REPUBLIQUE DU CAMEROUN
Paix-Travail-Patrie
****
MINISTERE DE L'ENSEIGNEMENT SUPERIEUR
****
UNIVERSITE DE YAOUNDE 1
****
FACULTE DES SCIENCES
****
CENTRE DE RECHERCHE ET DE FORMATION DOCTORALE EN SCIENCES, TECHNOLOGIES & GEOSCIENCES
****
UNITE DE RECHERCHE ET DE FORMATION DOCTORALE PHYSIQUE ET APPLICATIONS
****
DEPARTEMENT DE PHYSIQUE

UNIVERSITE DE YAOUNDE I
UNIVERSITY OF YAOUNDE I

REPUBLIC OF CAMEROON
Peace-Work-Fatherland
****
MINISTRY OF HIGHER EDUCATION
****
THE UNIVERSITY OF YAOUNDE I
****
FACULTY OF SCIENCE
****
POSTGRADUATE SCHOOL OF SCIENCE, TECHNOLOGY & GEOSCIENCES
****
RESEARCH AND POSTGRADUATE TRAINING UNIT IN PHYSICS AND ITS APPLICATIONS
****
DEPARTMENT OF PHYSICS

LABORATORY OF ENERGY, ELECTRICAL AND ELECTRONICS SYSTEMS (L.E.E.E.S)

THESIS

DEVELOPMENT OF A LOW DIMENSIONAL THERMAL MODEL FOR HEAT TRANSFERS IN A MULTIPHASE HOT CRUDE OIL FLOW THROUGH A LONG-SUBSEA PIPELINE COVERED WITH THERMAL INSULATION: EFFECT OF INSULATING MATERIALS

Thesis presented and defended in partial fulfillment to the award of
Doctorate/PhD in Physics

Speciality: Energy, Electrical and Electronics Systems
Option: Energy and Environment

By:
GOPDJIM NOUMO Prosper

Registration Number: 07W290
Master of Science in Physics

Publicly defended before the Jury composed of:

Président : WOAFO Paul, Professeur, Université de Yaoundé I

Rapporteurs : NJOMO Donatien, Professeur, Université de Yaoundé I

Membres : TCHAWOUA Clément, Professeur, Université de Yaoundé I

MEUKAM Pierre, Professeur, Université de Yaoundé I

DJANNA KOFFI Francis Lénine, Maître de conférences, Université de Douala

NANA NBENDJO Blaise Roméo, Professeur, Université de Yaoundé I

Year 2022

RÉPUBLIQUE DU CAMEROUN
Paix - Travail - Patrie
****
UNIVERSITÉ DE YAOUNDÉ I
****
FACULTÉ DES SCIENCES
****
DÉPARTEMENT DE PHYSIQUE

REPUBLIC OF CAMEROON
Peace - Work - Fatherland
****
THE UNIVERSITY OF YAOUNDÉ I
****
FACULTY OF SCIENCE
****
DEPARTMENT OF PHYSICS

ATTESTATION DE CORRECTION DE LA THÈSE DE DOCTORAT/PhD

Nous soussignés, **Professeur WOAFO Paul, Président** et Professeur **TCHAWOUA Clément, Examinateur** du jury de la soutenance de la **thèse de Doctorat/PhD** de Monsieur **GOPDJIM NOUMO Prosper**, Matricule **07W290**, préparée sous la direction du Professeur **NJOMO Donatien**, intitulée : « **Development of a low dimensional thermal model for heat transfers in a multiphase hot crude oil flow through a long-distance subse a pipeline covered with thermal insulation : Effect of insulating materials** », soutenue publiquement le **jeudi 28 juillet 2022** à la salle S01/02 de la Faculté des Sciences de l'Université de Yaoundé I en vue de l'obtention du **grade de Docteur/PhD de l'Université de Yaoundé I en Physique, spécialité : Énergie et Systèmes Électriques et Électroniques**, attestons que toutes les corrections demandées par le jury de soutenance ont été effectuées.

En foi de quoi la présente attestation lui est délivrée pour lui servir et valoir ce que de droit.

Fait à Yaoundé, le 21 OCT 2022

L'Examinateur

Pr. TCHAWOUA Clément

Le Président du jury

Pr. WOAFO Paul

Le Chef de Département de Physique

UNIVERSITE DE YAOUNDE I
FACULTE DES SCIENCES
Le Chef de Département
DEPARTEMENT DE PHYSIQUE

Pr. NDJAKA Jean-Marie Bienvenu

PLEDGE OF HONOUR

*I, the undersigned, **GOPDJIM NOUMO Prosper**, hereby declare that, this work is the result of my own research with the exception of quoted extracts from other works whose sources have been duly noted..*

DEDICATION

To the lovely memory of NOUMO Jean Paul, my father

ACKNOWLEDGMENT

I have presented here my doctorate thesis title "**development of a low dimensional thermal model for heat transfers in a multiphase hot crude oil flow through a long-distance subsea pipeline covered with thermal insulation: Effect of insulating materials**" which was given by my director and supervisor of study professor *NJOMO Donatien* and approve by me. The realization of this thesis would not have been possible without the help and support of so many people. I would like to express this gratitude to some of them in particular

First, I would like to sincerely thank my thesis supervisor professor *NJOMO Donatien* for the confidence he had toward me by given me this topic, for his continuous support throughout this study. I greatly appreciate his guiding advice, the constructive discussions that we had, his opening toward all my interrogations about my topic and his careful review of my thesis. I would also like to sincerely appreciate his availability.

I would like to thank the Vice-Chancellor of the University of Yaounde I, the Coordinator of the Research and Training Center in Science, Technology and Geosciences, and the Dean of the Physics Department, for allow me to continue my studies and to defend my doctoral thesis at this university.

I would like to thank the jury of pre-defense, Professor WOAFO Paul, Professor NJANDJOCK NOUCK Philippe and Professor TCHAWOUA Clément, for the constructive remarks and recommendations they made toward this work in order to highlights its quality.

I would like to thank the jury of audition, Professor BEN-BOLIE Germain Hubert, Professor SIEWE SIEWE Martin, Professor ZEKENG Serge and Professor BODO Bertrand, for the constructive critics and recommendations they made in order to ameliorate the quality of this work.

I would like to thank the external and internal experts for accepting to enrich this study with remarks and recommendations.

I would like to sincerely thank all the Professors in the Department of Physics for all the taught they gave to me since my first step in the Department. Special thanks to *Professor OBOUNOU Marcel*, to *Professor NDJAKA Jean Marie, Professor WOAFO Paul, Professor NJANDJOCK NOUCK Philippe, Professor TCHAWOUA Clément, Professor ZEKENG Serge, Professor BEN-BOLIE Germain Hubert* and to *Professor KOFANE Crépin* for all theirs taught and encouragement.

I would also like to thank the elders and friends of the Laboratory of Energy, of Electrical Systems and Electronics Systems (L.E.E.S.E.S), for all the unforgettable moments we had spent together. My thoughts are with: Professor TAMBA Jean Gaston, Dr. AKANA Nguimdo, Dr. MBOUMBOUE Edouard, Dr. TALLA Armel, Dr. FOTSING Rodrigues, Dr. SEUTCHE Calvin, BOUNOU Clovis, CHUISSEU Leonard, FOTSO Thierry, ZEPANG Kevin, WOUAPPI Corine, TEDONGMO Josiane, AVOTO Martial, KENFACK Stéphane, DJAMI Astelle, MAHAMAT Hasan, BISSAI Junior and all others.

I would also like to extend my gratitude to all my friends and colleagues at the Laboratory of Energy, of Electrical Systems and Electronics Systems of the University of Yaounde I, for theirs supports, remarks and observations they did toward this research work in order to ameliorate it quality.

I would like to express my gratitude to MABEU Thérèse and TCHAKONTIO Rachel, my mothers, for all what they have been doing for me, for all their wisdoms advises and love they have been given to me. Thank lovely mothers.

Finally, I would like to thank my family members, particularly to BAKAM Nadine, NOUMO Stephane, NOUMO Francis, KEGNE Agnès Solange, JIEUPA Dominique, CHOCOAGA Gabrielle, my great brothers BALLA Michel, TCHAPLE Christian and my lovely friend *MOLO Barbara and son MESSI GOPDJIM Paul* for always believing in me, supporting me, and encouraging me to achieve my dreams. Without their help during difficulties situations, I would never be able to be where I am now.

TABLE OF CONTENTS

NOMENCLATURE AND UNITS

A	cross section area, m²
B_o	oil formation volume factor, m³/m³
B_w	water formation volume factor, m³/m³
B_g	gas formation volume factor, m³/m³
C_d	profile parameter
C_o	isothermal compressibility of oil bar^{-1}
Cp	specific heat at constant pressure, j/kg K
d	inner diameter of pipe, m
f	friction factor,
GOR	gas-oil ration, m³/m³
g	acceleration of gravity, m/s²
h_i	inner convection heat transfer coefficient, W/m²-K
h_o	outer convection heat transfer coefficient, W/m²-K
H	hold up
k	thermal conductivity of pipe, W/m-K
k_{ins}	thermal conductivity of the insulation material, W/m-K
L	pipe length, m
M_g	mass of gas, kg
P	pressure, Pa
P_b	bubble point pressure, Pa
P_{pc}	pseudo-critical pressure, Pa
P_{pr}	pseudo-reduced pressure
q	heat flow rate, W/m²
$Q_w(P,T)$	volumetric flow rate of water at flow conditions, m³/D
$Q_o(P,T)$	volumetric flow rate of oil at flow conditions, m³/D

$Q_g(P,T)$	volumetric flow rate of gas at flow conditions, 158.99m³/D
$Q_{w\_sc}(P,T)$	volumetric flow rate of water at standard conditions, m³/D
$Q_{o\_sc}(P,T)$	volumetric flow rate of water at standard conditions, m³/D
$Q_{g\_sc}(P,T)$	volumetric flow rate of water at standard conditions, m³/D
Re	Reynolds number
R_S	solution gas-oil ratio, m³/m³
r	radius of pipe, m
T	temperature, °F, K
T_{pc}	pseudo-critical temperature, °R
T_{pr}	pseudo-reduced temperature
U	overall heat transfer coefficient, W/m² K
V_d	drift velocity, m/s
V_{sw}	superficial velocity of water, m/s
V_{so}	superficial velocity of oil, m/s
V_{sg}	superficial velocity of gas, m/s
V_g	velocity of the gas phase, m/s
V_m	mixture velocity, m/s
$V_o(P,T)$	volume of oil at pressure and temperature, m³
$V_g(P,T)$	volume of gas at pressure and temperature, m³
$V_w(P,T)$	volume of water at pressure and temperature, m³
V_{o_sc}	volume of oil at standard condition, m³
V_{w_sc}	volume of water at standard condition, m³
V_{g_sc}	volume of gas at standard condition, m³
W	mass flow rate, kg/s
WOR	water-oil ratio, m³/m³
Z	gas compressibility factor

SUBSCRIPTS

atm	Atmospheric
o	oil, outer
g	Gas
w	Water
l	liquid
m	Mixture
sc	standard conditions
pc	pseudo-critical
pr	pseudo-reduced
r	Reduced
tp	two phase
p	Pipe
i	Inner
a	Ambient
f	Fluid
n	no-slip
Av	Average

GREEK SYMBOLS

ρ	**density,kg/m³**
μ	**viscosity, Pa.s**
γ	**specific gravity**
α	**void fraction**
ε	**pipe roughness, m**
η	**joule Thomson coefficient,**
θ	**inclination angle of pipe, rad**
σ	**surface tension, j/m**

LIST OF FIGURES

LIST OF TABLES

ABSTRACT

In this thesis, we developed a thermal model for pressure and temperature predictions of an oil and gas flow through a long subsea pipeline based on energy conservation equation coupled with a pressure gradient formulation. Next, we determined by using three approaches, the optimum insulation thickness of three insulating material, that will be necessary to maintain a minimum temperature of 40°C, at any point of the flowing area in the pipe. In the first approach, we defined manually and gradually the range of insulation thickness and we determined by running numerical simulations, the optimum insulation thickness of the three insulating materials namely black aerogel (BA), calcium silicate (CS) and polyurethane foam (PUF). In the second approach, we combined genetic algorithm (GA) and power regression model using MATLAB software, to find out the optimum insulation thickness of each of the insulating material. Finally, the optimum insulation thickness was also determined using machine learning models namely: Generalized Linear Model (GLM), Decision Tree (DT), Deep Learning (DL), Random Forest (RF) and Support Vector Machine (SVM), in RAPIDMINER software. Further, we investigated the risks of formation of some flow assurance issues in pipeline using logistic regression. The results obtained from the numerical simulations of the temperature using MATLAB, is in good agreement with a relative error of 1.60% and 0.64% respectively on those from field data and the PIPESIM model. An absolute relative error of 1.64% was obtained with an existing model. In addition, the predicted pressure model matches with the measured value data with a relative pressure drop of 1.26%. Optimum insulation thickness, for the case of BA, was found to be 8.89 cm, 7.94 cm and 8.16 cm using respectively, the numerical simulation approach, power regression approach and RF approach. Next, for the case of CS, 71.12 cm, 69.5 cm and 69.77 cm were found respectively, following the three approaches. Finally, for the case of PUF, 22.86 cm, 22.30 cm and 22.43 cm were found respectively, for the numerical simulation approach, power regression approach and RF approach. It comes out that, the best insulating material for this study is BA. Finally, logistic regression model for the evaluation of flow assurance solids risk formation, using MATLAB, was validated using results from a statistical analysis software named STATGRAPHIC. Good accuracy was observed, indicating the capability of the software for making good predictions of the flow assurance solids risk formation during transportation of oil and gas in long subsea pipeline.

Keywords: Subsea pipeline, insulating material, two-phase flow, black oil model, heat transfer, numerical simulation, machine learning, temperature profile.

RESUME

Dans cette thèse, nous avons développé un modèle thermique à une dimension pour décrire la distribution de température et de pression d'un écoulement multiphasique de pétrole à partir de l'équation de conservation de l'énergie couplée avec l'équation du gradient de pression. Ensuite, nous avons déterminé, suivant trois approches, l'épaisseur optimale de trois matériaux d'isolation, nécessaire pour maintenir une température minimale de 40°C, en tout point de la conduite. Dans la première approche, nous avons défini manuellement et progressivement la plage d'épaisseur d'isolation et nous avons déterminé l'épaisseur optimale de trois matériaux d'isolation à savoir : le silicate de calcium (CS), la mousse de polyuréthane (PUF) et l'aérogel noir (BA) en effectuant des simulations numériques. Dans la deuxième approche, nous avons combiné les techniques d'algorithme génétique (GA) et le modèle de régression de puissance, à l'aide du logiciel MATLAB. Enfin, nous avons utilisé certains modèles d'apprentissage automatique dits « Machine Learning » à savoir : Modèle Linéaire Généralisé, Arbre de Décision, Apprentissage Profond, Forêt Aléatoire (FA) et Machine à Vecteur de Support, du logiciel RAPIDMINER. Nous avons finalement étudié, les risques de formation de certains solides, liés au transport d'hydrocarbures, en utilisant la régression logistique. Les résultats des simulations numériques de la température obtenus à l'aide de MATLAB, sont en accord avec une erreur relative de 1,60% et 0,64% respectivement, sur ceux issus des données de valeur mesurées et du modèle PIPESIM. Une erreur relative de 1,64% a été obtenue avec un modèle existant. Le modèle de gradient de pression, est également en accord avec les données mesurées, avec une erreur relative de 1,26%. L'épaisseur d'isolation optimale, pour le cas de BA, s'est avérée être de 8,89 cm, 7,94 cm et 8,16 cm, en utilisant respectivement l'approche par simulation numérique, par la régression de puissance combinée avec GA et par l'approche de FA combinée avec GA. Pour le cas du CS,71,12 cm, 69,5cm et 69,77 ont été obtenues respectivement, suivant ces trois approches. Pour le cas de PUF, 22,86 cm, 22,30 cm et 22,43 cm, ont été trouvées respectivement. Il en ressort que, le meilleur matériau isolant pour cette étude est le BA avec une épaisseur de 7,94 cm. Enfin, s'agissant de l'évaluation du risque de formation des solides, les résultats obtenus à l'aide de MATLAB, du modèle de régression logistique ont été validés par le logiciel STAGRAPHIC. Les différents modèles utilisés dans ce travail, ont été validés, indiquant leur capacité à pouvoir faire des prédictions assez précises.

Mots clés : pipeline sous-marin, matériaux isolants, écoulement multiphasique, modèle d'huile noire, transfert de chaleur, simulation numérique, machine learning, profil de température.

GENERAL INTRODUCTION

Offshore oil and gas production has become an essential part of global energy supply. It involves ever more advanced technologies and increasing attention to environmental impacts. According to [1], offshore production accounts for 30% of global oil production and 27% of gas production. These percentages have remained stable since the beginning of the 21st century, despite the strong onshore development of unconventional hydrocarbons such as tar sands or bituminous sands and shale hydrocarbons, it is estimated that offshore production represents 20% of world oil reserves and 30% of gas reserves [1]. Deep offshore accounts for 40% of Total's production and 70% of its 2015-2018 exploration goals. In 2017, 15% of global oil production comes from deep offshore (Total's forecast for 2019). 400 to 500 subsea wells operated and 8 Floating Production Storage and Outloading (FPSO) units [1]. Deep offshore hydrocarbons, once considered to be out of reach, now make up around 30% of the world's yet-to-be discovered conventional resources. Theirs exploitation, which takes place at greater and greater depths, in increasingly difficult seas and within increasingly isolated reserves characterized by complex fluids, represents a major challenge for the future of energy. From market predictions, the offshore industry is expected to invest $210 billion for new developments in five years (2011 - 2015), a 60% increase compared to the previous period (2006 - 2010), with pipelines and flow systems representing the 38% of this budget [2]. The implementation of new exploration and drilling technologies is expected to make the offshore industry to continue its growth towards deep (500 – 1500m) and ultra-deep (> 1500 m) waters.

One of the great challenges in subsea production result from unprecedented temperature and pressure conditions which leads to some flow assurance issues. According to [3], the offshore industry will face more challenging scenarios with production from deeper and colder waters. Subsea facilities will require longer subsea tiebacks in satellite fields to transport hydrocarbon fluids from the wellhead to existing production and processing platforms, and may require the transportation of processed gas and condensate streams to export facilities through subsea pipelines. The formation of solid deposits, such as gas hydrates, waxes, asphaltenes and mineral scale, may plug the flowlines, preventing production and generating a safety hazard. The flow assurance of the produced hydrocarbon stream has become a technical discipline that focuses on the design of safe and secure operation techniques for the uninterrupted transport of reservoir fluids from the reservoir to the point of sale.

Offshore pipelines are widely use as the unique mean of transportation of offshore fluids, which are generally consisting of oil, gas and water. These pipelines used for the transportation of offshore fluids

from the reservoir to the surface facility are known as infield pipelines and are designed for multiphase flow. These pipelines can be directly exposed to the seawater, buried or partially buried or event gathered as bundle. As conventional crude oil are more and more scarce, oil and gas industry are obliged to extract fluids from deeper water and at long tieback distances where the surrounding water is very cold. The lowest temperature of seawater, the presence of high water cut and changes in pressure and temperature of the fluids along the pipeline, will lead respectively to the cooling of the hot offshore fluids and to some flow assurance issues such as scales, asphaltenes, waxes and hydrates formation and deposition. As a consequence of these issues, the pipe effective flow area will reduce and in some cases, blockage of pipelines can occur (see figures 1.1 below) causing an interruption in production and therefore, resulting in colossal financial loss due to maintenance operations [4]. With today's low oil price and high rig rate, the industry is struggling with cost reduction [5]. Therefore, one of the important question is how to assure that, fluids will be safely and economically transported from the bottom of the wells all the way to the downstream processing plant. It is clear that, the fundamental challenge of any subsea project is to be able to transport the reservoir fluids, which is generally a multiphase fluid, consisting of oil, gas and water, from downhole to the processing facilities. One of the solutions to this problem is to find out the temperature and pressure profiles of the flowing fluid inside pipeline as well as to realize optimal insulation design because of it low resulting cost.

Figure 1.1: some flow assurance issues deposition inside pipeline [6]. In a) wax deposition, b) hydrate deposition and c) asphaltenes deposition.

Pressure and temperature are dependent variables that affect all the flow parameters. Due to their importance, the calculations of temperature and pressure profile during multiphase flow in wells and pipelines have been the scope of many researches [6]. [7] Presented temperature prediction model for flowing in wellbores and pipelines using both analytical model based on black oil model for fluids characterization. [4] Presented a model based on the general energy equation to describe the Explicit Temperature Drop Formula for an oil-gas steady flow in pipeline. They characterized the fluids properties using both black oil model and compositional model. [8] Developed two-phase flow wellbore thermal

models (oil–water and oil–gas) in both homogeneous and Drift-Flux forms. They used a compositional model to describe the fluids properties. [9] Presented the mathematical and numerical modeling of the oil biphasic flow in a partially submerged onshore pipeline. They analyzed the influence on the type of pipe insulation in the pressure and temperature gradients. All these researches show the interest that the scientific community have on this topic. Most of these studies focuses only on the modeling and simulation of pressure and temperature profiles in pipelines and wellbores during single-phase flow. Only few of them deals with the case of multiphase flow. These studies do not really take into account the need to perform thermal insulation of subsea pipeline, which is considered as one of the flow assurance thermal managements solutions.

Thermal insulation is used to slow down thermal energy loss of subsea production systems and therefore prevent solid deposits from precipitating. As subsea production systems move towards the deep sea, the cost of insulation systems will increase. A cost-effective insulation system is thus of great importance for subsea applications. Optimum insulation thickness need then to be calculated for an appropriate selection of the insulating material with respect to a proper thickness. In recent years, many researches have been carried out on this topic in the open literature showing the interest of scientific for the pipeline thermal design. For examples: NURFARAH and William [10] carried out a study on the optimum thermal insulation design for subsea pipeline. One of their objectives was to establish a workflow procedure in selecting thermal insulation materials, thickness and number of layers required for protective coating. The pipeline length considered was comprised between 500 and 1500m and the design criterion was that the output temperature should be above 20°C. They used Visual Basic Application with Excel for the simulations purpose. KIRAN [11], explored and compared the various types of insulation and find the optimum thickness of insulation required to maintain the temperature of the fluid inside the pipeline, above the hydrate/wax formation temperature of about 40°C to ensure smooth flow. Excel spreadsheet calculation was used to compare the effect of various insulation material with different thicknesses on the temperature profile of the fluid in deep-water environment. Ibrahim MASAUD Ahmed [12], focuses he study on the thermal insulation pipelines used for subsea crude oil transportation. He used MATLAB and Ansys fluent CFD to validate the MATLAB model. Briggs et al. [13] carried out a study using PIPESIM software to investigate the effects of flowlines sizes, flow rates, insulation material, type and configuration on flow assurance of waxy crude over 10.2 km between the wellhead and the first stage separator on the platform. Considering the implications of these factors for flow assurance. They used Polyurethane Foam, and pipe-in-pipe insulation type. MOBOLAJI et al. [14] investigated the best material that is suitable for the thermal insulation of subsea flowlines using the ANSYS software package, and then provided the best composite arrangement of insulation materials for better heat optimization. They used different insulating materials such as Aerogel, Paraffin Wax, Mineral Wool and Grooved Mineral to fill the gap between the inner pipe

and the outer pipe. S. A. MARFO et al. [15] used PIPESIM software to design a suitable pipeline for transporting condensate gas for the Jubilee and TEN Fields. The design comprises of two risers and two flowlines. Hydrate formation temperature was determined to be 72.5 °F at a pressure of 3 000 psig. The insulation thickness for flowlines 1 and 2 were determined to be 1.5 in. and 2 in. respectively. S. A. MARFO et al. [16] employed PIPESIM software to design a subsea pipeline for transportation of natural gas from Gazelle Field in Côte d'Ivoire to a processing platform located 30 km and to predict the conditions under which hydrate will form. They found that, an insulation thickness of 0.75 in, with specific pipe size of 10 in, could satisfy the arrival pressure condition of 800 psia. [12] Analyzed the temperature profile in steady state flow, heat loss, and transient flows of the startup mode for transporting crude oil in deep water pipeline. His study considers the determination of the effects produced with several thicknesses of insulation and several insulation materials for steady state and transient flow, using temperature profiles during the start-up of crude oil in subsea pipelines. However, most of these studies thermally design insulation material for pipelines using computational method and commercial software. Moreover, some of them are based on single-phase flow. As far as two-phase gas and liquid flow is concerned, few of these studies calculated the optimum insulation thickness based on a coupled temperature-pressure model. ALADE [17] carried out a study that focuses on choosing and sizing of an insulation material to meet an output temperature of an oil and gas wells. The criterion design output temperature was set at 20°C. The pipeline used was 1km long. The fluids properties were modeled using compositional model. Aspen Hysys software was used and polyurethane Foam was used as the insulating material.

This thesis aim to develop a thermal model for temperature and pressure predictions of a hot crude oil flowing through a subsea pipeline and to choosing and sizing an insulation material that will meet an output temperature of 40°C, using three approaches. Moreover, in this work, we used logistic regression to analyze the risk of formation of some flow assurance issues. The items accomplished during the course of this work are:

- Fluids properties characterized using black oil model
- Build pipeline model with PIPESIM software
- Build a thermal model that described pressure and temperature profiles inside subsea pipeline during two-phase flow
- Simulation of the pressure drop model for two-phase flow on MATLAB software and validation against field data and PIPESIM software
- Simulation of the temperature model for two-phase flow on MATLAB software and validation against field data and PIPESIM software
- Optimum insulation thickness calculation based on numerical simulations of three different insulation materials for different insulation thickness manually defined

- Optimum insulation thickness determination based on machine learning techniques for different insulation thickness randomly created using MATLAB
- Optimum insulation thickness determination based on machine learning techniques for different insulation thickness randomly created using RAPIDMINER.
- Evaluate the flow assurance risk probability for the best insulating material.

This thesis has been divided into 3 chapters. In chapter 1, after the introduction, a brief review on multiphase flow in pipelines is presented. The concepts on single and two-phase flow are presented, along with typical approaches for modeling flow behavior and pressure drop. In this chapter, heat transfer as well as insulation materials concepts are also presented. This chapter also highlights machine learning techniques and genetic algorithm concepts. The main focus of this Chapter is to provide the background to the fundamental concepts of fluid flow and heat transfer modeling during transportation in pipelines as well as machine techniques. Chapter 2 is devoted to methodology used in this work to achieve the objectives. Here, the thermal model that described the pressure and temperature profiles inside the considered subsea pipeline is presented. PIPESIM pipeline-built model is also presented. Machine learning techniques and RAPIDMINER software are briefly presented. Genetic algorithm chart is shown. Temperature and pressure profile obtained by numerical simulations using MATLAB and PIPESIM are discussed and compared each other with field data in chapter 3. The optimum insulation thickness as well as the best insulating material obtained by numerical simulations and by combining genetic algorithm with machine learning techniques are presented. Finally, this thesis is ended by conclusions and suggestions for further research.

CHAPTER 1 : LITERATURE REVIEW

Introduction

The aim of this study is to develop a thermal model for the prediction of temperature and pressure profiles of a hot multiphase fluid, consisting of oil and gas, flowing through a long subsea pipeline, in order to investigate the proper insulating material as well as the appropriated insulation thickness that will meet the thermal requirement of 40°C. Accurate prediction of temperature profile in subsea pipelines during multiphase flow required the simultaneous modeling of the hydrodynamic behavior of the biphasic fluids and the heat transfer occurring between the fluids and the pipeline wall. An appropriate formulation of the pressure drop and liquid hold up is essential to model the temperature profile. Therefore, this chapter provides a brief overview of the petroleum production system, the fundamentals of single-phase and multiphase flow. A review of steady state and transient models is provided, with a discussion of the key concepts behind each of them. The concepts of heat transfer and insulation material are also highlights in this chapter. Numerical tools used in this work is finally presented.

1.1 Multiphase flow modeling in offshore area

Multiphase flow is the area of fluid mechanics that deals with the simultaneous flow of two or more immiscible phases of matter (gas, liquid, or solid). Although this phenomenon may occur in many industrial applications, this thesis focuses on the multiphase flow of oil and gas in offshore pipelines. In this thesis, the terms multiphase and two-phase are used interchangeably. Multiphase flow has become increasingly important for the transportation of fluid from reservoir to the surface facility through pipelines. In offshore fields, produced fluids are transported to shore through long, large-diameter export pipelines for subsequent separation and processing. Tiebacks are often long pipelines that transport untreated produced fluids from marginal fields to an existing platform. These pipeline systems usually exhibit multiphase flow. Offshore pipelines are multiphase flow systems that require proper design and operation for safe and economic business. Accurate prediction of flow pattern, liquid holdup, pressure drop and flow characteristics along these pipeline systems is essential to enhance not only pipeline design, sizing, and routing, but also design of downstream separation and processing facilities to ensure safe and economic business operation. Therefore, it is important to have good understanding of the concepts of single and multiphase flow in pipelines.

1.1.1 Single and Multiphase flow concepts in offshore pipelines

It is very important to set some fundamental concepts of multiphase flow in pipeline, before talking about the temperature modeling. Any fluid flow consisting of more than one phase is referred to as

multiphase flow. Multiphase flow can be defined as a simultaneous flow of several phases. Gas-liquid two-phase flow is prevalent in various major industries such as petroleum, nuclear, space and geothermal [18]. In offshore production and transportation of oil and gas, multiphase flow occurs in horizontal as well as inclined pipes, in both the wellbore and flowlines. Flow assurance engineers require design methods to determine the pressure drop and liquid holdup to correctly size the transportation line and the separation facilities. In subsea area, multicomponent flow is generally encountered in infield pipelines through which, oil, gas and water are usually transported simultaneously either from manifold or the wells to the surface facilities, which can be a platform or a FPSO (Floating Production, Storage and Offloading). The flow of oil, gas and water can be treated as a biphasic flow where the oil and water constitute the liquid phase and gas is the gaseous phase. Because of the difference in densities of the two phases, they do not travel along the pipeline with the same velocity. For example, in downward flow, the liquid phase always flows faster than the gas phase [19]. Two-phase flow in horizontal, inclined or vertical pipeline, always display many configurations due to the difference in densities of the fluids and the pipeline geometry. These configurations are called flow regimes or flow patterns, which differ from each other in the spatial distribution of the interface of the fluids in presence. Pressure drop and liquid hold up calculations are strongly related to the type of flow pattern. Thus, multiphase flow reveals to be more complicated and complex to model than the single-phase flow. The modeling of multiphase flow in subsea pipeline required a good understanding of the petroleum production system.

1.1.2 Petroleum production systems in subsea area

Petroleum production systems can be classified in two main groups, which are reservoir system and piping system. The piping system is the means to transport reservoir fluids from the reservoir to surface facility. A schematic of this is presented at the Fig.1.2 below. From this figure, the following are the primary components:

- Reservoir, which is a porous and permeable rock that contains hydrocarbons.
- Wellbore, which is a vertical, deviated, or horizontal pipe connect to the reservoir to the surface.
- Wellhead, which is a combination of valves and chokes that control the flow.
- Flowlines, which are horizontal or slightly inclined pipes that transport reservoir fluids.
- Separator: which is a large vessel that separate reservoir fluids.

Petroleum production systems generally exhibit multiphase flow. Because of water flooding, water coning and production of interstitial water or water condensing in the well. Alternatively, free gas saturation in an

oil reservoir will lead to a gas-liquid mixture and retrograde condensation can result in hydrocarbons liquid condensing in a gas or condensate reservoir so that gas-liquid mixture can be encountered.

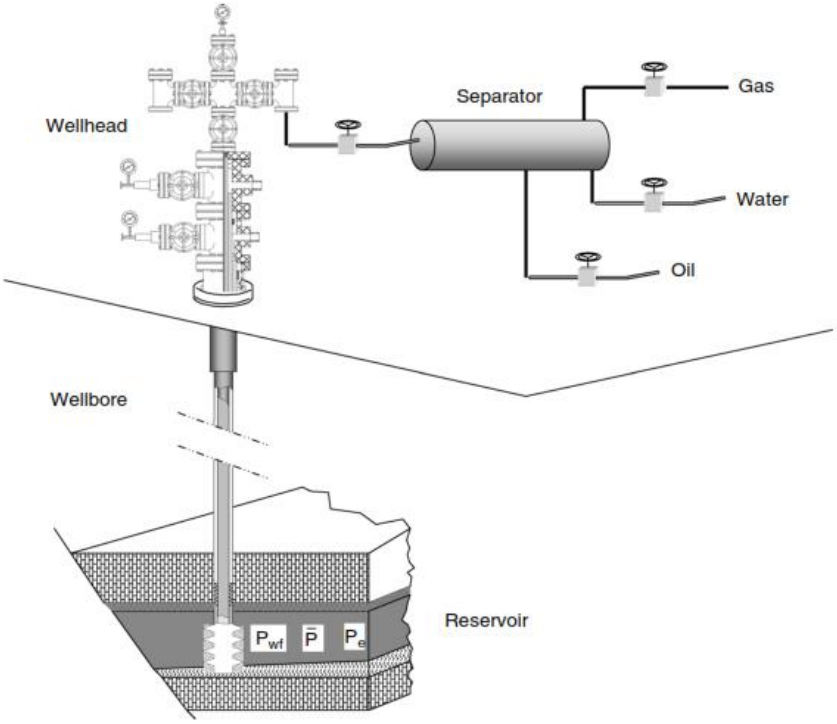

Figure 1.2: A schematic view of production system [20].

1.1.3 Single phase flow

The basis for virtually all computations involving fluid flow in pipes is conservation of mass, momentum, and energy. Application of these principles permits calculating changes in pressure and temperature along pipes. It is important to understand the fundamentals of single-phase flow in pipes before discussing multiphase flow in pipes. This section discusses the approach to calculate the steady state pressure drop in single-phase flow. This will provide the fundamental basis to build upon when moving to two-phase flow. It is important to understand fluid physical behavior along pipes before predicting its flow parameters. The two main fluid physical properties related to fluid flow in pipes are viscosity and density. On the basis of fluid viscosity, fluids can be classified into two categories-namely, Newtonian and non-Newtonian. Similarly, fluids can be classified into incompressible and compressible according to their density behavior [21].

a) Newtonian fluid

A Newtonian fluid is a fluid with constant viscosity, regardless of the shear force applied on it. This definition indicates that Newtonian fluid viscosity depends only on pressure, temperature, and composition,

and not on the shear forces. The constant viscosity behavior of a Newtonian fluid is represented by the constant slope of a straight line through the origin of a plot of shear stress vs shear rate. Newton's law for this type of fluid can be written as [21],

$$\tau_{xy} = -\mu \frac{dV_x}{dy} \tag{1.1}$$

where: τ_{xy} is the shear stress or momentum flux, Pa, $\frac{dV_x}{dy}$, is the shear rate, s^{-1}, and μ, the viscosity, Pa.s. The negative sign in front of the viscosity indicates that the shear stress transfers from high velocity to low velocity. All gases and homogeneous nonpolymeric liquids follow Newtonian behavior. Conversely, a non-Newtonian fluid is one that has an increasing viscosity trend (shear thickening) or decreasing viscosity trend (shear thinning) with shear stress. Furthermore, a non-Newtonian fluid may have a constant viscosity but require an initial shear force to flow (plastic flow). In oil and gas production, crude oil, formation water, and natural gas are all considered to Newtonian fluids. Others fluids, however, such as oil/water emulsions or slurries (oil and produced solids) are often found to display non-Newtonian behavior [21]. This study focuses assume that fluids are Newtonians

b) Incompressible fluid

A constant density with pressure and temperature characterizes an incompressible fluid. Although there is no truly incompressible fluid, this assumption simplifies the mathematical formulation and calculation significantly with minor error. Water is the best example of an incompressible fluid, whereas crude oil is considered a slightly compressible fluid. Conversely, natural gas is compressible fluid because of its low intermolecular forces that cause a density change with pressure and temperature. [21]

c) Steady state condition

A steady state condition is a special flowing condition in which the mass, linear momentum and energy inflow rates in pipe are equal to outflow rates. In other words, the rate change of mass, linear momentum, and energy along a pipe is zero. In steady state condition, the conservation laws are independent of time [21].

d) Conservation of mass

For a given control volume, such as a segment of pipe, conservation of mass simply implies that the mass in, minus the mass out, must equal the mass accumulation. The mass conservation equation for fluid flow in one dimension is then given by,

$$\frac{\partial \rho}{\partial t} + \frac{\partial (\rho V)}{\partial L} = 0 \tag{1.2}$$

Equation 2 is the continuity equation that describes the time rate change of fluid density at any time and pipe length. For steady state flow conditions, there is no mass accumulation and the equation above becomes:

$$\frac{d(\rho V)}{dL} = 0 \tag{1.3}$$

For an incompressible fluid, equation (1.3) reduces to the following

$$\rho \frac{d(V)}{dL} = 0 \tag{1.4}$$

Equation 4 indicates that for a steady state incompressible flow, the fluid velocity is constant along the pipe.

e) Conservation of momentum

From the Newton's first law, the rate of momentum out minus the rate of momentum in, plus the rate of momentum accumulation in a given pipe segment must equal the sum of all the forces on the fluids. Figure 1.3 defines the control volume and partial variables. Conservation of linear momentum can be expressed as:

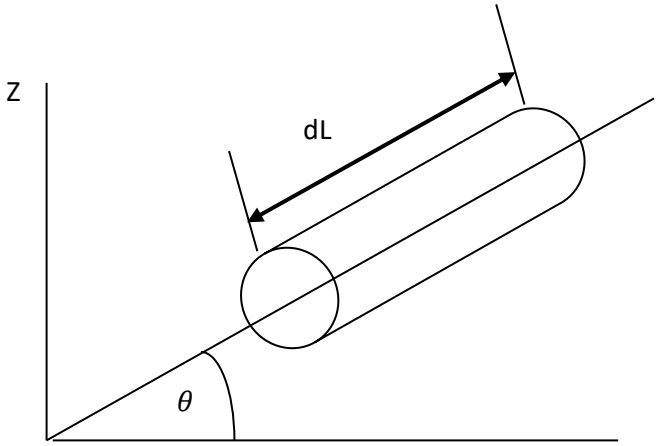

Figure 1.3 Segment of an inclined pipe [22]

$$(momentum\ rate)_{in} - (momentum\ rate)_{out} + (som\ of\ forces\ acting\ on\ fluid) = (rate\ of\ momentum\ accumulated)_{in\ the\ control\ volume} \tag{1.5}$$

Mathematically, we have:

$$momentum\ rate\ in = A_p \rho V\ (V)_{in}$$

$$momentum\ rate\ out = A_p \rho V\ (V)_{out}$$

$$som\ of\ forces\ acting\ on\ fluid = shear\ force + gravity\ force + pressure\ force$$

The shear force is a result of fluid shear along the pipe wall and is the product of shear stress and the inner pipe surface area ($\pi d \Delta L$). The shear force is always acting in the opposite direction of flow (negative). The shear force is defined as ($\tau_w . \pi d \Delta L$).

The gravity force is the weight of fluid and is the product of hydrostatic pressure ($\rho g \Delta L \sin\theta$) and pipe cross-sectional area ($A_p = \frac{\pi d^2}{4}$). The gravity force direction depends on the flow direction as follow:

- In upward flow, the gravity term is negative (i.e., pressure loss because of the positive inclination angle).
- In downward flow the gravity force is positive (i.e., pressure gain because of the negative inclination angle, which pulls the fluid in the direction of flow).
- In horizontal flow, the gravity force is zero.

The pressure force in a moving fluid is defined by the equation of state, ($\rho = f(p,T)$) and may increase or decrease along pipe depending on the magnitude and direction of the shear and gravity forces.

Equation 2.5 can therefore be rewritten as,

$$A_p \rho V\ (V)_{in} - A_p \rho V\ (V)_{out} + A_p P - A_p \left(P + \frac{\partial P}{\partial L} dL\right) - A_p\ \rho g \Delta L\ \sin\theta - A_p\ f \rho \frac{V^2}{2d} = A_p \frac{\partial(\rho V)}{\partial t} dL \tag{1.6}$$

From equation 6 above, we obtained,

$$\frac{\partial(\rho V)}{\partial t} + \frac{\partial(\rho V^2)}{\partial L} = -\frac{\partial P}{\partial L} - f \rho \frac{V^2}{2d} - \rho g \sin\theta \tag{1.7}$$

for steady state flow, we have:

$$\frac{\partial P}{\partial L} = -f \rho \frac{V^2}{2d} - \rho g \sin\theta - \frac{\partial(\rho V^2)}{\partial L} \tag{1.8}$$

Combining the equation above with the continuity equation, gives:

$$\frac{\partial P}{\partial L} = -f \rho \frac{V^2}{2d} - \rho g \sin\theta - \rho V \frac{\partial V}{\partial L} \tag{1.9}$$

where: d is the inside diameter of the pipe, m, f is the dimensionless friction factor. ρ is the density of the fluid, kg/m³, g is the acceleration of gravity, m/s², θ is the pipeline inclination, rad, V, is the velocity of the fluid, m/s, L, is the pipeline length, m, and P, is the pressure, Pa. Equation 2.9 applies for any fluid in

steady state, one-dimensional flow for which $f, p,$ and v can be defined. Definition of these variables is what causes most of the difficulty in describing two-phase flow. In two-phase flow, f may be a function of other variables besides the Reynolds number and relative roughness.

The pressure gradient prediction along a pipe is obtained by combining the mass and the momentum conservation equations. This equation indicates that, the total pressure gradient along a pipe is composed of three components, which are frictional, elevation and acceleration. The first term at the right of the equation is the pressure gradient term due to friction, the second term is the one due elevation and the last term is the one due to acceleration of fluids particles. For single-phase flow, this equation can be solved using analytical method. As far as multiphase flow is concerned, the resolution of this equation cannot be done without resorting to empirical techniques. More details are provides in [21-24]. Some aspects of the pressure gradient equation as it applies to single-phase flow are discussed to develop a thorough understanding of each component before modifying it for two-phase flow. The elevation change or hydrostatic component is zero for horizontal flow only. It applies for compressible or incompressible, steady state or transient flow in both vertical and inclined pipes. For downward flow, the sin of the angle is negative, and the hydrostatic pressure increases in the direction of flow. The friction loss component applies for any type of flow at any pipe angle. It always causes a drop of pressure in the direction of flow. The kinetic energy change or acceleration component is zero for constant area, incompressible flow. For any flow condition in which a velocity change occurs, such as compressible flow, a pressure drop will occur in the direction of the velocity increase. Although single-phase flow has been studied extensively, it still involves an empirically determined friction factor for turbulent flow calculations. The dependence of this friction factor on pipe roughness, which must usually be estimated, makes the calculated pressure gradients subject to considerable error. To calculate the pressure change in equation 1.9, the friction factor must be evaluated. The friction factor f, dependent on the Reynolds number, pipe wall roughness, and flow regime in the pipe (i.e., laminar or turbulent flow). Therefore, the procedure requires evaluating whether the flow is laminar or turbulent. This can be accomplished by first defining and calculating the Reynolds number.

- Reynolds Number and flow regime

The Reynolds number is a dimensionless number defined as the ratio of inertial to viscous forces. The Reynolds number is calculated as follow.

$$Re = \frac{V\rho d}{\mu} \tag{1.10}$$

Where, ρ is the density, $\mathrm{km/m^3}$, V is the velocity, $\mathrm{m/s}$, μ is the dynamic viscosity, $\mathrm{kg/(m.s)}$ and d is the pipe diameter, m. If the Reynolds number is less than 2000, flow is laminar otherwise, the flow is turbulent.

➢ Pipe wall relative roughness

The pipe wall relative roughness is the dimensionless roughness of the internal pipe wall and is a measure of the texture of the surface. It is characterized by the vertical irregularities and deviations of a real surface from its ideal form. If these deviations are large, then the surface is rough. If they are small, the surface is smooth. The roughness is often affected by corrosive fluids and solids particles flowing in the pipe. Thus it is a function of operation time, fluids and pipe material. The relative roughness is therefore the roughness divided by the pipe inside diameter. The roughness values of common material are available in literature.

➢ Friction factor

Friction factor can be determined from the Moody chart (see figure 1.4 below) which illustrate the flow regime regions and their respective friction factor behavior.

Friction factor can be calculated as follow:

- For Reynolds numbers lower than 2000 the flow is laminar, and f is given explicitly by

$$f = \frac{64}{R_e} \tag{1.11}$$

- For Reynolds numbers larger than 3000 the flow is turbulent, and f is given implicitly by:
- Smooth pipe friction factor (modified Blasius 1908)

$$f = 0.184 Re^{-0.2} \tag{1.12}$$

- Rough pipe friction factor (Colebrook, 1939)

$$\frac{1}{\sqrt{f}} = 1.74 + 2\log_{10}\left(2\varepsilon + \frac{18.7}{R_e\sqrt{f}}\right) \tag{1.13}$$

where, ε is the dimensionless pipe roughness defined as:

$$\varepsilon = \frac{e}{d} \tag{1.14}$$

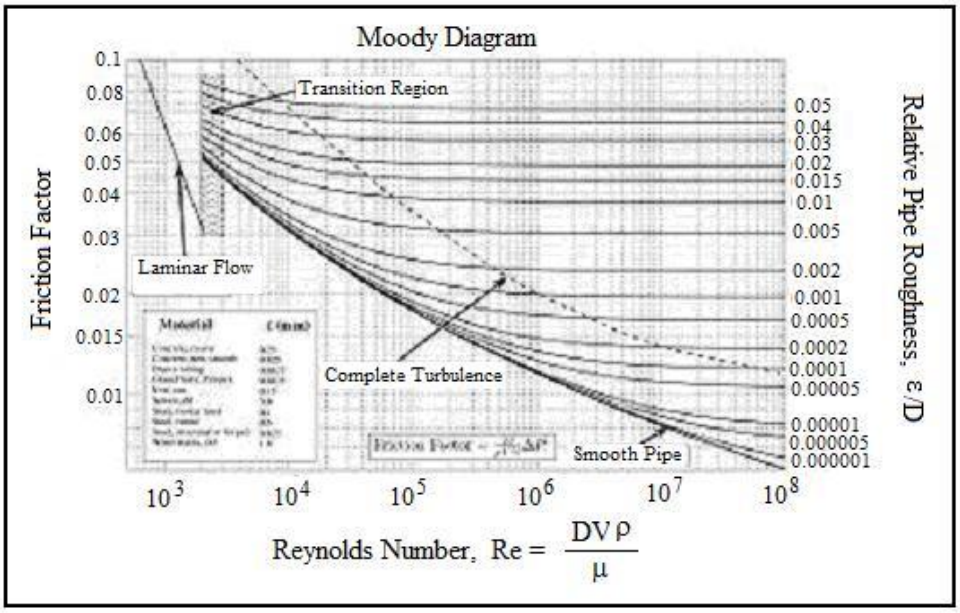

Figure.1.4: Moody Friction Diagram Source: http://www.thefullwiki.org/Moody_diagram

- For fully turbulent flow, that is, the friction factor is no longer a function of the Reynolds number and only a function of the relative roughness, friction factor is calculated as:

$$f = \left[1.74 - log\left(\frac{2\varepsilon}{d}\right)\right]^{-2} \tag{1.15}$$

Finally, the pressure gradient equation becomes by making use of derivatives definition, as:

$$\frac{dP}{dL} = -f\rho\frac{V^2}{2d} - \rho g \sin\theta - \rho V\frac{dV}{dL} \tag{1.16}$$

where: g is the acceleration of gravity in m/s² and θ is the inclination angle in rad. In pipeline engineering, the inclination θ is defined as the angle of the pipeline axis with respect to the horizontal plane. The term $\sin\theta$ is therefore a measure of the change in elevation of the pipeline axis per unit length of measured distance. Equation (1.16) above shows that the steady-state pressure gradient equation is made up of three components: friction, elevation and acceleration.

$$\left(\frac{dP}{dL}\right)_{tp} = \left(\frac{dP}{dL}\right)_f + \left(\frac{dP}{dL}\right)_h + \left(\frac{dP}{dL}\right)_a \tag{1.17}$$

The *frictional loss* is caused by the dissipation of energy by viscous forces in the fluid. This term depends strongly on the fluid properties, the flow regime (laminar or turbulent) and the fluid velocity. It is usually the most important component in pipelines. Friction losses normally represent 5 to 20% of the total

pressure drop in wells [25]. The *head loss or gravity loss* is the static change in pressure caused by the change in the pipe's elevation. In near-horizontal pipelines this component is negligible, but it is usually the most important component in a well. The pressure between surface and bottom hole changes greatly, simply due to the weight of the column of fluid in the well, even if it is not flowing. It usually contributes from 80 to 95% of the pressure gradient in the wells [25]. The *acceleration loss* is caused by the change in momentum when the fluid is accelerated in the well due to expansion. Generally, this term is less important and can be neglected in some cases. However, it can become of significance for very high rate gas wells [22].

1.1.4 Multiphase flow parameters in subsea pipeline

In petroleum production system, the term multiphase flow refers to the simultaneous flow of two or more different phases (oil, water, gas, solids) in pipeline. In this study, the term multiphase flow will refer to the flow of gas-liquid (oil and water) flow. In subsea area, we distinguish pipelines that transport untreated produced fluids from the reservoir to the surface facilities. These pipelines are called infield pipelines or Tiebacks and always exhibit multiphase flow. While pipelines that carried, fluids from surface facilities to shore are called export pipelines. In this study, pipelines are considered as infield pipelines. Some basic multiphase flow concepts definition in subsea pipeline are presented.

❖ **Flow patterns**

As summarize by [26], flow pattern of the multiphase flow is the description of how the liquid and gas are distributed in the pipe. The flow pattern can be affected by many parameters, such as pipe inclination, liquid/gas ratio and inlet flow rate. Generally, flow pattern can be divided into two categories: horizontal flow pattern and vertical flow pattern. Because the flow is directed by perpendicular gravity, the flow pattern of horizontal multiphase flow is distinct from vertical flow. Figure 1.5 below present some of the flow patterns generally encountered in horizontal pipeline. From this illustration, we can retain that:
Stratified flow occurs in a horizontal pipeline when gas and liquid flow with a relatively small flow rate. In horizontal flow, gas flows above the liquid, which flows along the lower portion of the pipe. Stratified flow is generally classified into two types, which are smooth and wave flow. Stratified smooth flow has no disturbance on the liquid surface when the gas velocities are low enough. Stratified wave flow happens at higher gas velocities, waves can be seen on the surface of the liquid. If the gas velocity increases, waves start to form, and these waves can get high enough to reach the top of the pipe. When that happens, the gas is throttled or even blocked for a moment so that the flow becomes discontinuous, thus leading to the formation of *slugs* or *elongated bubbles*. *Disperse bubble flow* occur when numerous tiny bubbles are transported by continuous liquid phase, causing no relative motion between the two phases. *Annular flow*

is characterized by the axial continuity of the gas phase in a central core with the liquid flowing upward, both as thin film along the pipe wall and as dispersed droplets in the core, leaving a very thin liquid film flowing along the wall.

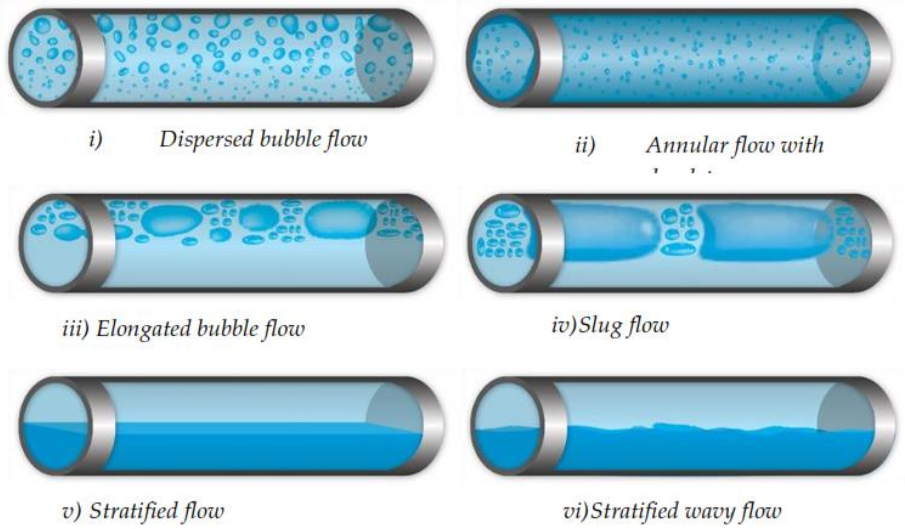

Figure 1.5: Gas-liquid flow regimes in horizontal pipes [26].

In vertical and near vertical systems, four major flow patterns are recognized: bubbly flow, slug flow, churn flow and annular flow. These flow patterns are clearly distinguishable and are generally recognized by all researchers. A schematic of different flow regimes in a vertical wellbore is shown in Figure 1.6 below.

- **Bubbly flow**: At low gas velocity, the liquid phase is the continuous phase and gas or vapor phase flows as bubbles in it. When the gas velocity is low, especially in vertical flow, the bubbles are uniformly distributed.
- **Slug flow:** As gas velocity increases, the bubbles coalesce and make larger bubbles. These large bubbles sometimes have almost the same diameter as the wellbore. Hence, as shown in Figure 1.8, the slug flow consists of two parts: large bubbles (Taylor bubbles) and continuous liquid phase containing small bubbles.
- **Churn flow**: This flow regime forms by the breakdown of slug flow Taylor bubbles because of high mixture velocity. The gas phase flows in a chaotic manner through the liquid phase and it is relatively unstable, hence the multiphase flow parameters such as holdup vary with time at each section when churn flow exists in the tubing.
- **Annular flow:** As the flow rate and fraction of the gas phase increases, this phase starts to flow through the center of the wellbore as a continuous core with some liquid droplets. The liquid phase forms a layer along the pipe wall and flows as an annulus.

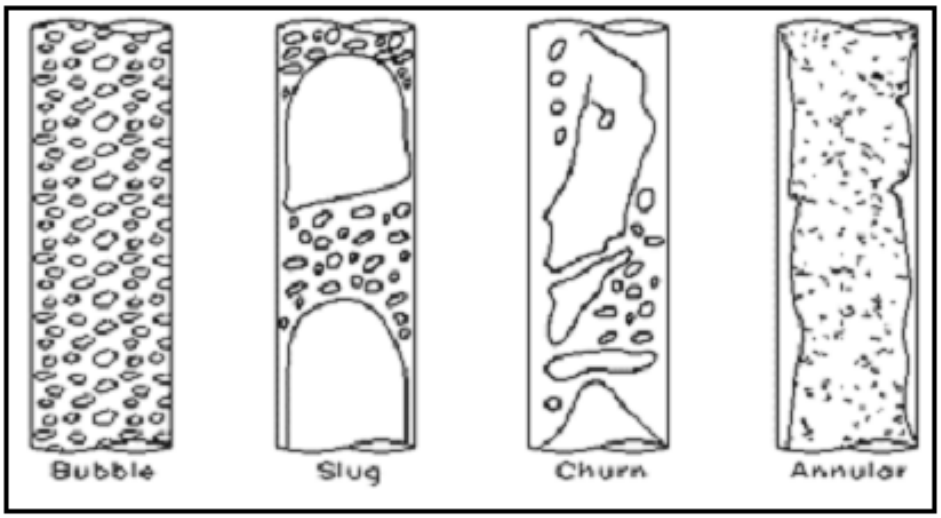

Figure 1.6. Schematic multiphase flow patterns in a vertical tube (From left to right: bubble flow, slug flow, churn flow and annular flow), picture from [25].

❖ **Two phase variables**

When performing multiphase flow calculations for wells and pipelines, single-phase flow equations are often modified to account for the presence of a second phase. This involves defining mixture expressions for velocities and fluid properties that use weighting factors, based on either volume or mass fractions. Therefore, it is important to understand the two-phase flow variables that are commonly used in two-phase flow calculations. These variables are known as liquid holdup and void fraction, and velocities

➢ **Liquid holdup and void fraction**

Liquid holdup can be defined as the fraction of a pipe volume increment or cross section that is occupied by the liquid phase. The expression "hold-up" is also often used in the oil industry to indicate the volume fractions occupied by gas and liquid, although in upward flow the gas is not actually held up, but to the contrary is speeded up. The liquid hold-ups H_L is defined as

$$H_L = \frac{V_L}{V_p} = \frac{A_L}{A_p} \tag{1.18}$$

The in-situ gas volume fraction is defined by the void fraction and is given as

$$H_g = \alpha = 1 - H_L \tag{1.19}$$

For the case of homogeneous flow, the no-slip holdup is the fraction of liquid in the pipe and can be calculated from the in-situ volumetric flow rates as:

$$\lambda_L = \frac{Q_L}{Q_m} = \frac{Q_L}{Q_L + Q_g} = \frac{V_{sl}}{V_m} \tag{1.20}$$

The no-slip gas void fraction is the fraction of the pipe cross-sectional area occupied by gas. It is calculated as:

$$\lambda_g = 1 - \lambda_L \tag{1.21}$$

When oil and water flow simultaneously in pipes, with or without gas, the slippage between them is normally small as compared to the slippage that can occur between gas and liquid. Therefore, assuming no-slippage, the oil fraction in a liquid phase is calculated as:

$$f_o = \frac{Q_o}{Q_o + Q_w} \tag{1.22}$$

The water cut, is defined as the ratio of water volumetric flow compared to the total volumetric liquid flow.

$$f_w = 1 - f_o = \frac{Q_w}{Q_o + Q_w} \tag{1.23}$$

- Velocities

Several velocities are used in multiphase flow, such as superficial, mixture, actual, and slip velocities.

Superficial velocity is defined as phase velocity, assuming it occupies the entire pipe cross-sectional area. Superficial velocity is smaller than actual phase velocity. Oil, water and gas superficial velocity are calculated as follow:

$$V_{So} = \frac{Q_o}{A_p} \tag{1.24}$$

$$\mathrm{V_{sw}} = \frac{Q_w}{A_p} \tag{1.25}$$

$$V_{Sg} = \frac{Q_g}{A_p} \tag{1.26}$$

For homogeneous flow of oil and water, the two phases may be combined as a single liquid phases as follows:

$$V_{SL} = \frac{q_L}{A_p} = \frac{Q_o + Q_w}{A_p} \tag{1.27}$$

- Mixture velocity

The mixture velocity is defined as the algebraic sum of the respective phase flow rates divided by the entire pipe cross-sectional area. In terms of superficial velocities, the mixture velocity of two and three-phase flows can be expressed as:

$$V_m = V_{SL} + V_{Sg} \tag{1.28}$$

- Actual velocity

The actual velocity represents the local or the true phase velocity of each phase in the pipe. It can be calculated as follow:

$$V_g = \frac{Q_g}{A_g} = \frac{Q_g}{A_p \alpha} = \frac{V_{sg}}{\alpha} \tag{1.29}$$

$$V_L = \frac{Q_L}{A_g} = \frac{Q_L}{A_p H_L} = \frac{V_{sL}}{H_L} \tag{1.30}$$

For homogeneous flow, the void fraction and liquid holdup are replaced by the no-slip void fraction and the no-slip liquid holdup in equation (1.29) and (1.30) respectively.

- Slip velocity

The slip velocity can be defined as the difference between the actual phase velocities.

$$V_S = V_L - V_g \tag{1.31}$$

In homogeneous flow, the slip velocity in equation (1.31) is reduced to zero because the no-slip liquid holdup is used as the liquid holdup.

❖ **Two-phase mixture properties**

From knowledge of single-phase in-situ densities and viscosities of oil, water, gas, gas-oil ratio, water oil ratio, gas-water ratio, surface tensions and no-slip liquid holdup, the multiphase in-situ mixture density, viscosity, and surface tension can be calculated. A wide variety of methods have been used to define mixture properties in the open literature [27-31].

- Oil water mixture

For both black-oil and compositional model cases, when free water exists, oil and water properties can be combined under the assumption of no-slip homogeneous flow using volumetric weighted-averaging methods as follows [22-24]: The liquid density at standard conditions and at flow conditions are given by:

$$\rho_{L\_sc} = f_w\rho_{w\_sc} + (1 - f_w)\rho_{o\_sc} = \frac{WOR}{1+WOR}\rho_{w\_sc} + \frac{1}{1+WOR}\rho_{o\_sc} \quad (1.32)$$

$$\rho_L = \frac{\rho_{g\_sc}R_{sL}+\rho_{L\_sc}}{B_L} \quad (1.33)$$

where: ρ_{w_sc} and ρ_{o_sc} are the water and oil densities at the standard conditions. B_L is the volume formation factor of the liquid given by [22] as follow:

$$B_L = \frac{WOR}{1+WOR}B_w + \frac{1}{1+WOR}B_o \quad (1.34)$$

and R_{sL} the gas-liquid ration defined as the ratio of the quantity of gas solubilized in the oil at flow condition to the liquid volume, both expressed at standard conditions.

$$R_{sL} = \frac{1}{1+WOR}R_s \quad (1.35)$$

From the above, the density of liquid homogeneous mixture can be obtained by:

$$\rho_L = \rho_o(1 - f_w) + \rho_w f_w \quad (1.36)$$

The liquid viscosity can be calculated using the water cut as follow:

$$\mu_L = \mu_o(1 - f_w) + \mu_w f_w \quad (1.37)$$

where μ_o and μ_w are respectively the oil and water viscosities.

The surface tension of the liquid mixture is given as follow:

$$\sigma_L = \sigma_o(1 - f_w) + f_w\sigma_w \quad (1.38)$$

where σ_o and σ_w are respectively the oil and water surface tensions.

- Gas-Liquid mixture

No-slip gas-liquid properties can be calculated using the no-slip liquid holdup as a volumetric weighting factor [25].

$$\rho_n = [\rho_o(1 - f_w) + \rho_w f_w]\lambda_L + \rho_g(1 - \lambda_L) \quad (1.39)$$

$$\mu_n = \mu_L\lambda_L + \mu_g\lambda_g \quad (1.40)$$

1.1.5 Multiphase pressure gradient models in offshore pipeline

For single-phase flow, the pressure gradient is calculated as in equation (1.16). As far as multiphase flow is concerned, the frictional pressure drop is the result of an irreversible work done due to shear at the pipe wall and at the gas-liquid interface. The frictional pressure drop in two-phase flow reveal to be much more complex to predict than single-phase flow. This is because it dependent on many flow parameters such as pipe diameter, mass flux, pipe orientation, pipe surface roughness, fluid properties and interfacial contact area between the phases. There are many two-phase flow pressure drop correlations in the open literature. Sometimes it becomes difficult to know which correlation would be more accurate or suitable for the task at hand. Moreover, the lack of good understanding of the two-phase flow behavior had led many researchers to develop correlations that are limited to a certain range of flow parameters. Therefore, the user of the correlation must understand those restrictions and must make sure the task at hand is within the restrictions [32]. In the following paragraphs, will be presented some of the pressure gradient correlations selected based on the works done by [23, 25 and 32]. From these works, the frictional pressure gradient is modeled based on separated flow approached or a well-mist flow approached or homogeneous models. Below, is presented some of the two-phase variables necessary for the modeling of fluid flow.

1.1.5.1 Homogeneous pressure gradient

The accurate design of oil and gas well tubing and surface flowlines requires the ability to predict flow behavior along the pipes. Here, we present the physical phenomena and prediction methodology of two-phase flow in pipes for homogeneous flow. Homogeneous can be defined as of uniform structure or composition throughout. In multiphase terminology, a homogeneous two-phase flow is defined as the flow structure in which the two phases travel at the same in-situ velocity. When the combined drag and buoyancy forces overcome the gravity force, the higher density phase will disperse throughout the higher-velocity phase, resulting in equal velocities of both phases and thus a no-slip homogeneous flow. The fundamental assumption in the homogeneous model is that fluid in the system are perfectly mixed so that there is no slip between each phase, hence forming a homogeneous mixture [33]. Treated as a single-phase fluid, the two-phase fluid is considered to have one velocity-mixture velocity. Fluid properties can be represented by mixture properties. The equality of the phase's velocities in homogeneous two-phase flow ignores a common two-phase flow physical phenomenon known as slippage. Therefore, a homogeneous two-phase flow results in no accumulation of one phase along the pipe. Pressure drop calculations for homogeneous

two-phase flow in pipes starts by calculating the in-situ physical fluid properties and flow rates for each phase. Detailed descriptions of this calculation using the black-oil model and the compositional are given in [23, 25]. The calculation steps is followed by calculating two-phase flow variables such as superficial velocities, mixture velocity, and no-slip liquid holdup. The two-phase mixture properties are then calculated, and the results are then used in calculating the pressure gradient. In the open literature, many correlations have been developed for the determination of pressure gradient in homogeneous flow with and without slippage condition. [25, 32]. The pressure gradient equation derived in equation (1.16) for single-phase flow can be modified for homogeneous multiphase flow by using homogeneous mixture properties and adding an acceleration term.

$$\frac{dP}{dL} = -f_{tp}\rho_n \frac{{V_m}^2}{2d} - \rho_n g \sin\theta - \rho_n V_m \frac{dV_m}{dL} \tag{1.41}$$

The elevation pressure gradient component requires the no-slip homogeneous density and inclination angle. This term has the highest contribution to the total pressure gradient. The pressure gradient caused by acceleration is negligible except for cases of high flow velocities. The frictional pressure gradient component requires determining a two-phase homogeneous friction factor, which requires a two-phase homogeneous Reynolds number, estimated as follows:

$$Re_{ns} = \frac{\rho_n V_m d}{\mu_n} \tag{1.42}$$

In equation (1.41), f_{tp} is the two-phase friction factor, which can be obtained from the Colebrook equation as given below:

$$\frac{1}{\sqrt{f_{tp}}} = -2log\left[\frac{2\varepsilon/d}{3.7} - \frac{5.02}{Re_{ns}} log\left(\frac{2\varepsilon/d}{3.7} + \frac{13}{Re_{ns}}\right)\right] \tag{1.43}$$

where ε, is the pipe roughness, d the pipe diameter and Re_{ns} is the Reynolds number of the mixture.

Homogeneous pressure gradient can also be calculated using some empirical correlations. Here, Beggs and Brill (1973) and modified Dukler et al (1969) correlations will be presented among others.

a) Beggs and Brill (1973) model [24]

The general expression for the pressure drop, where p is the pressure and L is the pipeline length, can be written as follow:

$$\left(\frac{dP}{dL}\right)_{total} = \left(\frac{dP}{dL}\right)_f + \left(\frac{dP}{dL}\right)_g + \left(\frac{dP}{dL}\right)_{acc} \tag{1.43}$$

The first term on the right side of equation (1.43) with subscript "f" is the pressure gradient due to friction, the second term with subscript "g" is the pressure gradient due to elevation and the last term with subscript "acc" is the pressure gradient due to acceleration. The Beggs and Brill (1973) correlation for the total pressure gradient is given generally as:

$$\frac{dP}{dL} = \frac{\frac{f_{tp}\rho_n V_m^2}{2d} + \rho_m g \sin\theta}{1 - E_k} \tag{1.44}$$

In which E_k is a dimensionless acceleration term that take into consideration the pressure gradient due to kinetic energy effects and is given by:

$$E_k = \frac{V_m V_{Sg} \rho_m}{P} \tag{1.45}$$

In equation.(1.44), f_{tp} is the friction factor for two-phase flow; ρ_n is the no-slip density of the fluids;ρ_m is the slip density of the fluids; V_m is the mixture velocity of the fluids; d is the pipe inner diameter; P is the pressure; g is the acceleration of gravity; θ is the inclination angle of the pipe; L is the pipeline length. . assuming the acceleration component to be negligible gives:

$$\frac{dP}{dL} = \frac{f_{tp}\rho_n V_m^2}{2ID} + \rho_m g \sin\theta \tag{1.46}$$

with ρ_m given by:

$$\rho_m = \rho_l H_L + \rho_g \alpha \tag{1.47}$$

In equation (1.44), the two-phase friction factor is calculated as follows:

$$f_{tp} = \left[4log\left(\frac{Re_{ns}}{4.5223\log(Re_{ns} - 3.8215)}\right)\right]^{-2} \times e^S \tag{1.48}$$

$$S = \frac{lnY}{-0.0523 + 3.182\ln(Y) - 0.8725(\ln(Y))^2 + 0.01853(\ln(Y))^4} \tag{1.49}$$

$$Y = \frac{\lambda}{H(\theta)} \tag{1.50}$$

In equation (1.50), $H(\theta)$ is the liquid holdup for any inclination angle of pipeline. For more details on this method, see [25].

b) Dukler and Taitel correlation

The Dukler and Taitel correlation [34] is given by:

$$\left(\frac{dP}{dL}\right) = \frac{f_{tp}\rho_m V_m^2}{2D} + \rho_m g \sin(\theta) \tag{1.51}$$

c) Drift-flux model

Similar to the homogeneous model, the drift-flux model treats the two-phase flow mixture as a whole, yet it does so with the relative motion of one phase with respect to the mixture. Drift-flux model considers the two-phase closely coupled by one mixture momentum equation. In the drift-flux model, the dominant relative motion of one phase to the other is caused by an external force such as gravity. The drift-flux model is considered an improvement over the homogeneous model and a simplification of the two-fluid model, which treats each phase separately. The drift-flux model was first developed by [35]. It is showed in [35] that, the void fraction can be predicted taking into consideration the non-uniformity in flows and the difference in velocity between the two phases. The mathematical expression of the drift-flux model of a gas and liquid flow in pipes is as follows:

The volumetric drift flux of the gas phase is given as:

$$J_g = \alpha(V_g - V_m) \tag{1.52}$$

Where J_g is the volumetric drift flux of the gas in m³/s-m² and α is the gas void fraction. Substituting the mixture velocity ($V_m = V_{SL} + V_{Sg}$) and the superficial phase velocities ($V_{SL} = \alpha V_g$) into equation (1.52) and simplifying gives.

$$J_g = \alpha\left(V_g - V_L\right) + \alpha^2(V_g - V_m) \tag{1.53}$$

Substituting the slip velocity ($V_S = V_g - V_L$) into equation (1.53) gives the following.

$$J_g = \alpha(1-\alpha)V_S \tag{1.54}$$

Alternatively, starting from equation (1.52) and using the actual velocity definition $V_g = \frac{V_{Sg}}{\alpha}$, equation (1.52) can be expressed in term of superficial gas and liquid velocities and gas void fraction as:

$$J_g = (1-\alpha)V_{Sg} - \alpha V_{SL} \tag{1.55}$$

Equating equation (1.54) and equation (1.55) yields:

$$\alpha(1-\alpha)V_S-(1-\alpha)V_{Sg}-\alpha V_{SL}=0 \tag{1.56}$$

Equation (1.56) gives the following implicit equation of gas void fraction, which can be solved for gas void fraction implicitly given a constant slip velocity. From this model, liquid holdup and thus pressure gradient can be calculated. Void fraction can also be calculated using correlations. When gas and liquid flow together in pipeline, due to the buoyancy effect, the gas phase velocity is different from the liquid phase. From [35] general law we have:

$$V_g = C_d V_m + V_d \tag{1.57}$$

Here, C_d is the profile parameter and V_d is the drift velocity. For a well-homogeneous model, $V_d = 0$ and $C_d = 1$. The void is defined as:

$$\alpha = \frac{V_{sg}}{C_d V_m + V_d} \tag{1.58}$$

The drift flux parameters C_d and V_d can be calculated using the correlation. In this study, the void fraction is approached using correlations of Woldesemayat and Ghajar (2007) as presented by [23].

- **Correlation developed by Woldesemayat and Ghajar (2007) [36].**

$$C_d = \frac{V_{sg}}{V_m}\left[1+\left(\frac{V_{sl}}{V_{sg}}\right)^{\left(\frac{\rho_g}{\rho_l}\right)^{0.1}}\right] \tag{1.59}$$

$$V_d = 2.9\left[\frac{g.ID.\sigma(1+\cos\theta)(\rho_l-\rho_g)}{\rho_l^2}\right]^{0.25}(1.22+1.22\sin\theta)^{\frac{P_{atm}}{P}} \tag{1.60}$$

$$\alpha = \frac{V_{sg}}{V_{sg}\left[1+\left(\frac{V_{sl}}{V_{sg}}\right)^{\left(\frac{\rho_g}{\rho_l}\right)^{0.1}}\right]+2.9\left[\frac{gd\sigma(1+cos\theta)(\rho_l-\rho_g)}{\rho_l^2}\right]^{0.25}(1.22+1.22\,sin\,\theta)^{\frac{P_{atm}}{P}}} \tag{1.61}$$

Homogeneous model can be applied with more or less reasonable prediction in several two-phase pipe flow production and transportation applications. The homogeneous model, because of its simplicity, works well only in a limited number of applications [22]. Its gives reasonable results if the density ratio of liquid and gas is less than 10 or if the total mass flux is greater than 2000 kg/m². s [22]. It is used as a reference case.

1.1.5.2 Separated flow models

In separated flow models, each phase is assumed to flow separately from one another. Most separated flow models assume different velocities for each phase unlike homogeneous flow models where both of the fluids are assumed to have the same velocity. In this type of flow, two-phase frictional pressure drop can be modeled based on the use of two-phase multiplier. In this work, the correlation presented by Wallis [37], Müller-Steinhagen [38] and Vierra and Garcia [39] were used to model the friction term in equation (1.43).

a) Wallis correlation (1969)

The two-phase multiplier is defined as the ratio of the frictional pressure gradient and the one considering that the total mass flow is flowing as liquid. The correlation proposed by Wallis (1969) [37] based on two-phase multiplier is given by:

$$\emptyset_{lo}{}^2 = \frac{\left(\frac{\partial P}{\partial L}\right)_f}{\left(\frac{\partial P}{\partial L}\right)_l} \tag{1.62}$$

$$\left(\frac{\partial P}{\partial L}\right)_l = \frac{f_l}{2\rho_l}\frac{G^2}{d} \tag{1.63}$$

$$\emptyset_{lo}{}^2 = \left(1 + x\left(\frac{\rho_l - \rho_g}{\rho_g}\right)\right)\left(1 + x\left(\frac{\mu_l - \mu_g}{\mu_g}\right)\right)^{-1/4} \tag{1.64}$$

where: subscripts 'l' and 'f' are used to indicate liquid only and frictional component of pressure, respectively. $\emptyset_{lo}$ is the two-phase multiplier, $\left(\frac{\partial P}{\partial L}\right)_f$ is the pressure gradient due to friction, $\left(\frac{\partial P}{\partial L}\right)_l$ is the pressure drop due to liquid flow only.

In equation (1.63), f_l is the friction factor of the liquid phase determined in this study by the Colebrook correlation given as:

$$\frac{1}{\sqrt{f_l}} = -2log\left[\frac{2\varepsilon}{3.7} - \frac{5.02}{Re_l}log\left(\frac{2\varepsilon}{3.7} + \frac{13}{Re_l}\right)\right] \tag{1.65}$$

$$Re_l = \frac{G.d}{\mu_L} \tag{1.66}$$

where, Re_l is the Reynolds number of the liquid phase, $G = \rho_g V_{Sg} + \rho_L V_{SL}$ is the total mass flux. x represents the vapor quality of the gas-liquid mixture and can be calculated as follow:

$$x = \frac{\dot{m}_g}{\dot{m}_g + \dot{m}_l} = \frac{Q_g\rho_g}{Q_g\rho_g + Q_l\rho_l} = \frac{Q_g\rho_g}{Q_g\rho_g + Q_o\rho_o + Q_w\rho_w}, \tag{1.67}$$

$\dot{m}_g$ and $\dot{m}_l$ are the gas and liquid mass flowrates.

Therefore, the Wallis model is described by equation (1.68) below:

$$\left(\frac{dP}{dL}\right) = \rho_m g \sin(\theta) + \emptyset_{lo}{}^2 \frac{f_l}{2\rho_l}\frac{G^2}{d} \tag{1.68}$$

b) Müller-Steinhagen and Hecck (1986)

This correlation was checked against other fourteen correlations using a data bank of 9300 measurements for a variety of fluids and flow conditions [38]. The proposed two-phase multiplier is:

$$\emptyset_{lo}{}^2 = \frac{G_c(1-x)^{1/3} + Bx^3}{B_1} \tag{1.69}$$

$$G_c = B_1 + 2(B - B_1)x \tag{1.70}$$

$$B_1 = \frac{f_l}{2\rho_l}\frac{G^2}{d} \tag{1.71}$$

$$B = \frac{f_g}{2\rho_g}\frac{G^2}{d} \tag{1.72}$$

Therefore, the Müller-Steinhagen model is obtained by replacing equations (1.69-172) into equation (1.68), hence:

$$\left(\frac{dP}{dL}\right) = \rho_m g \sin(\theta) + \emptyset_{lo}{}^2 \frac{f_l}{2\rho_l}\frac{G^2}{d} \tag{1.73}$$

c) Vierra and Garcia (2014)

As presented by [23], Vierra and Garcia (2014) [39] addressed the friction term in the two-phase multiplier approach by using a homogeneous two-phase flow model and considering the center of volume j and center of mass velocities. The two phase multiplier is given by:

$$\emptyset_{lo}{}^2 = \left(\frac{f}{f_l}\right)\left(\frac{\rho_L}{\rho}\right) \tag{1.74}$$

Using the correlation given by Swamee (1993) [40], the friction factor in equation (1.74) can be determined as follow:

$$f_l = \left(\left(\frac{64}{Re_l}\right)^8 + 9.5\left[\ln\left(\left(\frac{\varepsilon}{3.7} + \frac{5.74}{Re_l{}^9}\right) - \left(\frac{2500}{Re_l}\right)^6\right)\right]^{-16}\right)^{0.125} \tag{1.75}$$

For the liquid friction factor, f_l, the Reynolds number is calculated as:

$$Re_l = \frac{d.G}{\mu_L} \tag{1.76}$$

For the center of mass velocity approach,

$$Re_m = \frac{\rho_m V_m d}{\mu_m} \tag{1.77}$$

Therefore, the Vierra and Garcia model is obtained by replacing equations (1.74-1.77) into equation (1.68), hence:

$$\left(\frac{dP}{dL}\right) = \rho_m g \sin(\theta) + \emptyset_{lo}{}^2 \frac{f_l}{2\rho_l}\frac{G^2}{d} \tag{1.78}$$

Above, we have presented some of the pressure models generally used for single and multiphase flow in wellbores and pipelines. This work modified the pressure model presented by Dukler and Taitel, in which the liquid hold up was determined by the Drift-Flux model. In the following, we are presenting a brief review on heat transfer process during multiphase flow in subsea pipeline.

1.2 Review on heat transfer in subsea pipeline during multiphase fluid flow

In offshore area, pipelines carried hot petroleum fluids from the reservoir to the surface. The hot fluids will be losing heat as far as its travels along the pipeline because of the cooling surrounding. In this section, we will review the heat transfer mechanism during multiphase flow in subsea pipelines. This include conduction, convection and radiation. Heat transfer occurs whenever there exists a temperature difference in a medium or between media. Three mechanisms are responsible of the flow of heat in a medium: conduction, convection and radiation.

1.2.1 Conduction

Heat conduction, also called diffusion, is the term used to refer to the transport of heat from a high temperature to low temperature in a fix medium, which may be solid or a fluid, by the motion of molecules or electrons. This mechanism is governed by the Fourier's law of conduction expressed as follow, when considering the solid shown in figure 1.7 below.

$$Q = kA_p \frac{dT}{dx} \tag{1.116}$$

where Q is the rate of heat transfer per unit time, k is the thermal conductivity of the material, A_p is the area of the medium (pipe), T is the temperature distribution profile and $\frac{dT}{dx}$ is the temperature gradient. The negative sign in equation (1.116) indicates that heat is transferred in the direction of decreasing temperature.

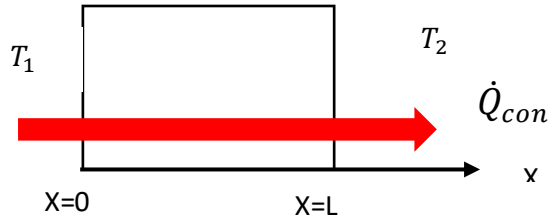

Figure 1.7: One dimensional heat transfer by conduction in a solid

1.2.2 Convection

Convection is a heat transfer mechanism, which is caused by the motion of fluid on a solid surface or inside a channel. Convection is called forced convection if the fluid is forced to flow over the surface by external means such as fan, pump, or the wind. In contrast, convection is called natural (or free) convection if the fluid motion caused by buoyancy forces that are induced by density differences due to the variation of temperature in the fluid (Figure 1.8).

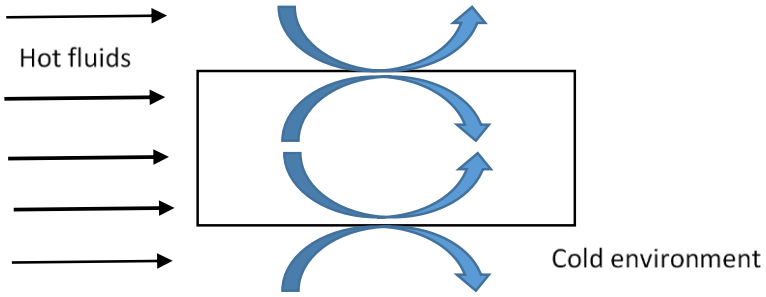

Figure 1.8: Schematic view of heat transfer by convection.

The rate of convection heat transfer between a bulk fluid at the temperature T_f and the surface of a channel at a temperature T_p, is expressed by Newton's law of cooling as:

$$\dot{Q}_{conv} = hA_p\left(T_f - T_p\right) \tag{1.117}$$

In equation (1.117) above, $\dot{Q}_{conv}$ is the rate of heat transfer per unit time, h is the convective heat transfer coefficient, A_p is the cross-sectional area of the medium (pipe), T_f is the temperature of the fluids and T_p is the temperature of the surface or the environment temperature.

1.2.3 Radiation

Every body with a temperature emits energy in the form of electromagnetic waves or photons, which is called radiation. The radiation energy does not require a medium for heat transfer. Most gases transmit nearly all incident radiation, but liquids rapidly attenuate radiation. Most solids, except for glasses and transparent plastics, are completely opaque to radiation. For subsea pipelines systems, because the fluids temperature is usually less than 200°C, this heat transfer mechanism is relatively insignificant compared with heat transfer from conduction and convection. The radiation energy per unit time from a blackbody is proportional to the fourth power of absolute temperature and can be described by Stefan-Boltzmann law as follow:

$$\dot{Q}_{Rad} = \sigma A_p T_p^4 \tag{1.118}$$

where $\sigma = 5{,}6703 \times 10^{-8}\ (w.m^{-2}.k^{-4})$ is the Stefan-Boltzmann constant. T_p is the temperature of the body and A_p is the area of the body.

Although these three heat transfer modes occur at all subsea systems, for typical pipelines, heat transfer from radiation is relatively insignificant compared with heat transfer from conduction and convection because the system temperature is below 200°C in generally. Therefore, conduction and convection will be solely considered here.

1.2.4 Heat transfer through pipelines

When fluid flows inside a pipe, the heat transfer process is a result of the convection inside the pipe, the conduction through the pipe and the convection outside the pipe. The Fourier's law in the radial coordinate gives the conduction heat transfer q . Whereas the Newton's law gives the convective heat transfer inside the pipe and outside the pipe.

1.2.4.1 Heat transfer through an exposed pipeline

Let us considered the figure (1.9) representing a horizontal pipeline without insulation, exposed to surrounding (seawater or soil). We analyzed the heat transfer through the pipe.

- For convection inside pipeline, the Newton's law is given as follow:

$$q = 2\pi r_1 \Delta L h_i (T_m - T_1) \tag{1.119}$$

where,

r_1 represent the inner radius of the pipeline,

ΔL is the pipeline segment,

h_i is the internal heat transfer coefficient,

T_m is the average temperature of the fluids,

T_1 the temperature of inner pipe wall.

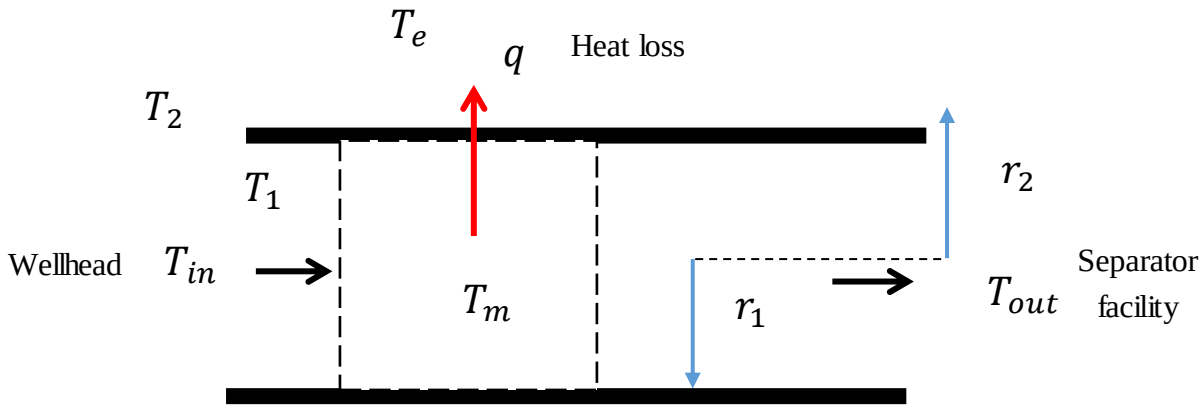

Figure 1.9: schematic of view of an exposed pipeline

- For conduction through the pipe, the Fourier's law is given by:

$$q = 2\pi\Delta L k_{pipe} \frac{(T_1 - T_2)}{ln\left(\frac{r_2}{r_1}\right)} \tag{1.120}$$

where: k_{pipe} is the pipe thermal conductivity. r_2 is the outer radius of the pipe and T_2 is the outer temperature of the pipe wall.

- For convection outside the pipe we have:

$$q = 2\pi r_2 \Delta L h_o (T_2 - T_e) \tag{1.121}$$

where: T_e is the surrounding seawater temperature; h_o is the outer convective coefficient of the seawater. Combining equations (1.119) through (1.121) yield,

$$(T_m - T_e) = \frac{q}{2\pi\Delta L}\left[\frac{1}{r_1 h_i} + \frac{log\left(\frac{r_2}{r_1}\right)}{k_{pipe}} + \frac{1}{r_2 h_o}\right] \tag{1.122}$$

1.2.4.2 Heat transfer through an exposed insulated pipeline with one layer

Let us considered figure 1.10, below representing a horizontal pipeline with one insulation layer. Heat transfer analysis gives:

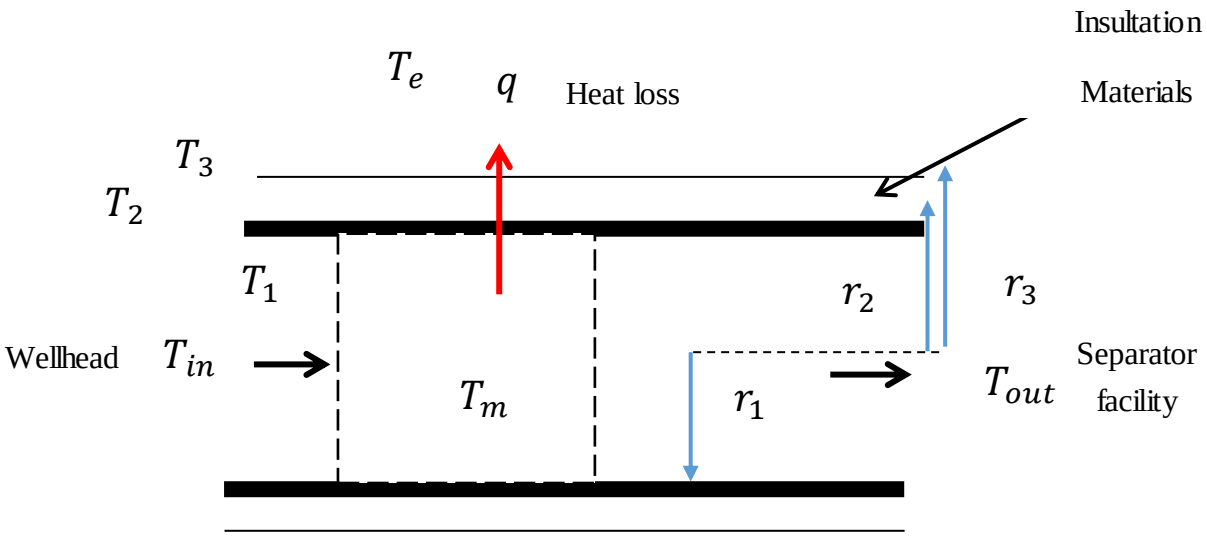

Figure 1.10: schematic view of pipeline with insulation layer exposed to seawater

- For conduction through the insulation material 1, Fourier`s law is given by:

$$q = 2\pi\Delta L k_{ins} \frac{(T_3 - T_2)}{ln\left(\frac{r_3}{r_2}\right)} \tag{1.123}$$

where, k_{ins} is the thermal conductivity of the insulation layer, T_3 is the temperature at the insulation layer and r_3 is the radius of the insulation.

The temperature difference between the internal film fluids and the surrounding is then given as:

$$(T_m - T_e) = \frac{q}{2\pi\Delta L}\left[\frac{1}{r_1 h_i} + \frac{log\left(\frac{r_2}{r_1}\right)}{k_{pipe}} + \frac{log\left(\frac{r_3}{r_2}\right)}{k_{ins}} + \frac{1}{r_3 h_o}\right] \tag{1.124}$$

1.2.4.3 Heat transfer through and exposed insulated pipeline with multilayer

More generally, from equation written above, the heat transfer from the internal film fluids to the surrounding can be given as, for a pipeline with multilayers of insulation materials,

$$q = \frac{(T_m - T_e)}{\left[\frac{r_o}{r_i h_i} + \sum_{j=1}^{n}\left(\frac{r_o log\left(\frac{r_{j+1}}{r_j}\right)}{k_j}\right) + \frac{1}{h_o}\right]} \tag{1.125}$$

where: r_o and r_i are respectively the outer and the inner radii of the pipe, h_o and h_i are outer and inner heat transfer coefficients. k_j is the conductivity of layer j and r_j is the radius of wall layer j. n is the number of wall layers.

1.2.5 Heat transfer coefficient

From the equation above, in order to determine the heat transfer to surrounding or the temperature difference between the fluids and the surrounding, is important to know the internal and outer heat transfer coefficient, hence the overall heat coefficient.

1.2.5.1 Internal convective coefficient

The internal heat transfer coefficient of two-phase flows is strongly dependent on the flow pattern and on the liquid film thickness of the circumference of the tube. According to the correlation developed by Ghajar and Tang (2005) [41] as presented by Stephane and Josua (2011) [42], we have:

- For turbulent flow:

$$h_i = h_{Li}F_p\left[1 + 0.7\left(\frac{x}{1-x}\right)^{0.08}\left(\frac{F_p}{1-F_p}\right)^{0.06}\left(\frac{P_{rg}}{P_{rL}}\right)^{0.03}\left(\frac{\mu_L}{\mu_g}\right)^{0.14}(I)^{0.65}\right] \quad (1.126)$$

where,

P_{rg} and P_{rg} are the liquid and gas Prandtl number.

I is the inclination factor that take into account the effect of the gravity on the heat transfer coefficient given by:

$$I = 1 + \frac{gd(\rho_l - \rho_g)\sin\theta}{\rho_l V_{SL}^2} \quad (1.127)$$

the pipe factor is given by:

$$F_p = \alpha + (1-\alpha)F_s \quad (1.128)$$

The shape factor F_s, is defined as:

$$F_s = \frac{2}{\pi}\tan^{-1}\left(\sqrt{\frac{\rho_g(V_g - V_L)^2}{gd(\rho_L - \rho_g)\cos\theta}}\right) \quad (1.129)$$

V_g and V_L are liquid and gas velocities respectively. α is the void fraction. θ is the inclination angle. The heat transfer coefficient h_{Li} can be calculated using various correlations. For fully turbulent flow, the correlation of Dittus and Boelter (1930) [36] can be used. Hence,

$$Nu_o = 0.027 \, . R_{eo}^{0.8} P_{ro}^{0.3} \quad (1.130)$$

$$Nu_i = h_{Li} d / k_f \quad (1.131)$$

$$P_{rL} = \frac{Cp_l \mu_L}{k_L} \quad (1.131)$$

$$k_L = \alpha_o k_o + \alpha_w k_w \quad (1.132)$$

where: μ_L is the liquid viscosity at the bulk temperature; Cp_l is the heat capacity of the liquid at bulk temperature. k_l is the thermal conductivity of the liquid at bulk temperature and wall temperature. R_{e_L} is the Reynolds liquid number.

- If the fluid is in a transitional region $2100 < R_{eL} < 5 \times 10^4$ the correlation of Gnielinski (1976) [43] can be used as follow:

$$h_{Li} = \frac{(f_L/8) R_{el} P_{rL}}{1+12.7\sqrt{(f_L/8)}\left(P_{rL}^{2/3}-1\right)} \left[1 + \left(\frac{d_i}{L}\right)^{2/3}\right] \left(\frac{P_{rm}}{P_{rw}}\right)^n \left(\frac{k_L}{d_i}\right) \quad (1.133)$$

Here, the Moody diagram can be used to obtain the friction factor, f_l.

$$f_L = [0{,}79 \ln(R_{e_l}) - 1{,}64]^{-2} \quad (1.134)$$

Equation (1.133) is valid for $0.5 < P_{rL} < 2000$ and $3 \times 10^3 < R_{eL} < 5 \times 10^6$.

- For laminar flow

$$Nu_i = 3.66. \quad (1.135)$$

1.2.5.2 External convective coefficient

Here, the surrounding pipeline can be exposed to the seawater, can be buried or partially buried under the subsea soil. For pipeline exposed to seawater, the external heat transfer coefficient can be calculated using the correlation presented in equation (1.130) for given seawater properties.

1.2.5.3 Heat transfer coefficient of soil for buried pipeline

From [44] and using figure.1.11, the heat transfer coefficient for a buried pipeline can be expressed as:

$$h_{soil} = \frac{k_{soil}}{\left(\frac{D}{2}\right)\cosh^{-1}\left(\frac{2Z}{D}\right)} \quad (1.137)$$

where, h_{soil} is the heat transfer coefficient of soil, k_{soil} is the thermal conductivity of soil, D is the outside diameter of buried pipe and Z is the distance between top of soil and centre of pipe.

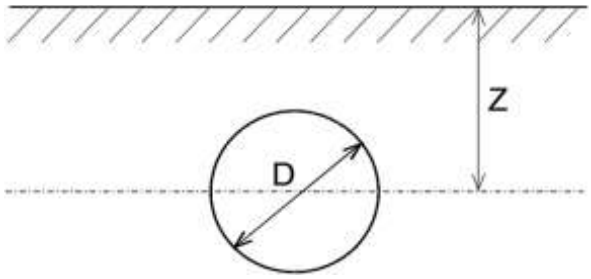

Figure 1.11: cross section of a buried pipeline [44].

For the case of Z> D/2,

$$\cosh^{-1}\left(\frac{2Z}{D}\right) = \ln[\left(\frac{2Z}{D}\right) + \left(\left(\frac{2Z}{D}\right)^2 - 1\right)^{0.5}] \quad (1.138)$$

$$h_{soil} = \frac{k_{soil}}{\mathrm{D}\ \ln\left[\frac{2Z+\sqrt{4Z^2-D^2}}{D}\right]} \quad (1.139)$$

1.2.5.4 Heat transfer coefficient for partially buried pipeline

The increase in the insulation effect for a partially buried pipeline is not large compared with a fully buried pipeline. Heat flow circumferentially through the steel to the section of exposure. Even exposure of just the crown of the pipeline results in efficient heat transfer to the surroundings due to the high thermal conductivity of the steel pipe. A trenched pipeline (partially buried pipeline) experiences less heat loss than an exposed pipeline but more than a buried pipeline [44]. Engineering judgment must be used for the analysis of trenched pipelines. The heat transfer may be calculated using a weighted average of the fully buried pipe and exposed pipe as follows:

$$h_{pb} = (1 - f_p)h_{o,buried} + f_p h_{o,exposed} \quad (1.140)$$

where, f_p is the fraction of outside surface of pipe exposed to the surrounding fluid.

1.2.6 Overall heat transfer coefficient

In the modeling of heat transfer, the overall heat transfer is an important parameter that has to be calculated accurately. Below, we present details on the calculation of this parameter is various cases.

1.2.6.1 Overall heat transfer coefficient for exposed pipeline with and without insulation

For an exposed pipeline, with or without insulation layer (s), the overall heat transfer coefficient is determined as follow:

$$U_o = \frac{1}{\left[\frac{r_o}{r_i h_i} + \sum_{j=1}^{n}\left(\frac{r_o log\left(\frac{r_{j+1}}{r_j}\right)}{k_j}\right) + \frac{1}{h_o}\right]} \quad (1.141)$$

1.2.6.2 Overall heat transfer coefficient for buried pipeline with and without insulation

For a buried pipeline, with or without insulation layer (s), the overall heat transfer coefficient is determined as follow:

$$U_o = \frac{1}{\left[\frac{r_o}{r_i h_i} + \sum_{j=1}^{n}\left(\frac{r_o log\left(\frac{r_{j+1}}{r_j}\right)}{k_j}\right) + \frac{1}{h_{soil}}\right]} \quad (1.142)$$

1.2.6.3 Overall heat transfer coefficient for partially buried pipeline with and without insulation

For a partially buried pipeline, with or without insulation layer (s), the overall heat transfer coefficient is determined as follow:

$$U_o = \frac{1}{\left[\frac{r_o}{r_i h_i} + \sum_{j=1}^{n}\left(\frac{r_o log\left(\frac{r_{j+1}}{r_j}\right)}{k_j}\right) + \frac{1}{h_{pb}}\right]} \quad (1.143)$$

Heat transfer characteristics such as the over all heat transferred coefficient and the convective heat transferred have been review for uninsulated and insulated pipeline, as well as for partial and fully buried pipeline. In the following, we will be presenting a review on different tool that are usually used to run numerical simulation of the temperature and pressure profile.

1.3 Machine learning techniques and genetic algorithm revue [45]

Machine Learning (ML) is a subset of Artificial Intelligence (AI), but the two are not entirely the same. While AI is the umbrella concept that deals with the creation of intelligent machines that can simulate human thinking capability and behavior, machine learning is an application that allows machines to learn

from data without being programmed explicitly. In fact, machine learning, as a sub-field and a concept that branched out of AI, started to flourish in the 1990s. The focus of this field gradually shifted from only achieving artificial intelligence to tackling solvable problems of a practical nature. The goal of machine learning is to generalize a detectable pattern or to create an unknown rule from given examples. Over a period and with more data, model predictions will become better. As organizations become more data-driven, machine learning is rapidly gaining prominence across multiple sectors. Industries that have widely adopted this advanced technology include:

- Retail

Retail sites that offer buying recommendations based on your previous purchases use machine learning technologies to analyze your shopping patterns. Today, leading retailers rely heavily on ML to capture and analyze buyer data to gain customer insights, optimize pricing, launch marketing campaigns, and to deliver a personalized shopping experience.

- Energy

Oil and gas companies deploy machine learning to analyze subsurface energy sources, predict refinery failures, and streamline distribution systems to maximize profits.

The scope of implementing machine learning in the energy sector is vast and expanding.

- Financial Services

The application of machine learning in the financial sector is diverse. Banks and financial institutions not only implement machine learning technologies to help customers and investors in several ways, but they also use ML for detecting high-risk profiles, cyber surveillance, and fraud prevention

- Healthcare

Thanks to advancements in sensor technologies and medical wearable devices, machine learning is increasingly becoming an integral part of the modern-day healthcare ecosystem. The breakthrough technology helps healthcare professionals analyze data to determine trends in real-time, which leads to better diagnosis and improved treatment.

- Transportation and Logistics

Data analysis, trend detection, and the modeling aspect of ML are crucial tools for transport organizations and delivery companies. The transportation and logistics industry uses machine learning to make more efficient routes and predict potential problems, translating into increased profitability.

- Government

Government agencies have various data sources. From utilities to public safety, government agencies are mining Big Data to gain actionable insights for improving efficiency, lowering risks, and increasing savings. Many agencies are also adopting machine learning to detect fraud and curb identity theft.

Machine Learning is great for [45]:

- Problems for which existing solutions require a lot of hand-tuning or long lists of rules: one Machine Learning algorithm can often simplify code and perform better.
- Complex problems for which there is no good solution at all using a traditional approach: the best Machine Learning techniques can find a solution.
- Fluctuating environments: a Machine Learning system can adapt to new data.
- Getting insights about complex problems and large amounts of data.

1.3.1 Classification of machine learning [45]

Machine learning is broadly classified into three categories but nonetheless, based on the situation, these categories can be combined to achieve the desired results for particular applications.

1.3.1.1 Supervised learning

This is teaching machines to learn the relationship between other variables and a target variable. In supervised learning, the training data you feed to the algorithm includes the desired solutions, called labels.

1.3.1.2 Unsupervised learning

In unsupervised learning, algorithms learn by themselves without any supervision or without any target variable provided. It is a question of finding hidden patterns and relations in the given data. The categories in unsupervised learning are as follows: Dimensionality reduction and Clustering.

1.3.1.3 Reinforcement learning

This allows the machine or agent to learn its behavior based on feedback from the environment. In reinforcement learning, the agent takes a series of decisive actions without supervision and, in the end, a reward will be given, either +1 or -1. Based on the final payoff/reward, the agent reevaluates its paths. Reinforcement learning problems are closer to the artificial intelligence methodology rather than frequently used machine learning algorithms.

In some cases, we initially perform unsupervised learning to reduce the dimensions followed by supervised learning when the number of variables is very high. Similarly, in some artificial intelligence applications, supervised learning combined with reinforcement learning could be utilized for solving a

problem; an example is self-driving cars in which, initially, images are converted to some numeric format using supervised learning and combined with driving actions (left, forward, right, and backward).

1.3.2 Overview of machine learning algorithms

Machine learning models are classified mainly into supervised, unsupervised and reinforcement learning methods.

1.3.2.1 supervised learning

Some of the most important supervised learning algorithms are:

- Logistic regression

Logistic regression is the appropriate regression analyses to conduct when the dependent variable is dichotomous (binary). Outcomes are discrete classes rather than continuous values in this problem. In statistical methodology, it uses the maximum likelihood method to calculate the parameter of individual variables. In contrast, in machine learning methodology, log loss will be minimized with respect to the weights. Logistic regression has a high bias and a low variance error.

- Lasso and ridge regression

This uses regularization to control overfitting issues by applying a penalty on coefficients. In ridge regression, a penalty is applied on the sum of squares of coefficients, whereas in lasso, a penalty is applied on the absolute values of the coefficients. The penalty can be tuned in order to change the dynamics of the model fit. Ridge regression tries to minimize the magnitude of coefficients, whereas lasso tries to eliminate them.

- Linear regression

This is used for the prediction of continuous variables. It utilizes error minimization to fit the best possible line in statistical methodology. However, in machine learning methodology, squared loss will be minimized with respect to the weights. Linear regression also has a high bias and a low variance error.

- Decision trees (classification trees)

Recursive binary splitting is applied to split the classes at each level to classify observations to their purest class. The classification error rate is simply the fraction of the training observations in that region that do not belong to the most common class. Decision trees have an overfitting problem due to their high variance in a way to fit; pruning is applied to reduce the overfitting problem by growing the tree completely. Decision trees have low a bias and a high variance error.

- Bagging classifier

This is an ensemble technique applied on decision trees in order to minimize the variance error and at the same time not increase the error component due to bias. In bagging, various samples are selected with a subsample of observations and all variables (columns), subsequently fit individual decision trees independently on each sample and later ensemble the results by taking the maximum vote (in regression cases, the mean of outcomes calculated).

- Random forest classifier

This is similar to bagging except for one difference. In bagging, all the variables/columns are selected for each sample, whereas in random forest a few subcolumns are selected. The reason behind the selection of a few variables rather than all was that during each independent tree sampled, significant variables always came first in the top layer of splitting. Which makes all the trees look more or less similar and defies the sole purpose of ensemble: that it works better on diversified and independent individual models rather than correlated individual models. Random forest has both low bias and variance errors.

- Boosting classifier

This is a sequential algorithm that applies on weak classifiers such as a decision stump (a one-level decision tree or a tree with one root node and two terminal nodes) to create a strong classifier by ensembling the results. The algorithm starts with equal weights assigned to all the observations, followed by subsequent iterations where more focus was given to misclassified observations by increasing the weight of misclassified observations and decreasing the weight of properly classified observations. Boosting might have an overfitting problem, but by carefully tuning the parameters, we can obtain the best of the self machine learning model.

- K-Nearest Neighbors (KNN)

The k-Nearest Neighbor algorithm is based on comparing an unknown Example with the k training Examples which are the nearest neighbors of the unknown Example. The first step of the application of the k-Nearest Neighbor algorithm on a new Example is to find the k closest training Examples. "Closeness" is defined in terms of a distance in the n-dimensional space, defined by the n Attributes in the training Example Set. Different metrics, such as the Euclidean distance, can be used to calculate the distance between the unknown Example and the training Examples. Due to the fact that distances often depends on absolute values, it is recommended to normalize data before training and applying the k-Nearest Neighbor algorithm. The metric used and its exact configuration are defined by the parameters of the Operator. In the second step, the k-Nearest Neighbor algorithm classify the unknown Example by a majority vote of the found neighbors. In case of a regression, the predicted value is the average of the values of the found neighbors.

It can be useful to weight the contributions of the neighbors, so that the nearer neighbors contribute more to the average than the more distant ones.

- Support Vector Machines (SVM) classifier

This maximizes the margin between classes by fitting the widest possible hyperplane between them. In the case of non-linearly separable classes, it uses kernels to move observations into higher-dimensional space and then separates them linearly with the hyperplane there.

1.3.2.2 unsupervised learning

In unsupervised learning, the training data is unlabeled. The system tries to learn without a teacher.

Unsupervised learning does not have as many algorithms as in supervised learning.

Some of the most important unsupervised learning algorithms are:

- Principal component analysis (PCA)

Principal components are calculated in place of the original variable in this dimensionality reduction technique. Principal components are determined where the variance in data is maximum; subsequently, the top n components will be taken by covering about 80 percent of variance and will be used in further modeling processes, or exploratory analysis will be performed as unsupervised learning.

- K-means clustering

This is an unsupervised algorithm that is mainly utilized for segmentation exercise. K-means clustering classifies the given data into k clusters in such a way that, within the cluster, variation is minimal and across the cluster, variation is maximal.

1.3.2.3 reinforcement learning

Reinforcement Learning is a very different beast. The learning system, called an agent in this context, can observe the environment, select and perform actions, and get rewards in return. It must then learn by itself what is the best strategy, called a policy, to get the most reward over time. A policy defines what action the agent should choose when it is in a given situation. This is the scenario in which multiple decisions need to be taken by an agent prior to reaching the target and it provides a reward, either +1 or -1, rather than notifying how well or how badly the agent performed across the path:

- Markov decision process

In reinforcement learning, MDP is a mathematical framework for modeling decision-making of an agent in situations or environments where outcomes are partly random and partly under control. In this model,

environment is modeled as a set of states and actions that can be performed by an agent to control the system's state. The objective is to control the system in such a way that the agent's total payoff is maximized

- Monte Carlo methods

Monte Carlo methods do not require complete knowledge of the environment, in contrast with MDP. Monte Carlo methods require only experience, which is obtained by sample sequences of states, actions, and rewards from actual or simulated interaction with the environment. Monte Carlo methods explore the space until the final outcome of a chosen sample sequences and update estimates accordingly.

- Temporal difference learning

This is a core theme in reinforcement learning. Temporal difference is a combination of both Monte Carlo and dynamic programming ideas. Similar to Monte Carlo, temporal difference methods can learn directly from raw experience without a model of the environment's dynamics. Like dynamic programming, temporal difference methods update estimates based in part on other learned estimates, without waiting for a final outcome. Temporal difference is the best of both worlds and is most commonly used in games.

1.3.3 Steps in machine learning model development and deployment

The development and deployment of machine learning models involves a series of steps that are almost similar to the statistical modeling process, in order to develop, validate, and implement machine learning models. The steps are as follows:

- **Collection of data**: Data for machine learning is collected directly from 1. structured source data, web scrapping, API, chat interaction, and so on, as machine learning can work on both structured and unstructured data (voice, image, and text).
- **Data preparation and missing/outlier treatment**: Data is to be formatted as per the chosen machine learning algorithm; also, missing value treatment needs to be performed by replacing missing and outlier values with the mean/median, and so on.
- **Data analysis and feature engineering**: Data needs to be analyzed in order to find any hidden patterns and relations between variables, and so on. Correct feature engineering with appropriate business knowledge will solve 70 percent of the problems. Also, in practice, 70 percent of the data scientist's time is spent on feature engineering tasks.
- **Train algorithm on training and validation data**: Post feature engineering, data will be divided into three chunks (train, validation, and test data) rather than two (train and test) in statistical

modeling. Machine learning are applied on training data and the hyperparameters of the model are tuned based on validation data to avoid overfitting.

- **Test the algorithm on test data**: Once the model has shown a good enough performance on train and validation data, its performance will be checked against unseen test data. If the performance is still good enough, we can proceed to the next and final step.
- **Deploy the algorithm**: Trained machine learning algorithms will be deployed on live
- **Streaming** data to classify the outcomes.

1.4 Genetic algorithm in Matlab [46]

The genetic algorithm is a method for solving optimization problems that is based on natural selection, the process that drives biological evolution. The genetic algorithm repeatedly modifies a population of individual solutions. At each step, the genetic algorithm selects individuals at random from the current population to be parents and uses them produce the children for the next generation. Over successive generations, the population "evolves" toward an optimal solution. You can apply the genetic algorithm to solve a variety of optimization problems that are not well suited for standard optimization algorithms, including problems in which the objective function is discontinuous, non-differentiable, stochastic, or highly nonlinear [46]. The genetic algorithm uses three main types of rules at each step to create the next generation from the current population [46]:

- Selection rules select the individuals, called parents that contribute to the population at the next generation.
- Crossover rules combine two parents to form children for the next generation.
- Mutation rules apply random changes to individual parents to form children.

The genetic algorithm differs from a standard optimization algorithm in two main ways, as summarized in the following [46]:

- **Standard Algorithm**
  - Generates a single point at each iteration. The sequence of points approaches an optimal solution.
  - Selects the next point in the sequence by a deterministic computation.
- **Genetic Algorithm**

- Generates a population of points at each iteration. The population approaches an optimal solution.
- Selects the next population by computations that involve random choices.

In this work, we proposed that GA be used to solve heat transfer problems of insulation material selection. The goal of the proposal is to estimate the optimal parameters using a GA. The GAs are approaches, which try to find the optimal solution and are based on evolutionary methodologies as state above. The process flow of a GA can be described as follow:

- As a first step, the initial population is generated, and the fitness for this population is calculated. The fitness is checked to determine whether it meets the stopping criterion. If the stopping criterion is not met, the selection algorithm is run to find the best solutions. The most commonly used selection algorithms are tournament, roulette wheel, proportionate, rank, and steady-state selection.
- The next step is to create new children according to the selected parents. At this stage, a crossover is made. Crossover is a matter of replacing some of the genes in one parent with the corresponding genes of the other.
- After the crossover phase, a mutation is made. Mutations consist of flipping the bit at a randomly chosen locus.
- After this process, the fitness of the generated children is calculated, and the best is selected. The error criterion is checked again, and this process is repeated until the desired point is reached. Genetic algorithms have a target based on the fitness function. Constraints and design variables are used while the target is found. Constraints are variables that include formulas and ranges and only affect the target function. Design variables are found in a certain range of values, and they are explored by the GA. They are effective on the constraints and target function. The target is the fitness value for which the maximum, minimum, and target values are to be determined.

1.5 Software

There exist many software for numerical simulations of thermal flow phenomena and machine learning predictions. Below, we are presenting the used in this study. In oil and gas industry, successful production system design and operations requires a detailed understanding of multiphase flow behavior. Flow modeling and simulation provides valuable insight into flow behavior, including the physics describing flow through the entire production systems, from reservoir pore to process facility. Simulators and numerical codes are often used for prediction, optimization, evaluation and support to decision maker.

The multiphase flow simulation now than ever has become a powerful engineering tool to conduct virtual experiments, to minimize cost of production system design and physical testing, and to assist development of new technologies particularly in the oil and gas industry. The major challenge of a petroleum engineer is to design wells and pipelines to ensure that produced fluids will be safely and economically transported to downstream processing facilities. One of the solution is to run multiphase flow simulation. The foundation for accurate modeling of these piping systems relies on three core areas of science: Multiphase flow; Heat transfer and Fluid behavior. Pipesim and Matlab among others software have been used in this study to model and simulate thermal multiphase flow in offshore pipelines. Rapidminer software was also used to design patterns in order to predict the temperature profile and combining this machine learning model to genetic algorithm, optimum insulation thickness was determined.

1.5.1 MATLAB software [47]

MATLAB (Matrix laboratory) is a software that enable to not only to work with built-in function, but also, to implement numerical algorithm from mathematical model (further detailed can be obtained by reading the MATLAB tutorial downloadable easily at www.mathwork.com). In this work, MATLAB software was used to implement thermal multiphase of oil and gas in long subsea pipeline.

1.5.2 PIPESIM software [48]

The PIPESIM simulator offers the most advanced steady state modeling capabilities in the industry to address these critical aspects:

- Multiphase flow modeling
- Heat transfer
- Fluid property modeling

The PIPESIM simulator together with OLGA simulator, offer the most rigorous modeling solution for multiphase flow systems.

1.5.3 Machine learning software: RAPIDMINER [49]

Machine learning techniques can skip all the physical theories and models to extract direct patterns between data, thereby providing computers with the ability to learn without being explicitly programmed. In this study, machine learning techniques were employed to establish a pattern between the minimum temperature and thickness of insulating materials. The goal in machine learning was to find an appropriate function to depict the pattern between minimum temperature and the insulation thickness. RAPIDMINER software provides an integrated and comprehensive environment for carrying out several task like data preparation, machine learning, deep learning, text mining as well as predictive analytics. It is popular for

its lightning-fast speed to drive revenue, reduce costs and avoid risk. One of its most essential features is its graphical unit interface-based drag and drop feature that allows the users to intuitively build data processing workflows that can be selected from over 2000 available nodes. Apart from building machine learning models, one can also optimize the model performance through bagging boosting and building the model ensembles.

Conclusion

In this chapter, we have carried out a brief literature review on single and multiphase flow in pipeline. Next, we presented an overview of some pressure gradient models existing in the literature. further, we presented an overview on heat transfer process and characteristic during multiphase flow in subsea pipeline. finally, machine learning models and genetic algorithm as well as some simulation tools such as PIPESIM, MATLAB and RAPIDMINER were presented. In the following chapter, we will be presenting the methods and materials used in order to achieve our objectives.

CHAPTER 2: METHODOLOGY FOR THERMAL MODEL DEVELOPMENT: INSULATION DESIGN

Introduction

In order to avoid precipitation and solid deposits, thermal insulation is applied to subsea pipelines to maintain the temperature of crude oil above a critical level, such as the wax appearance temperature (WAT), hydrate formation or even scales and asphaltenes. The position within the entire system where the lowest temperature is observed is a risk point. For insulation design, the insulation requirement for pipeline and flowline segments is to keep the temperature at the risk point higher than the critical level. In fact, various combinations of insulation thickness can lead to the same lowest temperature. Theoretically, for a certain subsea production system, there exists one insulation design that meets the insulation requirement with the lowest insulation volume [50]. Therefore, the optimizing approach adopted in this study is the same as that presented in [50]. The best minimum of insulation thickness that will guarantee a minimum material consumption will be found. Thus, the insulation volume is set as the objective function and the insulation requirement as the constraint. This work developed a low thermal model for temperature and pressure predictions and its determined optimum insulation thickness using three approaches: the numerical simulation, application of genetic algorithm to machine learning, based on MATLAB software and RAPIDMINER software. In order to achieve this goal, we applied the following methodology.

2.1 Pipeline geometry

The subsea pipeline geometry considered in this study is the same as that presented in [4] for the example 1 case. Figure 2.1 below represent a vertical section of the considered offshore pipeline. The figure was represented with MATLAB software based on data from the schematic in [4].

2.2 Fluid properties characterization

In this work, the black oil model was used to characterized the oil and gas thermophysical properties. The black oil model assumed that there are at most three distinct phases: oil, gas and water. Water and oil are assumed to be immiscible and they do not exchange mass or change phase. Gas is assumed to be soluble in oil but not in water. All black oil model variables are given in S.I units unless precise.

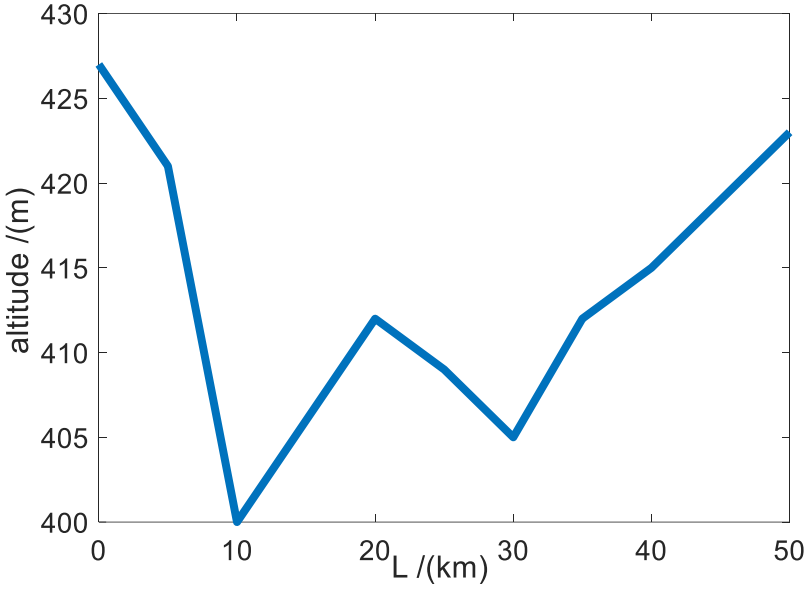

Figure 2.1: Vertical sectional profile of the pipeline [4]

2.2.1 Bubble point pressure P_b

The bubble point pressure can be determined by [51]:

$$P_b = 1.255\left[\left(\frac{GOR}{0.0059\gamma_g 10^{2.14/\gamma_o} 10^{-0.00198T}}\right)^{0.83} - 1.76\right] \quad (2.1)$$

with T is in $°k$, P_b in *Bar*.

2.2.2 Gas oil solution R_S

Standing in 1951 [51], proposed a correlation for the calculation of the gas-oil solution.

$$R_S = 0.00590\gamma_g 10^{2.14/\gamma_o} 10^{-0.00198T}(0.797.10^{-5}P + 1.4)^{1.205} \quad (2.2)$$

For pressures greater than bubble point pressure, $R_S = GOR$.

with T in $°k$ and P in Pa, R_S *in* Sm^3/Sm^3.

2.2.3 Oil formation volume factor B_o

B_o is defined as the ratio between the oil volume at flow conditions and the oil volume at standard conditions.

$$B_o = \frac{V_o(P,T)}{V_{o\_sc}} = \frac{Q_o(P,T)}{Q_{o\_sc}} = \frac{V_{so}}{V_{so\_sc}} \quad (2.3)$$

Oil formation volume factors at or less than bubble point pressures can be estimated by using the correlation obtained by Standing (1951) [51].

$$B_o = 0.9759 + 0.952.10^{-3}\left(R_S\left(\frac{\gamma_g}{\gamma_{OSC}}\right)^{0,5} + 0.401T - 103\right)^{1.2} \quad (2.4)$$

For pressures greater than bubble point pressure, oil formation volume factor is calculated as in [51] by:

$$B_o = B_{ob}exp[-C_o(P - 10^5 P_b)] \quad (2.5)$$

The coefficient of oil isothermal compressibility is calculated by [29] using the correlation below:

$$C_o = 10^{-9}\frac{2.81Rs + 3.10T + \frac{171}{\gamma_o} - 118\gamma_g - 1102}{P} \quad (2.6)$$

With, T in °k, P in *Bar*, B_o in m^3/m^3 and C_o in Bar^{-1}.

2.2.4 Oil viscosity μ_o

The oil viscosity is determined for three thermodynamic pressure levels

- For $P = P_{atm}$ The dead oil viscosity is calculated using the equation by Beal (1946) [27] as presented by [23]:

$$\mu_{od} = C_4\left(0.32 + \frac{1.8\times10^7}{API^{4.53}}\right)\left(\frac{360}{C_3 + 200}\right)^{10^{\left(0.43 + \frac{8.33}{API}\right)}} \quad (2.7)$$

- For $P_{atm} < P \leq P_b$ The live oil viscosity is calculated using Beggs and Robinson (1975) [28] formulation

$$\mu_o = 10.715C_4(C_1Rs + 100)^{-0.515}\left(\frac{\mu_{od}}{C_4}\right)^{\left(5.44(C_1Rs + 150)^{-0.338}\right)} \quad (2.8)$$

- For $P > P_b$, The relation from Vasquez and Beggs (1980) [29] is used

$$\mu_o = \mu_{ob}\left(\frac{P}{P_b}\right)^m \tag{2.9}$$

where,

$$m = 2.6(C_2P)^{1.187} \times e^{-11.513-8.9810^{-5}C_2P} \tag{2.10}$$

μ_{ob} is the viscosity at the bubble-point pressure obtained using and setting $R_s = GOR$.

$\mu_o$is given in $Pa.s$.

2.2.4.1 Oil specific gravity and oil density γ_o, ρ_o

In petroleum industry, the oil specific gravity and oil density are given by:

$$\gamma_o = \frac{141.5}{API+131.5} \tag{2.11}$$

$$\rho_{o\_sc} = \gamma_o \rho_{w\_sc} \tag{2.12}$$

$$\rho_o = \frac{\rho_{o\_sc}+\rho_{g\_sc}R_s}{B_o} \tag{2.13}$$

where,

ρ_{o_sc}, ρ_{w_sc} and ρ_{g_sc} are standard densities of oil, water and gas respectively. $\gamma_o$is the specific density of oil. $\rho_o$is the local density of oil at flow conditions.

2.2.5 Gas compressibility factor Z

Correlation presented by [23] approximating the abacus data in Standing and Katz (1942) [30] is given by:

$$Z = 1 - \frac{3.52}{10^{0.9813T_{pr}}} + \frac{0.274P_{pr}^2}{10^{0.8157T_{pr}}} \tag{2.14}$$

$$T_{pr} = \frac{T}{T_{pc}} \tag{2.15}$$

$$P_{pr} = \frac{P}{P_{pc}} \tag{2.16}$$

where, the pseudocritical properties were calculated using the Standing (1951) [51] correlation

$$T_{pc} = \frac{1}{C_5}\left(168 + 325\gamma_g - 12.5\gamma_g^2\right) \tag{2.17}$$

$$P_{pc} = \frac{1}{C_2}\left(677 + 15.0\gamma_g - 37.5\gamma_g^2\right) \tag{2.18}$$

2.2.6 Gas formation volume factor B_g

B_g is defined by the ratio of the free gas volume in flow condition to the volume at standard condition of the same mass of gas.

$$B_g = \frac{V_g(P,T)}{V_{g\_sc}} = \frac{\rho_{g\_sc}}{\rho_g} \tag{2.19}$$

$$B_g = \frac{P_{sc}}{T_{sc}}\frac{ZT}{P} \tag{2.20}$$

where, P_{sc} and T_{sc} are pressure and temperature at standard condition. T and P are temperature and pressure at flow conditions respectively.

2.2.7 Gas density ρ_g

$$\rho_g = 0.009225\frac{\gamma_g P}{ZT} \tag{2.21}$$

where T is in °k, P in Pa.

2.2.8 Gas viscosity μ_g

For the gas viscosity calculation, we used the Lee et al (1966) [31].

$$\mu_g = C_4 F_1 exp(F_2\left(C_4\rho_g\right)^{F_3}) \tag{2.22}$$

$$F_1 = \frac{\left(9.379+16.07M_g\right)(C_5T)^{1.5}}{209.2+19260M_g+C_5T} \tag{2.23}$$

$$F_2 = 3.448 + \frac{986.4}{C_5T} + 10.09M_g \tag{2.24}$$

$$F_3 = 2.447 - 0.2224F_2 \tag{2.25}$$

where T is in °k

2.2.9 Water formation volume factor B_W

B_W is defined as the ratio between the water volume at flow conditions and the water volume at standard conditions.

$$B_w = \frac{V_w(P,T)}{V_{w\_sc}} = \frac{Q_w(P,T)}{Q_{w\_sc}} \tag{2.26}$$

It can be calculated using the McCain correlation [52].

$$B_W = (1 + \Delta V_{wT})(1 + \Delta V_{wP}) \tag{2.27}$$

where ΔV_{wT} and ΔV_{wP} are respectively the volume corrections for temperature and pressure, obtained by:

$$\Delta V_{wT} = -1.00010(10^{-2}) + 1.33391(10^{-4})C_3 + 5.50654(10^{-7}){C_3}^2 \tag{2.28}$$

$$\Delta V_{wP} = -1.95301(10^{-9})C_2C_3P - 1.72834(10^{-13}){C_2}^2C_3P^2 - 3.58922(10^{-7})C_2P - 2.25341(10^{-10}){C_2}^2P^2 \tag{2.29}$$

T is given in °k and P in Pa.

2.2.10 Water density

The water density at local flow condition is calculated as:

$$\rho_w = \frac{\rho_{w\_sc}}{B_w} \tag{2.30}$$

where ρ_{wsc} and γ_{wsc} are respectively water density at standard conditions and specific gravity of water at standard condition.

2.2.11 Water viscosity

The water viscosity was estimated by using the correlation of Collins (1987) [53], neglecting salinity effect as presented by [23].

$$\mu_{w_{sc}} = 109.574 C_4 C_3^{-1.12166} \tag{2.31}$$

$$\mu_w = \mu_{w_{sc}}(0.999 + 4.029510^{-5} k_6 + 3.1062 \times 10^{-9} k_6^2) \tag{2.32}$$

$$k_6 = (C_2 P + 14.7) \tag{2.33}$$

2.2.12 Volumetric flow rate

Volumetric flow rate of petroleum fluids (gas, oil and water) at flow conditions are defined as follow:

$$Q_g = (Q_{g\_sc} - Rs Q_{o\_sc}) B_g = Q_{o\_sc}(GOR - Rs) B_g \tag{2.34}$$

$$Q_o = Q_{o\_sc} B_o \tag{2.35}$$

$$Q_w = Q_{w\_sc} B_w \tag{2.36}$$

$$Q_l = Q_{o\_sc} B_o + Q_{w\_sc} B_w = Q_{o\_sc}(B_o + WOR . B_w) \tag{2.37}$$

where, Q_{g_sc}, Q_{w_sc} and Q_{o_sc} are the flow rates of gas, water and oil at standard conditions. Q_g, Q_w, Q_o and Q_l are the flow rates of gas, water, oil and liquid at flow conditions. GOR and WOR are gas oil ratio and water oil ratio at surface.

2.3 Multiphase pressure prediction model

Pressure model used in this work was derived by replacing in the Dukler et al pressure model equation (2.38), the liquid hold up in the original model by using drift flux parameters obtained from Woldesemayat and Ghajar [36]. The Dukler and Taitel correlation [37] is given by:

$$\left(\frac{dP}{dL}\right) = \frac{f_{tp} \rho_m V_m^2}{2D} + \rho_m g \sin(\theta) \tag{2.38}$$

In this equation, the fluid density, mixture velocity and friction factor are calculated by combining black oil correlations with drift flux parameters. Thus,

The liquid density at standard conditions and at flow conditions are given by:

$$\rho_{l\_sc} = f_w \rho_{w\_sc} + (1 - f_w)\rho_{o\_sc} = \frac{WOR}{1+WOR} \rho_{w\_sc} + \frac{1}{1+WOR} \rho_{o\_sc} \tag{2.39}$$

$$\rho_l = \frac{\rho_{g\_sc} R_{sl} + \rho_{l\_sc}}{B_l} \tag{2.40}$$

in these equations, ρ_{w_sc} and ρ_{o_sc} are the water and oil densities at the standard conditions. B_l is the volume formation factor of the liquid given by Andreolli (2017) as follow:

R_{sl} the gas-liquid ration defined as the ratio of the quantity of gas solubilized in the oil at flow condition to the liquid volume, both expressed at standard conditions.

$$R_{sl} = \frac{1}{1+WOR} R_s \tag{2.41}$$

From the above, the density of gas and liquid homogeneous mixture for no slip condition can be obtained by:

$$\rho_n = [\rho_o(1 - f_w) + \rho_w f_w]\lambda_L + \rho_g \lambda_G \tag{2.42}$$

$$B_l = \frac{WOR}{1+WOR} B_w + \frac{1}{1+WOR} B_o \tag{2.43}$$

For slippage between phases:

$$\rho_m = \frac{\rho_{g\_sc} R_{sl} + \rho_{l\_sc}}{B_l} \alpha_l + \rho_g \alpha \tag{2.44}$$

$$\mathrm{V_{sg}} = \frac{Q_g}{A_p} = \frac{(Q_{g\_sc} - Q_{o\_sc} R_s) B_g}{A_p} = \frac{Q_o (GOR - R_s) B_g}{A_p} \tag{2.45}$$

$$V_{so} = \frac{Q_o}{A_p} = \frac{Q_{o\_sc} B_o}{A_p} \tag{2.46}$$

$$\mathrm{V_{sw}} = \frac{Q_w}{A_p} = \frac{Q_{w\_sc} B_w}{A_p} \tag{2.47}$$

$$V_{sl} = \frac{Q_{o\_sc} B_o}{A_p} + \frac{Q_{w\_sc} B_w}{A_p} \tag{2.48}$$

The actual velocity represents the local or the true phase velocity of each phase in the pipe. It can be calculated as follow:

$$V_g = \frac{Q_g}{A_g} = \frac{Q_g}{A_p \alpha} = \frac{V_{sg}}{\alpha} \tag{2.49}$$

$$V_L = \frac{Q_L}{A_g} = \frac{Q_L}{A_p \alpha_l} = \frac{V_{sL}}{\alpha_l} \tag{2.50}$$

The mixture velocity can then be defined as the sum of the superficial gas and liquid velocities. Thus,

$$\mathrm{V_m} = \frac{Q_{o\_sc} B_o}{A_p} + \frac{Q_{w\_sc} B_w}{A_p} + \frac{Q_o (GOR - R_s) B_g}{A_p} \tag{2.51}$$

Combining these equations yields the final pressure model developed in this work.

$$\left(\frac{dP}{dL}\right) = \frac{f_{tp}\left(\frac{\rho_{g\_sc} R_{sl} + \rho_{l\_sc}}{B_l}\alpha_l + 0.009225\frac{\gamma_g P}{ZT}\alpha\right)\left(\frac{Q_o (GOR - R_s) B_g}{A_p}\right)^2}{2D} + \left(\frac{\rho_{g\_sc} R_{sl} + \rho_{l\_sc}}{B_l}\alpha_l + 0.009225\frac{\gamma_g P}{ZT}\alpha\right) g \sin(\theta) \tag{2.52}$$

The pressure model obtained depend on the drift flux parameter and black oil properties. This model was compared to four others pressure models presented herein described by equations (1.46), (1.68), (1.73) and (1.78). It was also compared to field data and PIPESIM model in order to evaluate its accuracy.

2.4 Temperature prediction model

The temperature profile is derived from the energy conservation equation. The mixture energy conservation equation used in this work is based on a homogeneous fluid model, where the gas and liquid phases are treated as a pseudo-phase, and the properties are the volume average of the independent phases [54]. The energy balance equation was derived from [55] where the hydrate terms was neglected. This equation includes terms for the transient behavior of the system enthalpy, the convection of energy, the transient change in system pressure, fluid viscous dissipation, change in potential energy, pipe wall heat transfer to the environment. The energy balance equation in terms of the pseudo-phase enthalpy is,

$$\frac{\partial h}{\partial t} - v_m \frac{\partial h}{\partial x} = \frac{1}{\rho_m}\frac{\partial P}{\partial t} - v_m \frac{\partial v_m}{\partial t} - v_m v_m \frac{\partial v_m}{\partial t} - v_m g \sin(\theta) - \frac{\dot{q}\pi d}{A_p \rho_m} \tag{2.53}$$

Where h is mixture enthalpy per unit mass and $\dot{q}$ is the wall heat flux.

The following is the procedure to express the mixture energy conservation equation explicitly in terms of temperature. From the thermodynamic theory, entropy (s) is a function of pressure (P) and temperature (T).

$$ds_k = \left(\frac{\partial s_k}{\partial T_k}\right)_{Pk} dT_k + \left(\frac{\partial s_k}{\partial P_k}\right)_{Tk} dP_k \tag{2.54}$$

The specific enthalpy is also a function of temperature and pressure

$$dh_k = C_{Pk} dT_k + \left(\frac{\partial h_k}{\partial P_k}\right)_{Tk} dP_k \tag{2.55}$$

For simple compressible systems of fixed chemical composition subject to an internally reversible process, the first law of thermodynamic can be written as,

$$ds_k = \frac{dh_k}{T_k} - v_k \frac{dP_k}{T_k} \tag{2.56}$$

Where, v_k is specific volume and k denotes either gas or liquid. By substituting (2.55) into (2.56), we have,

$$ds_k = \frac{C_{Pk} dT_k}{T_k} + \frac{1}{T_k}\left[\left(\frac{\partial h_k}{\partial P_k}\right)_{Tk} dP_k - v_k\right] dP_k \tag{2.57}$$

From equations (2.54) and (2.57), the following equation can be obtained,

$$\left(\frac{\partial s_k}{\partial T_k}\right)_{Pk} = \frac{C_{Pk}}{T_k} \tag{2.58}$$

$$\left(\frac{\partial s_k}{\partial P_k}\right)_{Tk} = -\left(\frac{\partial V_k}{\partial T_k}\right)_{Pk} \tag{2.59}$$

$$ds_k = \frac{C_{Pk}}{T_k} dT_k - \left(\frac{\partial V_k}{\partial T_k}\right)_{Pk} dP_k \tag{2.60}$$

Solving for the enthalpy gives

$$dh_k = C_{Pk} dT_k + \left[-T_k \left(\frac{\partial V_k}{\partial T_k}\right)_{Pk} + v_k\right] dP_k \tag{2.61}$$

Deriving equation (2.60) with respect to pressure at constant enthalpy gives,

$$\eta_k = \left(\frac{\partial T_k}{\partial P_k}\right)_{hk} = \frac{1}{C_{Pk}}\left[T_k\left(\frac{\partial V_k}{\partial T_k}\right)_{Pk} - v_k\right] \tag{2.62}$$

Where η_k is the Joule-Thomson coefficient of phase k. by substituting equation (2.62) into equation (2.61) we have,

$$dh_k = C_{Pk}dT_k + \eta_k C_{Pk}dP_k \tag{2.70}$$

Substituting equation (2.70) into equation (2.53) gives the energy balance equation in terms of temperature,

$$C_{Pm}\left(\frac{\partial T_m}{\partial t} + v_m\frac{\partial T_m}{\partial L}\right) - \chi\left(\frac{\partial P}{\partial t} + v_m\frac{\partial P}{\partial L}\right) - \frac{1}{\rho_m}\frac{\partial P}{\partial t} + v_m\left(\frac{\partial v_m}{\partial t} + v_m\frac{\partial v_m}{\partial L}\right) = -v_m g\sin\theta - \frac{\dot{q}\pi d}{A_p\rho_m} \tag{2.71}$$

Where:

$$\chi = \frac{\rho_g\alpha\eta_g C_{p,g} + \rho_L H_L\eta_L C_{p,L}}{\rho_m} \tag{2.72}$$

Cp_m is the average specific heat capacity of the multiphase flow calculated using equations (2.73) and (2.74) below as in [56].

$$Cp_m = Cp_g\alpha\frac{\rho_g}{\rho_m} + Cp_L(1-\alpha)\frac{\rho_L}{\rho_m} \tag{2.73}$$

$$Cp_L = \left(\frac{Q_o}{Q_o+Q_w}\right)Cp_o + \left(\frac{Q_w}{Q_o+Q_w}\right)Cp_w \tag{2.74}$$

η_m, is the average Joule-Thomson coefficient calculated as shown in equation (2.75 through equation (2.79) as shown below,

$$\eta_m = -\frac{1}{w_m Cp_m}\left(w_g Cp_g\eta_g + w_l Cp_l\eta_l\right) \tag{2.75}$$

$$\eta_g = \left(\frac{1}{\rho_g C_{p_g}}\right)\left[\frac{T_m}{Z}\left(\frac{dZ}{dT_m}\right)_p\right] \tag{2.76}$$

$$\eta_L = \frac{1}{\rho_L C_{p_L}}(T_m\beta - 1) \tag{2.77}$$

Equation (2.78) below calculated the thermal expansion of the liquid phase β.

$$\beta = \frac{1}{V_L}\left(\frac{\partial V_L}{\partial T}\right) = \frac{1}{B_L}\left(\frac{\partial B_L}{\partial T}\right) = \frac{WOR}{1+WOR}\frac{\partial B_w}{\partial T} + \frac{1}{1+WOR}\frac{\partial B_o}{\partial T} \tag{2.78}$$

w_m is the average mixture mass flow rate given by,

$$w_m = \rho_m V_m A_p \tag{2.79}$$

The heat exchange between the hot fluids inside pipeline and the cooler environment is given by:

$$q = U_o(T_m - T_e) \tag{2.80}$$

U_o is the overall heat transfer coefficient given by equation (2.81) below:

$$\frac{1}{U_o} = r_{ins}\left(\frac{1}{r_i h_{in}} + \frac{1}{h_{pipe}} + \frac{1}{h_{ins}} + \frac{1}{h_{sur}}\right) \tag{2.81}$$

where parameters h_{in}, h_{pipe}, h_{ins} and h_{sur} are, respectively, the heat transfer coefficient of the multiphase fluid flowing in the pipe ("*in*"), the thermal conductivity of the metallic pipe ("*pipe*"), the thermal conductivity of the insulation layer ("*layer*"), and the heat transfer coefficient of the surrounding environment ("*sur*"), which can be either water or soil. r_{ins}, r_i and r_o are respectively the pipeline outer radius including insulation, the pipeline inner radius and the pipeline outer radius excluding insulation.

According to [57], the terms h_{in} at the right hand of equation (2.81) can be calculated using equation (2.82) through equation (2.92):

$$h_{in} = \frac{K_{tp} Nu_{tp}}{D} \tag{2.82}$$

where:

$$K_{tp} = \alpha k_g + (1-\alpha)k_L \tag{2.83}$$

For laminar flow in long pipe ($Re_T \leq 2000$)

$$Nu_{tp} = 1.86\left[Re_T Pr_m \left(\frac{D}{L}\right)\right]^{\frac{1}{3}} \tag{2.84}$$

For turbulent flow ($Re_T \geq 6000$)

$$Nu_{tp} = 0.023\ \mathrm{Re}_{\mathrm{T}}^{0.8}\mathrm{Pr}_{\mathrm{m}}^{0.33}\left(1 + \left(\frac{D}{L}\right)^{0.7}\right) \tag{2.85}$$

For transition flow regime ($2000 \leq Re_T \leq 6000$)

$$Nu_{tp} = Nu_{laminar}\left[\frac{Re_T}{6000}\right]^a \tag{2.86}$$

where, parameter a is given by:

$$a = \frac{\ln\left(\frac{Nu_{turbulent}}{Nu_{laminar}}\right)}{ln\left(\frac{Re_{max}}{Re_{min}}\right)} \tag{2.87}$$

The total Reynolds number is calculated as follow:

$$Re_T = \frac{\rho_L V_{sL} D}{\mu_L} + \frac{\rho_g V_{sg} D}{\mu_g} \tag{2.88}$$

The Prandtl number of the mixture is given by:

$$Pr_m = \frac{\mu_m Cp_m}{K_m} \tag{2.89}$$

The mixture thermal conductivity is given as:

$$K_m = \frac{k_g k_L}{(1-\alpha)k_g + \alpha k_L} \tag{2.90}$$

The thermal conductivity of the metallic pipe h_{pipe} and that of the insulation layer h_{ins} are calculated as follow:

$$h_{pipe} = \frac{k_{pipe}}{\ln\left(\frac{r_o}{r_i}\right)} \tag{2.91}$$

$$h_{ins} = \frac{k_{ins}}{\ln\left(\frac{r_{ins}}{r_o}\right)} \tag{2.92}$$

The surrounding heat transfer coefficient h_{sur} depend on the nature of the surrounding environment. The correlation of average external heat transfer coefficient is calculated by the equation following, from [54]. For seawater environment, we have:

$$Nu_o = 0.027 \, . R_{eo}^{0.8} P_{ro}^{0.3} \tag{2.93}$$

$$Re_o = \frac{\rho_o V_o D}{\mu_o} \tag{2.94}$$

$$Pr_o = \frac{\mu_o Cp_o}{K_o} \tag{2.95}$$

$$h_{sur} = \frac{K_o Nu_o}{D} \tag{2.96}$$

In steady state conditions, assuming the kinetic term to be negligible, equation (2.71) becomes:

$$\frac{dT_m}{dL} = -\frac{U_o \pi d (T_m - T_e)}{C_{p_m} w_m} + \eta_m \frac{dP}{dL} - \frac{g \sin(\theta)}{C_{p_m}} \tag{2.97}$$

Equation (2.97) represents the temperature model of a mixture of gas-liquid flowing through an offshore pipeline in which the pressure gradient is obtained by using equation (2.52).

2.6 Numerical simulations algorithm

The finite difference method was used to discretize the temperature model given by equation (2.97). All the equations in this study are solved simultaneously using MATLAB software. Numerically, we divide the pipeline into sections, and each section was divided into cells and consider average value of temperature and pressure in the cells. The numerical solution obtained using iterative approached is therefore given by:

$$\frac{T_m(i+1) - T_m(i)}{\Delta x} = \left(\frac{T_e - T_m}{A} + \eta_m \frac{dP}{dL} - \frac{g \sin(\theta)}{C_{p_m}}\right)_i \tag{2.98}$$

In which, the parameter A is:

$$A_i = \left(\frac{C_{p_m} w_m}{U_o \pi D}\right)_i \tag{2.99}$$

i. Given the initial value of temperature and pressure at node i, guess an initial predicted temperature and pressure at node $i+1$ by setting for example $T_{i+1,} = T_i$ and $P_{i+1} = P_i$.

ii. Calculate the average quantities for the temperature and pressure $T_{Av} = \frac{T_{i+1}+T_i}{2}$ and $P_{Av} = \frac{P_{i+1}+P_i}{2}$.

iii. Calculate all the flow parameters and the physical properties at T_{Av} and P_{Av}.

iv. Computes pressure predicted ${P_{i+1}}^{pred}$ from the models.

v. Test convergence for pressure by comparing the calculated pressure to the guess pressure as follow:= $\frac{|{P_{i+1}}^{pred} - P_{i+1}|}{P_{i+1}}$, If $\varepsilon < 10^{-6}$ the procedure converge. If not, set $P_{i+1} = {P_{i+1}}^{pred}$ and calculate a new average pressure and repeat step 3 to 5 until the condition is match.

vi. Calculate the temperature ${T_{i+1}}^{pred}$ from the temperature model

Again, if temperature is not the same as the assumed one, we need to go back to the process 2 until converge is achieved.

2.7 PIPESIM thermal model

PIPESIM multiphase thermal model was built in this study in order to validate the pressure and the temperature models developed and presented here. A PIPESIM model is a representation of a flowing system that can be used to simulate fluid flow through the system. A model can be a single well with or without connected surface piping and equipment, a pipeline transporting fluid from one point to another, or multiple wells, pipeline, and surface equipment connected together to represent a large and complex flow network.

2.7.1 Basic model building workflow

The network schematic model was used to build the pipeline model in PIPESIM. Figure 2.2 below shows a sketch of the simulation modeling of the pipeline in PIPESIM

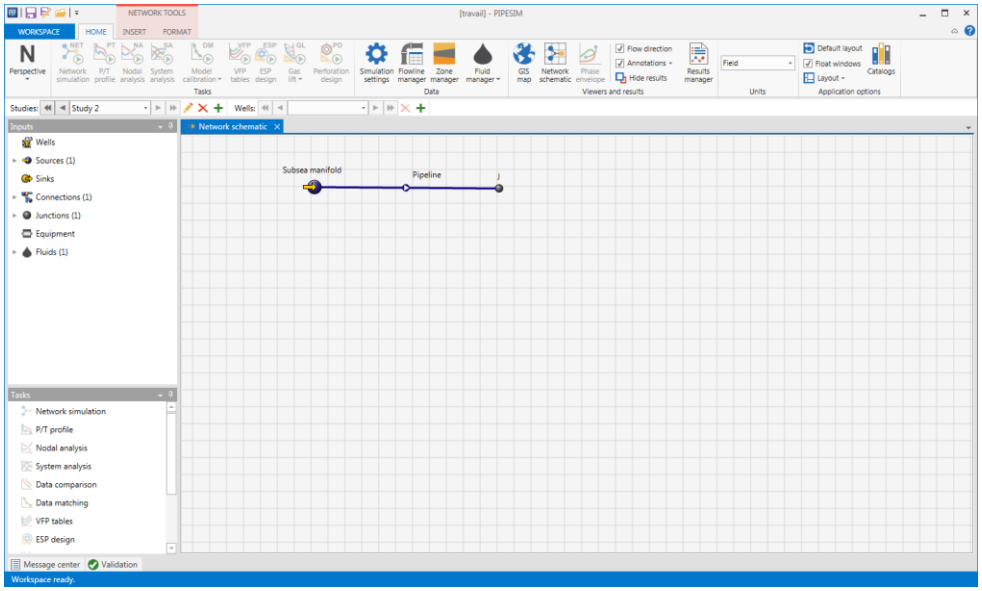

Figure 2.2: Sketch of the simulation modeling of subsea pipeline in PIPESIM.

Next, pipeline data was introduced in the PIPESIM as it is shown in figure 2.3 below,

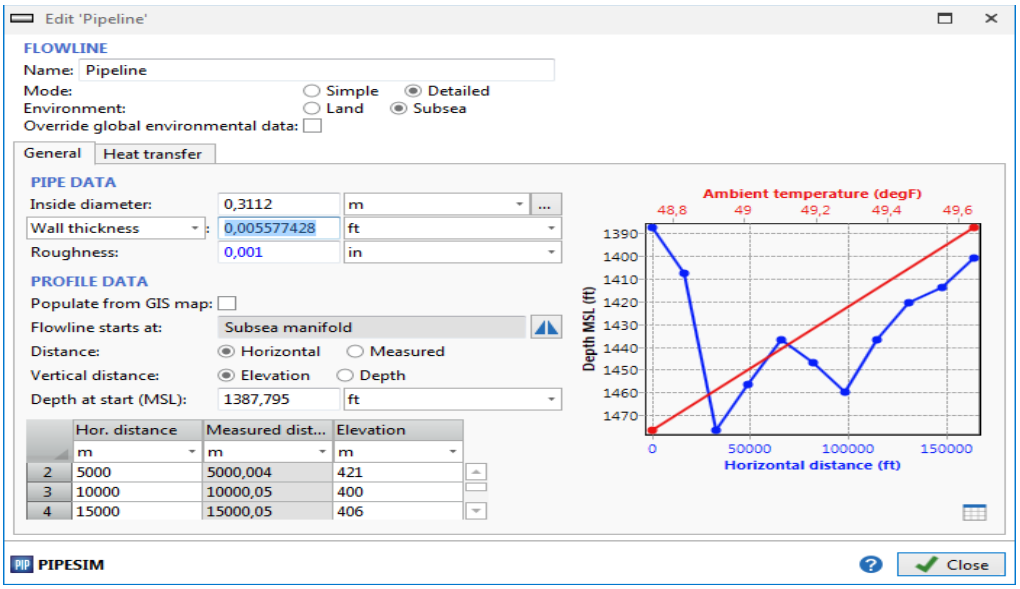

Figure 2.3: Editing pipeline data with PIPESIM.

2.7.2 Create or edit fluid models

Fluid modeling is a fundamental aspect of multiphase flow simulation. Before running any simulations, you need to create one or more fluid models. Fluid models are used to describe phase behavior and provide physical and transport properties of the fluid required for any simulation run. PIPESIM supports several types of fluids. After you select a fluid type on the home tab, all the objects within the model automatically use that fluid type. Even though you

can store multiple types of fluids within an object, PIPESIM only displays the one you selected on the home tab and uses it in simulation. These fluid types are currently available: Black oil and Compositional Fluid models. Black oil model was also used in pipesim for the fluid characterization. After the pipeline model was built, the fluid model was edited as it is shown in figure 2.4 below.

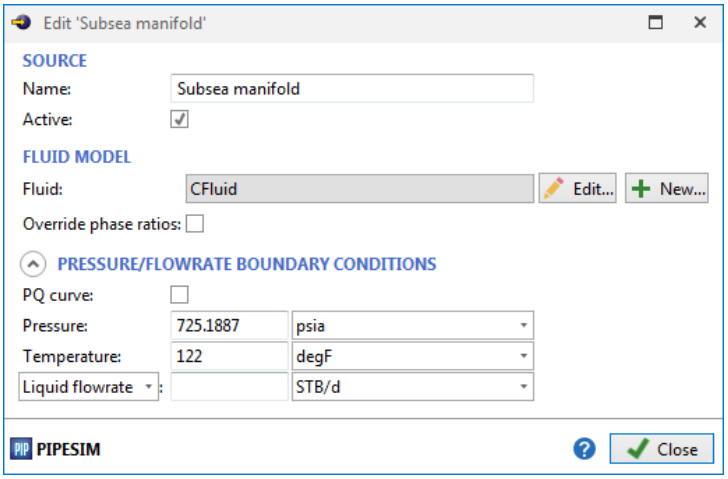

Figure 2.4: Sketch fluid model edited in PIPESIM

In this work, the revised Beggs and brill model was chose for the simulation of the pressure gradient, see figure 2.5

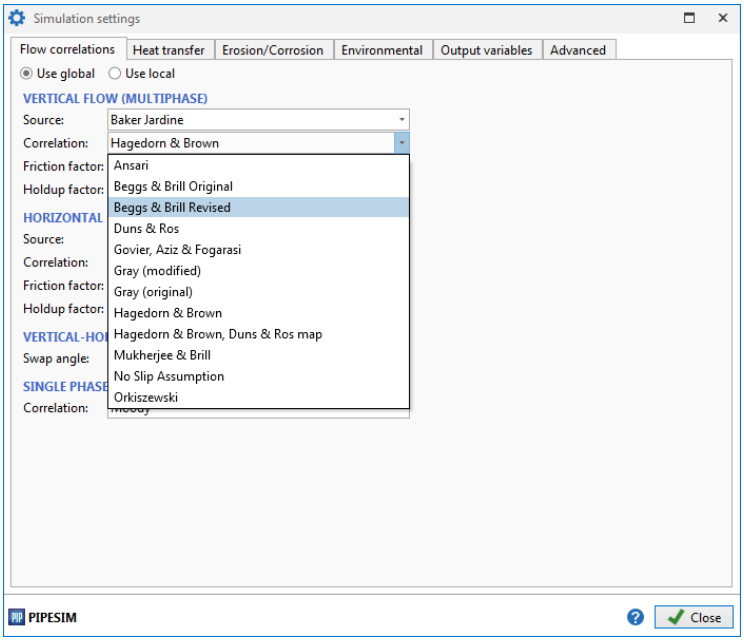

Figure 2.5: setting correlation for multiphase simulation using PIPESIM.

2.7.3 Energy equation for steady-state flow

PIPESIM uses the first law of thermodynamics to perform a rigorous heat transfer balance on each pipe segment. The first law of thermodynamics is the mathematical formulation of the principle of conservation of energy applied to a process occurring in a closed system (a system of constant mass m). It equates the total energy change of the system to the sum of the heat added to the system and the work done by the system. For steady-state flow, it connects the change in properties between the streams flowing into and out of an arbitrary control volume (pipe segment) with the heat and work quantities across the boundaries of the control volume (pipe segment). For a multiphase fluid in steady-state flow, the energy equation is given by:

$$\Delta\left[\left(H+\frac{1}{2}V_m^2+gz\right)dm\right]=\sum\delta Q-\delta W \tag{2.100}$$

where the specific enthalpy

$$H=U+PV \tag{2.101}$$

is a state property of the system since the internal energy U the pressure P and the volume V are state properties of the system. It is clear from the left-hand side of equation 2.100, that the change in total energy is the sum of the change in enthalpy energy,

$$\Delta[Hdm]=\Delta[(U+PV)dm] \tag{2.102}$$

The change in gravitational potential energy:

$$\Delta\left(E_p\right)=\Delta[(gz)dm] \tag{2.103}$$

Moreover, the change in total kinetic energy (based on the mixture velocity)

$$\Delta(E_k)=\Delta\left[\left(\frac{1}{2}V_m^2\right)dm\right] \tag{2.104}$$

Which is assumed to be negligible.

On the right-hand side of equation 2.100, $\sum\delta Q$ includes all the heat transferred to the control volume (pipe segment) and δW represents the shaft work, that is work transmitted across the boundaries of the control volume (pipe segment) by a rotating or reciprocating shaft.

2.7.4 Run simulations

You can perform nodal analysis, reservoir simulation, and use other analytical tools (such as pressure/temperature (P/T) profiles, VFP tables, and network simulation) to calculate the distribution of flowrates, temperatures, and pressures throughout the system and plan new field developments. In figure 2.6 below, a sketch of pipeline simulation model is presented.

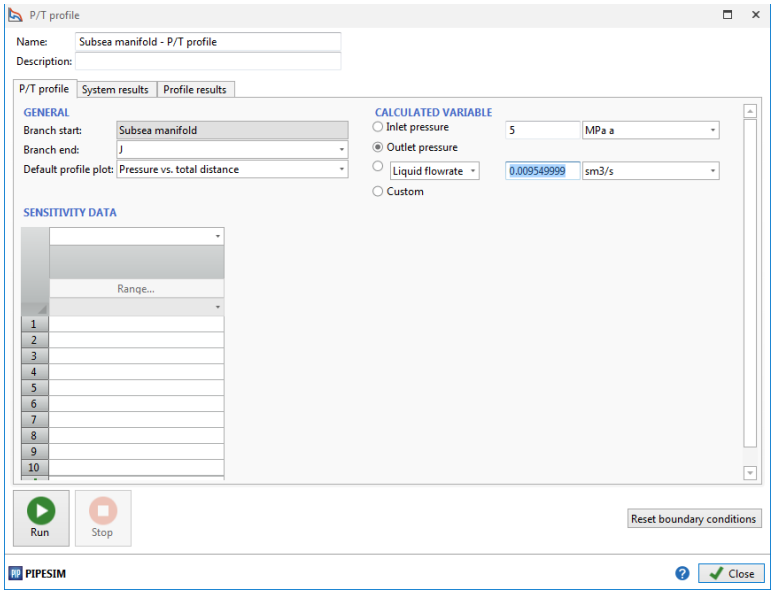

Figure 2.6: sketch of pipeline simulation model with PIPESIM.

2.8 Optimum insulation

In previous sections, we developed a thermal model that described the distribution of pressure and temperature through a subsea pipeline. In order to avoid some flow assurance issues such as precipitation and solid deposits, thermal insulation is applied to subsea pipelines to maintain the temperature of crude oil above a critical level, such as the wax appearance temperature (WAT). The position within the entire system where the lowest temperature is observed is a risk point. The problem here is to find out the optimum insulation thickness that meets the insulation requirement along with the lowest insulation material consumption. This objective has been achieved using three approaches: numerical simulations, combined machine learning with genetic algorithm using MATLAB and simulation run using RAPIDMINER.

2.8.1 Numerical simulations

For the numerical approach, we defined manually and gradually the different insulation thickness. Firstly, the insulation thickness was ranged from 0.0254 to 0.0635m. Moreover, it was further extended with an increasing step of 0.0127m until the requirement is satisfied. For

each insulation thickness and for each insulating material, numerical simulation was performed until the stopping criterial defined by equation (2.105):

$$Tmin \geq C \tag{2.105}$$

$Tmin$ is the minimum temperature of the system given in (°K) and C is the requirement set here at 40°C.

2.8.2 Genetic algorithm combined with machine learning techniques using MATLAB

The problem here is to find out the optimum insulation thickness of three different insulating materials that meets the thermal criteria by applying genetic algorithm to machine learning techniques using MATLAB. As state by [50], for insulation design, the insulation requirement for pipeline and flowline segments is to keep the temperature at the risk point higher than the critical level. In fact, various combinations of insulation thickness can lead to the same lowest temperature. Theoretically, for a certain subsea production system, there exists one insulation design that meets the insulation requirement with the lowest insulation volume. The optimizing approach adopted here was to set the insulation volume as the objective function and the insulation requirement as the constraint. The objective function is defined by

$$F = \sum_{i=1}^{n=200} \pi L \left((X_i + D_i)^2 - \left(D_i^2 \right) \right) \tag{2.106}$$

where, n is the number of gathered data points, X_i is the insulation thickness at the ith data point given in (m), D_i is the external diameter at the ith data point in (m). L is the length of the subsea pipeline in (m).

For a certain subsea production system, the minimum temperature of the whole system is a function of the insulation thicknesses as shown in equation (2.107) below:

$$T_{min} = f(X_i) \tag{2.107}$$

As state in [50], machine learning techniques can skip all the physical theories and models to extract direct patterns between data, thereby providing computers with the ability to learn without being explicitly programmed. In this study, machine learning techniques were employed to establish a pattern between the minimum temperature of the system and the insulation thickness. Supervised machine learning technique was used here because as

mentioned above, in supervised learning, the training data you feed to the algorithm includes the desired solutions. Hence, for a given X_i and $Y_i = T_{min}(i)$, the goal in machine learning is to find an appropriate function $f(X_i)$ that will be able to depict the pattern between T_{min} and X as follow:

$$Y = f(X) + \varepsilon_{error} \tag{2.108}$$

Y is the corresponding minimum temperature of the system and $f(X)$ is the predicted minimum temperature. Defining the equation $f(X)$ form, is the first step, which includes the selection of the equation form from types such as polynomial, exponential, power function , natural logarithm and so on. The arrangement of the variables is also critical in this step. The second step is to train the unknown parameters in the equations by feeding a large number of examples to the learning algorithm. A polynomial equation is commonly used in linear regression. The ordinary form of a polynomial equation is:

$$Y = \theta_0 + \theta_1 X_1 + \cdots + \theta_n X_n + \theta_{n+1} X_1^2 + \cdots + \theta_{2n} X_n^2 + \varepsilon \tag{2.109}$$

$$X^T = [1, X_1, X_2, \dots, X_n, X_1^2, X_2^2, \dots, X_n^m] \tag{2.110}$$

$$\theta^T = [\theta_0, \theta_1, \dots, \theta_n, \theta_{n+1}, \dots \theta_{2n}] \tag{2.111}$$

The learning features are X^T and the unknown parameters are θ^T. These parameters are determined by minimizing the cost function below:

$$J(\theta) = \frac{1}{2}\sum_{j=1}^{n}\left(\theta^T X^j - Y^j\right)^2 + \frac{\lambda}{mn1}\sum_{j=1}^{mn1}\theta_j^2 \tag{2.112}$$

Where $\frac{\lambda}{mn}\sum_{j=1}^{mn}\theta_j^2$ is the regularization term to prevent overfitting. n is the number of training examples, m is the maximum power index of a polynomial equation, $n1$ is the number of first-order features of a polynomial equation, and λ is the tuning factor. Because the relationship between the minimum temperature of the system and the insulation thickness is non-linear, the form of the predicted function proposed was the same as in equation (2.109) with the difference that the exponential index of each variable was not fixed to an integer, but was considered an unknown constant, which was trained by the supervised learning algorithm. More specifically, the predicted function equation form for this study was given by:

$$Y = \theta_0 + \theta_1 X^{\theta_2} + \varepsilon \quad (2.113)$$

The form of this equation was inspired by an observation in the scatter plot of the minimum temperature of the system and the insulation thickness. Once an appropriate θ^T was obtained by training, which makes the error ε small enough, the direct pattern between minimum temperature and insulation thickness was then established as:

$$T_{min}{}^{j} = \theta_0 + \theta_1 X_j{}^{\theta_2} \quad (2.114)$$

The database for the training process was generated by simulation. After obtaining equation (2.114), optimization algorithms was then used to assess the best set of insulation thickness. The fitting function equation form was trained by machine learning techniques with the database. The database was divided into three parts: training data set (70%), cross-validation data set (10%), and testing data set (20%). The fitting parameters were trained with the training data and the fitting function was tested with the testing data. The cross-validation data was then used to validate some special fitting parameters. Finally, all the trained equations were evaluated by their performance in terms of prediction accuracy. Below are the different steps that we employed in determining the optimum insulation thickness:

- 200 insulation thickness were created randomly between 10 to 700 mm
- For each insulation thickness created, the minimum temperature of the system was calculated using the thermal model built in this thesis.
- Based on these dataset, supervised machine learning technique was used in order to establish a pattern between the minimum temperature and the insulation thickness.
- The database was then divided into three parts: training data set (70%), cross-validation data set (10%), and testing data set (20%). The fitting parameters are trained with the training data and the fitting function is tested with the testing data. The cross-validation data can be used to validate some special fitting parameters.
- Finally, the genetic algorithm was then employed to find out the optimum insulation thickness with respect to the thermal requirement.

In MATLAB, there are two ways you can use the genetic algorithm with the toolbox:

- Calling the genetic algorithm function ga at the command line.
- Using the Genetic Algorithm Tool, a graphical interface to the genetic algorithm see figure 2.7 below.

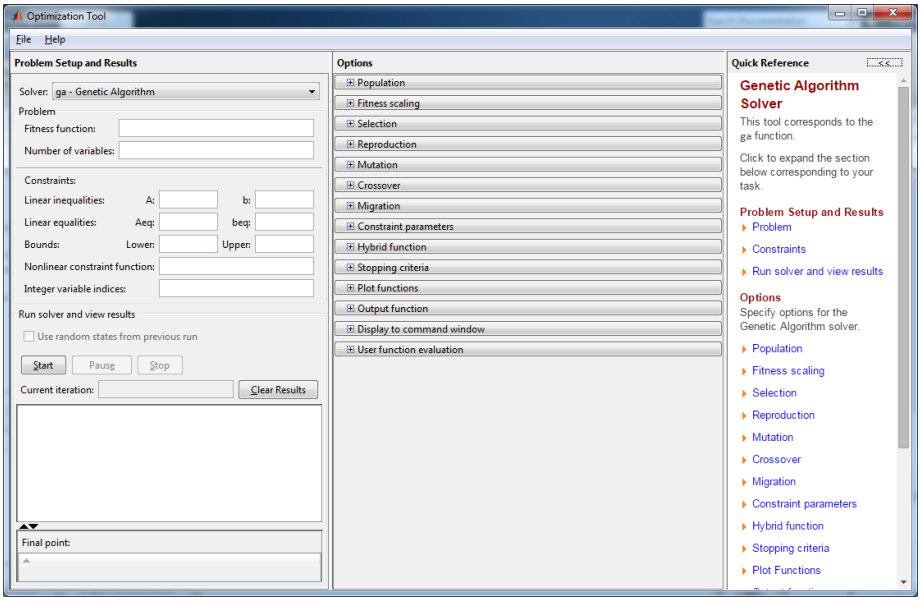

Figure 2.7 below is a sketch of graphical interface of genetic algorithm in MATLAB.

This MATLAB toolbox was used to find out the optimum insulation thickness in this study.

2.8.3 Optimum insulation using RAPIDMINER software

In RAPIDMINER, we built and run six supervised machine learning algorithms and we applied genetic algorithm operator to find out the optimum insulation thickness that meets the thermal requirement. The steps in building a genetic algorithm optimization using machine learning techniques in RAPIDMINER are as follow:

- Basic processing
  - Load and process data
  - Creates training and a validation set
  - Performs some basic feature engineering and preprocessing such as missing value handling or encoding.
- Feature engineering and modeling
  - Handle text columns if desired and stores the text processing model
  - Performs automatic feature engineering if desired. This happens in addition to the basic feature engineering done before text processing, date handling encoding etc.
  - Performs the actual model training and automatic hyperparameter tuning (parameter optimization) if desired.
- Transform validation and scoring data

- Transform the validation data (known target value) using the same preprocessing and features
- Transform the scoring data (no know target value) using the same preprocessing and features

➢ Scoring m validation explanations, weights and simulator

- Applies the model on the validation and the scoring data sets for scoring. Also explain the predictions and calculate model-specific weights.
- Perform a multiple hold-out set validation with robust estimation which provides similar quality of performance estimations than a cross validation with smaller runtimes.

➢ Production model

- Creates a final production model by training a model with the same parameters on the combined training and validation data sets.

The figure 2.7 below presents the RAPIDMINER process interface.

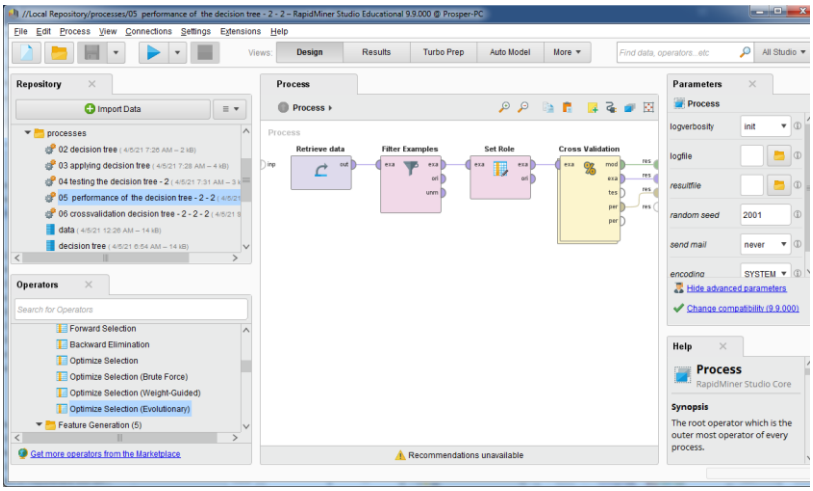

Figure 2.8 below is a sketch of graphical interface of genetic algorithm in RAPIDMINER.

Generally, for a subsea production system, the optimization steps were as follows:

- Build a subsea system model and gather enough model results to prepare the training database (the performance of the linear regression depends on the number of model results).
- Run a non-linear regression algorithm to extract a direct pattern between minimum temperature and insulation thickness.

- Run GA to find the insulation design, which meets the insulation requirements using the minimum volume of insulation material.

2.9 Flow assurance solids risk formation analyses with logistic regression

As state earlier, flow assurance solids formation is increasingly important issue in subsea oil and gas production pipelines due to its unexpected disaster such as reduction of the flow area resulting in a decreasing production rate. To ensure that these issues do not occur suddenly, factors such as temperature that mostly contribute to its formation should be analyzed seriously. Logistic regression model describes a relationship between an outcome and a set of independent variables. It has been using widely either in the medical field, business and marketing studies or as simple as determining yes or no in the decision-making process [58]. Here, the logistic regression analyses are used to answer whether yes or no the solids formation will occur during transportation of oil and gas in long subsea pipeline for given insulation thickness and minimum temperature of the system. The features used include insulation thickness and minimum temperature of the system. The Logistic Regression procedure is designed to fit a regression model in which the dependent variable Y characterizes an event with only two possible outcomes. Two types of data may be modeled:

- Data in which Y consists of a set of 0's and 1's, where 1 represents the occurrence of one of the 2 outcomes.
- Data in which Y represents the proportion of time that one of the 2 outcomes occurred.

The fitted regression model relates Y to one or more predictor variables X, which may be either quantitative or categorical. In this procedure, it is assumed that the probability of an event is related to the predictors through a logistic function. The procedure fits a model using either maximum likelihood or weighted least squares. The logistic model relates the probability of occurrence P of the outcome counted by Y to the predictor variables X. The model takes the form:

$$P(z1) = \frac{1}{1+e^{-z1}} \tag{2.115}$$

with,

$$z1 = \beta_0 + \beta_1 x_1 + \beta_2 x_2 + \cdots + \beta_n x_n \tag{2.116}$$

where x_1, x_2, …, x_n are the independent variables of interest and β_0, β_1, …, β_n are the coefficient representing unknown parameters. Estimates of these parameters are obtained using a mathematical technique called maximum likelihood. This likelihood mean the probability has been evaluated as a function of the parameters with fix data [59]. Likelihood allows the estimation of unknown parameters based on known outcomes. Initially, $\beta_0 = 0$, and at each iteration the value of this parameter will be updated. The iteration will stop when the percentage of error decreases to the smallest value that approximately becomes zero.

Alternatively, the model in equation (2.115) can be written in the form:

$$\log\left(\frac{P(z1)}{1-P(z1)}\right) = e^{-(\beta_0+\beta_1 x_1+\beta_2 x_2+\cdots+\beta_n x_n)} \tag{2.117}$$

where the left-hand side of the above equation is referred to as the logit transformation.

To determine the contribution of insulation thickness and the minimum temperature of the system on the risk analyses of the flow assurance issues formation, logistic regression analyses was applied here using MATLAB script. The following steps were considered:

- The dataset of the minimum temperature of the system was obtained using numerical simulations of the thermal model developed in this study. The insulation thickness was generated randomly. The flow assurance solids formation threshold is the thermal requirement. Thus, flow assurance issues risk is treated as binary data. If minimum temperature less than requirement then solids formation risk=1 and 0 otherwise.
- All possible variables were defined: the response variable is the solids risk formation whereas the insulation thickness and the minimum temperature of the system are the quantitative variables.
- Input of variables data into logistic regression function
- Estimate parameter using maximum likelihood estimation to determine goodness of fit: from the logistic function, the logistic regression model is attained through the parameter z1 that can be composed as linear sum of the explanatory variables as follows:
- Test the significance of each parameter and eliminate insignificance variables: once a full logistic regression model is developed, the backward stepwise elimination procedure will be used to remove the independent variable with an

insignificant coefficient. The backward stepwise elimination procedure begins with a full model. Then the variable that are found to be insignificant are eliminated from the model in an iterative process.

- Determine the most influential factor subject to solids risk formation. Next, analyses the tested model to ensure that the model still adequately fits the data.

For model validation, other model was built and used in a statistical analyses tool name STATGRAPHIC.

In RAPIDMINER see figure 2.9 below, the following steps were employed to build the logistic regression model:

- Load the dataset containing all the variables in the process
- Select the target attribute
- Split the data into three: 70% training, 20% test and 10% validation
- Used the logistic regression model tool
- Apply the model
- Validate the model by evaluating its performance by using the classification performance tool

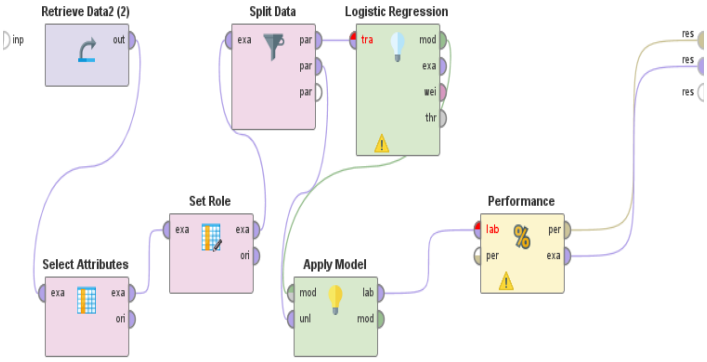

Figure 2.9: overview of the logistic regression model built in RAPIDMINER.

In STATGRAPHIC software see figure 2.10 below, the steps below where done:

- Load the dataset containing all the variables
- Precise the dependent variable and the independent variable
- Choose method of evaluating the parameters. Here the maximum likelihood method was selected.

- The backward selection was choosing for fit, and the model order was set to first order.

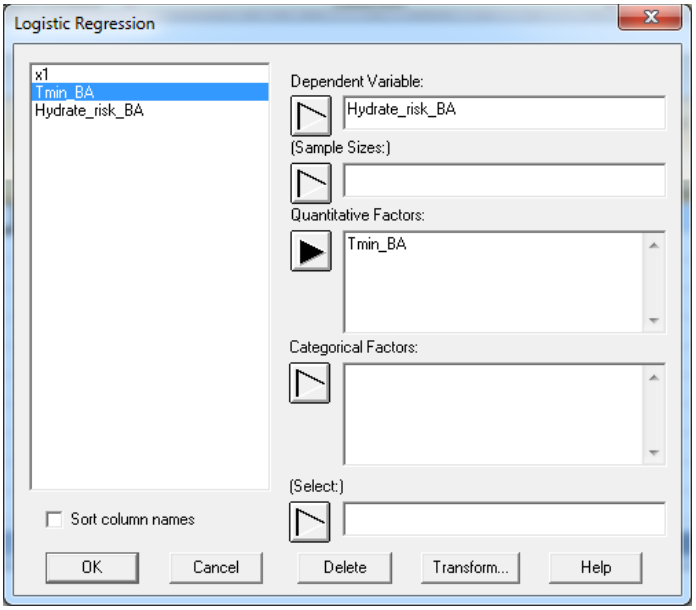

Figure 2.10: sketch of the precision of the variable's names for logistic regression in STATGRAPHIC.

2.10 Operating parameters

Below, the necessary parameters for the models' simulations are presented.

2.10.1 Pipeline and insulation materials parameters

The studied system presented here is consisting of a production subsea pipeline. The pipeline geometry considered is the same as that presented in [4] for the example 1 case. The geometrical parameters of pipeline and insulation materials are presented in table 3.1 below and the thermophysical properties of the insulation materials are given in table 3.2 below.

Table 2.1: Geometrical parameters of the subsea pipeline [4].

Internal diameter of pipeline (m)	External diameter of pipeline (m)	Thickness of pipeline (m)	Pipeline length (m)	Insulation materials thickness (m)
0.3112	0.3239	0.0127	50,000	0.0254
-	-	-	-	0.0381
-	-	-	-	0.0508
-	-	-	-	0.0635

Table 2.2: Thermophysical properties of the insulation materials [19]

Insulation materials	Thermal conductivity (W/m K)	Specific heat (Kj/Kg K)	Density (Kg/m^3)
Calcium Silicate	0.069	0.96	260
Polyurethane	0.04	1400	45
Black Aerogel	0.012	950	140

2.10.2 Data of fluids and operating parameters

The data of fluids used as well as the operating parameters are the same as in [4].

Table 2.3: Operating parameters [4]

Oil flow rate	$0.00955 m^3/s$
Gas flow rate	$9.05 Nm^3$
Density of natural gas	$0.710 Kg/m^3$
Density of crude oil (20°C)	$886.9 Kg/m^3$
Surrounding temperature	277.15 K
Inlet temperature	323.15 K
Outlet temperature	278.75 K
Inlet pressure	5 MPa
Outlet pressure	2.4 MPa
Over all heat transfer coefficient	$2 (W/m^2 K)$

Conclusion

In this chapter, we presented the mathematical models, which describes the temperature and pressure profiles existing inside a subsea pipeline carrying a hot multiphase fluid. Further, we presented the PIPESIM model employed herein. Next, we presented the approaches that we used to find out the optimum insulation thickness of three insulating materials for subsea pipeline insulation design. Finally, the machine learning technique such as power regression model was presented. RAPIDMINER tool, MATLAB tool for genetic algorithm optimization and STAGRAPHIC tool used for logistic regression model were presented. All these models were simulated and the results will be presented in the final chapter

CHAPTER 3: RESULTS AND DISCUSSION

Introduction

In this chapter, the numerical results obtained with MATLAB by using the pressure and temperature models developed herein, are compared with those from measured values, PIPESIM model and existing model from literature. Next, optimum insulation thickness of black aerogel, calcium silicate and polyurethane were assessed using numerical simulation, genetic algorithm combined with power regression and machine learning respectively, by using MATLAB and RAPIDMINER software. Finally, logistic regression model for prediction of the occurrence of flow assurance solids risk formation built with MATLAB was compared with the results displayed by STAGRAPHIC. Results are presented in graphical form using profiles. Tables are also used to observe difference and performance parameters that evaluates the accuracy of models.

3.1 Pressure profile comparison

We considered a pipeline system of 50 km long in a subsea bed. Pressure measurements values are available at both the inlet and outlet. Operating parameters have been displayed in Table 2.1 to Table 2.3 above. The existence of several models in literature such as homogeneous approaches, two-phase multiplayer and drift-flux approaches for the modeling of the pressure in pipeline during two-phase flow reflects the many uncertainties in characterizing actual fluid. Figure 3.1 and figure 3.2 below, represents the curves of some selected pressure models described by equations ((1.44), (1.68), (1.73) and (1.78)) and PIPESIM models respectively, with our model. Simulations revealed that, for the considered pipeline geometry, the transportation of fluid would experience a decrease in pressure, resulting in an increase of pressure drop, due to the contributions of the gravitational and friction components. Based on this first simulation, we observed from figure 3.1 that, the predicted model (equation (2.52)) and the Beggs and Brill correlation (equation (1.46)) are closed than Wallis et al, model (equation 1.68)), Müller-Steinhagen model (equation (1.73)) and Vierra and Garcia model (equation (1.78)). From figures 3.2 and 3.3, it can be observed that, the model proposed here predict the pressure gradient better than the PIPESIM model and other models. This is because, in the predicted model, new correlations for calculating the gas compressible factor and the liquid hold up correlation were incorporated in the original pressure model. The proposed model predicted the liquid holdup using void fraction correlation from a drift flux model.

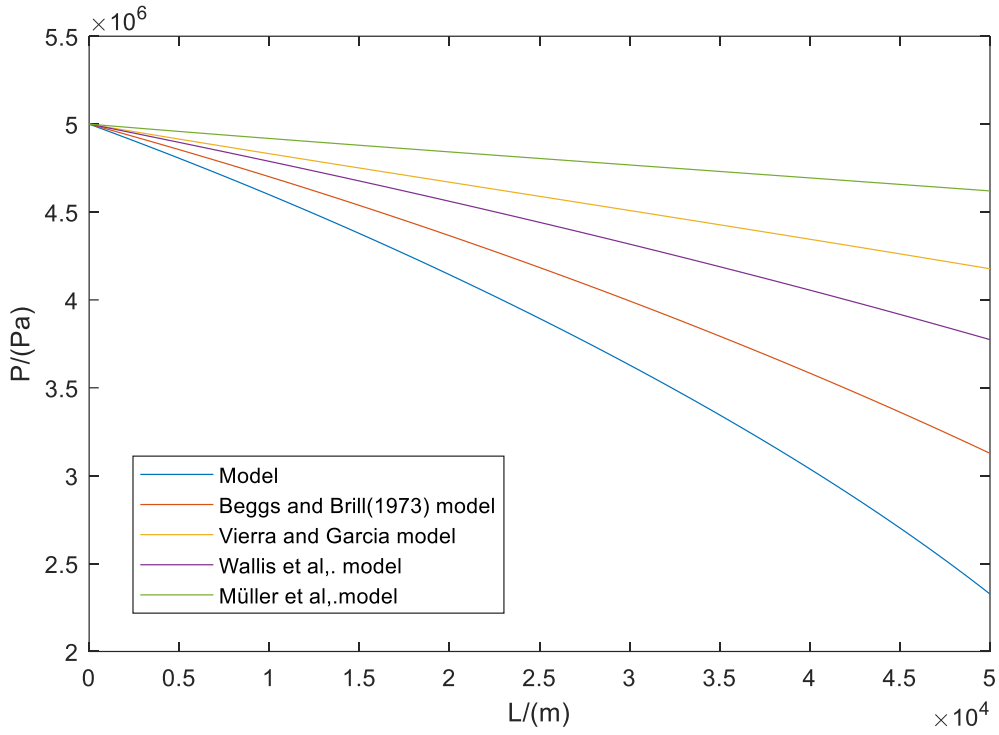

Figure 3.1: Comparison of the pressure gradient correlation

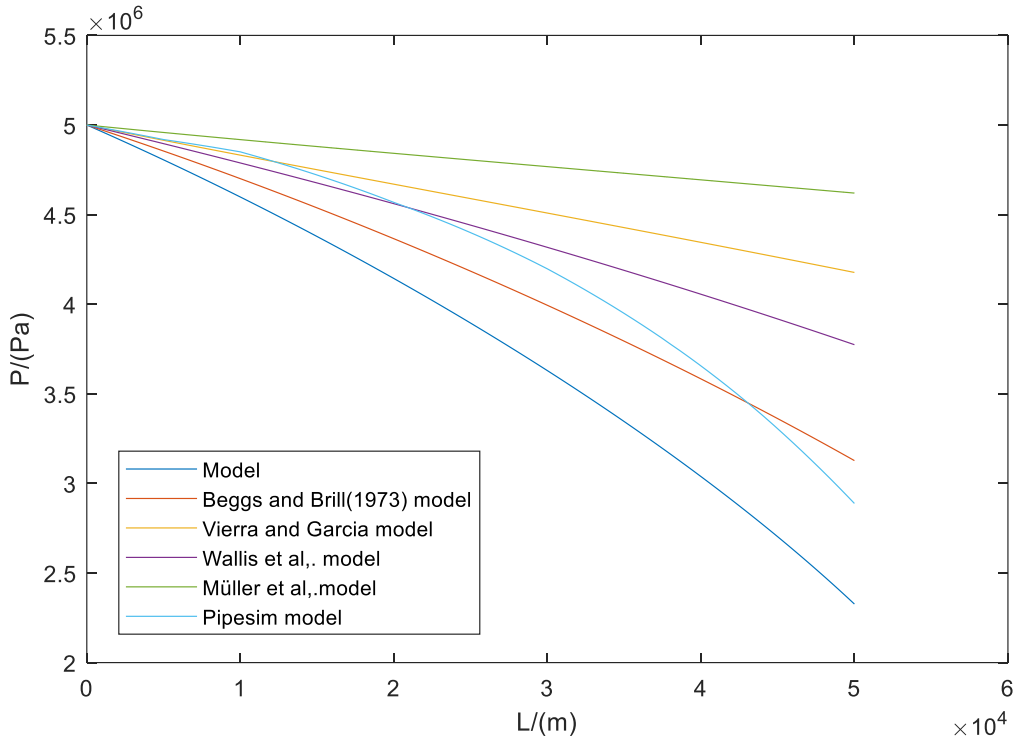

Figure 3.2 Comparison of the pressure gradient correlation with PIPESIM model correlation

From figure 3.3, we noticed that the pressure decreases along the offshore pipeline from 5×10^6Pa to 2.4327×10^6Pa. This can be explained by the fact that, the nature of the oil being transported is heavy crude oil. Heavy crude oil, have extremely low mobility due to their high viscosity. In subsea environment, their transportation is more challenging. As pressure and temperature are depending variables, a decrease in temperature may lead to the formation of some flow assurance issues such as asphaltenes, heavy metals, wax, and even hydrates, making it more challenging to production or transportation of the fluid. One can also observed that the resulting pressure drop is not linear in figure 3.3; this is due to the presence of more than one phase.

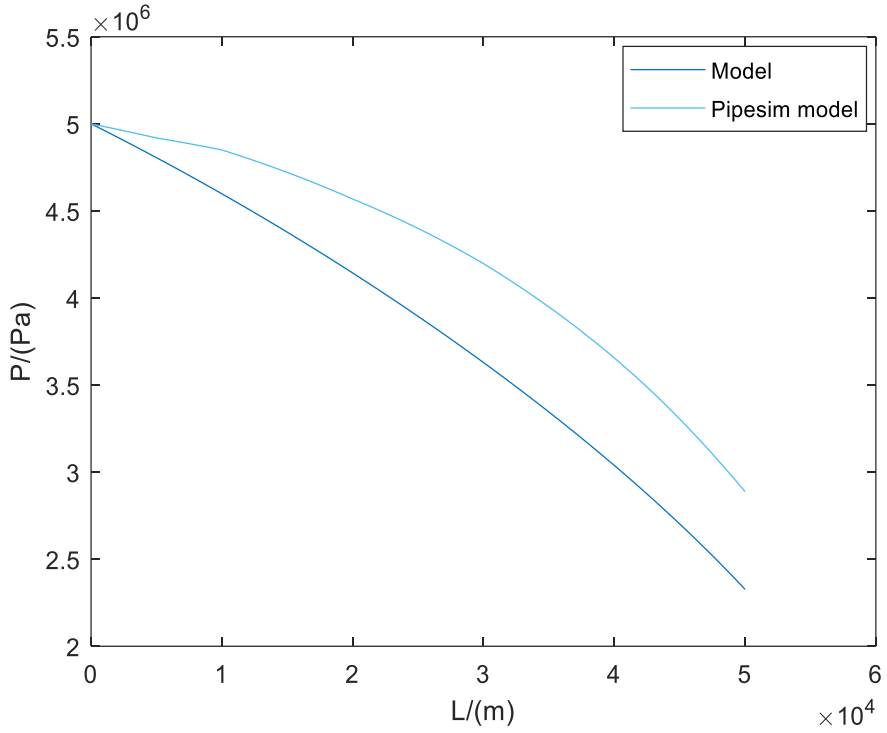

Figure 3.3: pressure profile along offshore pipeline obtained using proposed model.

From the results shown above, and when comparing with those from measured values as indicated in Table 3.1 below, it can be said that, the predicted model is the model that best described the pressure gradient along the considered subsea pipeline with a relative error of 1.26%. This performance indicator shows the capability of the model presented herein, for capturing the flow of oil and gas in subsea pipeline, and to characterize the actual fluid properties using black oil model. It also confirms that, the liquid fraction was well described using our approach .

Table.3.1: Pressure comparison and validation with the measured value (MV) [4].

Methods	Inlet pressure/ (MPa)	Endpoint pressure/ (MPa)	Pressure drop /(MPa)	REPD
Model	5	2.43	2.57	1.16%
MV	5	2.40	2.60	

3.2 Validation of the temperature profile

The temperature profile along subsea pipeline using the predicted model (equation (2.97)) is compared with the PIPESIM model, the unified predicting temperature and pressure (UPTP) model, and the measured value (MV) from [4]. From figure 3.4 below, it can be seen that, the temperature decreases along the pipeline for the both model from 323.15°k to an end point value of 278.29°k for PIPESIM and 277.99°k for our model. This is due to the heat exchanged between the hot flowing fluid inside the pipeline and surrounding cold water. It can also be observed that, the both curves have the same trend. From Table.3.2 below, it is shown that, the results obtained from our model is in good agreement with results from others models and those of the measured value (MV). In addition, our model prediction matches with the PIPESIM prediction with a relative error of 0.7%. These results indicates that, the proposed thermal model presented here is verified and accurate.

Table 3.2: Temperature drop validation (MV) as presented in [4]

Methods	Inlet temperature (°k)	Endpoint temperature (°k)	Temperature drop (°k)	RETD
Model	323.15	277.99	45.16	1.68%
PIPESIM	323.15	278.29	44.86	1.03%
UPTP	323.15	277.25	45.90	3.27%
MV	323.15	278.75	44.40	

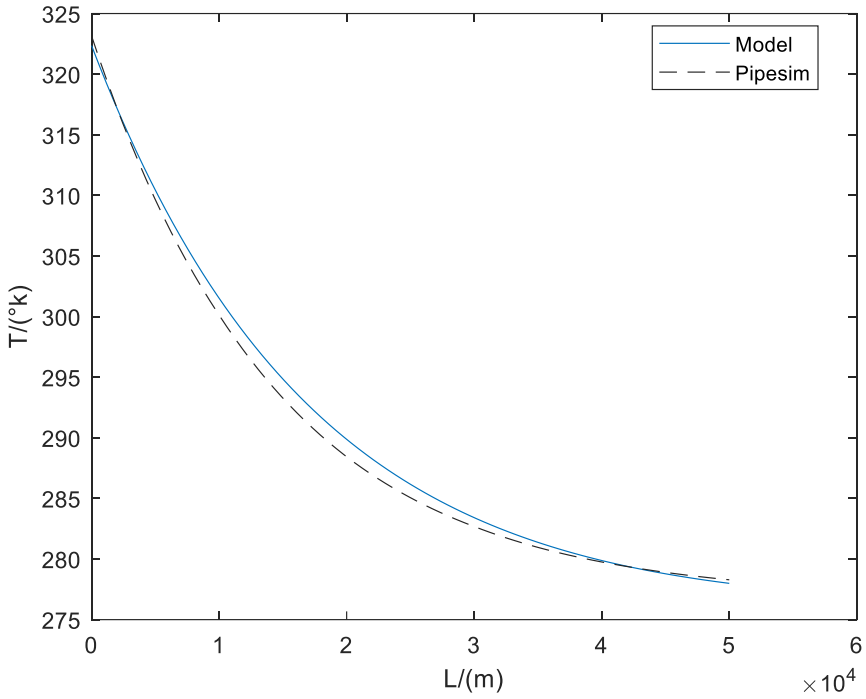

Figure.3.4 Temperature profile comparison between our model and PIPESIM model.

In this Table 3.2, the relative temperature drop (RETD) is calculated as follow:

$$RETD = \frac{Temperature\ drop\ predicted - Measured\ Value}{Temperature\ drop\ predicted} \times 100\%$$

3.3 Heat flux exchanged between the warm fluids and the seawater environment

As hot fluid flows inside pipeline surrounded by cold water, heat will flow from the hottest body to the coolest body until an equilibrium state will reach. This will result in a decrease in temperature of the warm body. Thus, figure.3.5 below, represents the curve of heat flux along the transportation pipeline. It can be observed that, heat flux decreases rapidly and tends to flattened after at about 3.5 km of flow, indicating that, warm and the cold bodies have reached to an equilibrium state.

3.4 Oil viscosity and oil flowrate variations with temperature

From figure 3.6 below, we observed that, as the temperature decreases along the pipeline, the oil viscosity increases. This increase in oil viscosity is mainly due to the heat exchanged between the surrounding seawater and hot fluid inside pipeline. The increase in oil viscosity will obviously lead to a decrease in production. While in figure.3.7 below, it is shown that, the oil flowrate decreases as the temperature decreases. This is due to the fact that, the decrease in

temperature and pressure along the pipeline, will lead to a very slow mobility of the fluid, making the transportation more difficult.

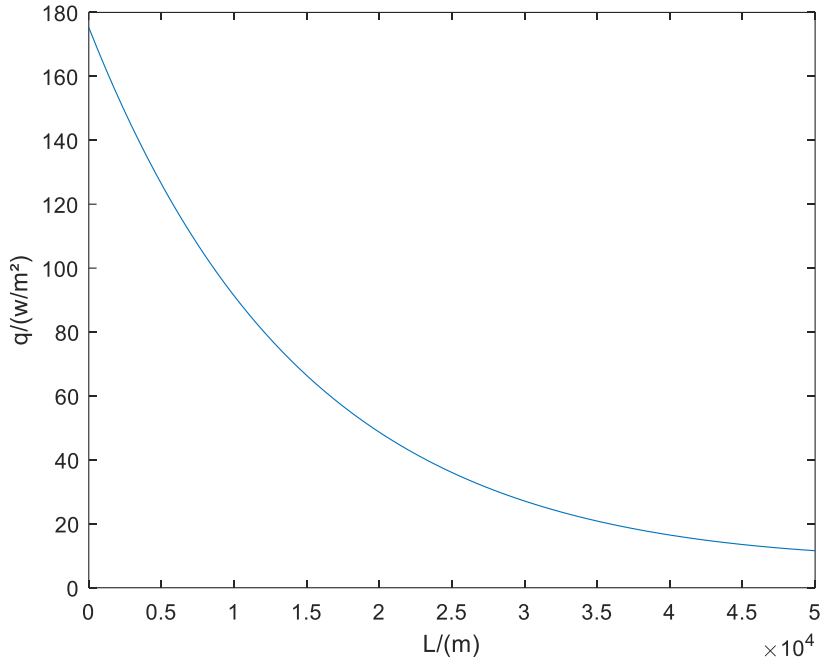

Figure 3.5 Heat flux exchange between the warm oil and gas flow and the seawater environment.

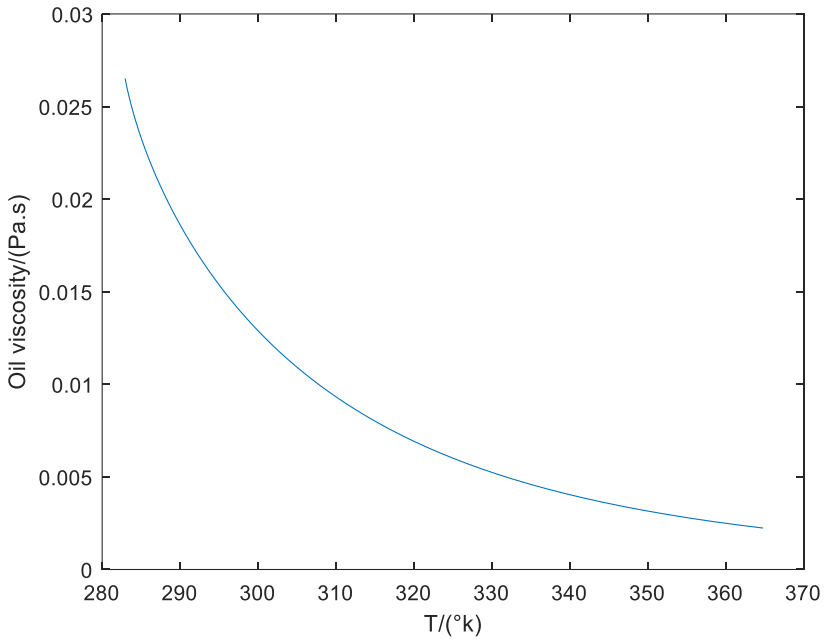

Figure 3.6: Variation of the oil viscosity with the temperature.

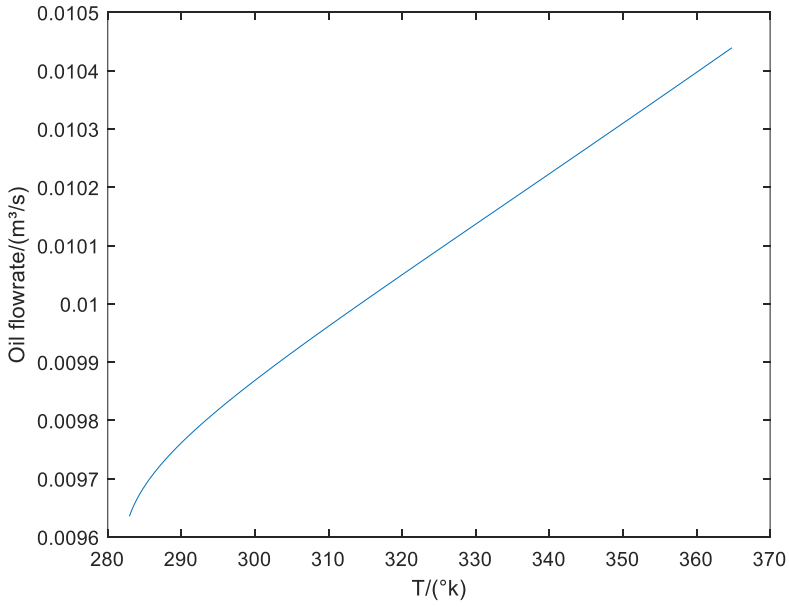

Figure 3.7 Variation of the oil flowrate with the temperature.

3.5 Effect of oil flow rate on the temperature profile

Effect of the oil flowrate was also investigated see figure 3.8 below. Results showed that as oil flowrate increases, the temperature drop decreases. This is because, increasing oil flowrate, increases the Reynolds number, which influence the overall heat transfer coefficient. Flow becomes rapid and the heat flux diminishes.

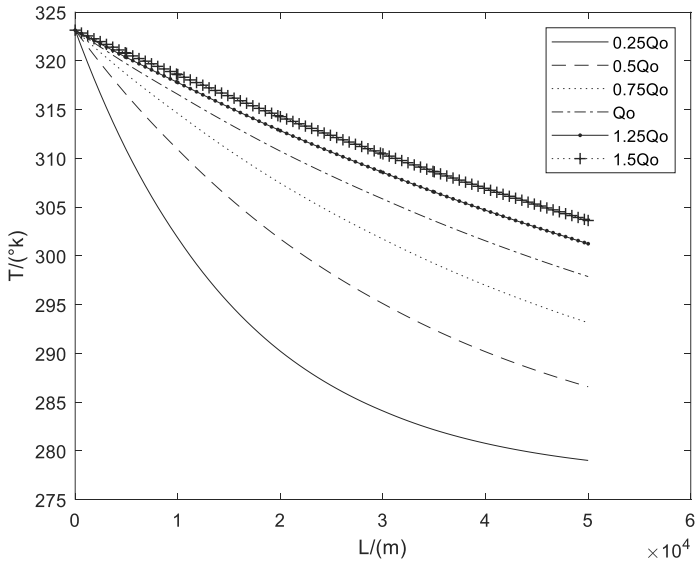

Figure 3.8 Variation of the oil flowrate with the temperature.

3.6 Optimum insulation thickness determination

After the validation of the proposed thermal model, we now used it to find out the best insulating material as well as the optimum insulation thickness by applying numerical simulations on the model and by combining genetic algorithm with supervised machine learning model. The goal is to find out the best approach to use for insulation thickness design in order to avoid material consumption and to reduce the resulting cost.

3.6.1 Application of numerical simulation for optimum insulation thickness

Here, the insulation thickness was manually defined from 254 mm to 700 mm with a step of 254 mm. for each insulation thickness value and for each insulating material, the simulation was carried out. The process ended when the minimum temperature of the system was greater or equal to the thermal requirement set in this case at 40°C.

3.6.1.1 Numerical simulations for optimum insulation thickness using Calcium Silicate insulating material

The simulations results presented in figure 3.9 below indicates that, the minimum insulation thickness that can meets the thermal requirement using calcium silicate material is comprised between 68.58 cm and 71.12 cm. More specifically, a true insulation thickness of 69.47cm will meet the requirement. This value was obtained after several simulations run and was not captured by the proposed approach. It was set as the true numerical insulation thickness of this problem for the considered case. 71.12cm was the value captured by our manual and gradual simulation. The material consumption volume was evaluated and presented in Table 3.3 below. From this Table, we observed that, the predicted values from this approach would not capture the appropriate insulation thickness that would meet the requirements of 313.15°K. This approach is time consuming and fastidious.

Table 3.3: Calcium insulation volume for different thickness

Insulation thickness (cm)	68.58	**69.47**	71.12
Absolute Relative Error	0.89		1.65
Minimum temperature (°K)	313.11	**313.15**	313.17
Insulation volume (m^3)	143589.51	**146416.62**	148123.22

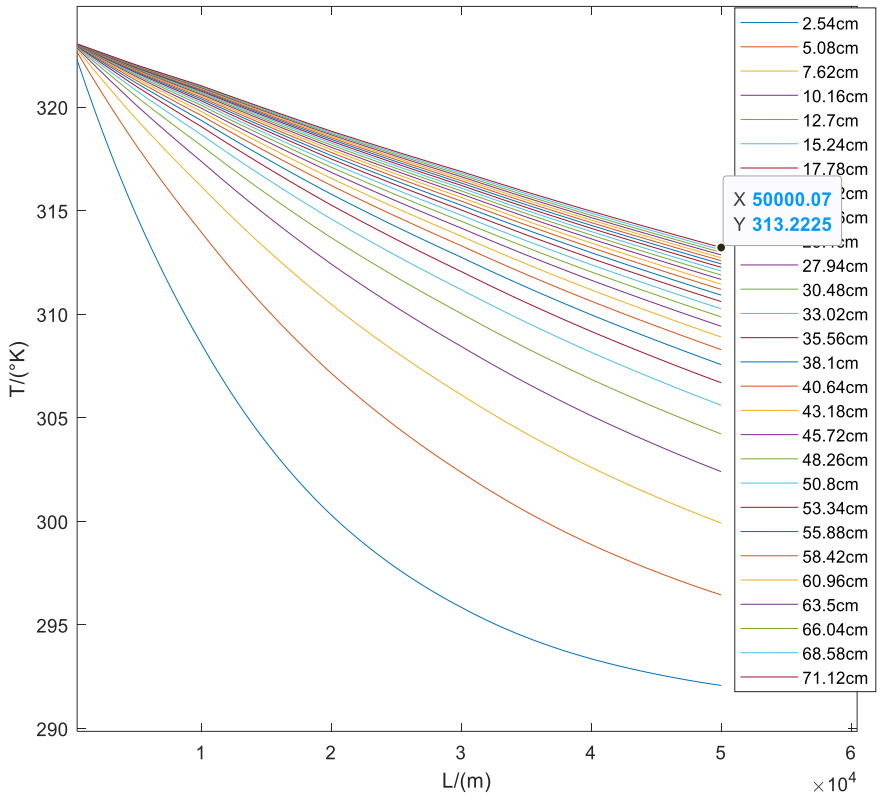

Figure 3.9: Temperature profiles of the flowing fluids inside subsea pipeline with different insulation thickness of Calcium Silicate.

3.6.1.2 Numerical simulations for optimum insulation thickness of Black Aerogel

The simulations results presented in figure 3.10 below indicates that, the minimum insulation thickness that can meets the thermal requirement using black aerogel material in this case is comprised between 7.62 cm and 10.16 cm. A true insulation thickness of 7.98 cm will meet the requirement. The material consumption volume can be seen in Table 3.4 below.

Table 3.4: Minimum temperature and insulation volume for different thickness of BA

Insulation thickness (cm)	7.62	**7.98**	**8.89**	10.16
Absolute Error	0.36		**0.91**	2.18
Minimum temperature (°K)	312.86	**313.15**	**313.78**	314.50
Insulation volume (m^3)	8661.50	**9111.37**	**9759.57**	11953.83

The minimum temperature of the predicted value of 7.62 cm is not greater nor equal to the requirement temperature of 313.15°K. From this table the nearest local minimum insulation

thickness close to the true value that is captured by our simulation with respect to the requirement is 8.89 cm. As in the case of CS presented above, we can said that, it is not obvious to find the appropriate thickness that would meet the requirements without over-estimation of raw material.

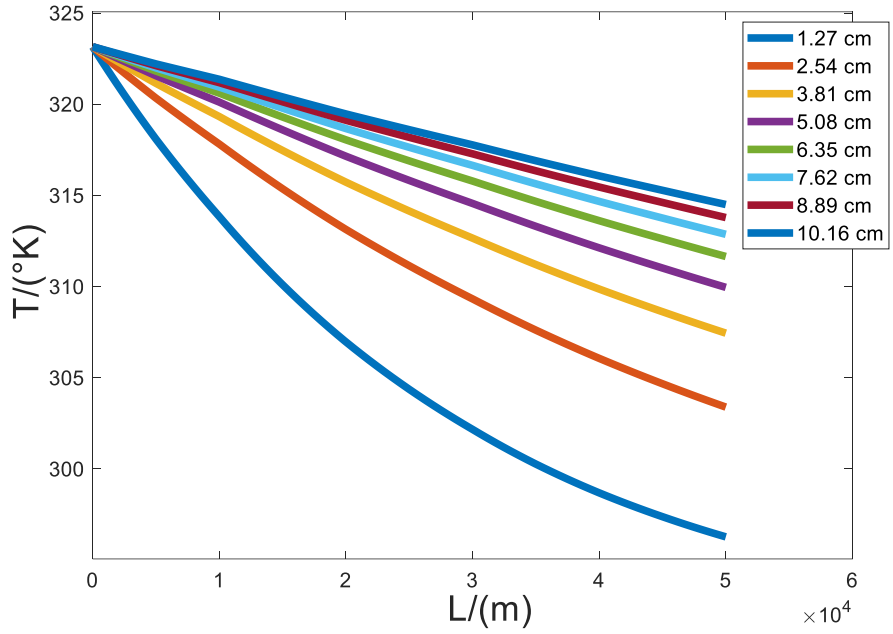

Figure 3.10: Temperature profiles of the flowing fluids inside subsea pipeline with different insulation thickness of BA

3.6.1.3 Numerical simulations for optimum insulation thickness of Polyurethane foam

The simulations results presented in figure 3.11 below indicates that, the minimum insulation thickness that can meets the thermal requirement using polyurethane foam material is comprised between 20.32 cm and 25.4 cm. more specifically, an insulation thickness of 22.30 cm will meet the requirement. The material consumption volume can be seen in Table 3.5 below. From this Table, it can be observed that, the predicted value of 22.86 cm is closely to the true value of 22.30 cm with absolute error of 0.56%.

Table 3.5: Minimum temperature and insulation volume for different thickness of PUF

Insulation thickness (m)	20.32	25.40	22.86	**22.30**
Absolute Error	1.98	3.1	0.56	
Minimum temperature (°K)	312.71	313.71	313.26	**313.15**
Insulation volume (m^3)	27148.94	35961.98	31454.17	**30491.01**

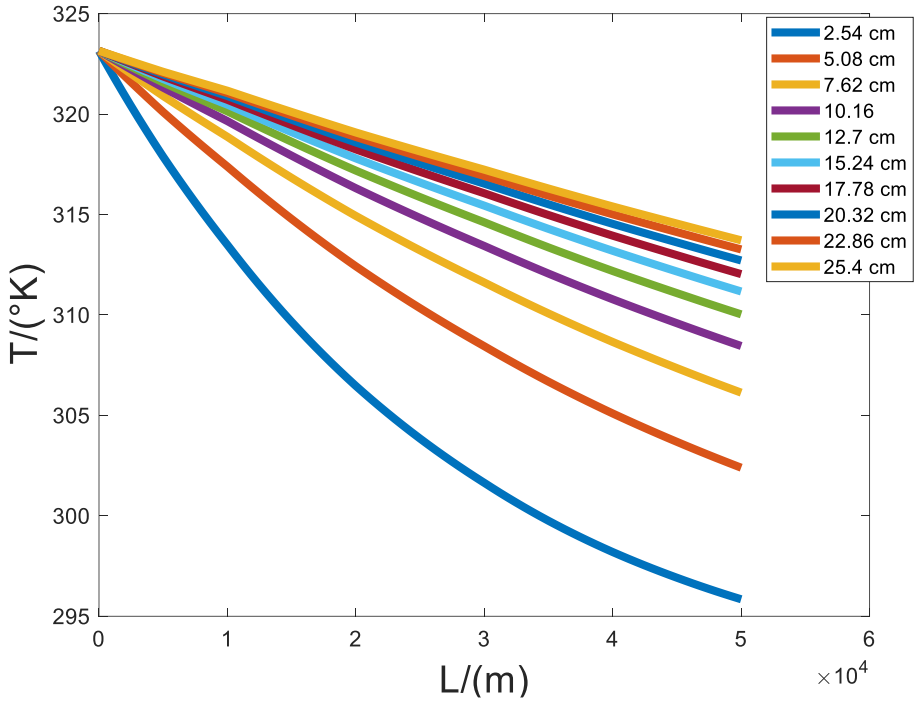

Figure 3.11: Temperature profiles with different insulation thickness of PUF.

The results obtained from Table 3.3 to Table 3.5 were summarized in Table 3.6 below.

Table 3.6: comparison of optimum insulation thickness from each insulating material

Insulating materials	Optimum insulation thickness (m) predicted	True optimum insulation thickness (m)	Insulation volume (m^3)	True insulation volume (m^3)
Calcium silicate	71.12	69.47	148123.22	146416.62
Black aerogel	**8.89**	**7.98**	**8661.50**	**9111.37**
Polyurethane foam	22.86	22.30	31454.17	30491.01

From this Table 3.6, we observed that, the insulating material that will withstand the requirement with a low insulation volume consumption is black aerogel.

3.6.2 Application of genetic algorithm combined with machine learning techniques for optimum insulation thickness using Matlab.

The purposes here was first to find out the appropriated function that best describes the relation between insulation thickness and minimum temperature of the system. Next, to verify the accuracy of the ML model and finally to combine the GA with the ML model to find out the optimum insulation thickness. For each insulating material, 200 examples of insulation configurations were randomly generated and simulated. The insulation thickness is ranged from 10 mm to 700 mm. The simulation results were randomly divided into three parts: 70% training examples (140), 10% validation examples (20), and 20% test examples (40). The type of fitting function was one of the key factors dictating the performance of the regression model. Equation (2.114) was used to fit the data of each insulating material. The regression model trained several functions with different exponential orders. Equation (3.1) below was then used to calculate the root mean square error (RMSE). Root Mean Square Error help to find how much error there is between two data sets. In order words, it compares a predicted value and an observed or known value. The smaller an RMSE value, the closer predicted and observed values are. It can be calculated using the formula below:

$$RMSE = \sqrt{\frac{\sum_{i=1}^{n}(Predicted_i - Observed_i)}{n}} \tag{3.1}$$

For the case of black aerogel, the RMSE and the correlation coefficient were plotted against the exponential power of the fitting function. These curves were displayed in order to determine the order of the exponential power of the fitting function in the regression model. Figure 3.12 below and figure 3.13 were obtained after several simulations for the case of BA. The training error indicates how well the algorithm is fitting the training data. The validation error and test error indicate the prediction accuracy of the trained. As shown in Figure 3.12 below, the three errors decreased in relation to a decrease exponential order, and they flattened after the -0.75 order, thus indicating that, adding terms with an order smaller than this order would not improve regression performance. From figure 3.13 below, we observed that, the correlation coefficient of the predicted function increases as the exponential order decreases and flattened after the order of -0.75. Thus, the fitting function with an order of -0.75 were then chosen for the optimization algorithm used in this case. The same process were performed for the cases of calcium silicate and polyurethane foam and the results were represented by the graphs in figure 3.14 to figure 3.17.

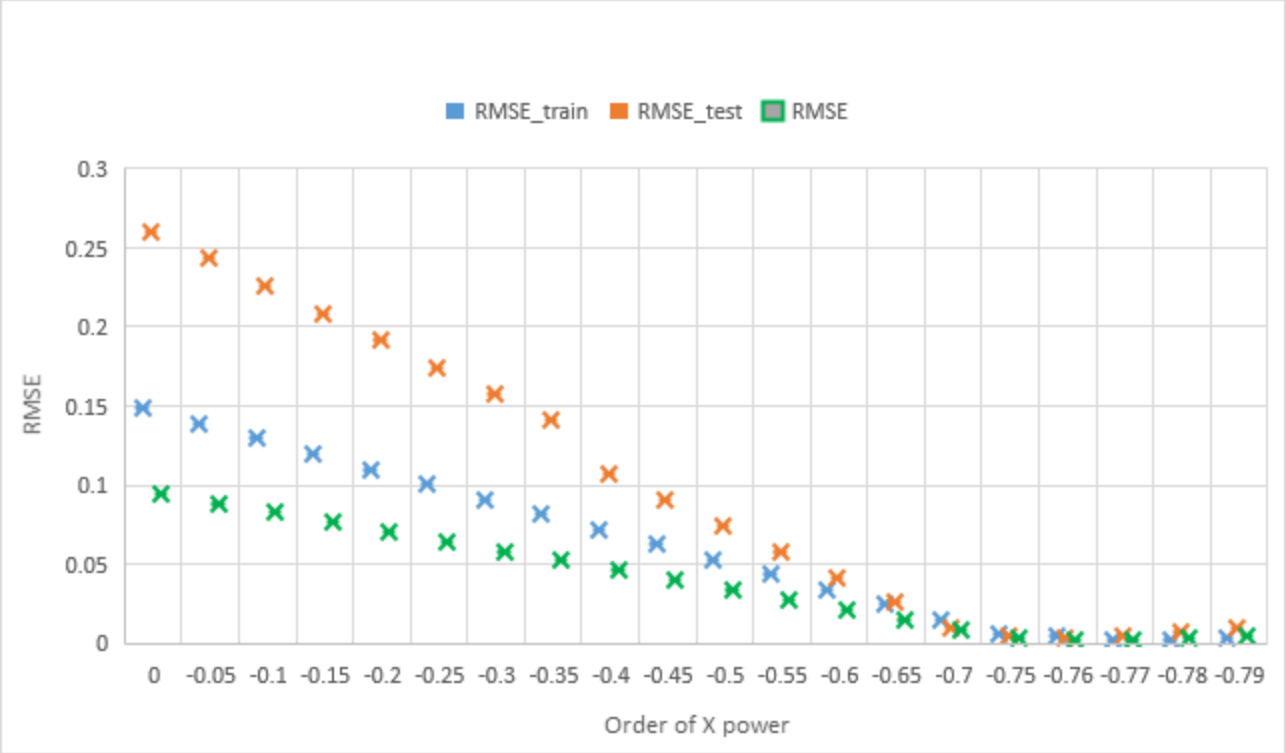

Figure 3.12: RMSE vs order of X power in the fitting function: case of BA material

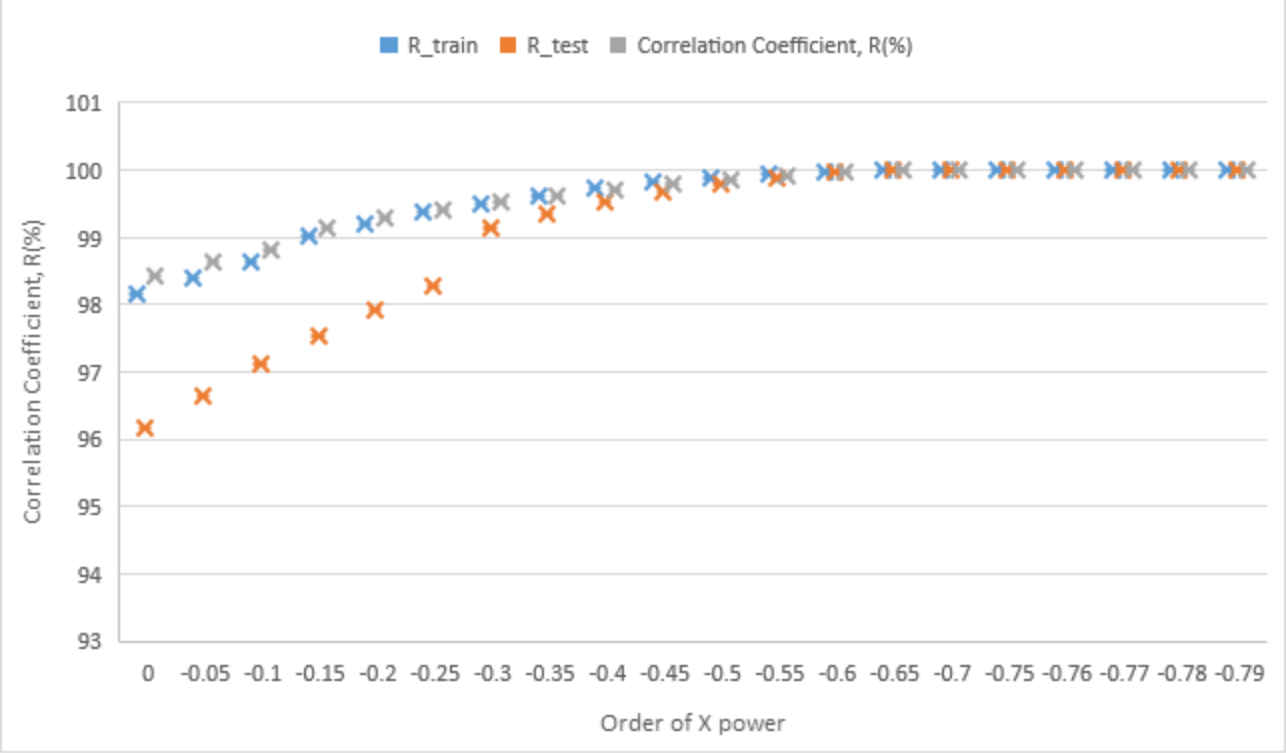

Figure 3.13: Correlation coefficient R (%) vs X order in the fitting function: B.A case

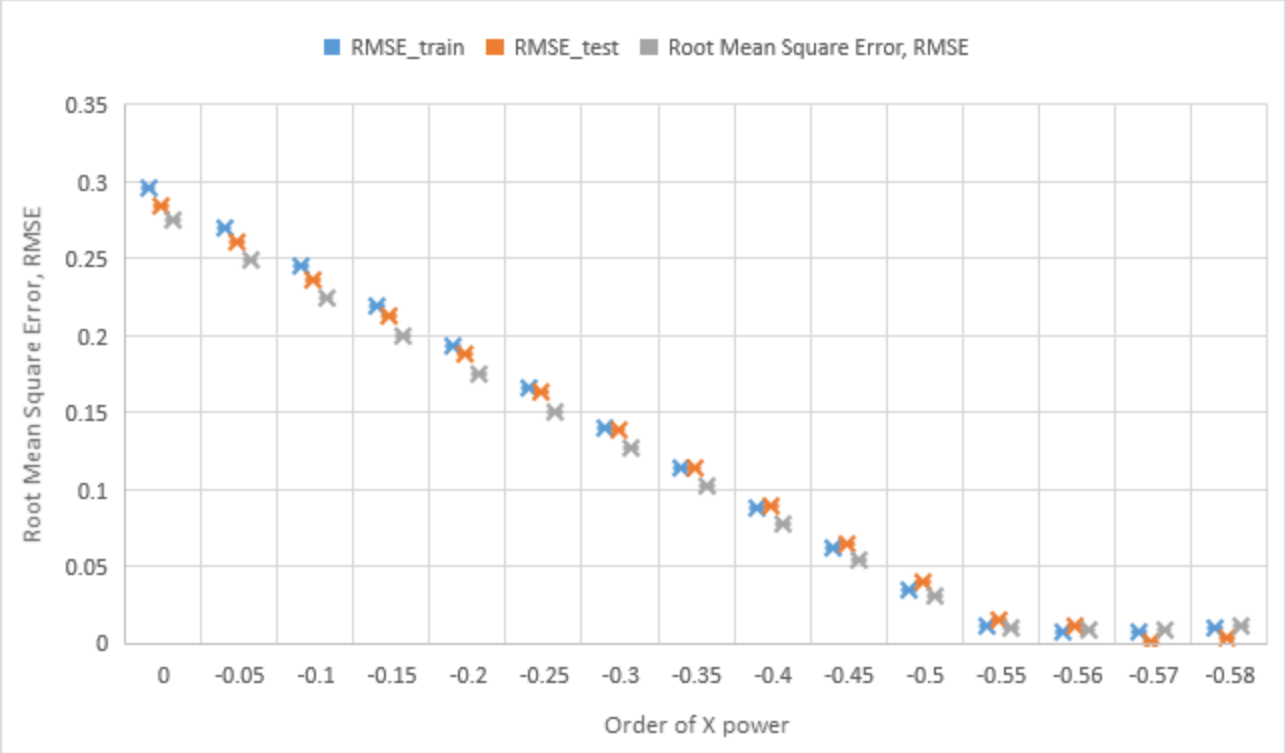

Figure 3.14: Root mean square error vs X order in the fitting function: Calcium silicate case

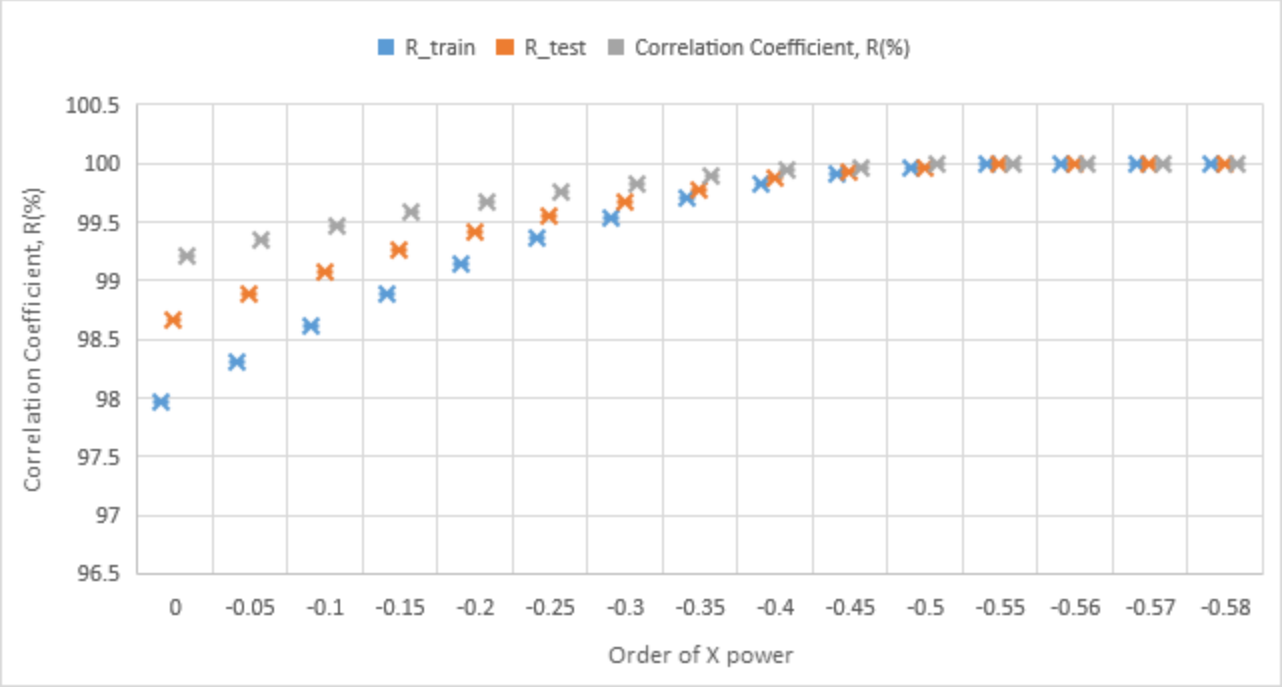

Figure 3.15: Correlation coefficient vs X order in the fitting function: Calcium silicate case

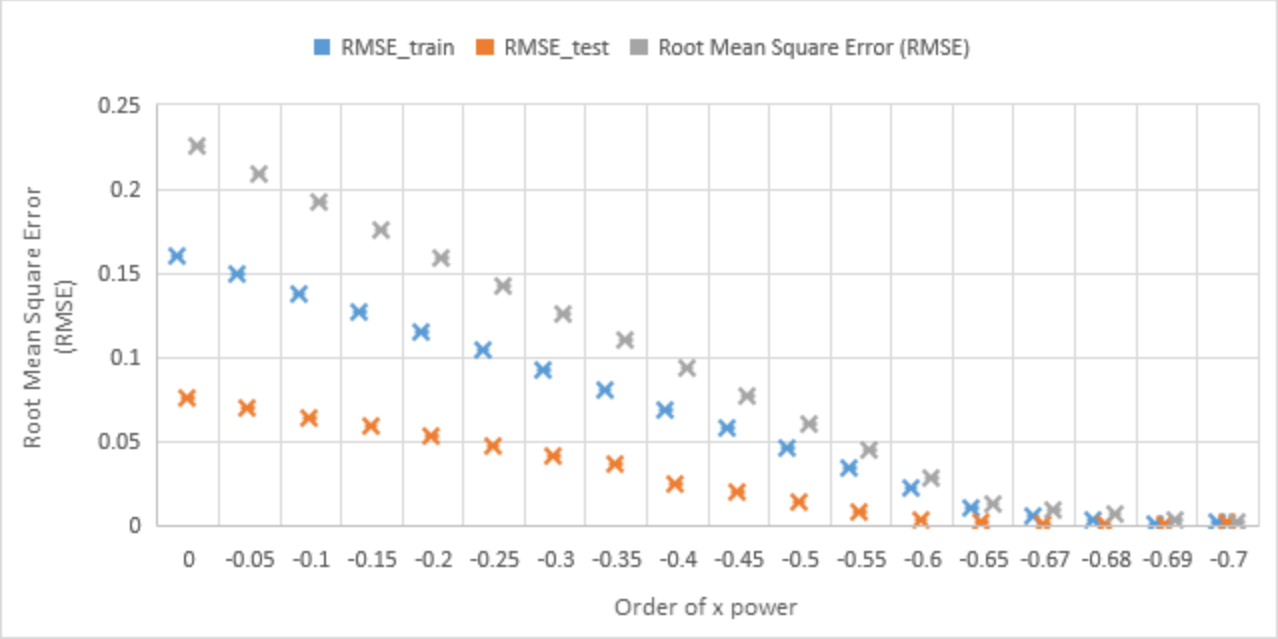

Figure 3.16: RMSE vs X order in the fitting function: Polyurethane foam case.

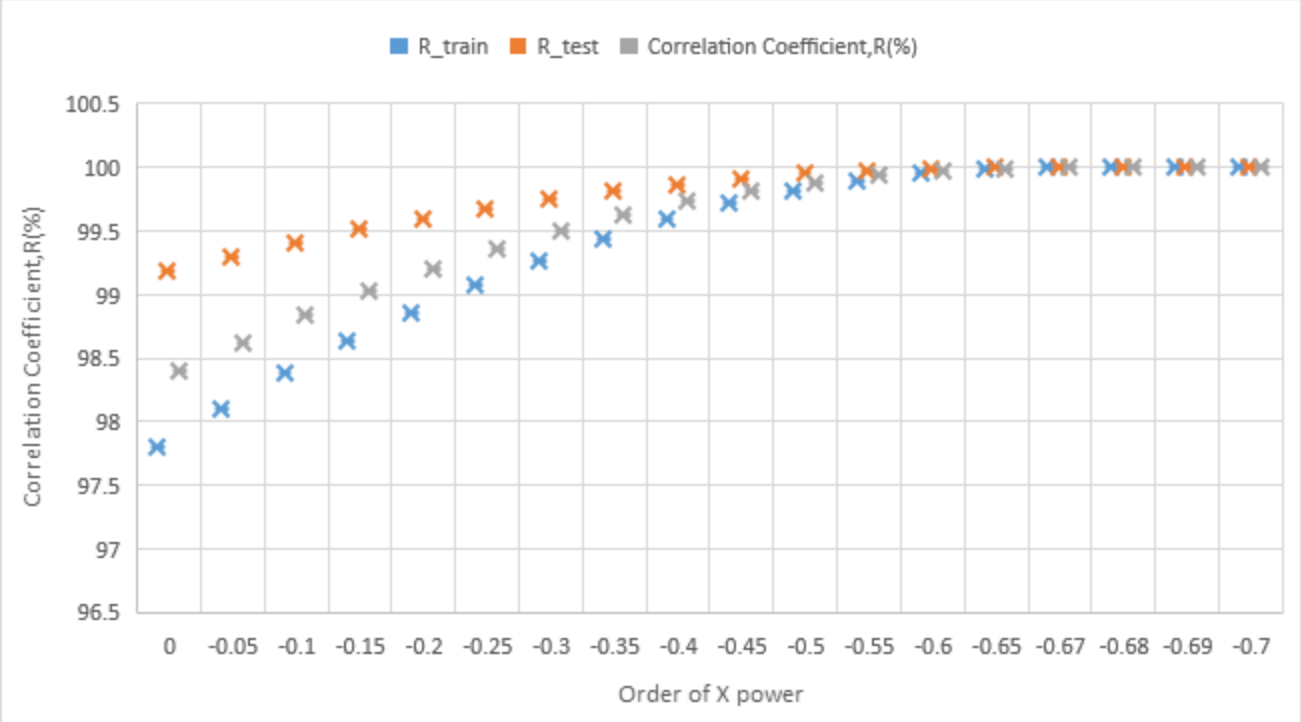

Figure 3.17: Correlation coefficient vs X order in the fitting function: Polyurethane foam case.

From the curves displayed above, the order of each fitting function for each insulating material was determined and the form of each equation was obtained after several simulations by verifying in each run simulation that the fitting function has neither a high variance nor a

high bias. The controlled factor was set to zero. Table 3.7 below presents the various equations forms for each insulating material.

Table 3.7: forms of predicting equation for each insulating material

Insulating materials	Equation forms
Black Aerogel	$T_{\min BA} = 321.164 - 212 * X^{-0.75}$
Calcium Silicate	$T_{\min CS} = 318.638 - 228.48 * X^{-0.57}$
Polyurethane Foam	$T_{\min PUF} = 319.734 - 274.699 * X^{-0.69}$

In order to test the performance of these functions, ten insulation thickness, which had never been fed to the learning functions, were randomly created. The minimum temperatures were calculated using the trained functions and compared with results given by thermal model. Figure 3.18 to figure 3.23 below illustrates the comparison and the performance of the fitting functions for each insulating material. As shown in Tables 3.8, 3.9 and 3.10, the regression model performed well in predicting the minimum temperature. The average absolute error was 2% for the case of black aerogel, 7.37% for the calcium silicate case and 2.5% for the polyurethane foam case. The regression successfully built a nonlinear and accurate pattern between insulation thickness and the minimum temperature of the subsea production system for each insulating material.

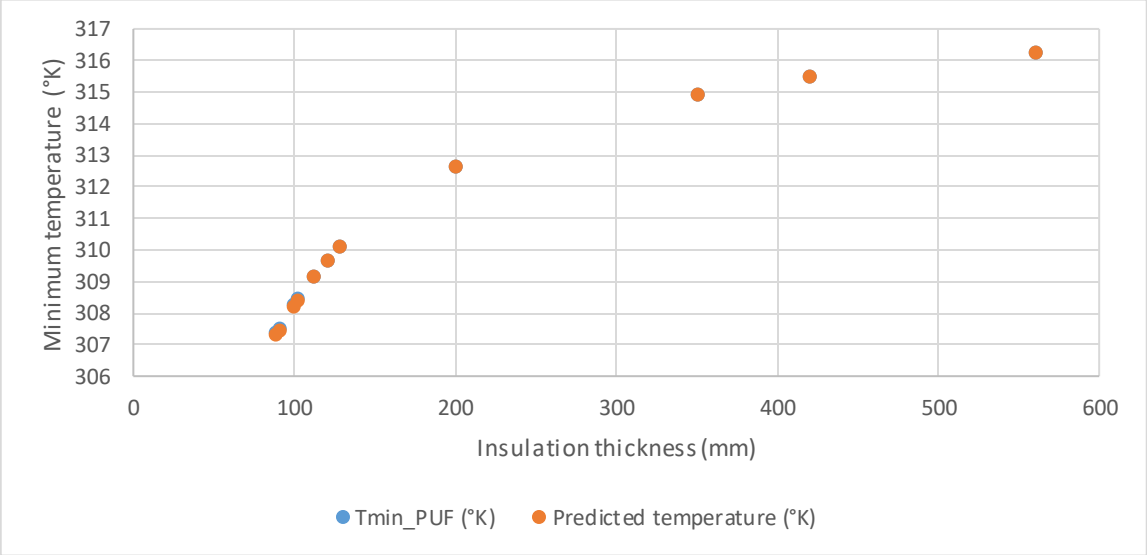

Figure 3.18: comparison of the predicted Tmin of PUF and the Tmin of PUF obtained from the thermal model.

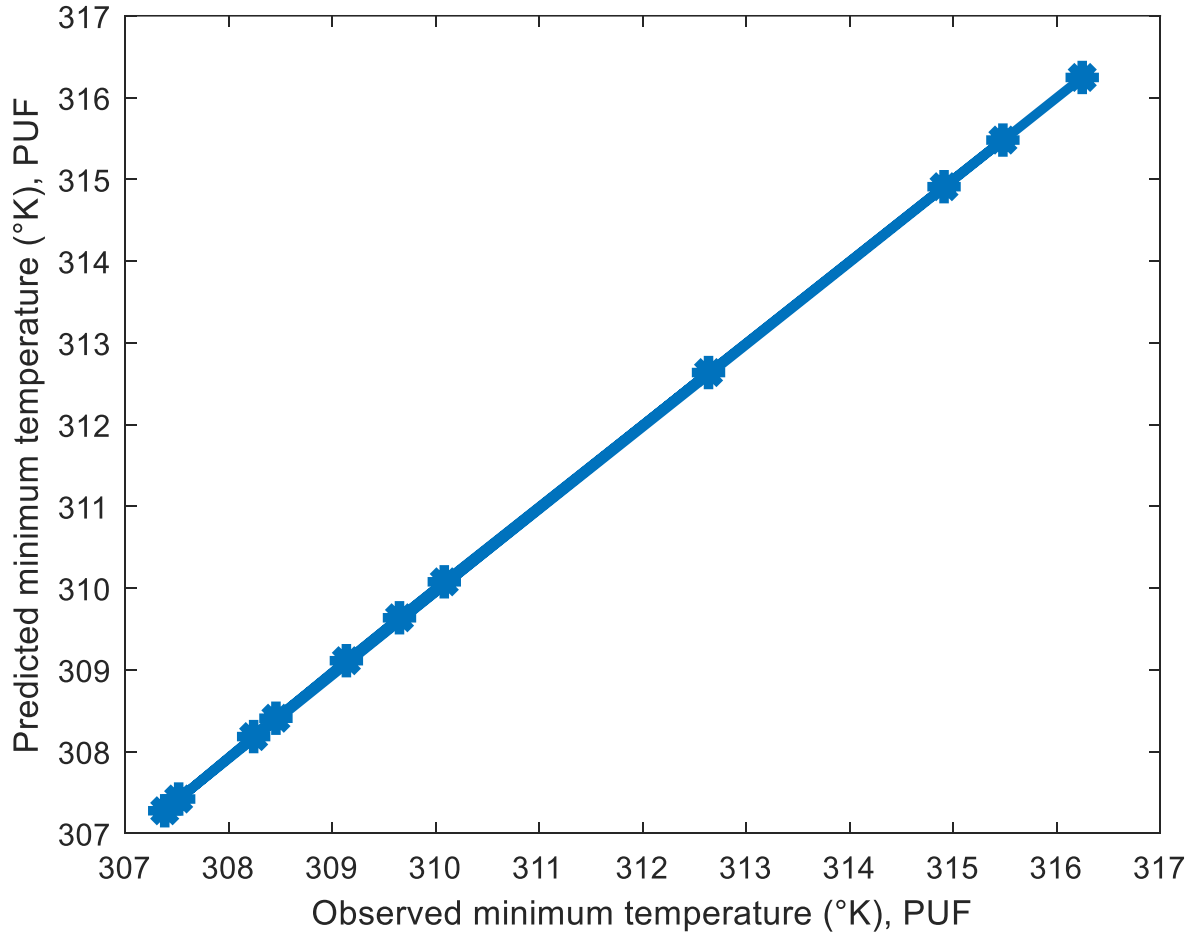

Figure 3.19: Fitting of the predicted Tmin of PUF and the Tmin of PUF obtained from the thermal model.

Table 3.8: Minimum temperature calculated and minimum temperature predicted of PUF

Insulation thickness (mm)	Tmin Observed (°K)	Tmin Predicted (°K)	Absolute Error
101.6	308.45	308.40	0.05
200	312.63	312.63	0.00
90	307.51	307.41	0.10
120	309.64	309.63	0.01
420	315.47	315.47	0.00
350	314.91	314.90	0.01
128	310.08	310.07	0.01
111.5	309.13	309.11	0.02

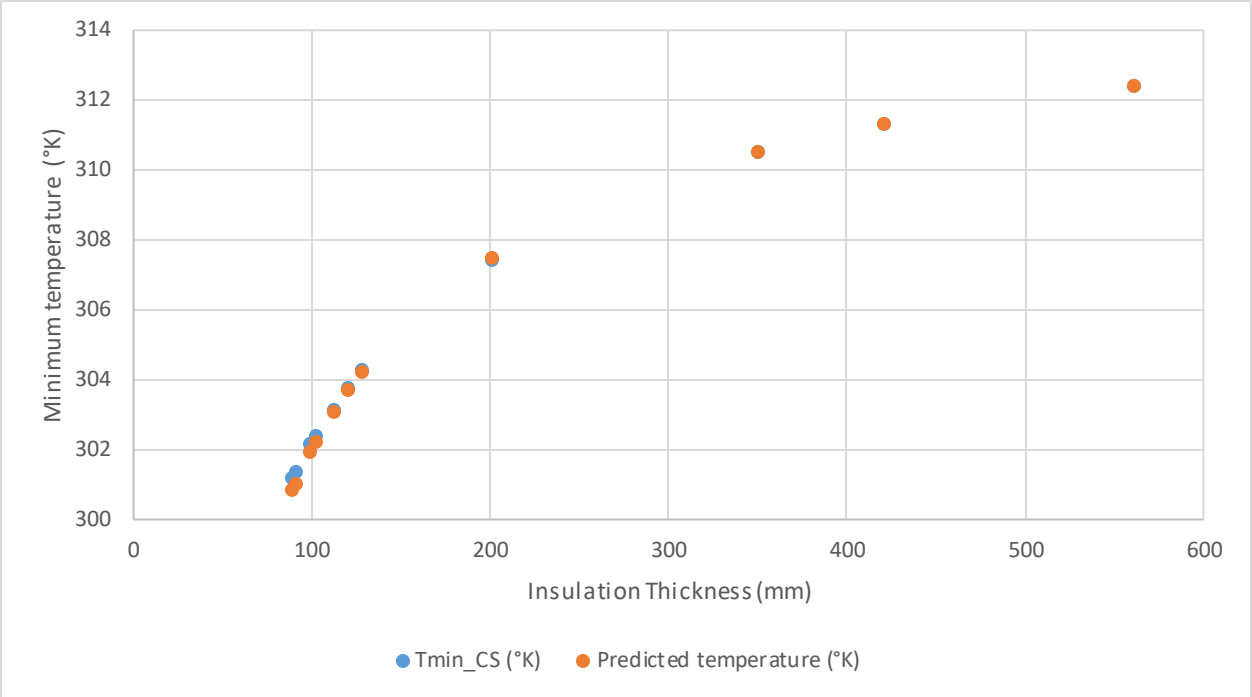

Figure 3.20: comparison of the predicted Tmin of CS and the Tmin of CS obtained from the thermal model.

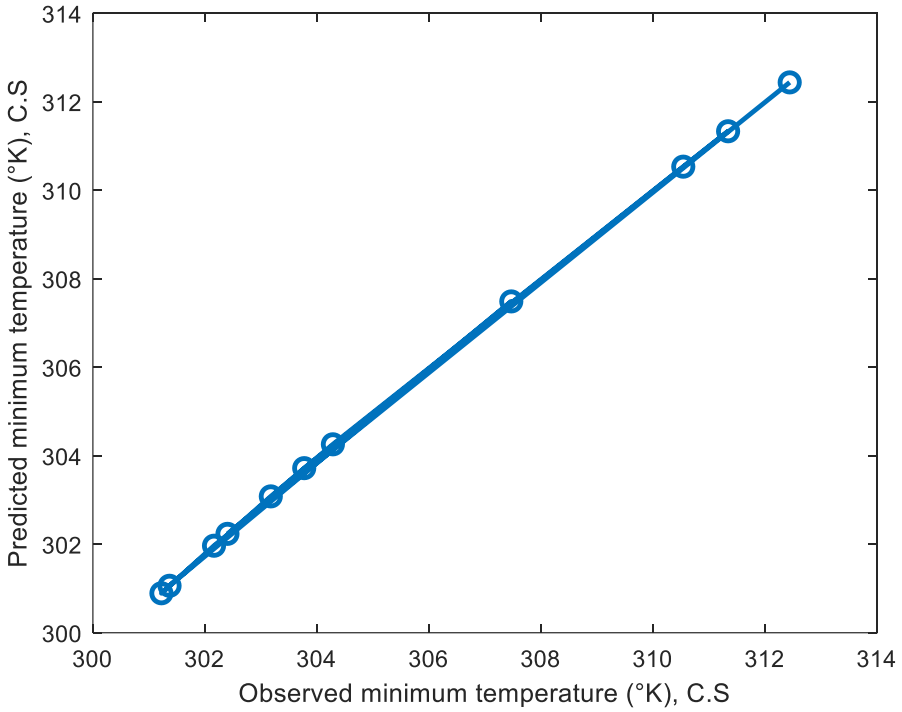

Figure 3.21: Fitting of the predicted Tmin of CS and the Tmin of CS obtained from the thermal model.

Table 3.9: Minimum temperature calculated and minimum temperature predicted of CS.

Insulation thickness (mm)	Tmin Observed (°K)	Tmin Predicted (°K)	Absolute Error
101.6	302.40	302.23	0.17
200	307.46	307.48	0.02
90	301.36	301.06	0.30
120	303.77	303.71	0.07
420	311.33	311.33	0.00
350	310.53	310.53	0.00
128	304.28	304.25	0.03

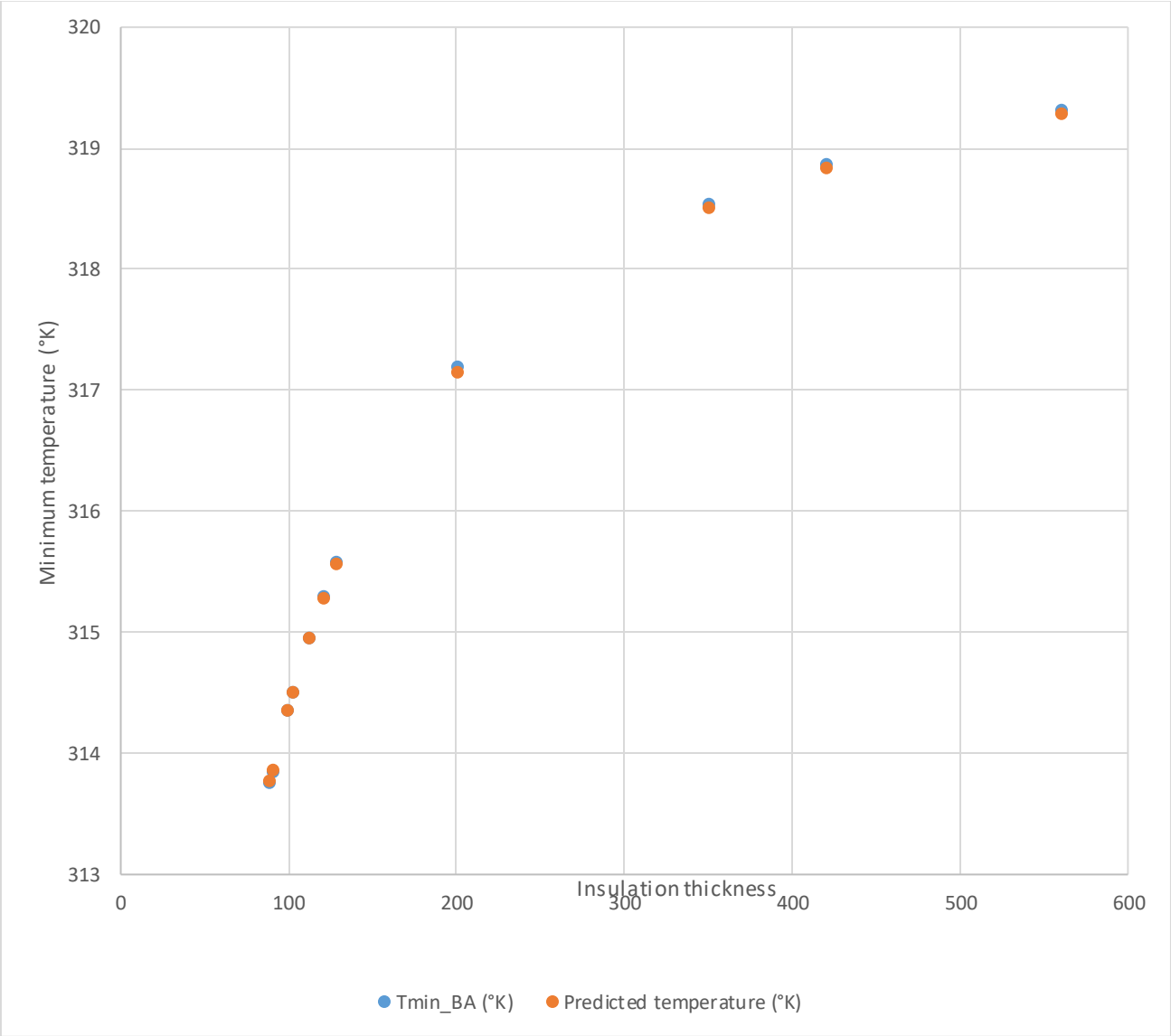

Figure 3.22: comparison of the predicted Tmin of B.A and the Tmin of B.A obtained from the thermal model

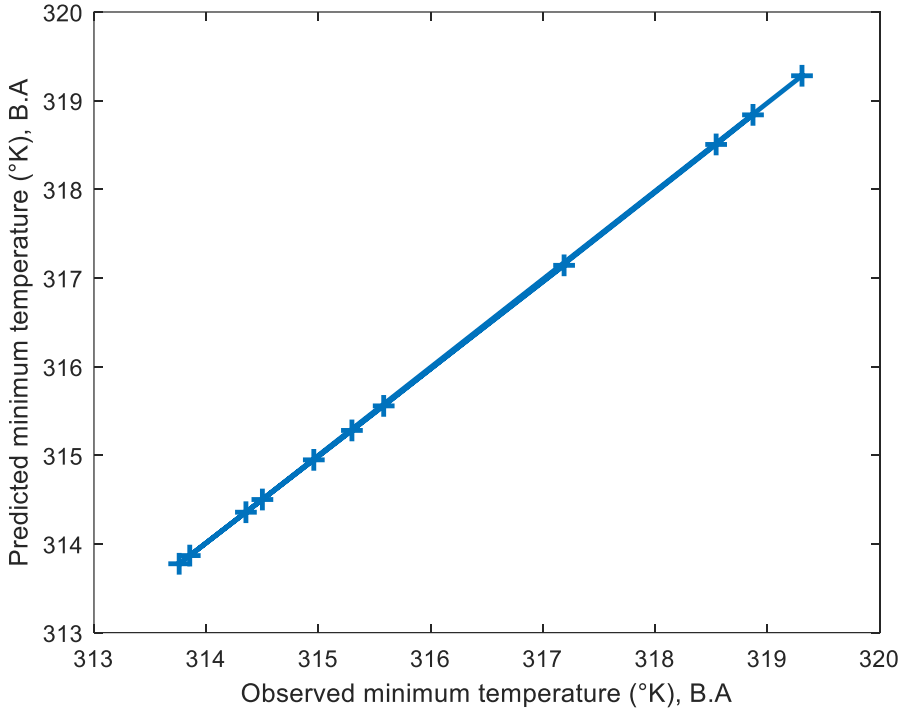

Figure 3.23: Fitting of the predicted Tmin of B.A and the Tmin of B.A obtained from the thermal model.

Table 3.10: Minimum temperature calculated and minimum temperature predicted of B.A.

Insulation thickness (mm)	Tmin Observed (°K)	Tmin Predicted (°K)	Absolute Error
101.6	314.50	314.50	0.00
200	317.18	317.14	0.04
90	313.85	313.86	0.01
120	315.29	315.28	0.01
420	318.87	318.83	0.04
350	318.54	318.50	0.04
128	315.58	315.55	0.03

Further, we carried out optimization to minimize the volume of insulation material using genetic algorithm (GA) taking into account the constraint for steady state flow set herein at 40°C. We make used of the MATLAB optimization toolbox. The population size was set at 50, because we had fewer variables, not up to five, and the maximum iteration was 100. The GA toolbox was then applied in programming the algorithm. GA was run for each insulating material and the results were plotted as shown below.

For the case of black aerogel (B.A), figure 3.24 is a plot of the best objective function value in each generation. It can be seen that, the best insulation volume is about 9067.194 m^3 for an optimum insulation thickness of 79.38 mm. These solutions are obtained after only 7 generations.

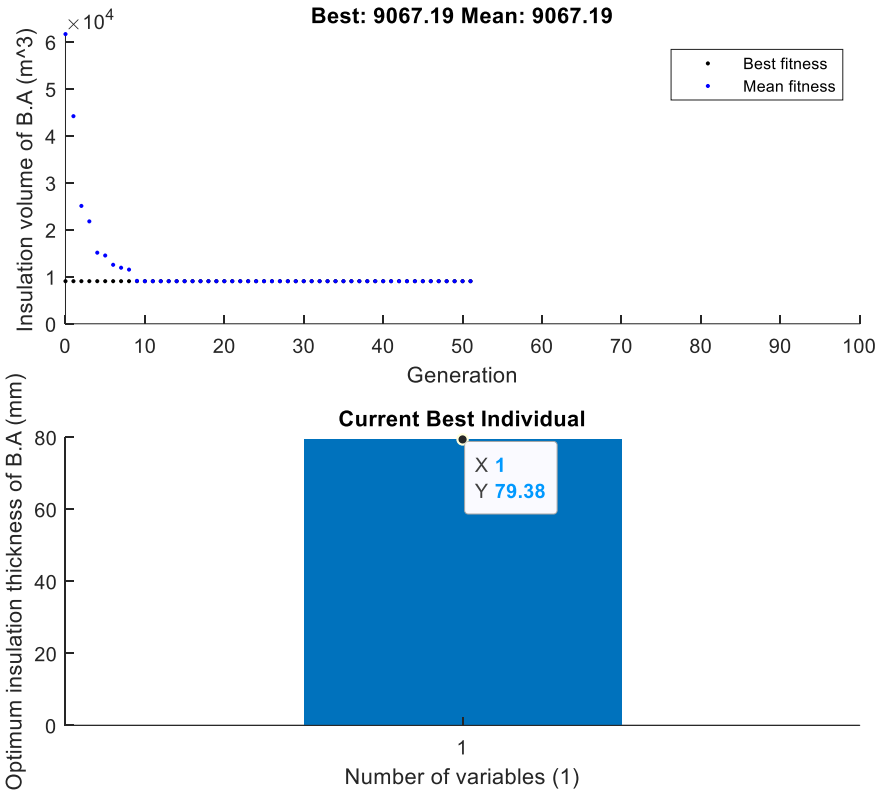

Figure 3.24: Best insulation volume and optimum insulation thickness of B.A using G.A

We run multiple objective function optimization in order to find out the best set of optimal solutions. The goal was to minimize the insulation volume and the minimum temperature of the system. Figure 3.25 is a plot of the first objective function (insulation volume) against the second function (minimum temperature). From this figure, one can easily see the non-dominated solution point of the two objectives functions. This solution point is given by 313.15°K for the minimum temperature of the system and 9067.194 m^3 for the insulation volume. The corresponding optimal insulation thickness is 79.38 mm. Figure 3.26 represents the plot of the maximum violation constraint. This constraint converged to 0, indicating that the insulation design would meet the requirement. The Pareto front in figure 3.25 as well as the maximum constraint given in figure 3.26 below ensured that, the insulation design would meet the temperature constraint.

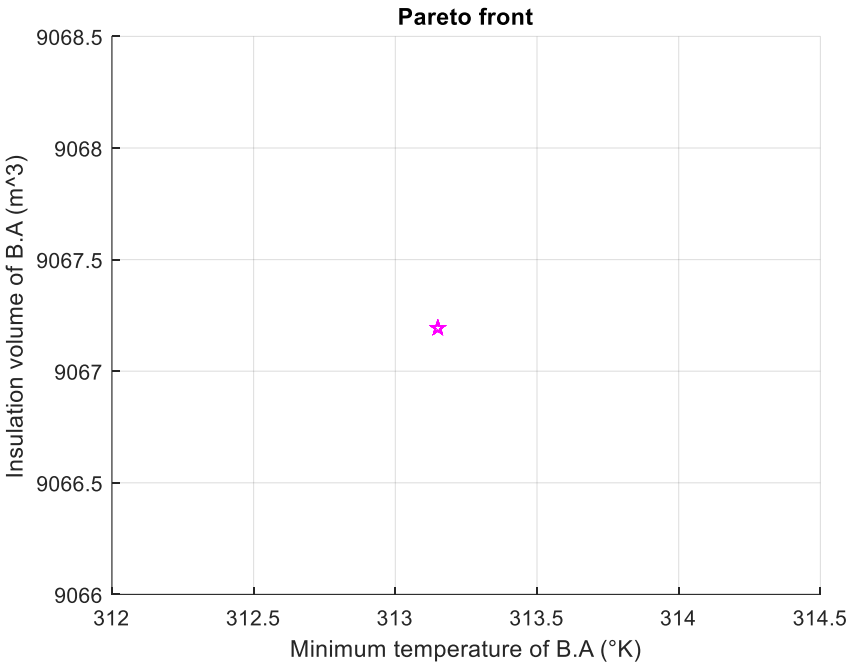

Figure 3.25: Pareto front of insulation volume against minimum temperature of B.A using G.A

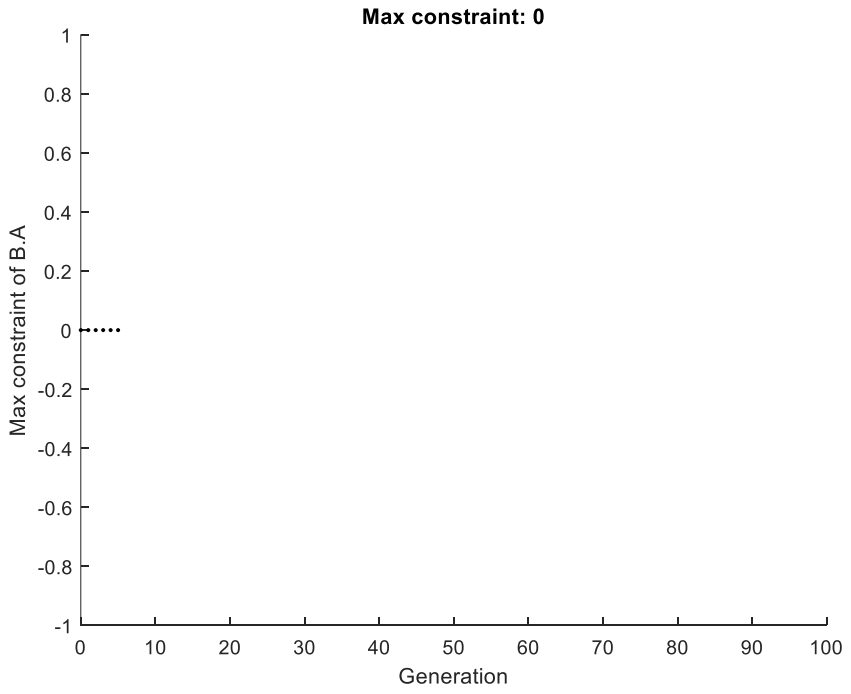

Figure 3.26: Maximum constraint violation for the case of B.A

The same analysis was applied in the cases of calcium silicate (CS) and polyurethane foam (PUF). Thus, from figure 3.27 below, it is shown that, the minimum insulation volume of

the calcium silicate insulating material is 146148 m^3 and the best insulation thickness is 693.605 mm.

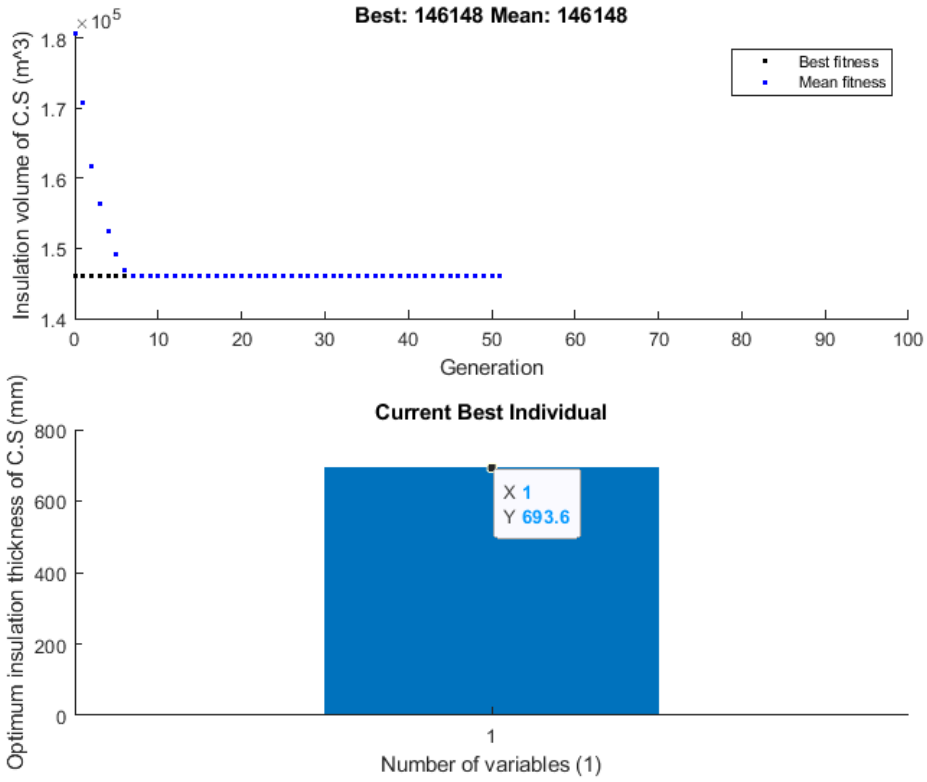

Figure 3.27: Best insulation volume and optimum insulation thickness of C.S using G.A

The Pareto front represented in figure 3.28 below shows the optimal solution of the multiple objective's optimization run. In this figure, it can be observed that, the best solution of the minimization of the insulation volume and the minimum temperature of the system is given by 313.15°K and 146148 m^3. In figure 3.29, we observed that, the maximum constraint violation converged to 0, indicating that the objective function would satisfy the constraint requirement.

For the polyurethane case, figure 3.30 below is a plot of the best insulation volume using the G.A. from this figure, it is shown that the optimal insulation volume is 30507,8 m^3. This result was obtained after 10 generations. In figure 3.31 below, the Pareto front shows the optimal solution of the multiple objective's optimization run. In this figure, we can observe that the best solution of the minimization of the insulation volume and the minimum temperature of the system is given by 313.15°K and 30507.8 m^3. The maximum constraint violation

converged to 0 from figure 3.32 above. This indicates that the objective function satisfied the constraint requirement.

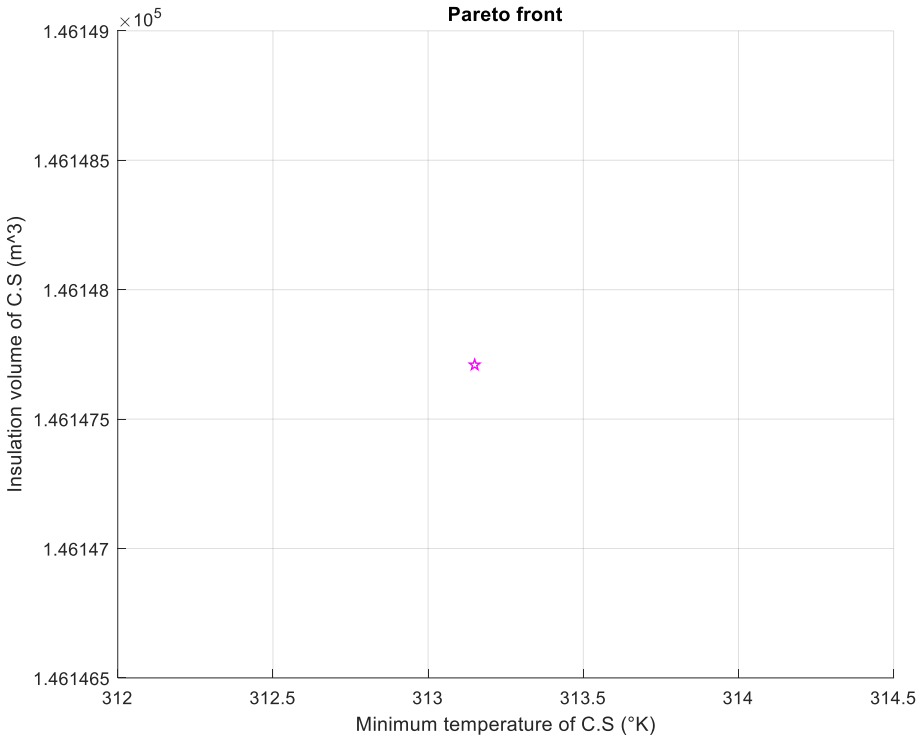

Figure 3.28: Pareto front of insulation volume and minimum temperature of C.S using G.A

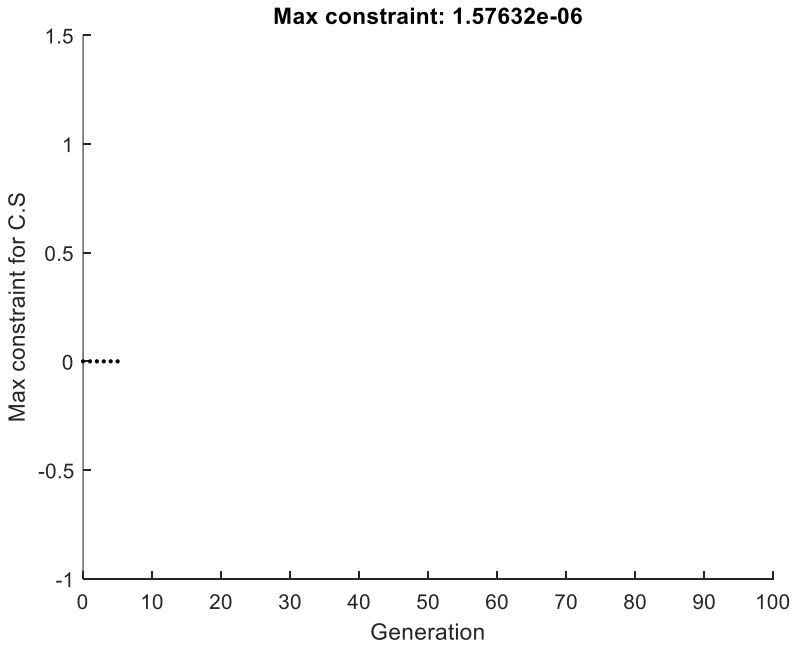

Figure 3.29: maximum constraint violation for the case of C.S

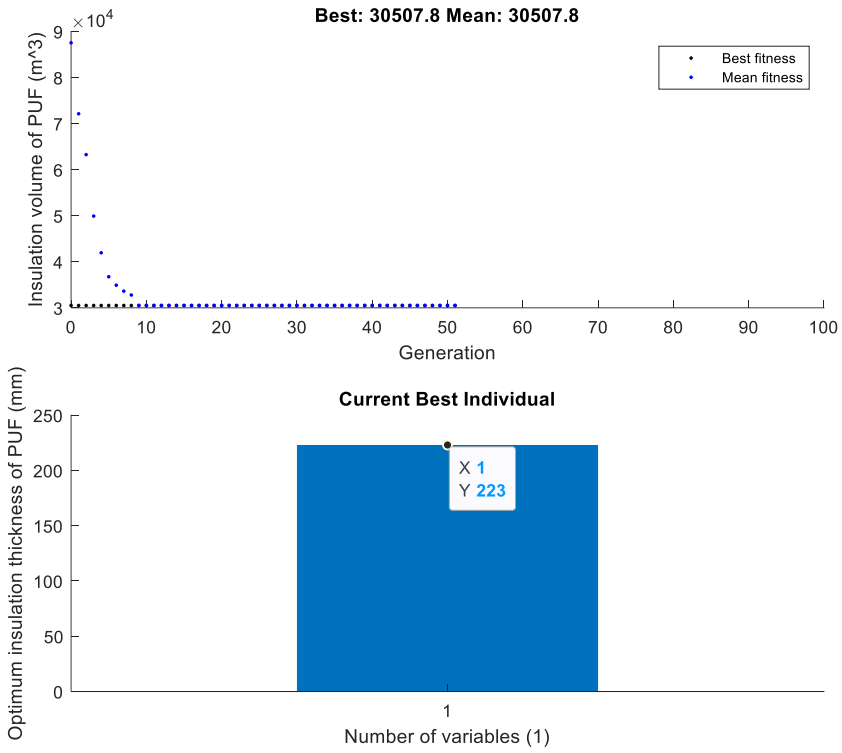

Figure 3.30: Best insulation volume and optimum insulation thickness of PUF using G.A

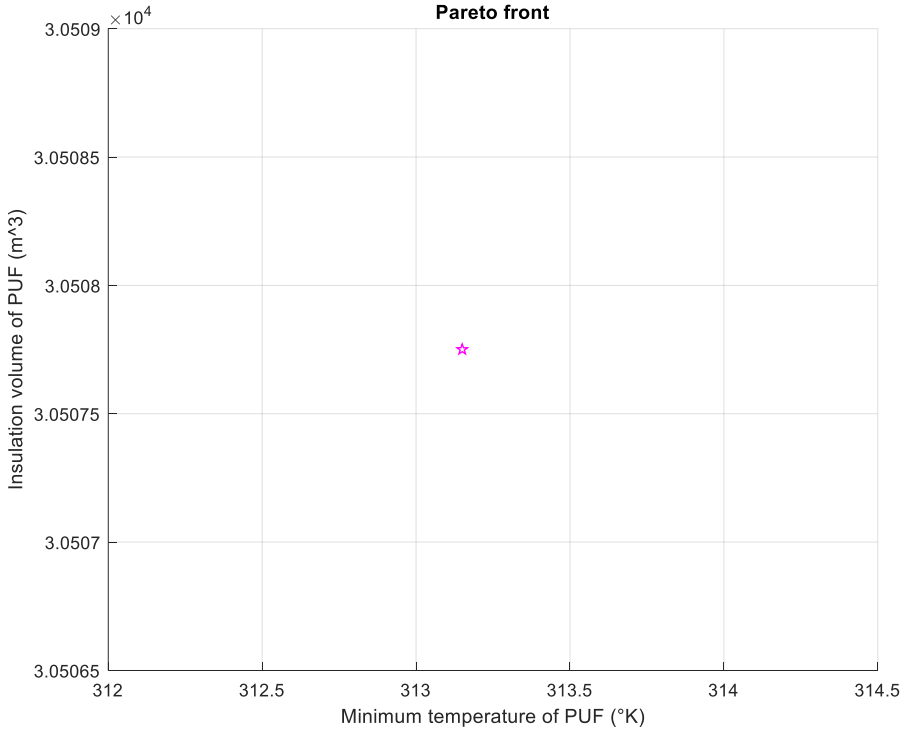

Figure 3.31: Pareto front of insulation volume and minimum temperature of PUF using G.A

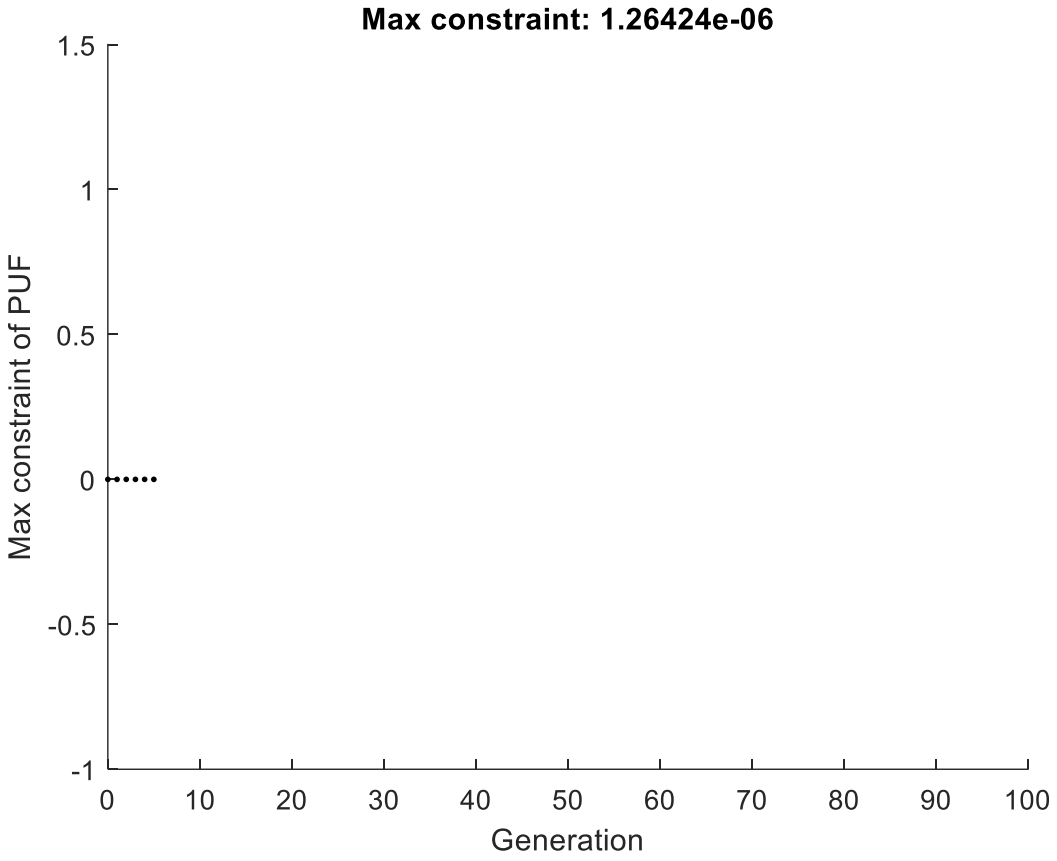

Figure 3.32: maximum constraint violation for the case of PUF

3.6.3 Application of genetic optimization on machine learning techniques for optimum insulation thickness using RAPIDMINER

For the purpose of validation and comparison, RAPIDMINER was used with the same objective and constraint functions. RAPIDMINER proposed various machine-learning techniques to solve optimization problems. Using RAPIDMINER, five machine learning models were used to train, test and validate dataset from numerical simulations. After the models were validated, we used the model to find out the optimum insulation thickness by applying genetic algorithm. The five models were applied to each insulating material. The results obtained from this software are presented here below.

3.6.3.1 Optimum insulation thickness of B.A using RAPIDMINER

Five machines learning models: generalized linear model (GLM), deep learning (DL), decision tree (DT), random forest (RF) and support vector machine (SVM) were used to predict the minimum temperature of the system. After validation of the models by evaluation of the

performance, genetic algorithm optimization method is applied to find out the best global minimum insulation of B.A material using RAPIDMINER. Figures 3.33, 3.36, 3.39, 3.42 and 3.45 are respectively the plots of the predicted minimum temperature of the system given by GLM, DL, DT, RF and SVM against the true values of the minimum temperature obtained by numerical simulation. From these plots, it can be seen that, the five models' predictions are likely close to the true prediction. The performance parameters of these models are shown in Table 3.11 below. In this Table, we noticed that, only GLM has a small correlation coefficient less than 0.9. DT and RF have the greater scoring and training time as it can be seen in figure 3.48. In addition, DT and RF have greater correlation coefficient indicating a good relationship between the predicted and the true value of the minimum temperature. After the five models were tested and validated, we applied the GA to each of the model in order to find out the best global minimum insulation thickness. GA is a concept based on natural selection. It evolves over time so that a better solution can be obtained. GA is used to find out the optimum solution of a problem. This can be done based on fitness function. Initially, we have an initial possible solution call initial parent or candidate solution. So, for every parent or selected candidate, it fitness value is found out. This fitness value decides whether the solution is best or not. Fitness function is simply a function which takes a candidate solution to the problem as input and produces as output how fit or good a solution is. In the case study, the fitness function is incorporate in RAPIDMINER software. When the fitness of each candidate is evaluated, the solution which satisfied the fitness criteria during the evaluation is kept in the population and those which do not satisfied the fitness criteria are discarded from the population after the fitness evaluation. Next, genetic operators like selection, crossover and mutation are applied on the selected parent for the generation of the new offspring. Thus, figures 3.34, 3.37, 3.40. 3.43 and 3.46 represent the plot of the fitness values of the fitness function over times of GLM, DL, DT, RF and SVM respectively. It can be seen that, in these figures, the fitness value increases rapidly. This increase in fitness values indicates the major role of the mutation operator in the changing of the genetic pool. In general, mutation affect a small portion of the population and provides an advantage to the individual by increasing its fitness value. We can easily observed that, the fitness value increases from -1.75 to 0 in figure 3.42. The reproduction or crossover operator role is to select among the previously selected chromosomes in the initial population, two chromosomes according to the fitness value in order to produce an offspring for next generation of new population. The selection, crossover, and mutation operation will be repeated on current population until the new population is complete. The converge is satisfied when the

absolute value of the fitness value remains constant across generation. The plot represented in figures 3.34, 3.37, 3.40, 3.43 and 3.46, meets this criterion. The fitness values converge to 0 for most of the models indicating the termination of the genetic algorithm. After the GA is terminated, the optimum solution of displays by each model can be visualized. Model that did not meet the requirement are discarded. In the case study, although DT has the best performance it did not meet the requirement. The RF model was then choosing the machine learning modeling, which displays the best insulation thickness of BA and the minimum insulation volume as, presented in Table 3.11 and Table 3.12 below. In Table 3.11 below, it is shown the best optimal insulation thickness of B.A as displayed in figures 3.34, 3.37, 3.40, 3.43 and 3.45.

Table 3.11: Comparison of the performance and optimum insulation thickness of B.A predicted using machine learning models with RAPIDMINER

Models	RMSE	Mean Absolute Error	Correlation Coefficient	Optimum insulation thickness (mm)
Generalized Linear Model	0.93	0.79	0.89	118.72
Deep Learning	0.95	0.76	0.92	118.72
Decision Tree	**0.19**	**0.09**	**0.99**	**81.63**
Random Forest	**0.41**	**0.25**	**0.97**	**81.63**
Support Vector Machine	0.46	0.33	0.96	65.88

Table 3.12: comparison of insulation thickness and insulation volume of various models for the case of B.A

Models	Optimum insulation thickness (mm)	Absolute error	Insulation volume (m^3)
True Numerical value	79.80		**9111.37**
Numerical model	**88.90**	**9.10**	**9759.56**
Generalized Linear Model	118.72	38.92	14288.16
Deep Learning	118.72	38.92	14288.16
Decision Tree	**81.63**	**1.83**	**9349.07**
Random Forest	**81.63**	**1.83**	**9349.07**
Support Vector Machine	65.88	13.92	7382.56
Regression model	**79.38**	**0.42**	**9067.19**

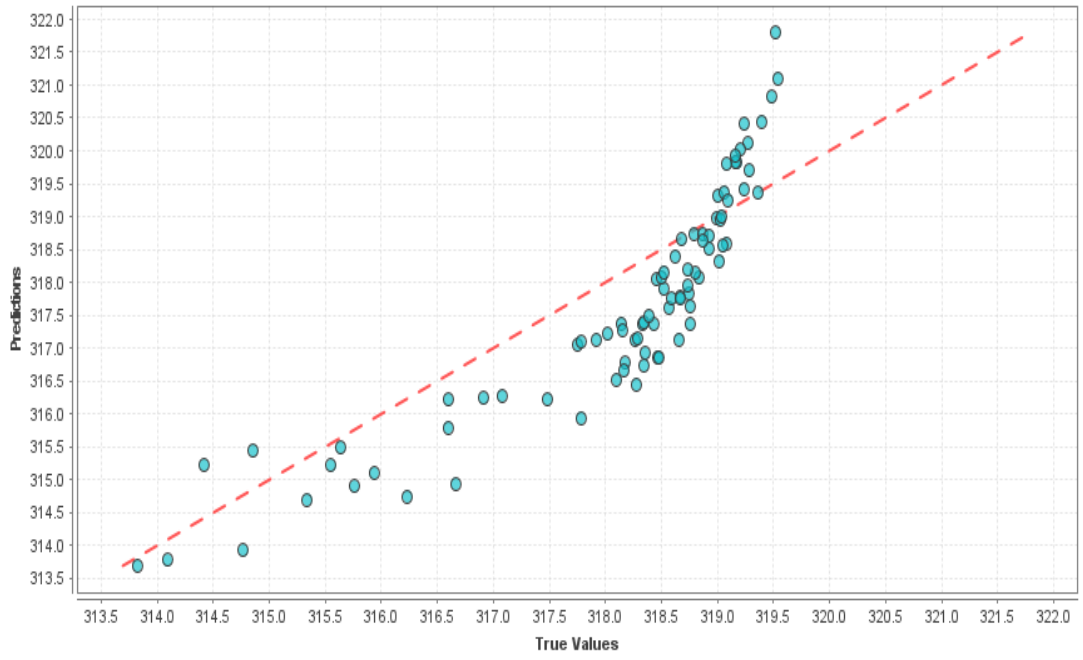

Figure 3.33: predicted values vs true values of the minimum temperature of the system given by the GLM using RAPIDMINER with B.A insulating material.

In Table 3.12 above, the value of the optimal insulation volume of B.A are calculated for the corresponding insulation thickness. From this Table, we noticed that the numerical model, RF, and Regression model predict value of the insulation thickness with small absolute error though. From this table, we also noticed that best model that performed well is the regression model over the numerical model. This is because the search procedure of the numerical model was based on manual and gradual step of the insulation thickness, which do not lead to the nearest best global optimum insulation thickness. This result simply confirms the importance of making use of machine learning in engineering processes.

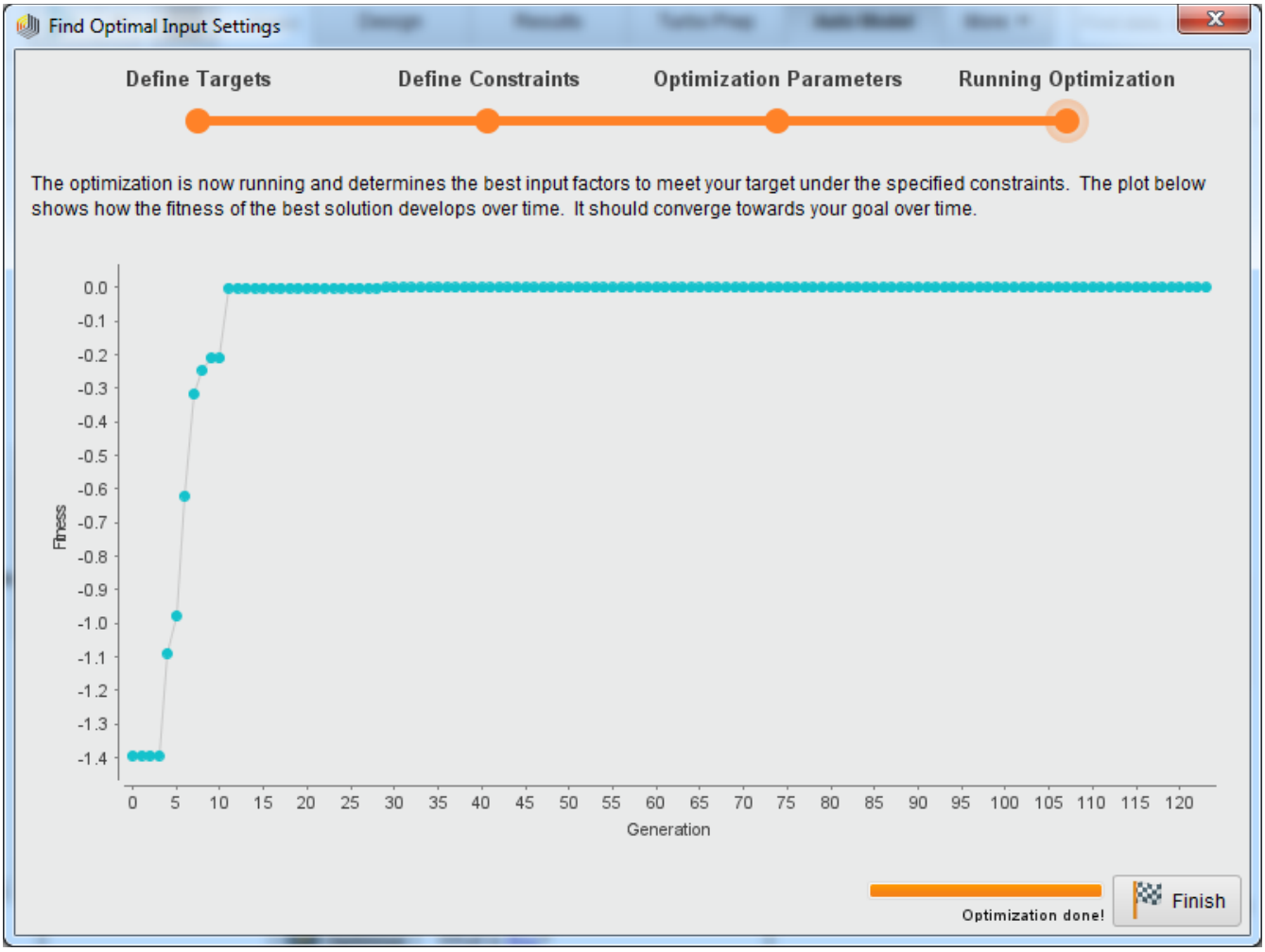

Figure 3.34: Application of G.A to GLM for optimal insulation thickness of B.A using RAPIDMIN

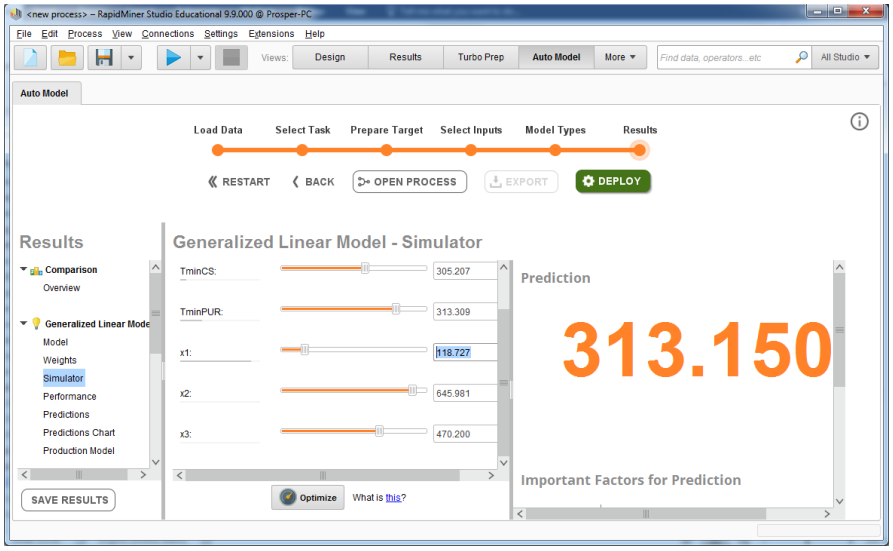

Figure 3.35: visualization of the optimum insulation thickness of B.A material given by GLM using RAPIDMINER

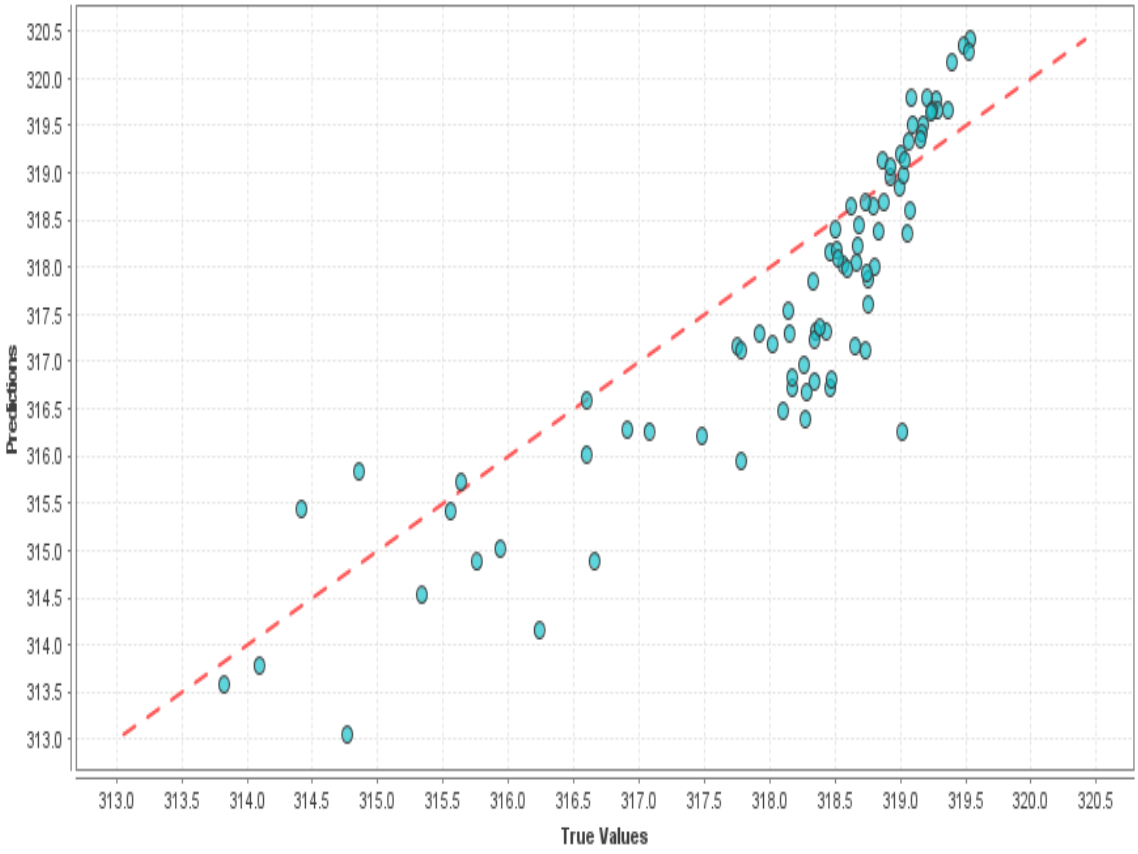

Figure 3.36: predicted values vs true values of the minimum temperature of the system given by the DL using RAPIDMINER with B.A insulating material.

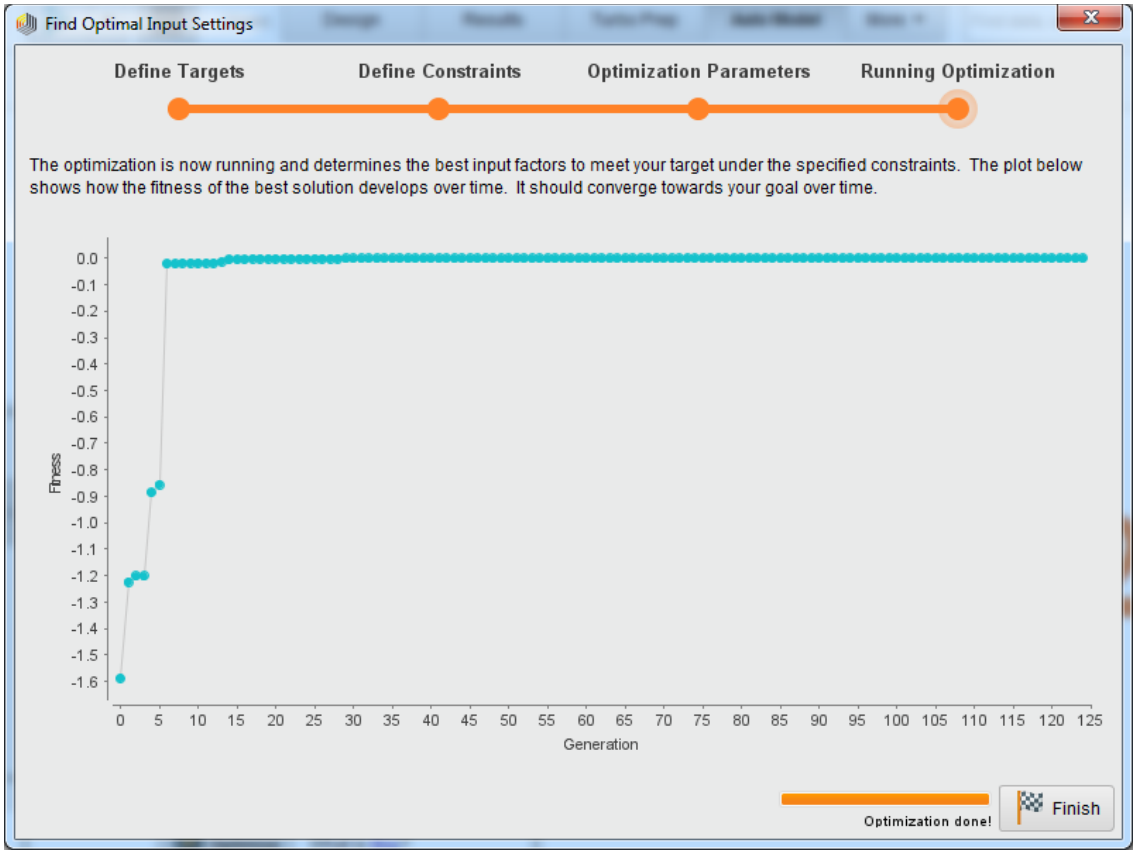

Figure 3.37: Application of G.A to DL for optimal insulation thickness of B.A using RAPIDMINER

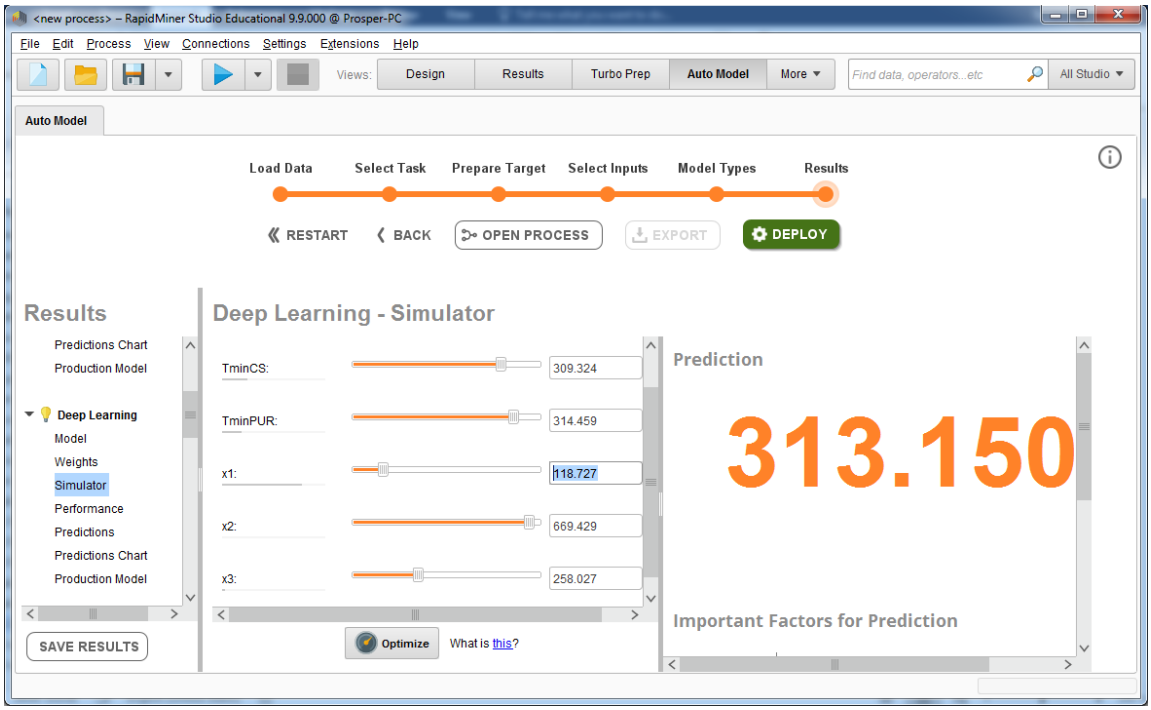

Figure 3.38: visualization of the optimum insulation thickness of B.A material given by DL using RAPIDMINER.

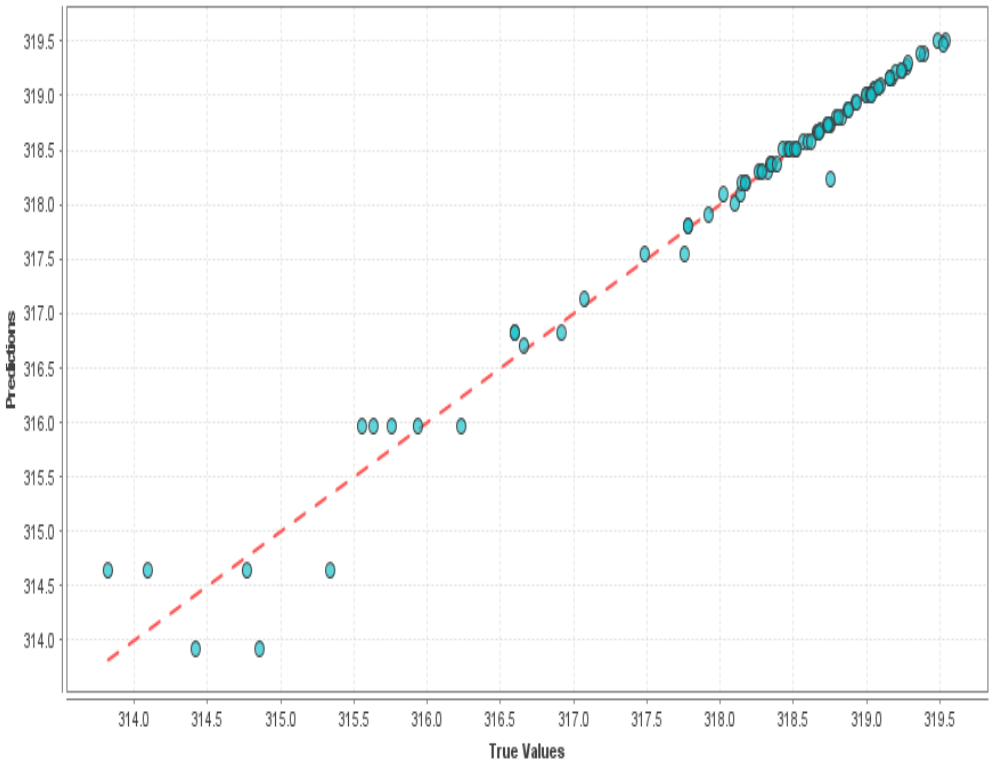

Figure 3.39: predicted values vs true values of the minimum temperature of the system given by the DT using RAPIDMINER with B.A insulating material.

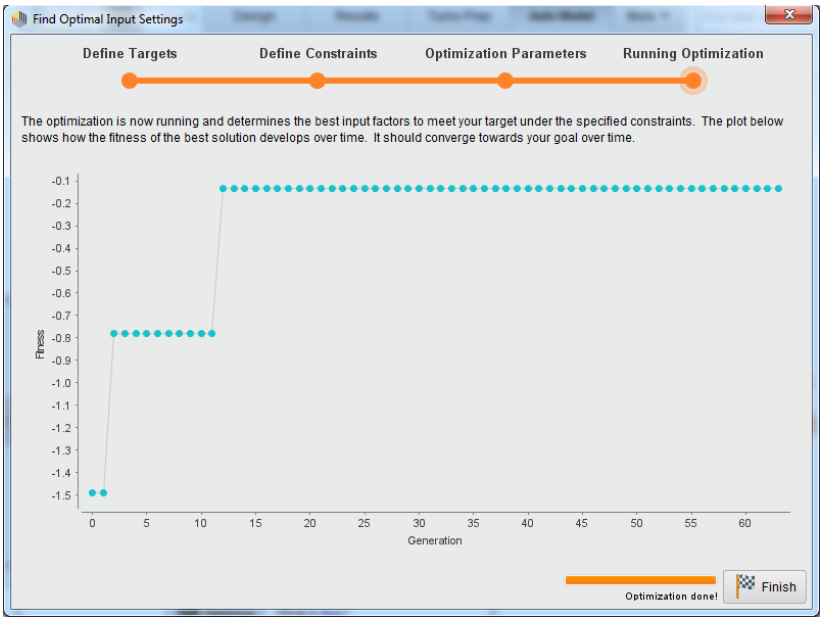

Figure 3.40: Application of G.A to DT for optimal insulation thickness of B.A using RAPIDMINER

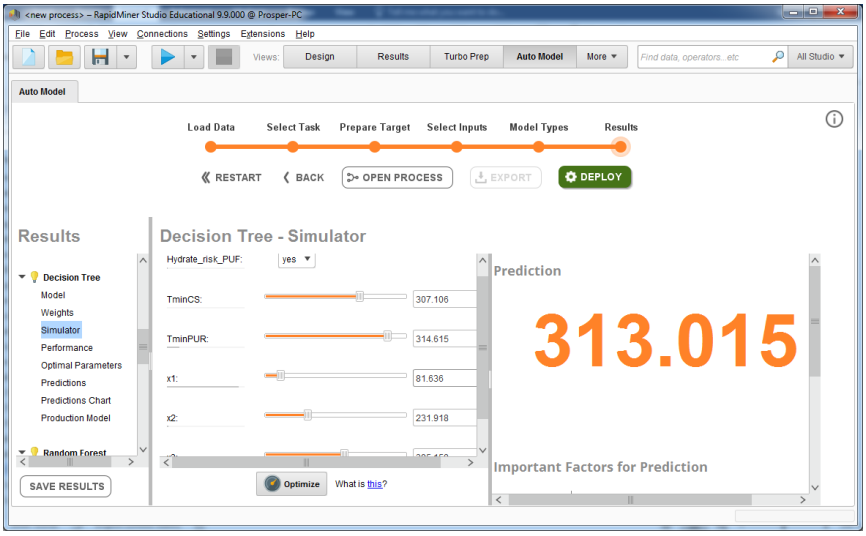

Figure 3.41: visualization of the optimum insulation thickness of B.A material given by DT using RAPIDMINER.

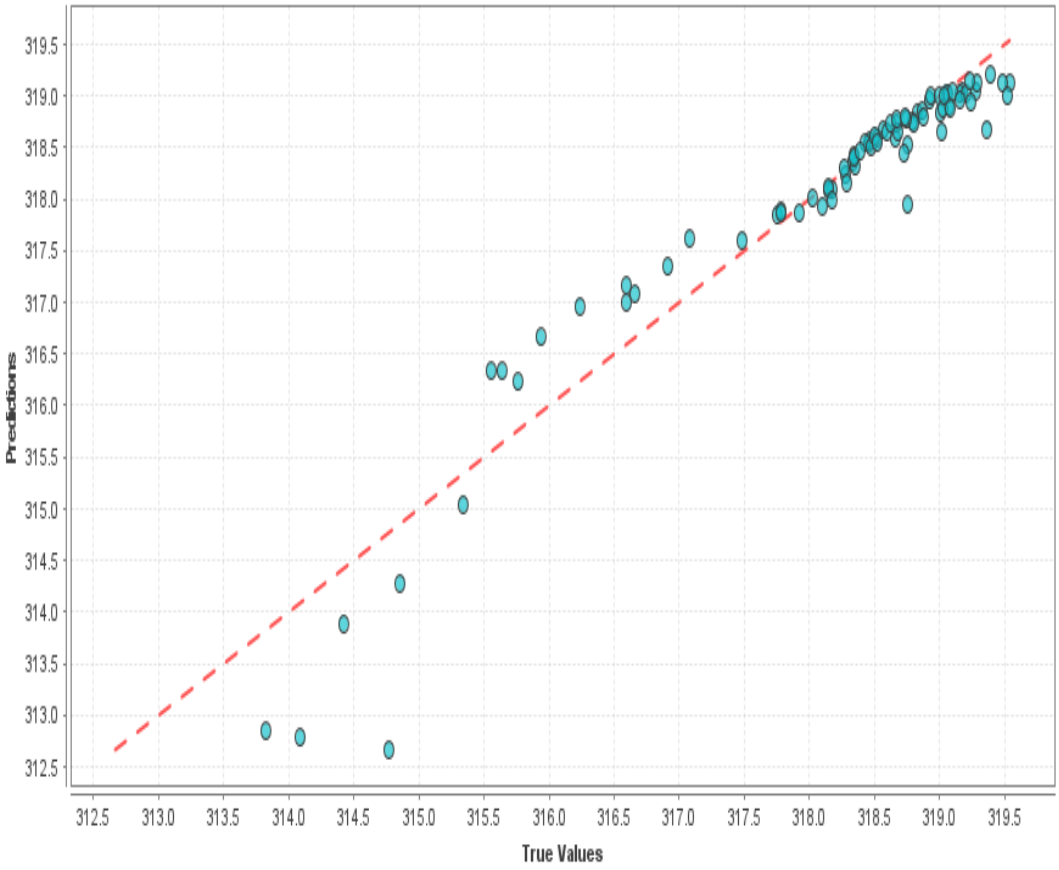

Figure 3.42: predicted values vs true values of the minimum temperature of the system given by the RF using RAPIDMINER with B.A insulating material

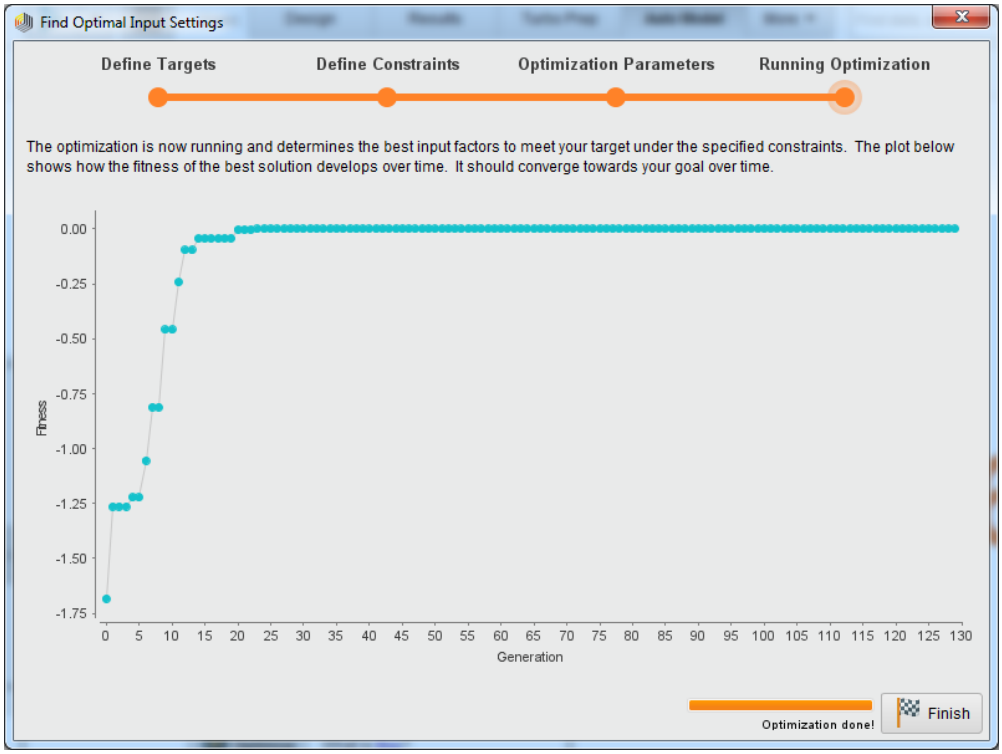

Figure 3.43: Application of G.A to RF for optimal insulation thickness of B.A using RAPIDMINER

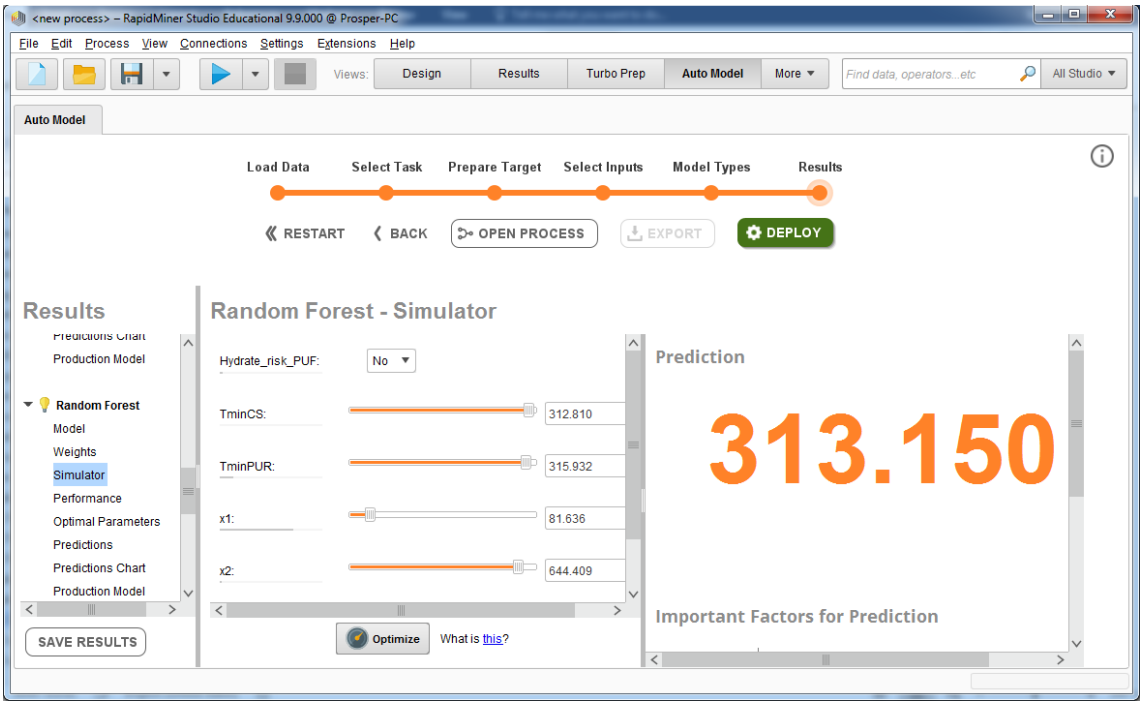

Figure 3.44: visualization of the optimum insulation thickness of B.A material given by RF using RAPIDMINER

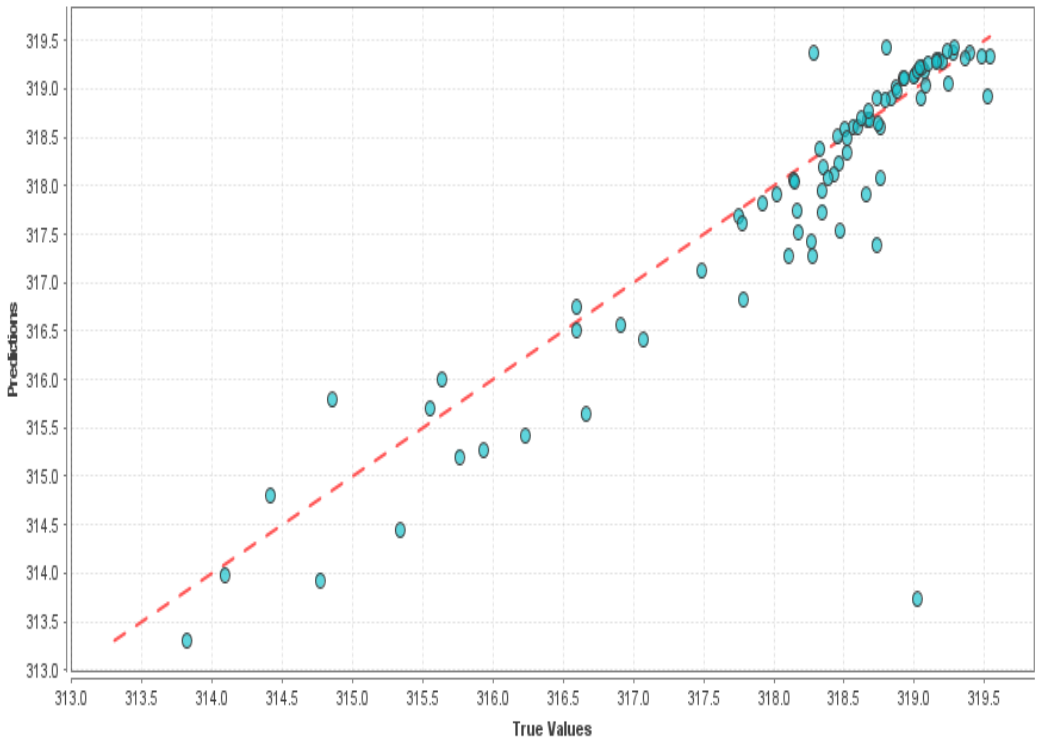

Figure 3.45: predicted values vs true values of the minimum temperature of the system given by the SVM using RAPIDMINER with B.A insulating material.

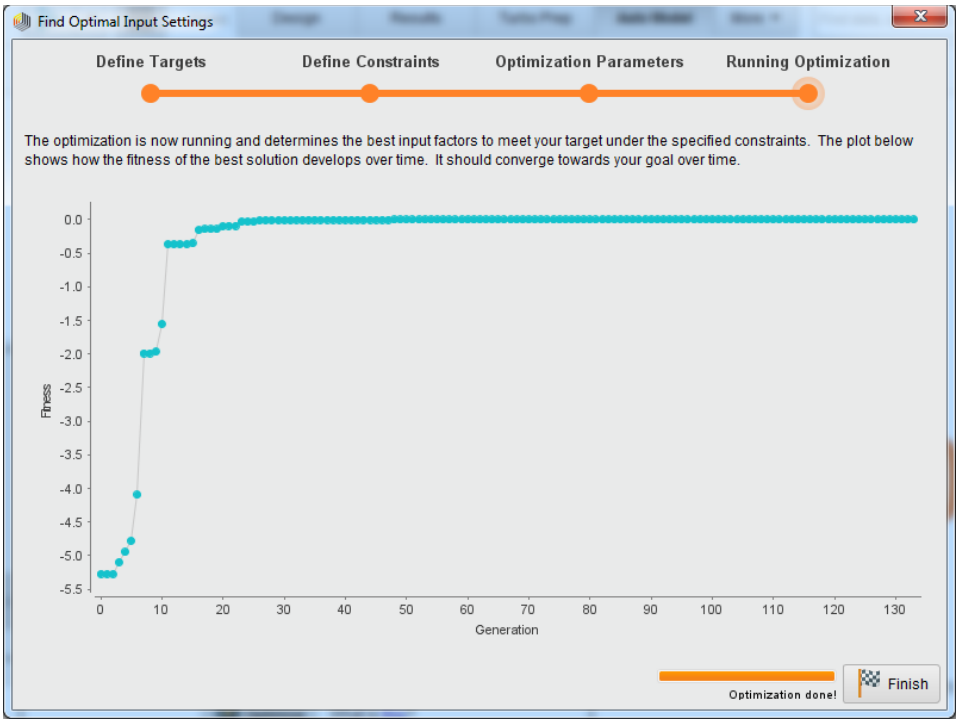

Figure 3.46: Application of G.A to SVM for optimal insulation thickness of B.A using RAPIDMINER

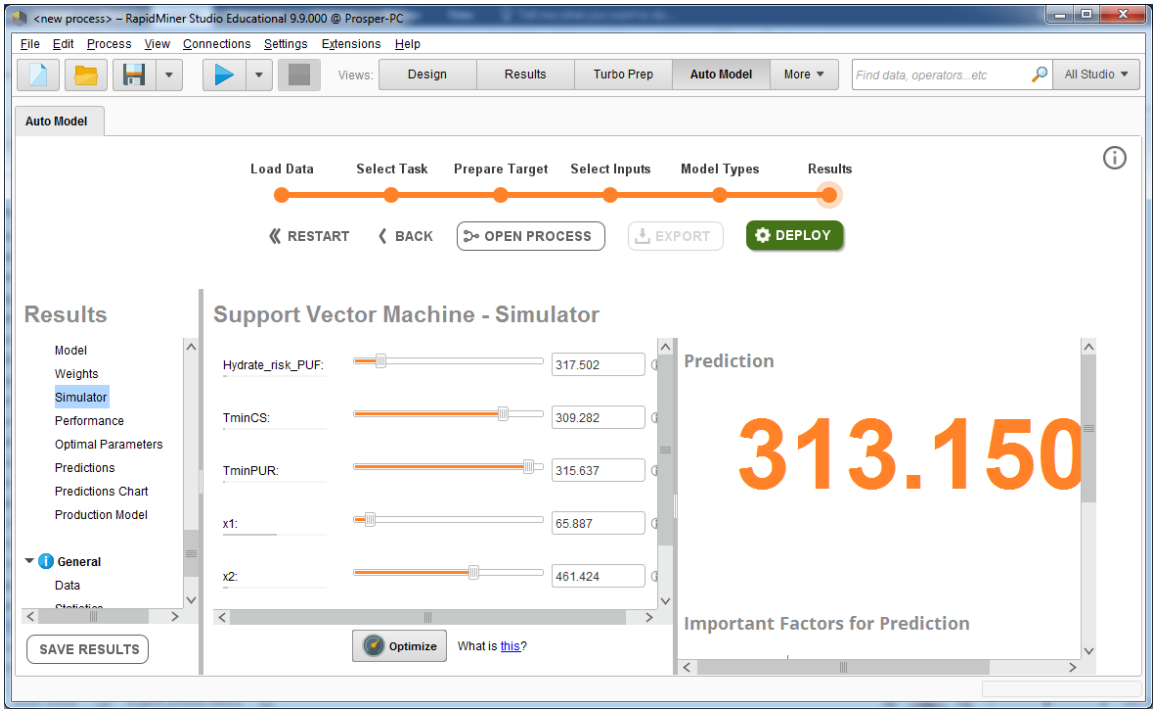

Figure 3.47: visualization of the optimum insulation thickness of B.A material given by SVM using RAPIDMINER.

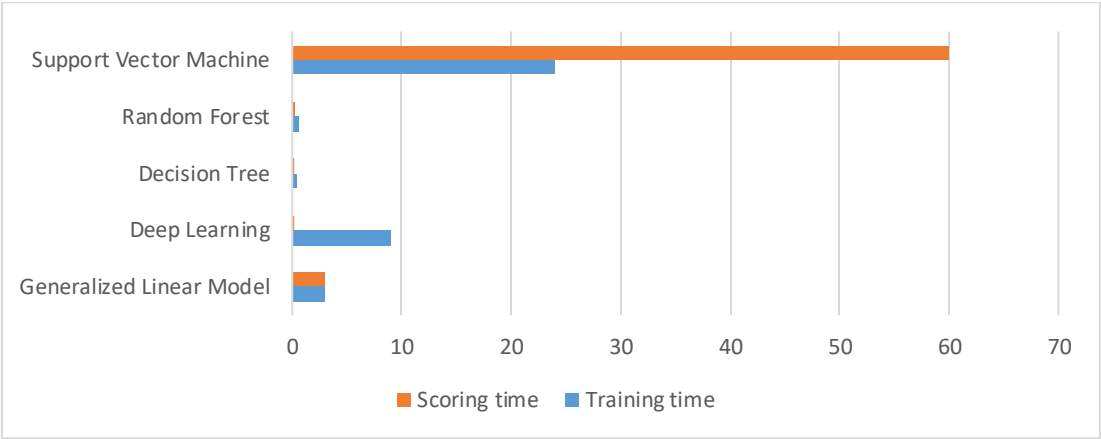

Figure 3.48: comparison of the training and scoring times of the five machine learning models

3.6.3.2 Optimum insulation thickness of CS with RAPIDMINER

The same analysis done in the B.A case was performed for the CS case. Results of these simulations are presented below. Figures 3.49, 3.52, 3.55, 3.58 and 3.61 are respectively the plots of the predicted minimum temperature of the system by GLM, DL, DT, RF and SVM against the true minimum temperature obtained by numerical simulation. In Table 3.13 below, we can see that, all the models performed well with a correlation coefficient greater than 0.9. Next, the genetic algorithm was then applied using RAPIDMINER to find out the optimum

insulation thickness. Moreover, it is shown in figure 3.64 that the DT has the fastest training time while the DL has the fastest scoring time.

Figures 3.450, 3.53, 3.56, 3.59 and 3.62 are plots of the fitness values across each generation in the GA process. The increase in fitness value indicates the major role of the mutation in the changing of the genetic pool In general, mutation affect a small portion of the population and provides an advantage to the individual by increasing its fitness value. We can easily observe that the fitness value increases over generations and converge. A constant fitness value indicates that the individual solution does not change or improve for the given period. The reproduction or crossover operator role is to select among the previously selected chromosomes in the initial population, two chromosomes according to the fitness value in order to produce offspring for next new generation of new population. The selection, crossover, and mutation operation will be repeated on current population until the new population is complete. The GA terminates when the absolute value of the fitness value is constant across generation. The plot represented in all these figures meets this criterion.

In Table 3.13 below, it is shown that the DT, DL and RF models performed well the prediction with high correlations coefficients and low RMSE. An analysis of this Table revealed that, RF though having a small RMSE and the greater correlation coefficient predicted a nearest optimum value. Table 3.14 below shows the comparison of all the models presented in this thesis for predicting the optimum insulation thickness of calcium silicate. From this Table, it can be seen that, the numerical simulation and the RF models predicted the optimum insulation thickness with a relative error of 0.77% and 0.48% respectively.

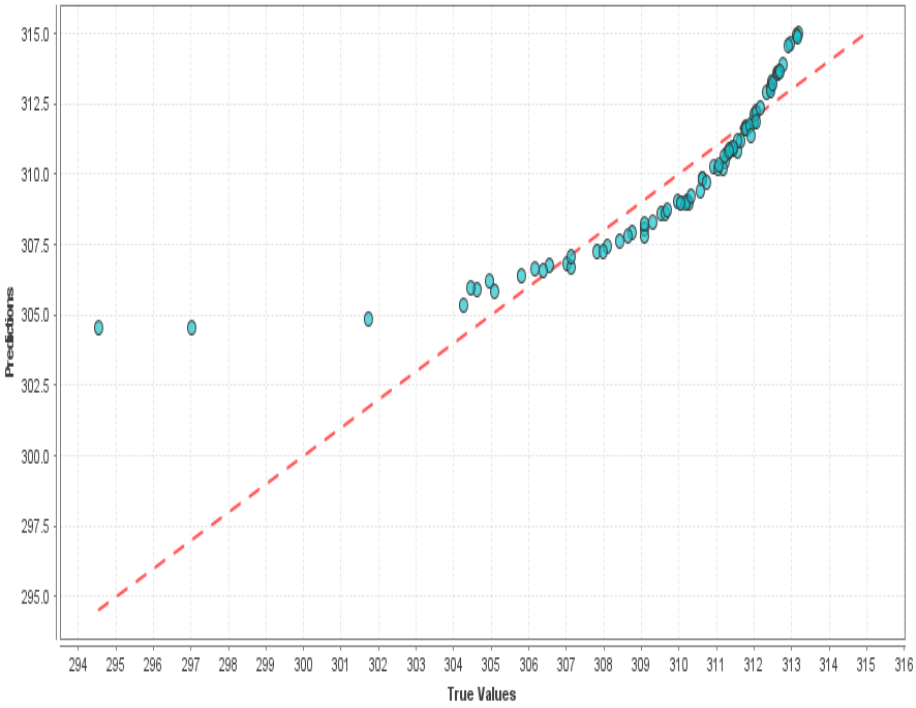

Figure 3.49: predicted values vs true values of the minimum temperature of the system given by the GLM using RAPIDMINER with CS insulating material

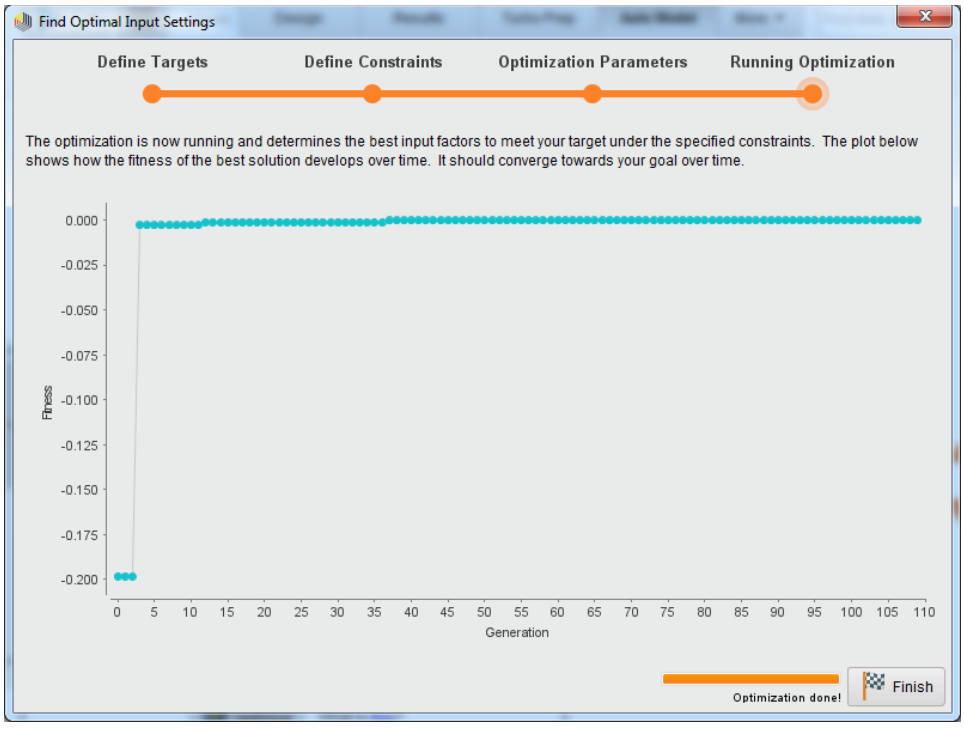

Figure 3.50: Application of G.A to GLM for optimal insulation thickness of C.S using RAPIDMINER

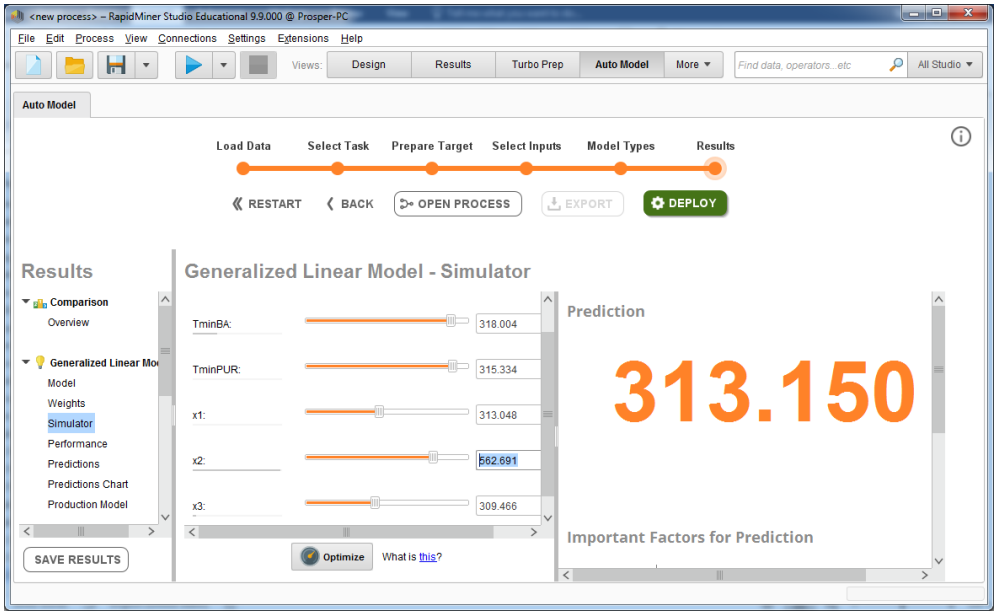

Figure 3.51: visualization of the optimum insulation thickness of CS material given by GLM using RAPIDMINER.

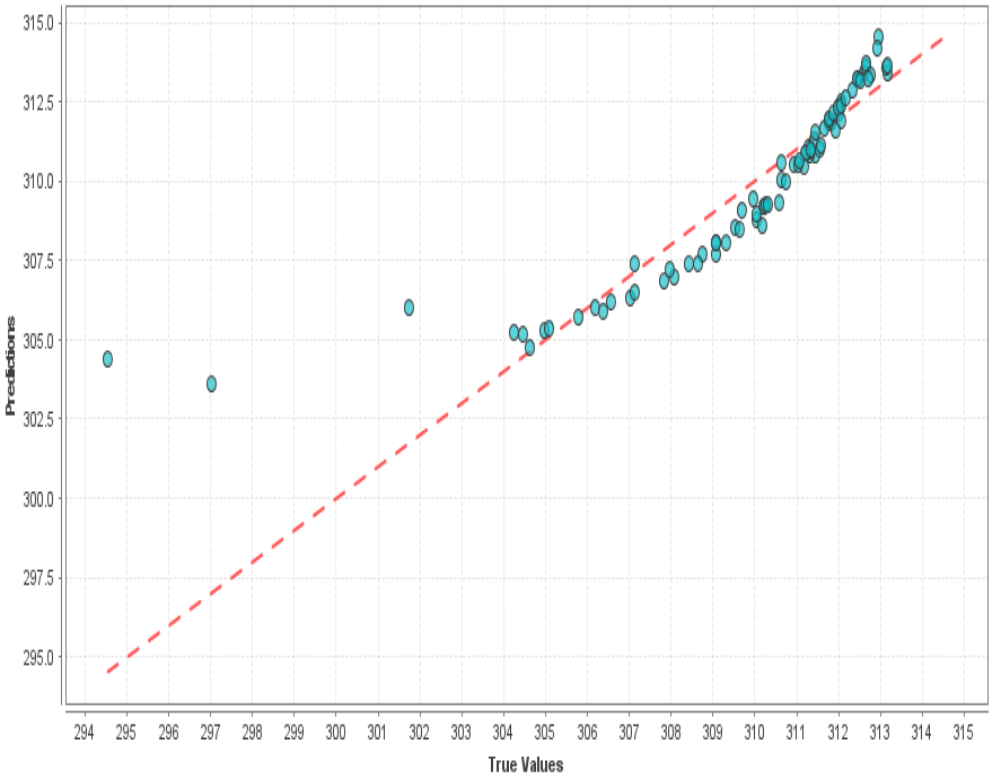

Figure 3.52: predicted values vs true values of the minimum temperature of the system given by the DL using RAPIDMINER with CS insulating material

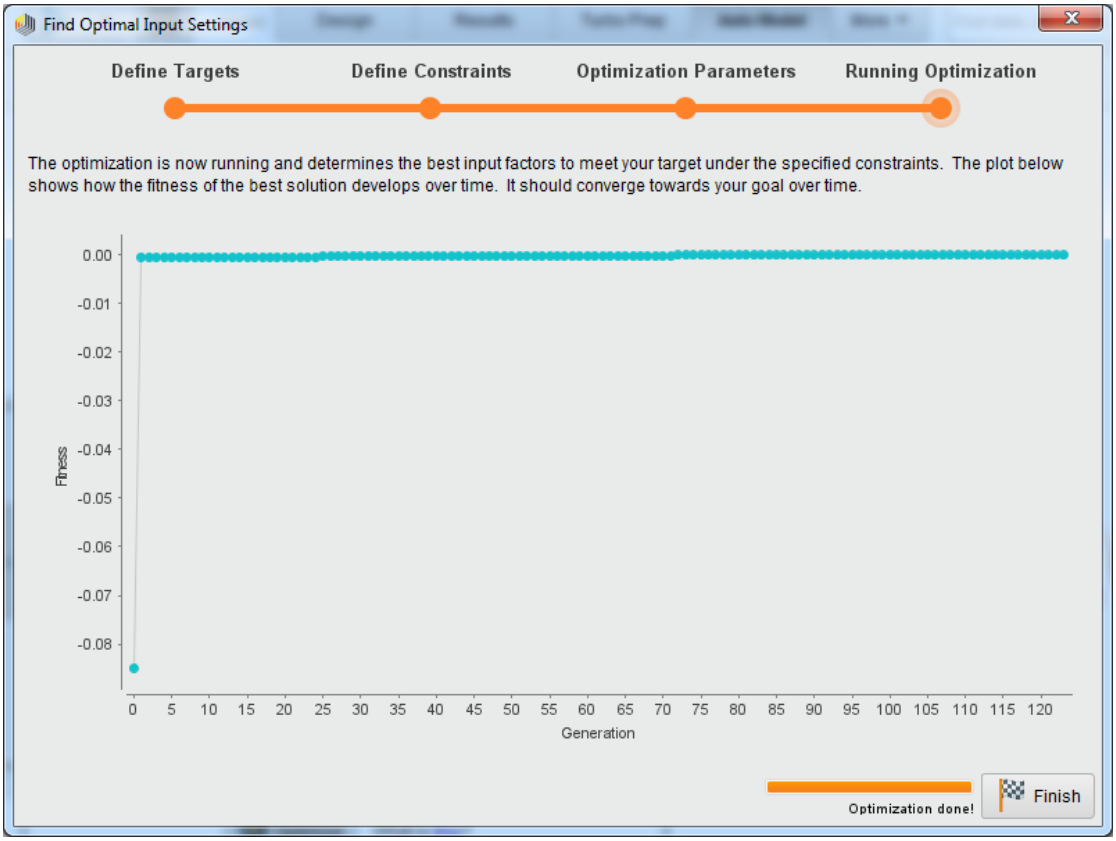

Figure 3.53: Application of G.A to DL for optimal insulation thickness of C.S using RAPIDMINER

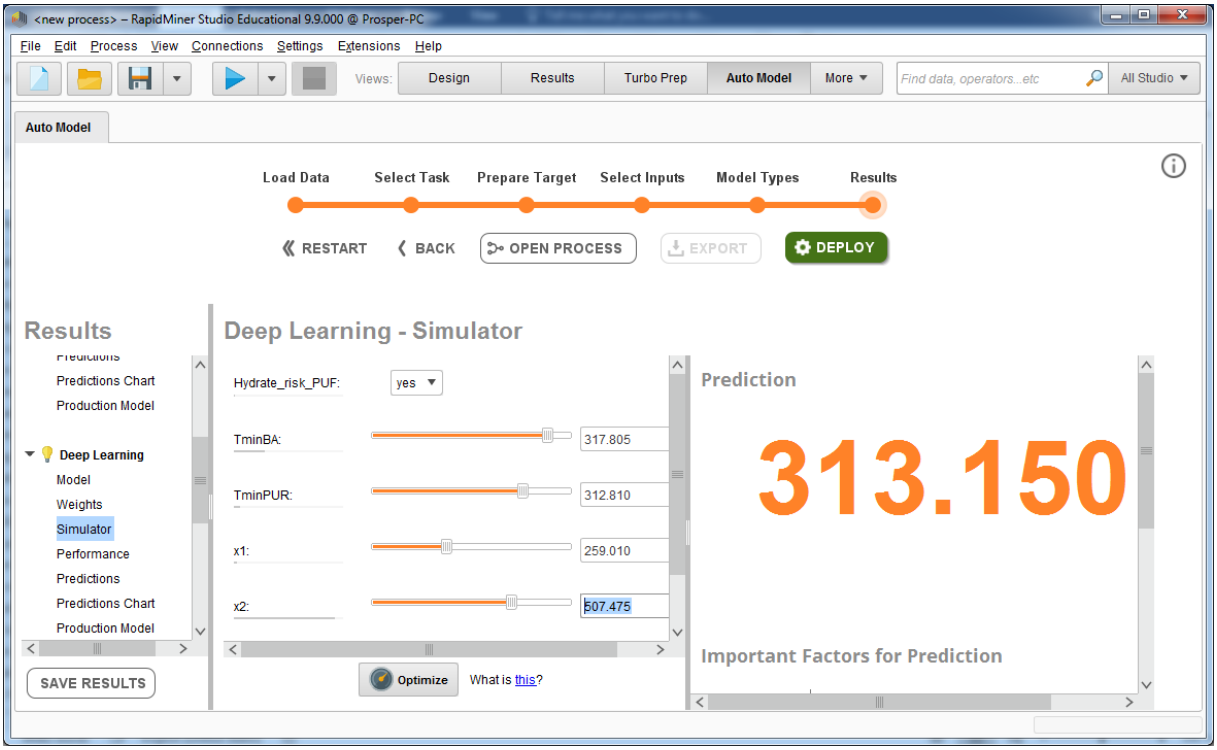

Figure 3.54: visualization of the optimum insulation thickness of CS material given by DL using RAPIDMINER.

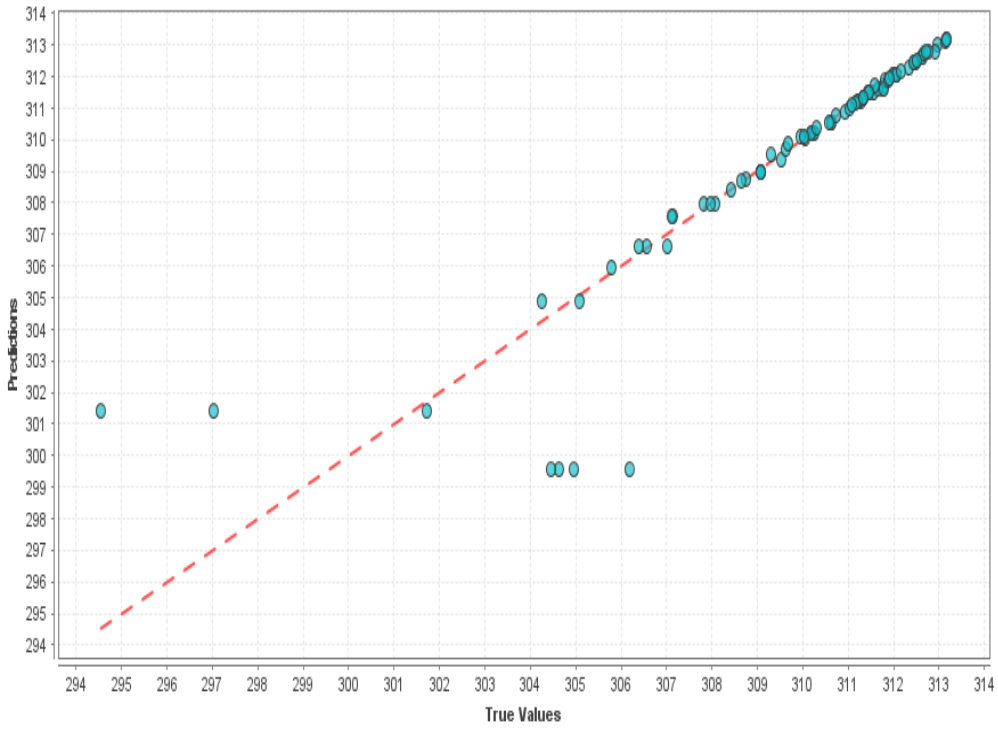

Figure 3.55: predicted values vs true values of the minimum temperature of the system given by the DT using RAPIDMINER with CS insulating material

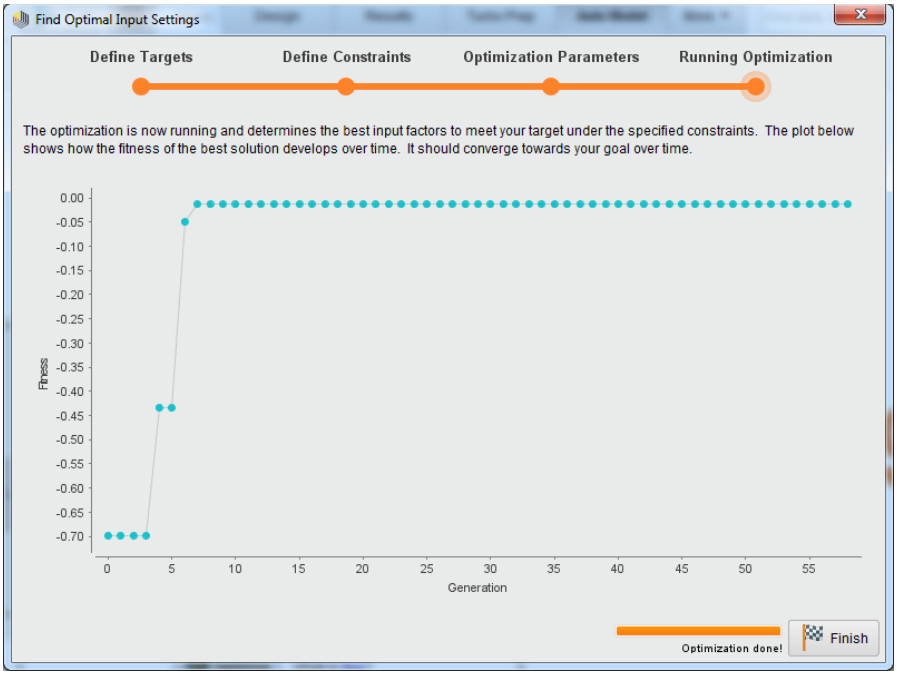

Figure 3.56: Application of G.A to DT for optimal insulation thickness of C.S using RAPIDMINER

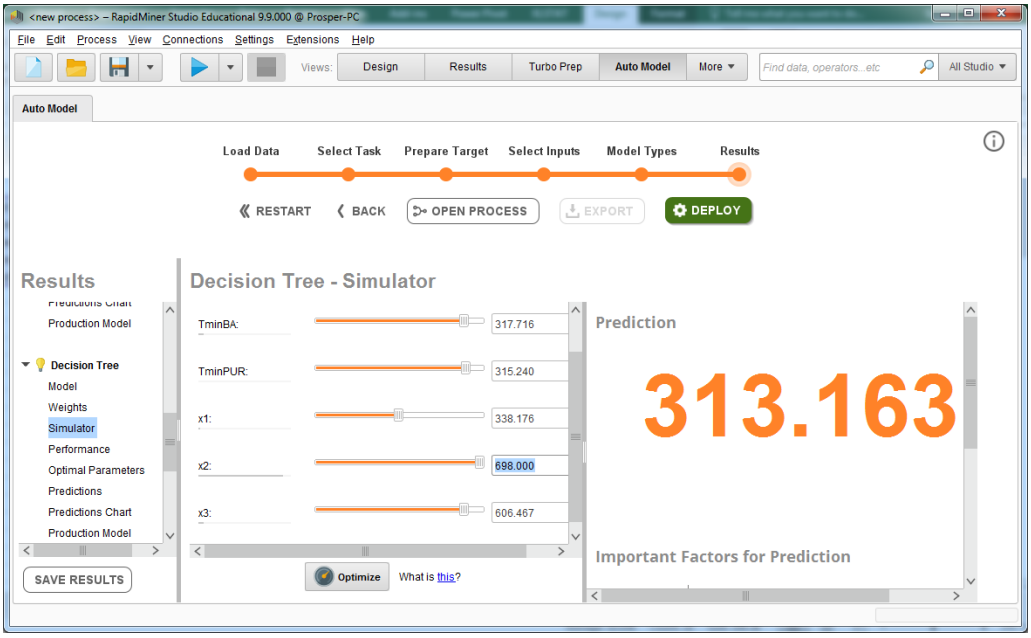

Figure 3.57: visualization of the optimum insulation thickness of CS material given by DT using RAPIDMINER.

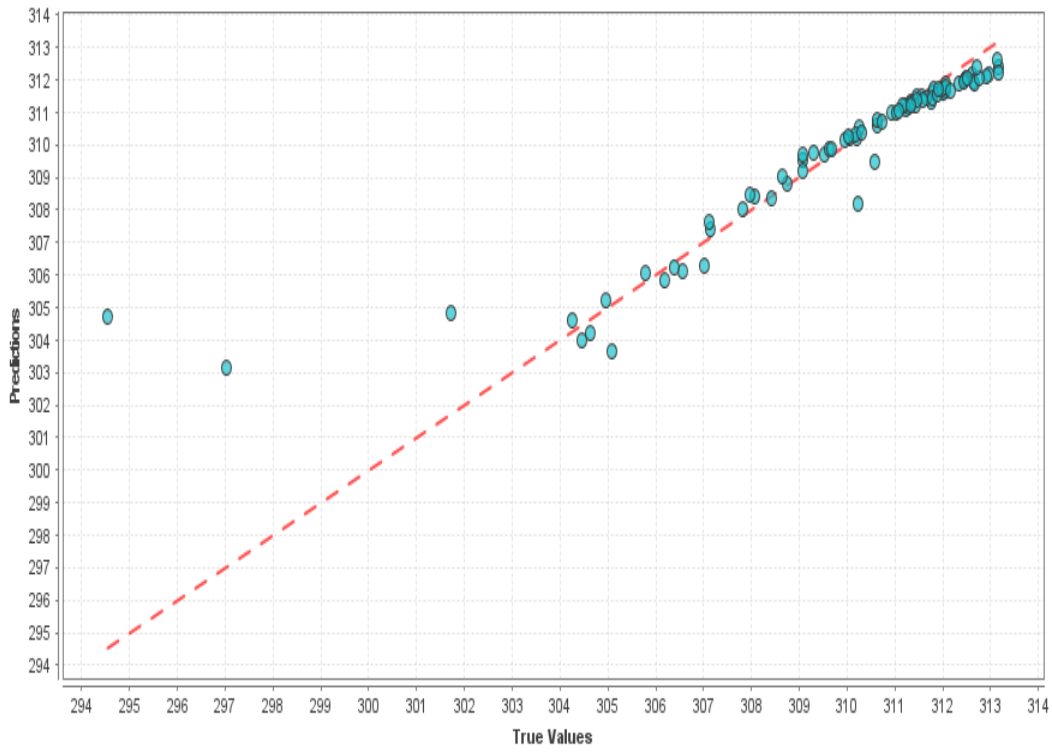

Figure 3.58: predicted values vs true values of the minimum temperature of the system given by the RF using RAPIDMINER with CS insulating material

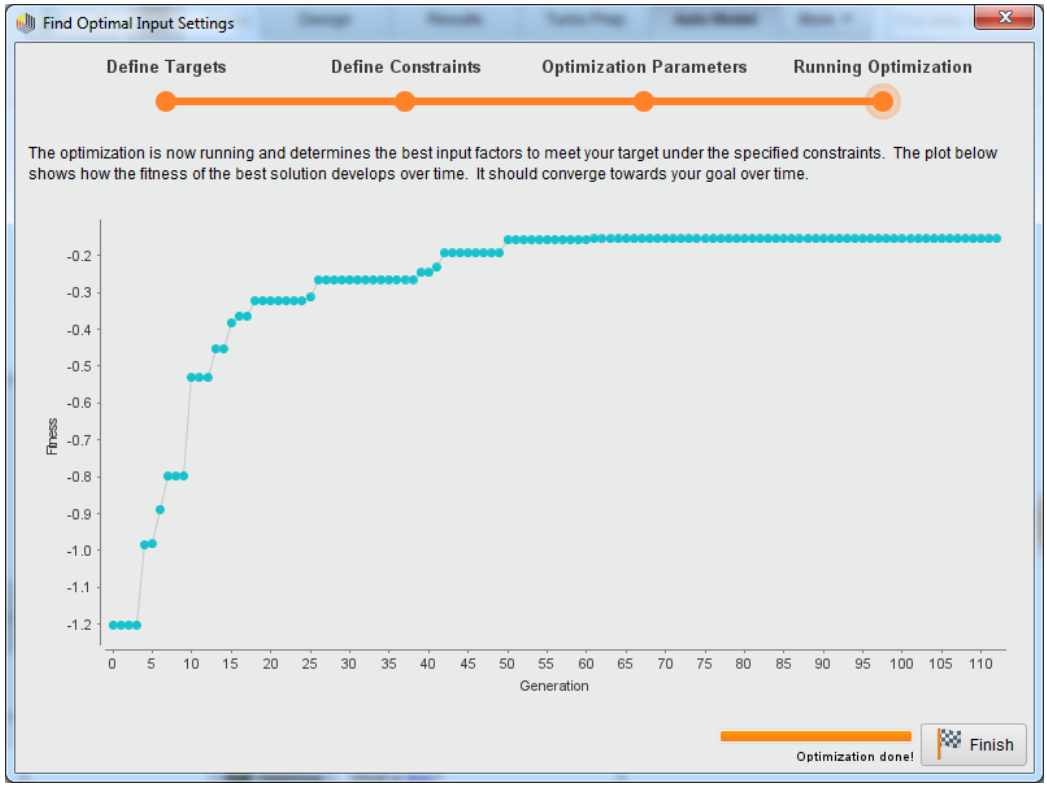

Figure 3.59: Application of G.A to RF for optimal insulation thickness of C.S using RAPIDMINER

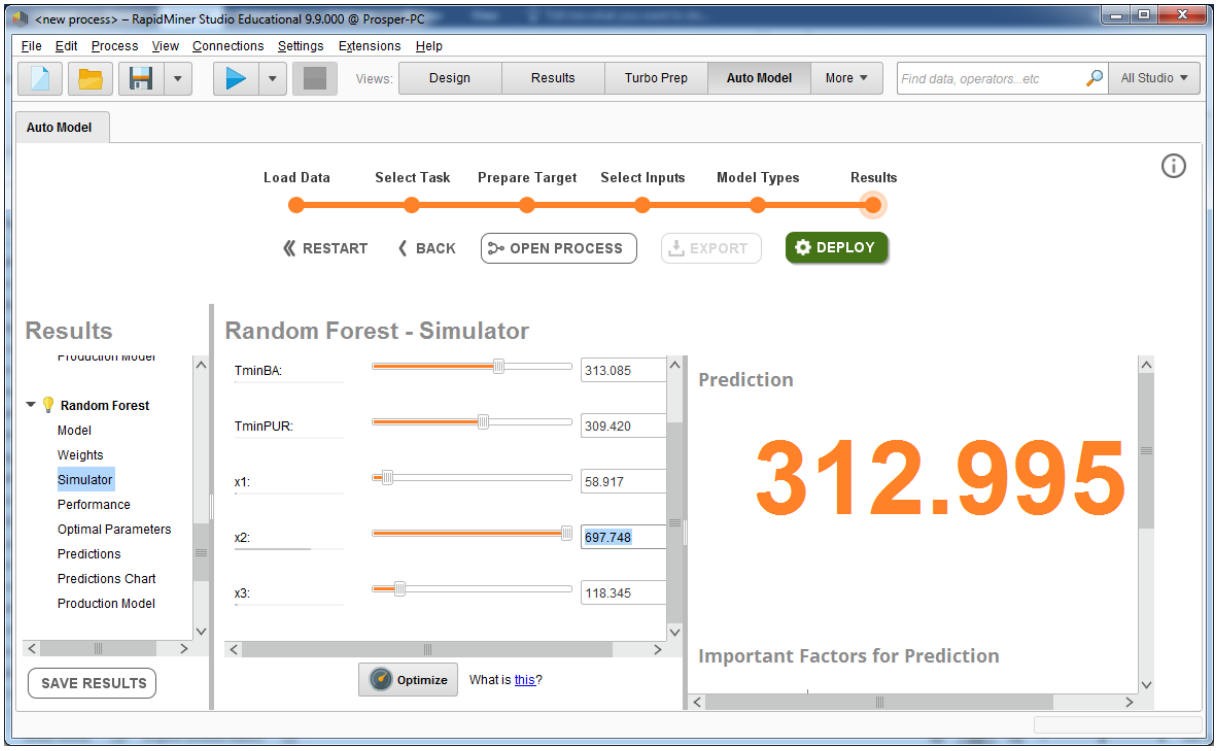

Figure 3.60: visualization of the optimum insulation thickness of CS material given by RF using RAPIDMINER.

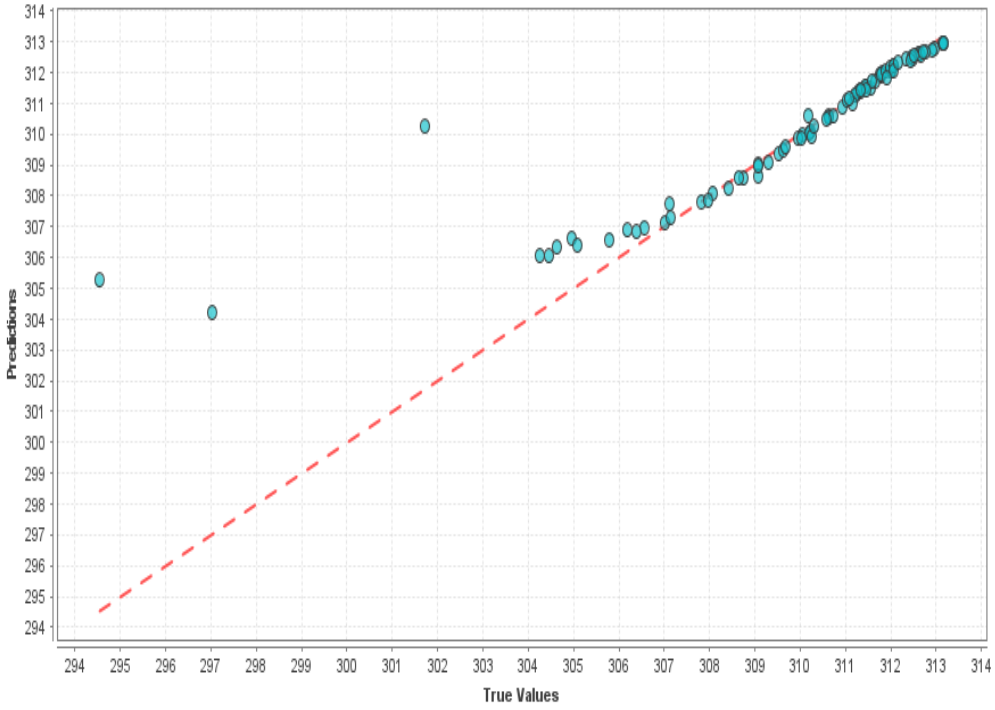

Figure 3.61: predicted values vs true values of the minimum temperature of the system given by the SVM using RAPIDMINER with CS insulating material

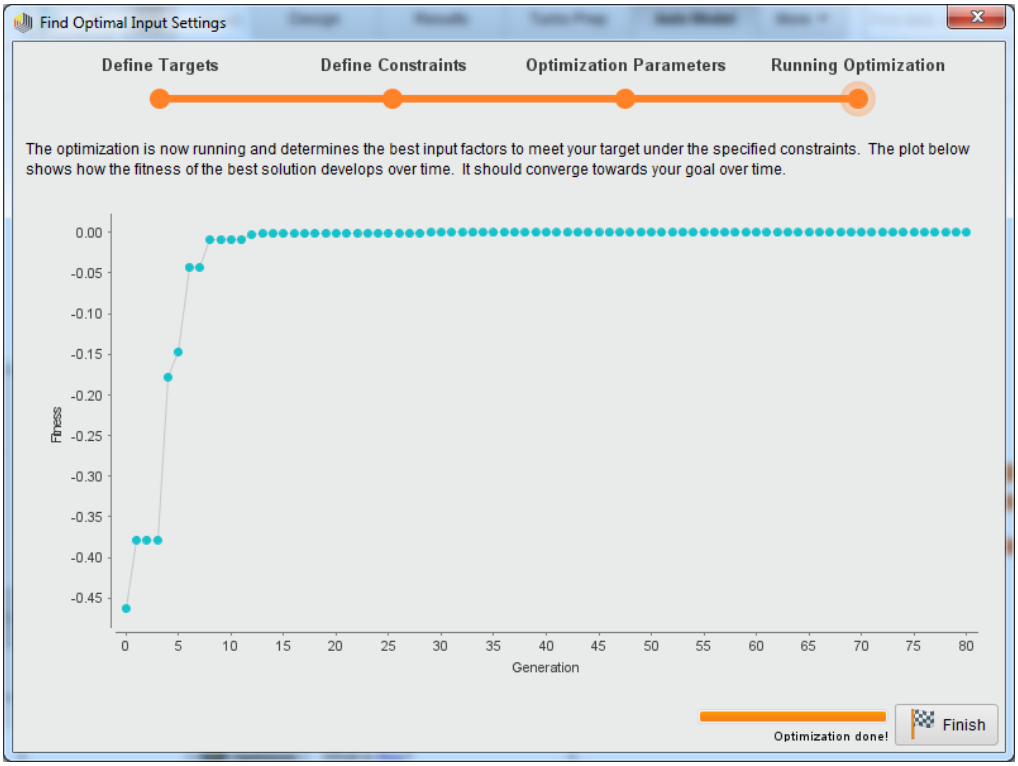

Figure 3.62: Application of G.A to SVM for optimal insulation thickness of C.S using RAPIDMINER

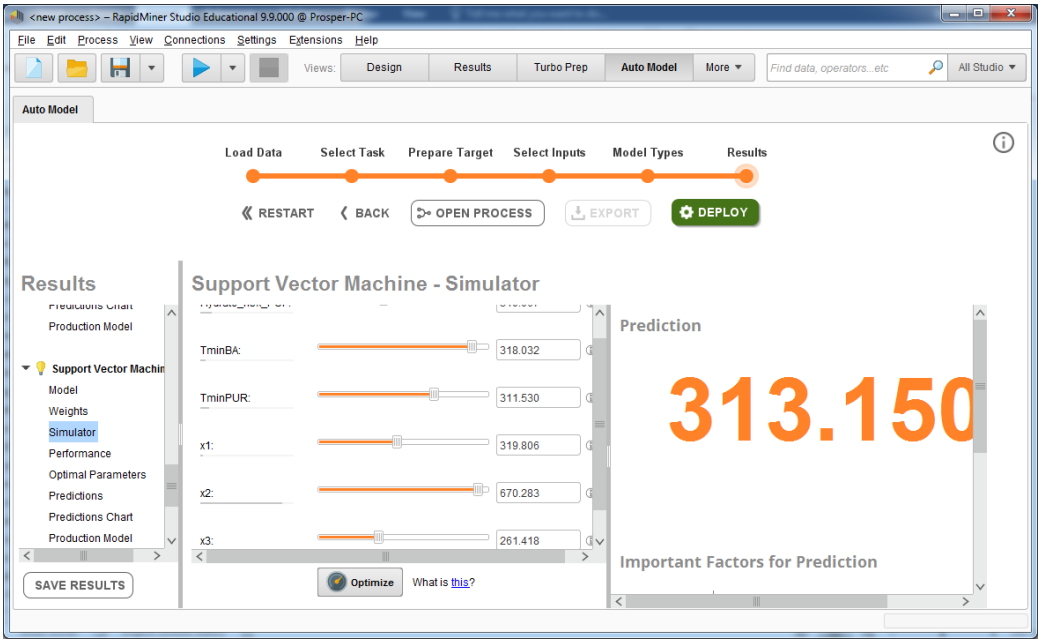

Figure 3.63: visualization of the optimum insulation thickness of CS material given by SVM using RAPIDMINER.

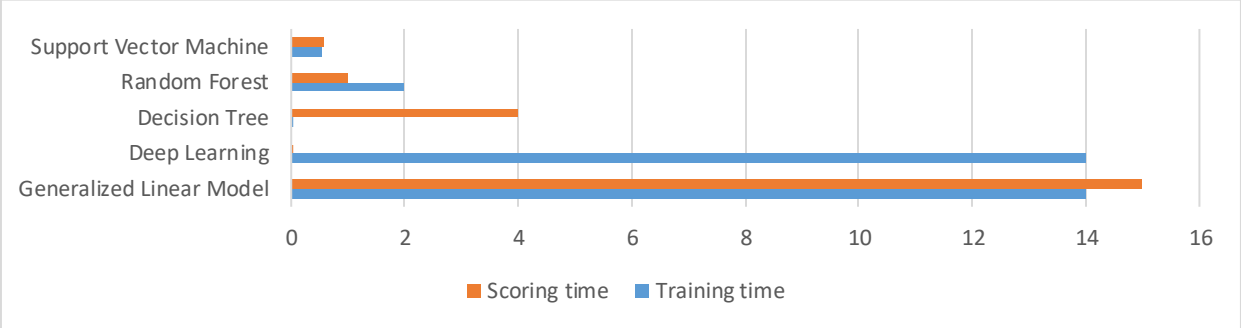

Figure 3.64: comparison of the training and scoring times of the five machine learning models

Table 3.13: performance and optimum insulation thickness of CS using machine learning model with RAPIDMINER

Models	RMSE	Mean Absolute Error	Correlation Coefficient	Optimum insulation thickness (mm)
Generalized Linear Model	1.22	0.90	0.93	562.69
Deep Learning	1.13	0.79	0.94	507.47
Decision Tree	**1.13**	**0.44**	**0.95**	**698.00**
Random Forest	**0.85**	**0.47**	**0.97**	**697.74**
Support Vector Machine	1.16	0.48	**0.90**	**670.28**

Table 3.14: comparison of insulation thickness and insulation volume of various models for the case of CS

Models	Optimum insulation thickness (mm)	Absolute error	Insulation volume (m^3)
True numerical value	**694.70**		**146416.61**
Numerical model	**711.20**	**16.5**	**92181,98**
Generalized Linear Model	562.69	132.01	106937.78
Deep Learning	507.47	187.23	92044.88
Decision Tree	698.00	3.3	147480.83
Random Forest	697.74	**3.04**	147399.98
Support Vector Machine	670.28	24.42	138707.71
Regression model	693.60	**1.1**	146148.00

3.6.3.3 Optimum insulation thickness of PUF with RAPIDMINER

The same analysis done in the B.A and CS cases was performed and the results of these simulations are presented below. Figures 3.65, 3.68, 3.71, 3.74 and 3.77 are respectively the plots of the predicted minimum temperature of the system by GLM, DL, DT, RF and SVM against the true minimum temperature obtained by numerical simulation. From these plots. In table 3.18 below, we can see that all the models performed well with a correlation coefficient greater than 0.9. From figure 3.80, it can be seen that the DT has the fastest scoring time while the DL has the fastest training time. After, the models were tested and validated; the genetic algorithm was then applied using RAPIDMINER to find out the optimum insulation thickness.

In Table 3.16 below, it is shown that, the DT, DL and RF models performed well the prediction with high correlations coefficients and low RMSE. An analysis of this Table revealed that, RF though having a small RMSE and the greater correlation coefficient predicted a nearest optimum value. Table 3.17 below shows the comparison all the models presented in this thesis for predicting the optimum insulation thickness of PUF.

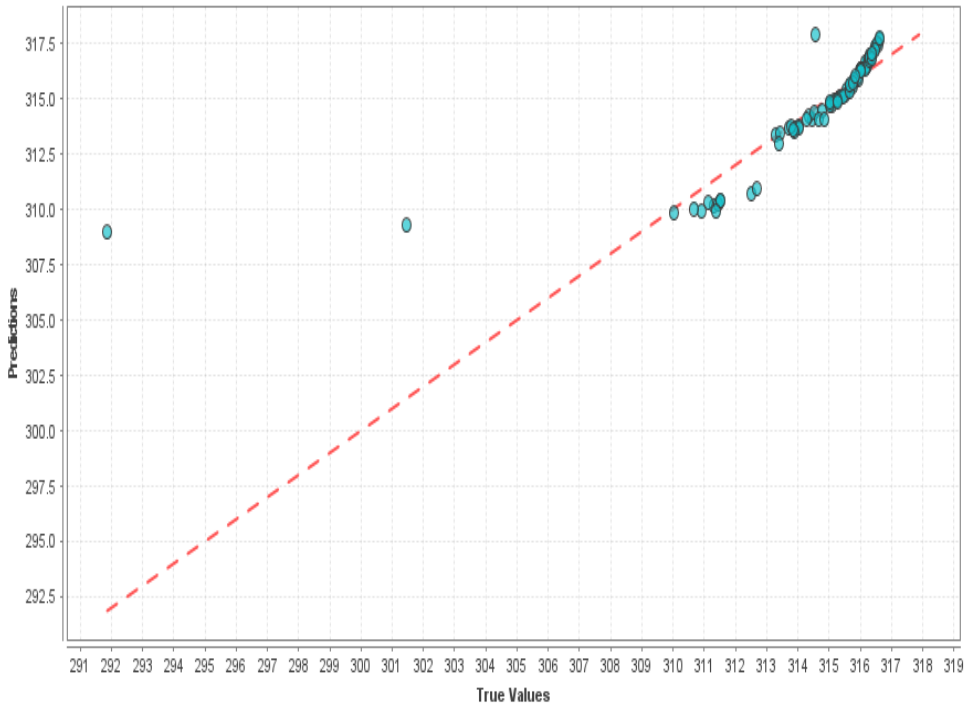

Figure 3.65: predicted values vs true values of the minimum temperature of the system given by the GLM using RAPIDMINER with PUF insulating material

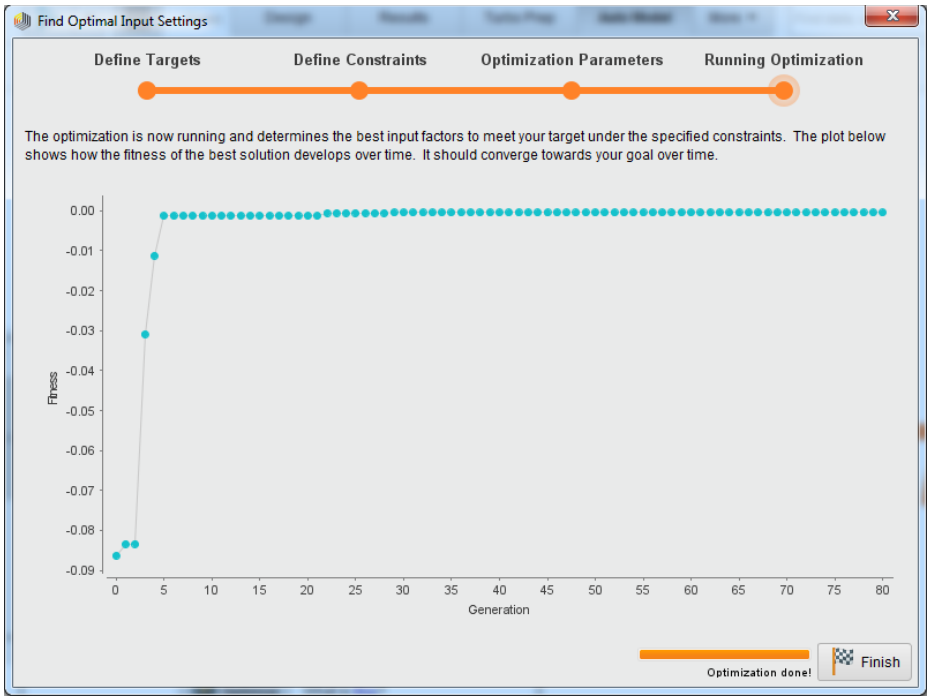

Figure 3.66: Application of G.A to GLM for optimal insulation thickness of PUF using RAPIDMINER

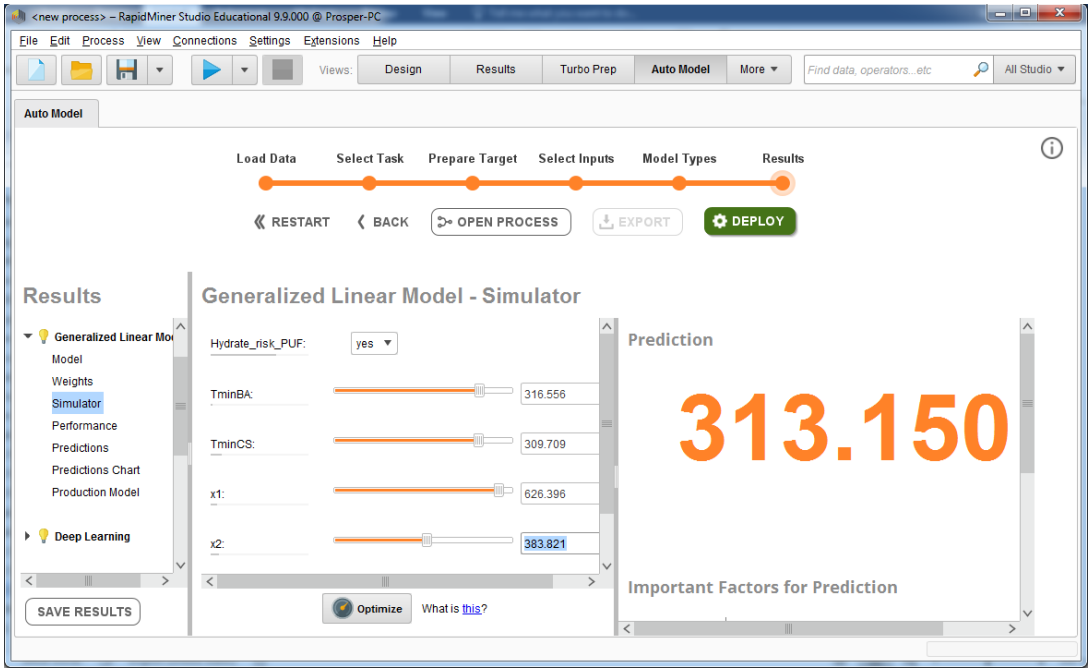

Figure 3.67: visualization of the optimum insulation thickness of PUF material given by GLM using RAPIDMINER.

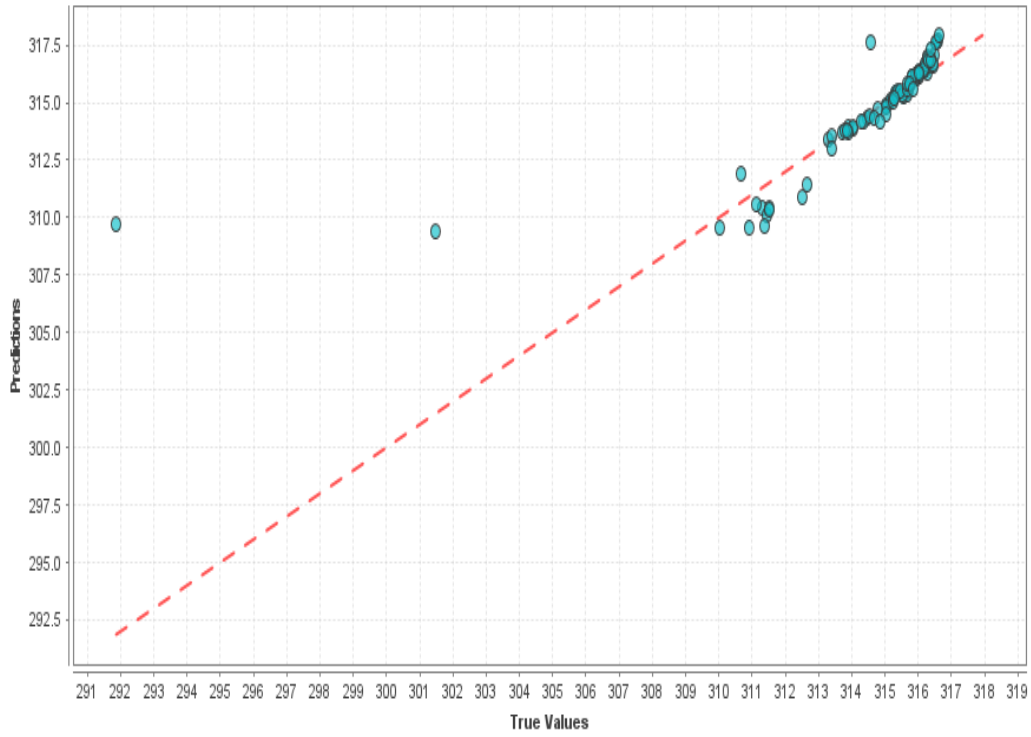

Figure 3.68: predicted values vs true values of the minimum temperature of the system given by the DL using RAPIDMINER with PUF insulating material

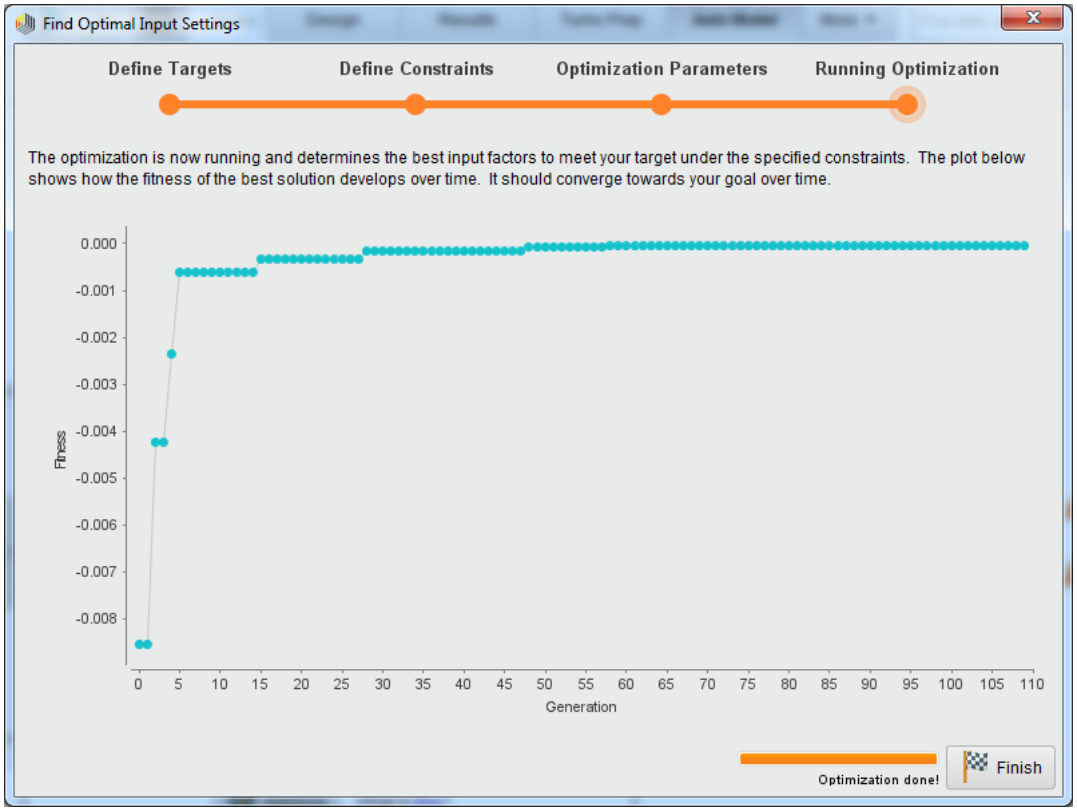

Figure 3.69: Application of G.A to DL for optimal insulation thickness of PUF using RAPIDMINER

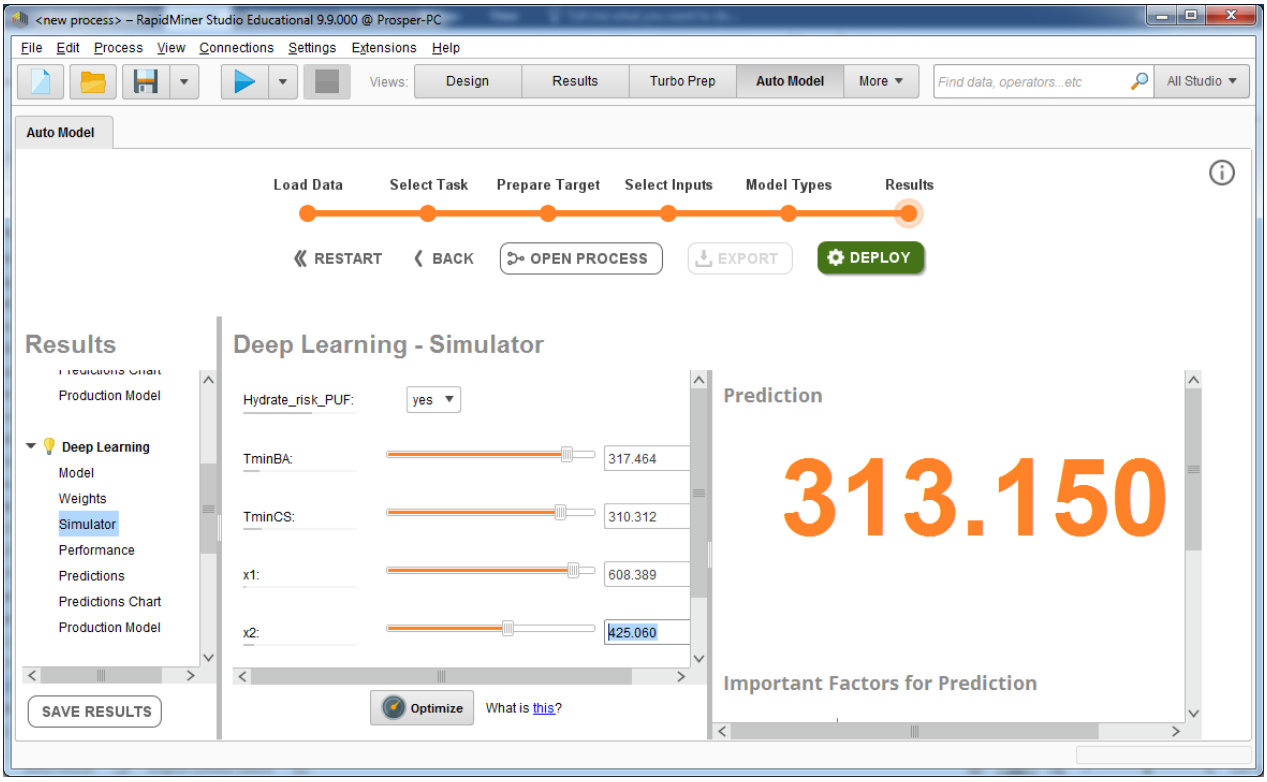

Figure 3.70: visualization of the optimum insulation thickness of PUF material given by DL using RAPIDMINER

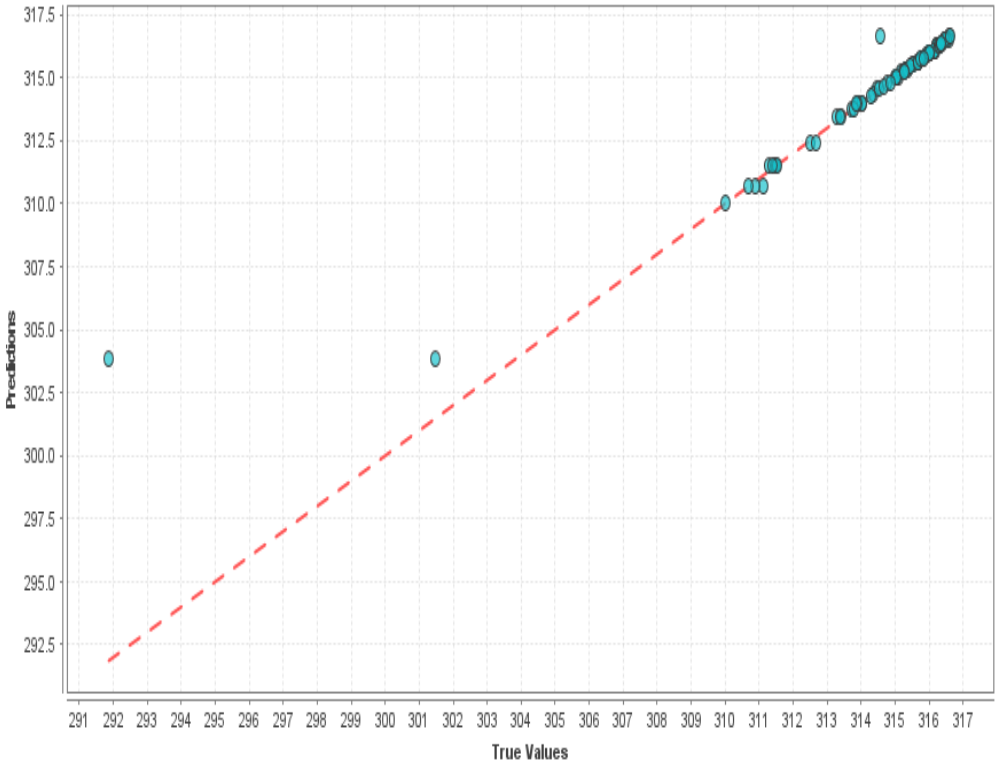

Figure 3.71: predicted values vs true values of the minimum temperature of the system given by the DT using RAPIDMINER with PUF insulating material

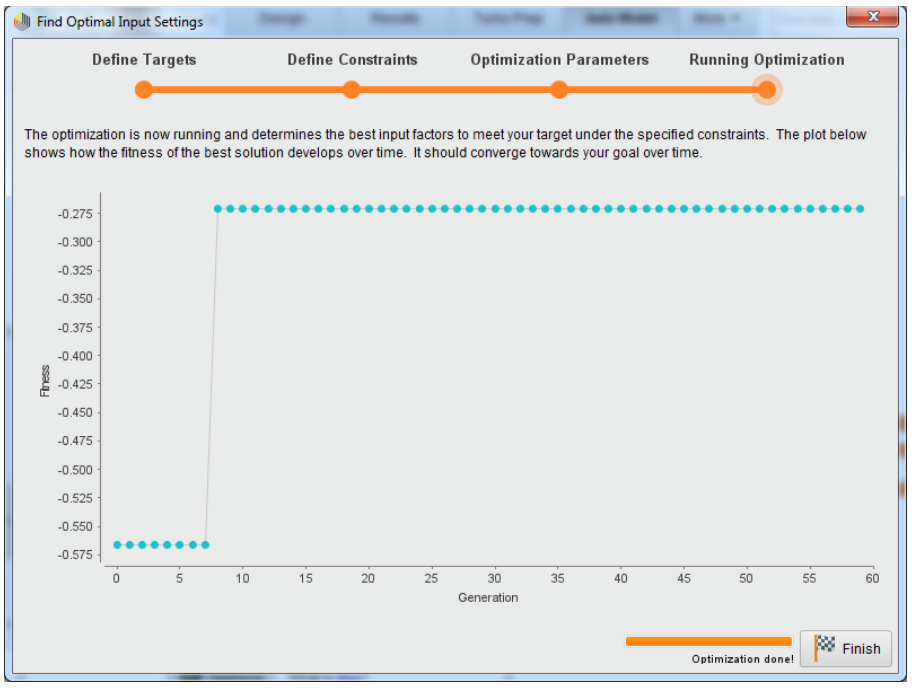

Figure 3.72: Application of G.A to DT for optimal insulation thickness of PUF using RAPIDMINER

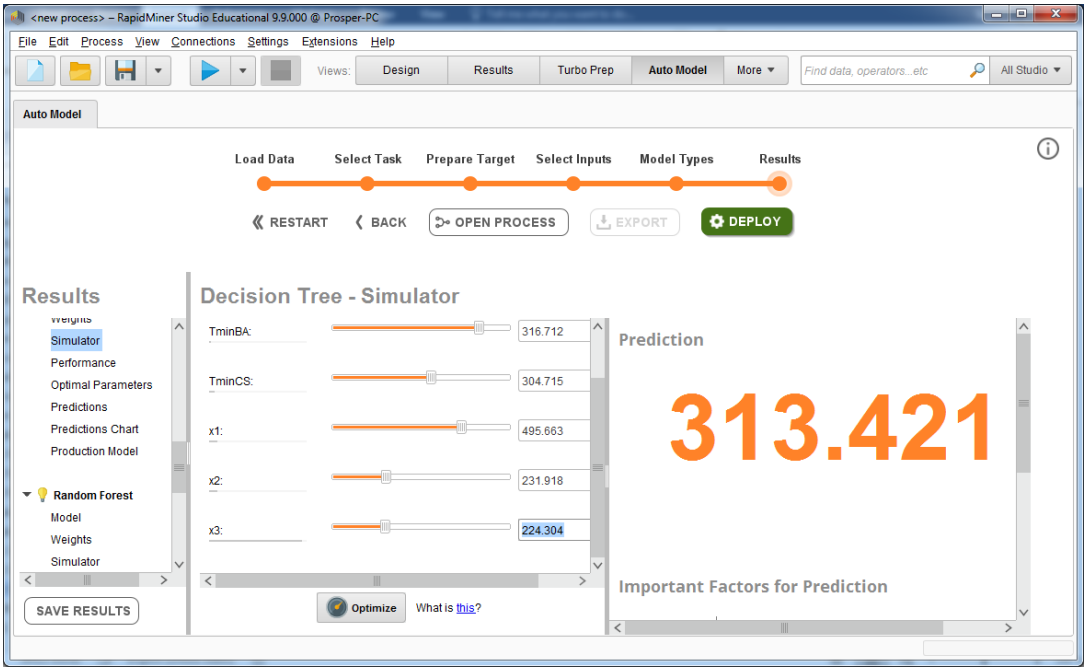

Figure 3.73: visualization of the optimum insulation thickness of PUF material given by DT using RAPIDMINER

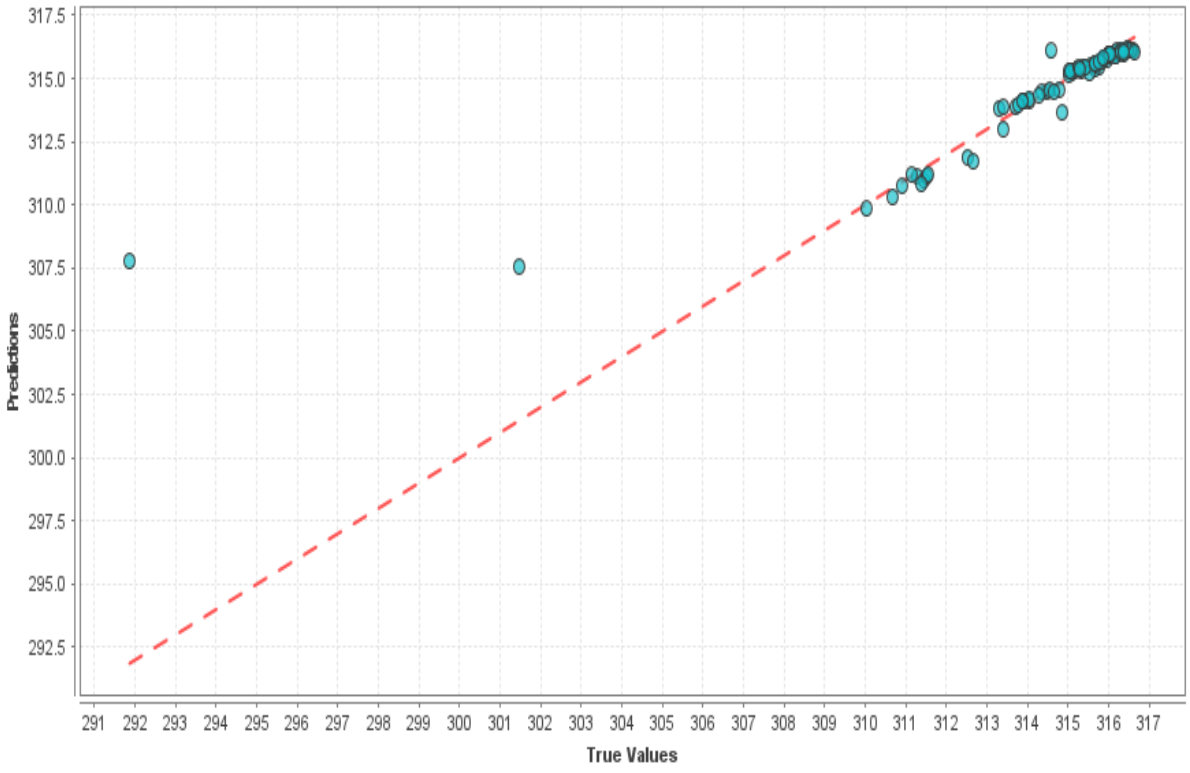

Figure 3.74: predicted values vs true values of the minimum temperature of the system given by the RF using RAPIDMINER with PUF insulating material

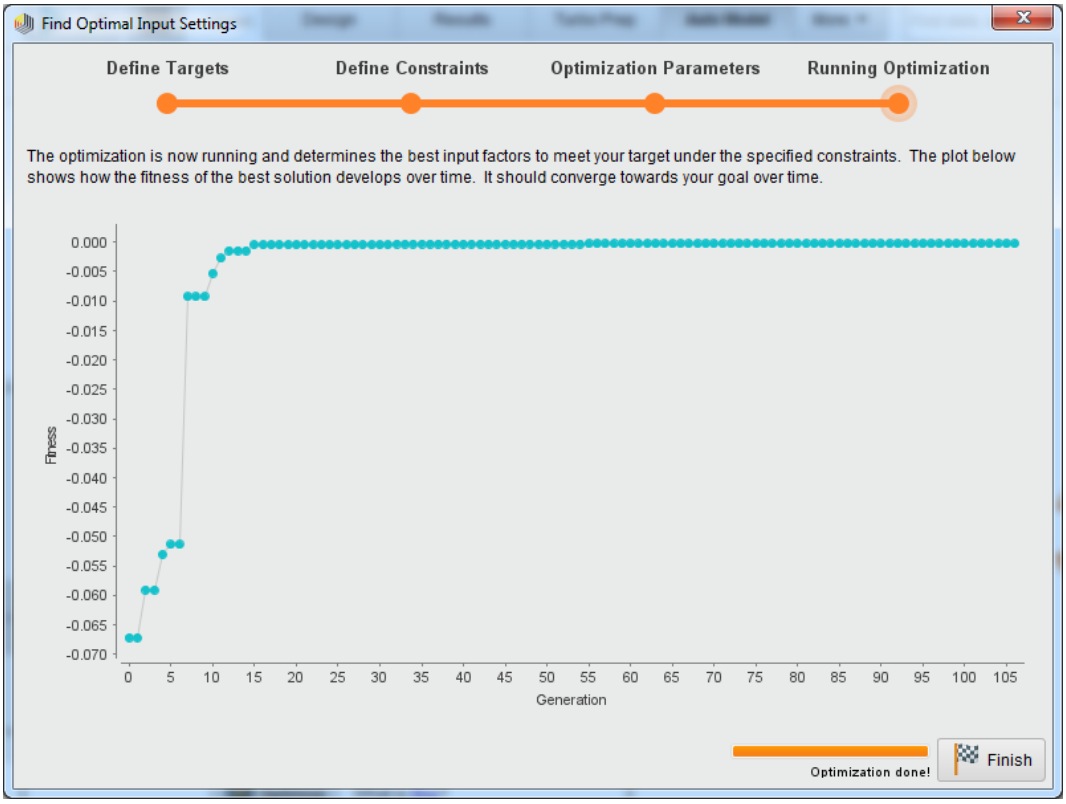

Figure 3.75: Application of G.A to RF for optimal insulation thickness of PUF using RAPIDMINER

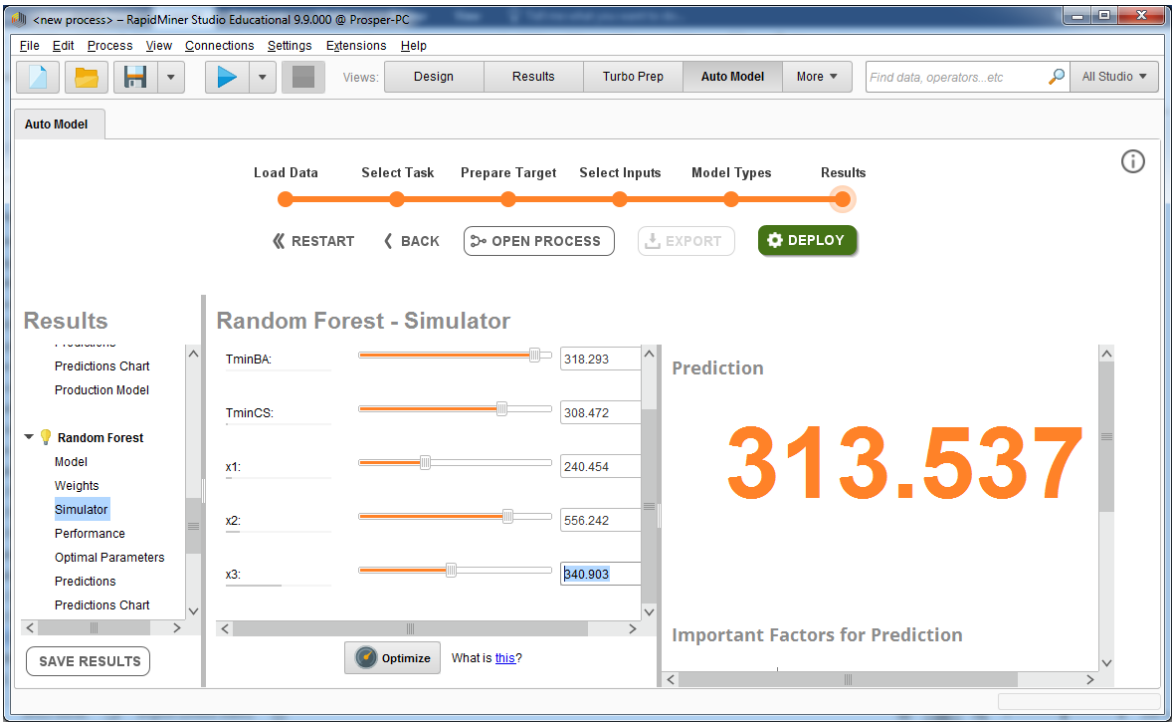

Figure 3.76: visualization of the optimum insulation thickness of PUF material given by RF using RAPIDMINER

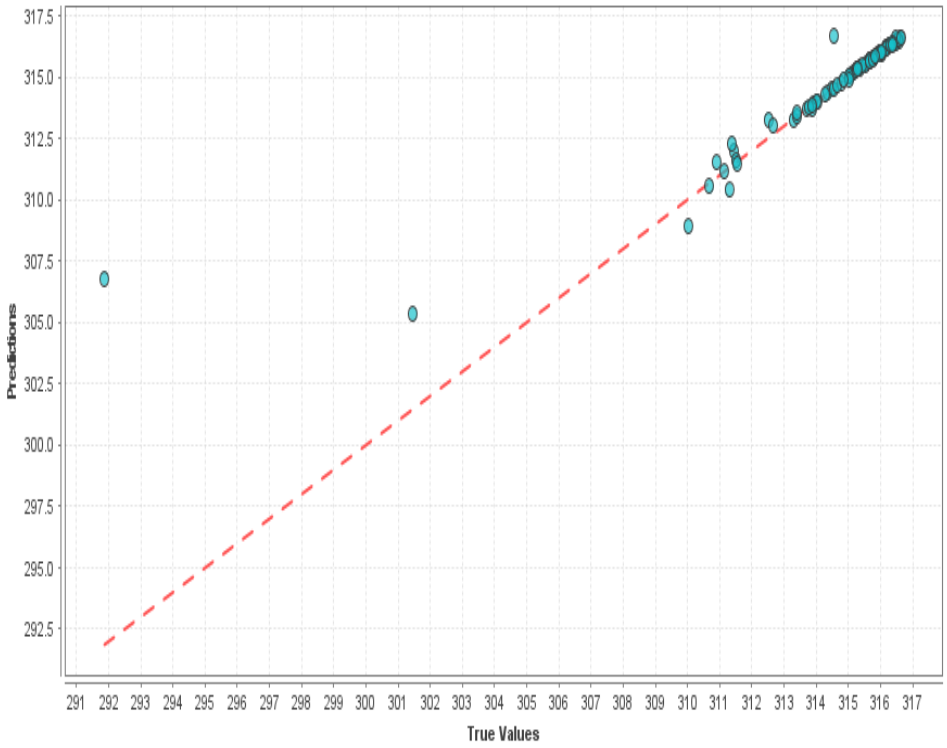

Figure 3.77: predicted values vs true values of the minimum temperature of the system given by the SVM using RAPIDMINER with PUF insulating material

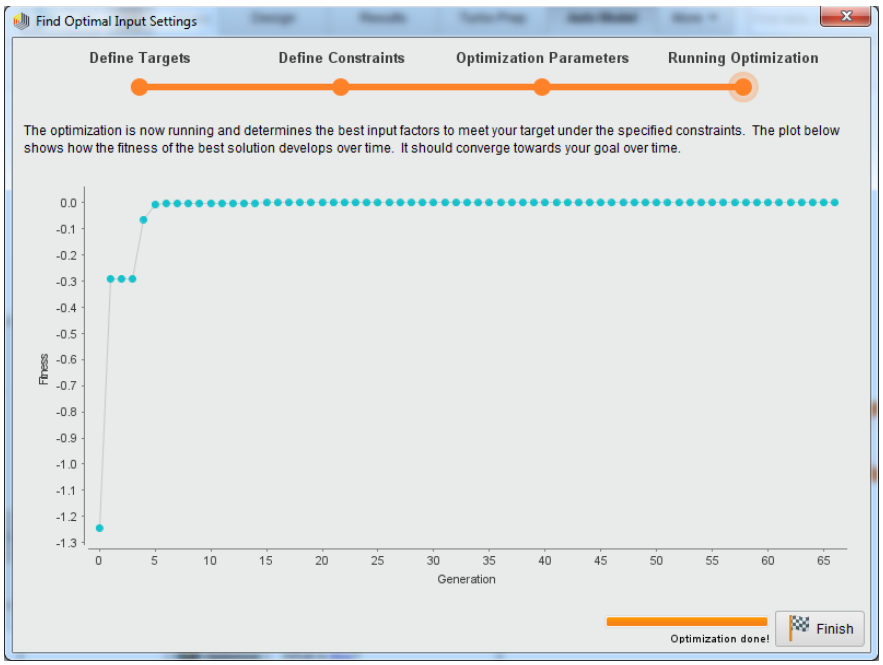

Figure 3.78: Application of G.A to SVM for optimal insulation thickness of PUF using RAPIDMINER

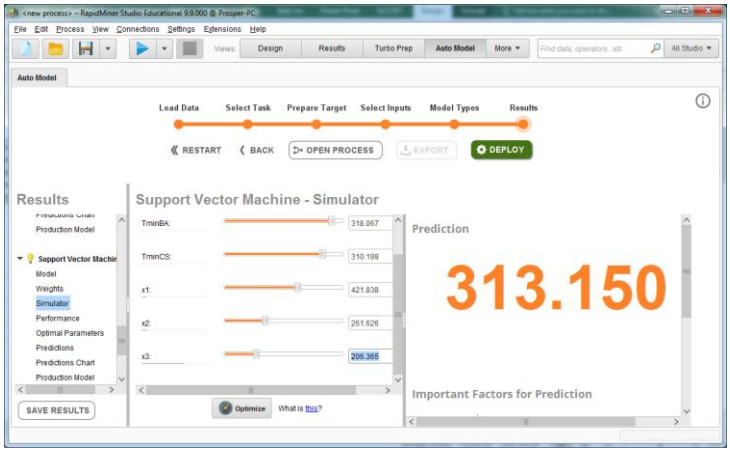

Figure 3.79: visualization of the optimum insulation thickness of PUF material given by SVM using RAPIDMINER

Table 3.15: performance and optimum insulation thickness of PUF using machine learning model with RAPIDMINER

Models	RMSE	Mean Absolute Error	Correlation Coefficient	Optimum insulation thickness (mm)
Generalized Linear Model	0.74	0.53	0.96	449.55
Deep Learning	0.71	0.48	0.96	424.29
Decision Tree	**0.19**	**0.08**	**0.98**	**224.30**
Random Forest	0.37	0.27	0.97	340.90
Support Vector Machine	**0.35**	**0.13**	**0.98**	**206.36**

Table 3.16: comparison of insulation thickness and insulation volume of various models for the case of PUF

Models	Optimum insulation thickness (mm)	Absolute error	Insulation volume (m^3)
True Numerical value	**223.02**		**30491.01**
Numerical model	**228.60**	**5.58**	**31454.17**
Generalized Linear Model	449.55	226.53	77451.70
Deep Learning	424.29	201.27	71415.69
Decision Tree	**224.30**	**1.28**	**30711.77**
Random Forest	340.90	117.88	52917.13
Support Vector Machine	206.36	16.66	27674.35
Regression model	**223.02**	**0.00**	**30507.80**

3.6.4 Optimum insulation thickness of the subsea pipeline

Here we summarized the results presented above and we select the best insulating material as well as the best global minimum insulation thickness for the considered subsea pipeline.

Table 3.17: comparison of insulation thickness and insulation volume of various models.

Models	Optimum insulation thickness (mm)			Insulation volume (m^3)		
	BA	CS	PUF	**BA**	CS	PUF
Numerical model	**88.90**	694.70	228.60	**9759.56**	92181.98	31454.17
Generalized Linear Model	**118.72**	562.69	449.55	**14288.16**	106937.78	77451.70
Deep Learning	**118.72**	507.47	424.29	**14288.16**	92044.88	71415.69
Decision Tree	**81.63**	698.00	224.30	**9349.07**	147480.83	30711.77
Random Forest	**81.63**	697.74	340.90	**9349.07**	147399.98	52917.13
Support Vector Machine	65.88	670.28	206.36	7382.56	138707.71	27674.35
Regression model	**79.38**	693.60	223.02	**9067.19**	146148.00	30507.80

From the results presented above and the results shown in Table 3.17, we observed that, the black aerogel insulating material is the best option and the best minimum insulation thickness is comprised between 79.38 and 81.636 mm. The regression model was the best model among the others and predicted a global minimum of insulation thickness for the B.A insulating material of 79.38mm. The difference between the true numerical value is **9.52mm** corresponding to a gain in insulation volume of about **982.45m^3**. This result indicate that machine learning algorithm combined to G.A is appropriate for the consumption material limitation.

3.7 Flow assurance solids risk formation assessment using logistic regression

Here we analyzed the effect of the best insulating material selected above, that is black aerogel as well as the effect of the minimum temperature of the system on the flow assurance (F.A) solids risk formation

in subsea pipeline using logistic regression model via MATLAB. The model validation is further done by comparing results generated via MATLAB script and the results displayed by STATGRAPHIC.

3.7.1 Flow assurance solids risk formation assessment using logistic regression via MATLAB

In this section, we are presenting the results of the logistic regression model applied for the flow assurance solids risk formation during oil and gas transportation in subsea pipeline. The logistic regression using two independent variables (insulation thickness and minimum temperature of the system is first applied on the dataset. Figure 3.80 below represents the plot of the train logistic regression model. From this figure, we can observe that the logistic regression model performed well by given a good prediction of the different data. However, the predicted model did not give correct results between 312°K and 314°K. The 0 mean that flow assurance solids will not form and the 1 simple mean that solids formation may occur. For insulation thickness located at far distance to the right, no risk of flow assurance exists. Equation (2.115) is used to find out the probability of flow assurance solids risk formation inside the subsea pipeline. Figure 3.81 below shows the plot of this result obtained using only minimum temperature of the system as independent variable. From this figure, we noticed that the logistic regression model fits the training model. One can note that at a minimum temperature of 312°K flow assurance solids formation will have a 100% probability to occur while at a minimum temperature of 314°K, the flow assurance solids will have an occurrence probability of 0%. Similar results were obtained using insulation thickness as the independent variable.

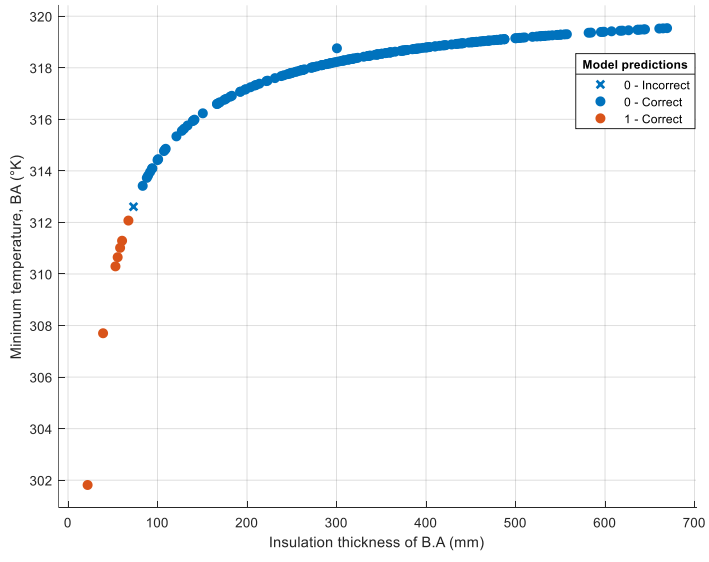

Figure 3.80: plot of flow assurance solids risk formation using two variables: insulation thickness and minimum temperature

In figure 3.82 below, it can be seen that, the logistic train model and the predicted model are in good agreement. Furthermore, one can notice that the probability of solids formation increases to a value of 1 as the insulation thickness of the black aerogel insulating material get lower and lower than an approximatively value of 83.45 mm. for all insulation thickness greater than this value, no flow assurance solids risk exists.

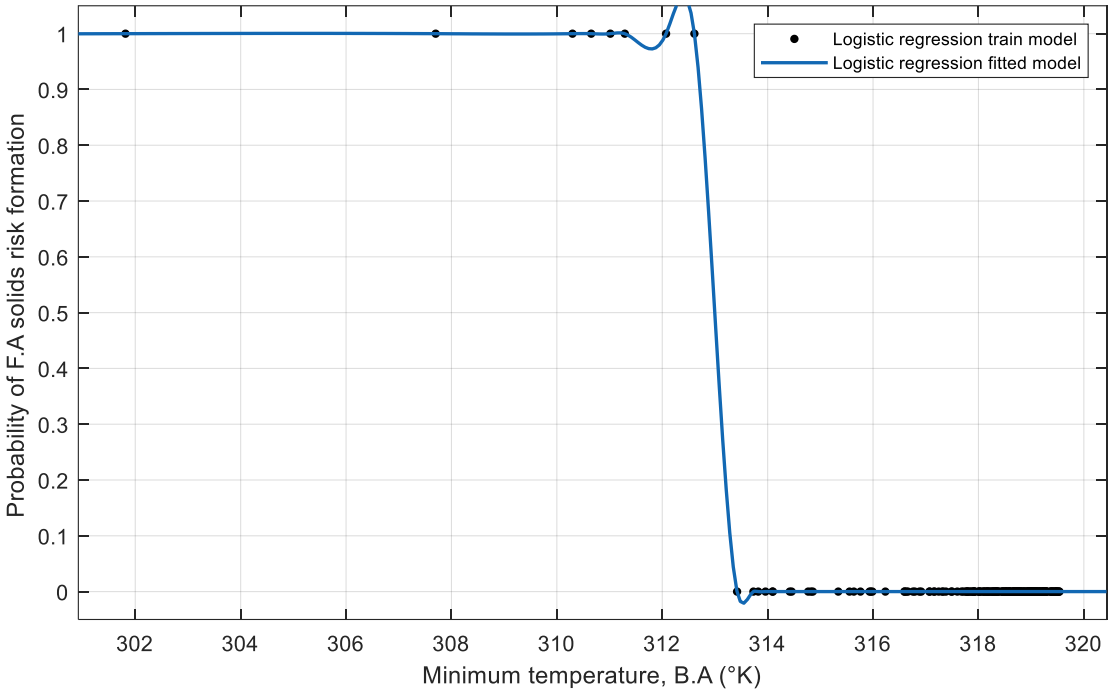

Figure 3.81: plot of the probability of F.A solids risk formation vs minimum temperature.

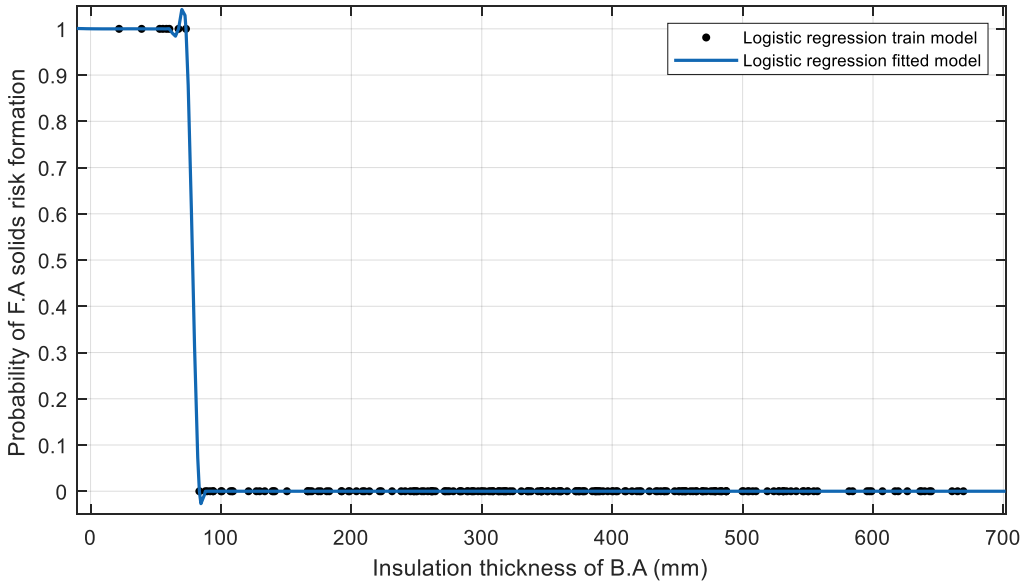

Figure 3.82: plot of the probability of F.A solids risk formation vs insulation thickness of B.A .

3.7.2 Flow assurance solids risk formation assessment using logistic regression via STATGRAPHIC

For the purpose of validation, logistic regression model was also built in STATGRAPHIC version 19 software.

- In the first case, one independent variable was used, the minimum temperature of the system. 210 observations were achieved. Moreover, the flow assurance solids risk formation was evaluated using the maximum likelihood. The Table 3.18 gives the value of the parameters defining the logistic regression in equation (2.115) and Table 3.19 present the deviance values.

Table 3.18: Estimated Regression Model (Maximum Likelihood)

Parameter	Estimate	Standard Error	Estimated Odds Ratio
Constant	4321.99	1397.02	
Minimum temperature	-13.80	4.44	0.00

The output shows the results of fitting a logistic regression model to describe the relationship between flow assurance solids risk formation and 1 independent variable, the minimum temperature of the system. The equation of the fitted model is

$$P(Tmin) = \frac{\exp(z1)}{1+\exp(z1)} \tag{3.2}$$

where

$$z1 = 4321.99 - 13.8075 * Tmin \tag{3.3}$$

Table 3.19: Analysis of deviance

Source	*Deviance*	*P-Value*
Model	67.95	**0.001**
Residual	0.02	1.00
Total (corrected.)	67.97	

Because the P-value for the model in the Analysis of Deviance table is less than **0.05**, there is a statistically significant relationship between the variables at the 95.0% confidence level. In addition, the P-value for the residuals is greater than **0.05**, indicating that the model is not significantly worse than the best possible model for this data at the 95.00% or higher confidence level. The percentage of deviance explained by model = 99.97 and the adjusted percentage = 94.09. The pane also shows that the percentage of deviance in flow assurance solid risk formation explained by the model equals 99.97%. This statistic is similar to

the usual R-Squared statistic. The adjusted percentage, which is more suitable for comparing models with different numbers of independent variables, is 94.09%. In figure 3.83 below, the plot of the logistic regression model with a 95% confidence is presented. The Plot of this figure displays the estimated probability of the flow assurance solids risk formation versus the minimum temperature. We can observe that, the figure in 3.81 and figure 3.84 shows similarities. The curve in blue represents the model while the red curves are the low and high boundary of the curve model with a 95% confidence. From this figure, it can be seen that at a minimum temperature of 312°K, the solids risk formation probability is 100% and at minimum temperature of 314°K, the occurrence risk of the solids is 0%. These are in good agreement as those shown in figure 3.81 above.

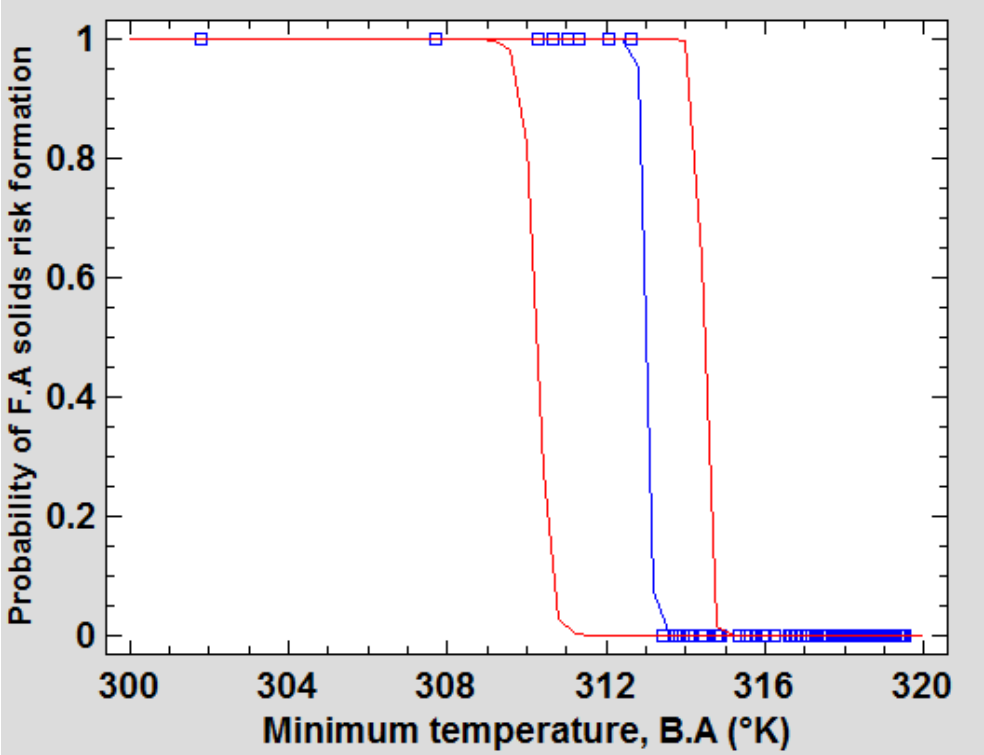

Figure 3.83: plot of the probability of F.A solids risk occurrence vs minimum temperature

In the second case, insulation thickness is used as the independent variable. Table 3.20 below gives the parameters defining the model and Table 3.21 present the deviance values.

Table 3.20: Estimated Regression Model (Maximum Likelihood)

Parameter	Estimate	Standard Error	Estimated Odds Ratio
Constant	37.27	6.09	
Insulation thickness	-0.47	0.06	0.62

Table 3.21: Analysis of deviance

Source	Deviance	P-Value
Model	67.59	0.001
Residual	0.37	1.00
Total (corrected.)	67.97	

The percentage of deviance explained by model = 99.44 and adjusted percentage = 93.55. Figure 3.84 below, shows the results of fitting the logistic regression model to describe the relationship between flow assurance solids risk formation and one independent variable.

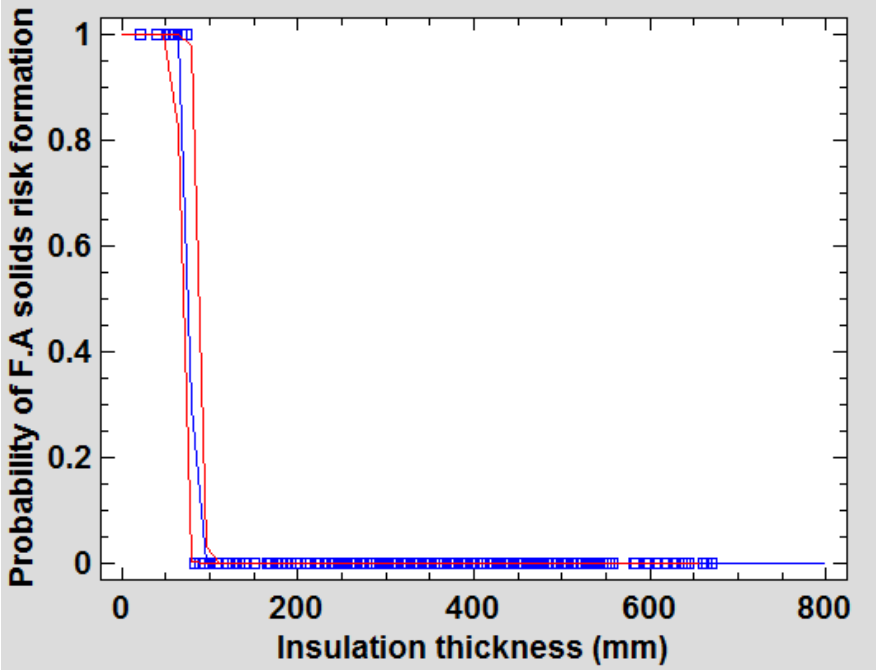

Figure 3.84: flow assurance solids risk formation vs insulation thickness

The equation of the fitted model is

$$P(Insulation\ thickness) = \frac{\exp(z1)}{1+\exp(z1)} \quad (3.4)$$

where

$$z1 = 37.2701 - 0.47657 * insulation\ thickness \quad (3.5)$$

Because the P-value for the model in the Analysis of Deviance table is less than 0.05, there is a statistically significant relationship between the variables at the 95.00% confidence level. In addition, the P-value for

the residuals is greater than or equal to 0.05, indicating that the model is not significantly worse than the best possible model for this data at the 95.00% or higher confidence level. The pane also shows that the percentage of deviance in solids risk formation probability explained by the model equals 99.40%. This statistic is similar to the usual R-Squared statistic. The adjusted percentage, which is more suitable for comparing models with different numbers of independent variables, is 93.55%. This value indicates when considering two independent variables, the insulation thickness might not be statistically significant at the 95.00% and may be ignored because the adjusted value of the minimum temperature which is 94.09% appear to be greater than the 93.55%. It can also be seen that figure 3.84 and figure 3.81 are similar. Furthermore, one can notice that the probability of solids formation increases to a value of 1 as the insulation thickness of the black aerogel insulating material get lower and lower than an approximatively value of 83.45 mm. for all insulation thickness greater than this value, no flow assurance solids risk exists.

Conclusion

In this chapter, the results from the simulation of the temperature and pressure models using MATLAB are presented. It is shown that, results generated by our model via MATLAB, and those obtained from: PIPESIM model, measured value in literature and the unified pressure temperature profile (UPTP) developed by [4] are in good agreement. The optimum insulation thickness of three insulating materials was determined. For each thickness, the thermal requirement condition was verified. Based on this information, the best insulating material was the Black Aerogel material, with an insulation thickness of 79.38mm. Results from the determination of insulation thickness of each insulating material based on the three approaches mentioned above, indicates that, machine learning combined to genetic algorithm is the ideal method to find out the best insulation distribution in terms of reduction in material consumption volume, thus for cost related to pipe-insulation. Next, it is also showed that, neither the polyurethane nor the calcium silicate fulfilled the objective function constraint and the requirement constraint. Therefore, using calcium silicate or polyurethane will demand more material consumption than that of black aerogel insulating material. Finally, logistic regression model built using MATLAB for assessing the risk of some flow assurance solids formation was validated using STATGRAPHIC software. This result indicates that, the two software are able to capture the problem of flow assurance risk in subsea pipeline, using logistic regression.

CONCLUSION AND RECOMMENDATIONS FOR FUTURE WORK

In summary, a low thermal model was developed in this thesis. The model was used to predict pressure and temperature profile. Further, a nonlinear and accurate pattern between the insulation thickness and the minimum working temperature was successfully established using regression model. The trained algorithm was able to predict the minimum temperature of the subsea production pipeline with a smaller relative error of 0.4%. Incorporating machine learning techniques and an optimization algorithm is the ideal method to find out the best insulation distribution. The results obtained by the GA optimization algorithms are optimistic in terms of reducing the insulation material consumption. In the case study, the black aerogel, calcium silicate and polyurethane foam were used as insulating materials and the optimization algorithm combined to machine learning gave the best optimum insulation thickness. It was shown that, optimization algorithm combined with machine learning technique lead to a reduction of insulation volume of about 44.18m³ when compared to the manually approach, which demonstrates somehow, the great potential of the optimization method. It is also important to note that we have two options of providing the training data in machine learning: using numerical simulation software or by in-situ measurements. Some of the significant points of this thesis can be listed below:

- Multiphase fundamental of oil and gas flow have been review herein
- Oil and gas fluid properties were characterized using black oil model using MATLAB software
- Pressure profile for and oil gas flow in long subsea undulated pipeline was predicted during transportation using MATLAB software
- Temperature profile of oil and gas flow was predicted during transportation using MATLAB software
- Pipeline model was built in PIPESIM software
- Temperature and pressure profile were calculated using PIPESIM software
- Insulation thickness was designed using numerical simulation based on manually defined thickness
- Machine leaning techniques such as Deep leaning, decision tree, support vector machine, random forest, generalized linear model, logistic regression and regression model were implemented using MATLAB, RAPIDMINER and STATGRAPHIC software
- Genetic algorithm was used for optimization

- Finally, logistic regression was used to investigate the probability of formation of some flow assurance solids component

Temperature is an important parameter that help to design production system. The knowledge of how temperature is being distributed along subsea pipeline is very important in oil and gas production system. A complete thermal design is obtained by combining steady and transient state simulation. This could be useful in optimizing the requirement constraint. For example, it will be very interesting to know within how many hour solids precipitation and deposition will start to form after shut-in and shutdown time. There are nowadays, many new insulating materials with better thermal performance and properties. These insulating materials could also be investigated for the conservation heat of subsea pipeline. Compositional option of characterizing fluids could also be used. So, for future work, the following recommendations are suggested:

- Transient temperature profile could be coupled to the steady state model developed here to complete the thermal design analysis.
- Compositional oil model could be used for fluid characterization and compared to the black oil model approached.
- Analysis of the effect of a large amount and new insulating materials on the temperature effect is also suggested.
- The objective function constraint could include the cost of insulating material, the maintenance cost, the total cost of the project.
- Shut-in and shutdown time could be analyzed in this work.
- Another optimization algorithm such as particle swarm optimization could be used in this work and compared to the GA.
- Others numerical simulations tools such as COMSOL Multiphysics and Olga software could be used and compared to our numerical results.
- Finally, more data greater than 200 for example 2000 data or 10000 data could be generated experimentally or by numerical simulations to prepare machine learning models.

REFERENCES

[1] www.Total.com, accessed on 09/27/2013

[2] Davis, L., (2011). Offshore tide on the rise, in: E&P Magazine. Hart Energy, Houston, Texas, USA. (http://www.epmag.com/item/Offshore-Tide-The-Rise 92764, accessed 09/17/2012).

[3] Kaczmarski, A.A., Lorimer, S.E., (2001). Emergence of flow assurance as a technical discipline specific to deepwater: Technical challenges and integration into subsea systems engineering. Offshore Technology Conference, Houston, Texas, USA, 30 Apr-3 May. https://doi.org/10.4043/13123-MS.

[4]: Duan, J.M., Wang, W., Zhang, Y., Zheng, L.J., Liuand, H.S., Gong, J., (2013). Energy Equation Derivation of the Oil-Gas Flow in Pipelines. *Oil & Gas Science and Technology – Rev. IFP Energiesnouvelles*, https://doi.org/10.2516/ogst/2012020.

[5]: Knut, V.L., (2015). Advanced Temperature Model for HPHT Conditions. Master Thesis in Petroleum Geoscience and Engineering, Department of Petroleum Engineering and Applied Geophysics, Norwegian University of Science and Technology.

[6] Sharifian, R., (2016). Temperature Modeling for Nodal Analysis. Master of Science in Applied Earth Sciences, Faculty of Civil Engineering & Geosciences, Delft University of Technology.

[7] Onuh, Y.C., (2011). Temperature Prediction Model for Flowing Distribution in Wellbores and Pipelines. Master of Science in Petroleum Engineering, Faculty of the African University of Science and Technology Abuja-Nigeria.

[8] Ayala, L.F., Dong, T., (2015). Thermodynamic analysis of thermal responses in horizontal wellbores. J Energy Resour Technol. http://doi.org/10.1007/s13202-015-0166-x

[9] Romero, O.J., Saad, H.C., Pereira, I.B., Romero, M.I., (2016). Influence of heat transfer on two-phase flow behavior in on-shore oil pipelines.*Ingeniería e Investigación*. http://dx.doi.org/10.15446/ing.investig.v36n1.51570.

[10] Nurfarah, H.B.Z., William, P., (2016). Optimum Thermal Insulation Design for Subsea Pipeline Flow Assurance. Researchgate. http://doi.org/10.13140/RG.2.2.33853.05603.

[11] Kiran, D., Sadafule, S., (2014). Study on effect of insulation design on thermal-hydraulic analysis: an important aspect in subsea pipeline designing. Technical Report, Maharashtra Institute of Technology. https://www.researchgate.net/publication/263426807.

[12] Ibrahim, M.A., (2018). Modeling and development of insulation materials in subsea pipeline. Master thesis, Faculty of Engineering and Applied Science, University of Newfoundland. https://www.semanticscholar.org.

[13] Briggs, T.A., Onyegiri, I.E., Ekwe, E.B., (2020). Investigation of the effects of flowlines sizes, flow rates, insulation material, type and configuration on flow assurance of waxy crude. Innovative Systems Design and Engineering. https://doi.org/10.7176/ISDE/11-3-02.

[14] Mobolaji, A., Adekola, A., (2020). Optimization of Thermal Insulation of Subsea Flowlines for Hydrates. Society of Petroleum Engineers. https://doi.org/10.2118/203721-MS.

[15] Marfo, S.A., Opoku, A.P., Kpami, L.A.A., (2018). Subsea pipeline design for natural gas transportation: A case study of côte d'ivoire's gazelle field. International Journal of Petroleum and Petrochemical Engineering (IJPPE). http://dx.doi.org/10.20431/24547980.0403003

[16] Marfo, S.A., Opoku, A.P., Acquah, J., Amafio, E.M., (2019). Flow assurance in subsea pipeline design-A case study of Ghana's Jubilee and TENfield, Ghana Minig Journal. https://dx.doi.org/104314/gmv19i1.9.

[17] Alade, O., (2018). Sizing surface production flowlines insulation thickness for a desired output temperature. Petroleum & Petrochemical Engineering Journal. https://doi.org/10.23880/ppej-16000178

[18] Abduvayt, P., Arihara, N., Manabe, R., Ikeda, K., (2003). "Experimental and modeling studies for gas-liquid two-phase flow at high pressure conditions." *Journal of the Japan Petroleum Institute.* https://doi.org/10.1627/jpi.46.111.

[19] Fidan., (2011). Wellbore heat loss calculation during steam injection in onshore & offshore environments. Master Thesis, Department of Ressources Engineering, STANFORD UNIVERSITY.

[20] Boyun, G., William, C., Lyons, A.G., (2007). Petroleum Production Engineering: A Computer-Assisted Approach. Publisher: Elsevier Science & Technology Books. ISBN: 0750682701.

[21] Eissa, M.A., Brill, J.P., (2017). Applied Multiphase Flow in Pipes and Flow Assurance, Oil and Gas Production. Society of Petroleum Engineers. 222 Palisades Creek Drive Richardson, TX 75080-2040 USA. ISBN 978-1-61399-492-4.

[22] Jansen, J.D., (2016). Nodal analysis of oil and gas wells – system modeling and numerical implementation. SPE Textbook Series. SPE, Richardson. In production.

[23] Andreolli, I., Zortea, M., Baliño, J.L., (2017). Modeling offshore steady flow field data using drift-flux and black-oil models, Journal of Petroleum Science and Engineering. https://doi.org/10.1016/j.petrol.2017.07.001.

[24] Beggs, H.D., Brill, J.P., (1973). A study of two-phase flow in inclined pipes. *Journal of Petroleum Technology*. https://doi.org/10.2118/4007-PA .

[25] Brill, J.P., Mukherjee, H. K., (1999). Multiphase flow in wells. Society of Petroleum Engineers. SPE Monograph series vol.17. ISBN:978-1-55563-080-5. 164pp.

[26] Ove, B., (2010). Pipe Flow 2: Multi-phase Flow Assurance, International Energy Agency, USA About Oil & Gas Technologies for the future. ISBN 978-616-335-926-1, drbratland.com.

[27] Beal, C., (1946). The viscosity of air, water, natural gas, crude oil and its associated gases at oil field temperatures and pressures. Transactions of the AIME. . https://doi.org/10.2118/946094-G

[28] Beggs, D.H., Robinson, J.R., (1975). Estimating the viscosity of crude oil systems. Journal of Petroleum technology. https://doi.org/10.2118/5434-PA

[29] Vazquez, M., Beggs, H.D., (1980). Correlations for fluid physical property prediction. Journal of Petroleum Technology. https://doi.org/10.2118/6719-PA

[30] Standing, M.B., Katz, D.L., (1942). Density of natural gases. Transactions of the AIME. https://doi.org/10.2118/942140-G

[31] Lee, A.L., Gonzalez, M.H., Eakin, B.E., (1966). The viscosity of natural gases. Journal of Petroleum Technology. https://doi.org/10.2118/1340-PA

[32] Henock, M.M., (2004). Comparison of frictional pressure drop correlations for isothermal two-phase horizontal flow. Master thesis, Department of Mechanical Engineering, Bahir Dar University, Ethiopia.

[33] Hasan, A.R., Kabir, C.S., (2002). Fluid flow and heat transfer in wellbores, Society of Petroleum Engineers, Richardson. ISBN:978-1-55563-094-2. 175pp.

[34] Taitel, Y., Dukler, A.E., (1976). A model for predicting flow regime transitions in horizontal and near horizontal gas-liquid flow, AIChE Journal. https://doi.org/10.1002/aic.690220105.

[35] Zuber, N., Findlay, J.A., (1965). Average volumetric concentration in two-phase flow systems. J Heat Transfer. https://doi.org/10.1115/1.3689137 .

[36] Woldesemayat, M., Ghajar, A.J., (2007). Comparison of void fraction correlations for different flow patterns in horizontal and upward inclined pipes. International Journal of Multiphase Flow. https://doi.org/10.1016/j.ijmultiphaseflow.2006.09.004

[37] Wallis, G.B., (1969). One-dimensional Two-phase Flow. McGraw-Hill, New York, 243.ISBN:978007067942900679428. 408pp.

[38] Müller, H., Heck, K., (1986). A simple friction pressure drop correlation for two-phase ow in pipes. Chemical Engineering and Processing: Process Intensification. https://doi.org/10.11016/0255-2701(86)80008-3 .

[39] Vieira, R.A., Garcia, A. P., (2014). Combination of petroleum correlations and drift-flux approaches: A new model for two-phase flow pressure gradient calculation for horizontal and slightly inclined upward flowlines. In: ASME 2014 33rd International Conference on Ocean, Offshore and Arctic Engineering. American Society of Mechanical Engineers.

[40] Swamee, P. K., (1993). Design of a submarine oil pipeline. Journal of transportation Engineering. https://doi.org/10.11061/(ASCE)0733-947X(1993)119:1(159)n .

[41] Afshin, J.G., Clement, C.T., (2010). Importance of Non-Boiling Two-Phase Flow Heat Transfer in Pipes for Industrial Applications.Taylor&Francis.https://doi.org/10.1080/01457630903500833

[42] Stéphane, L., Josua, P., (2011). Two-phase flow in inclined tubes with specific reference to condensation: A review. International Journal of Multiphase Flow, Elsevier https://doi.org/10.1016/j.ijmultiphaseflow.2011.04.005 .

[43] Gnielinski, V., (1976). New equations for heat and mass transfer in the turbulent pipe and channel flow. Int. Chem.Eng.

[44] Qiang, B., Yong, B., (2005). Subsea Pipeline Design, Analysis, and Installation. Technology &Engineering.

[45] Aurélien, G., (2019). Hands-on Machine Learning with Scikit-Learn, Keras, and TensorFlow. Published by O'Reilly Media, Inc., 1005 Gravenstein Highway North, Sebastopol, CA 95472. Printed in the United States of America.

[46] Mathwork., (2004). Genetic Algorithm and Direct Search Toolbox User's Guide for use in MATLAB. MathWorks, Inc.

[47] www.Mathworks.com, accessed on 05/28/2013

[48] www.pipesim.com, accessed on 07/20/2014

[49] www.Rapidminer.com, accessed on 04/17/2016

[50] Yang, J.L., Estefen, S.F., (2018). Thermal insulation of subsea pipelines for different materials. *Int Journal of Pressure Vessels and Piping*. https://doi.org/10.1016/j.ijpvp.2018.09.009 .

[51] Standing, M.B., (1951). Volumetric and phase behavior of oil field hydrocarbon systems: PVT for engineers. California Research Corp.

[52] McCain, W.D., (1990). The properties of petroleum fluids. PennWell Books, Tulsa. ISBN: 9781615838066. 548pp

[53] Collins, A. G., (1987). Petroleum engineering handbook. SPE, Dallas.

[54] Cazarez, O., Vasquez, M.A., (2005). Prediction of pressure, temperature, and velocity distribution of two-phase ow in oil wells. Journal of Petroleum Science and Engineering, https://doi.org/10.1016/j.petrol.2004.11.003.

[55] Zerpa, L.E., (2013). A practical model to predict gas hydrate formation, dissociation and transportability in oil and gas flowlines. PhD thesis, Faculty and the Board of Trustees of the Colorado School of Mines.

[56] Pourafshary, P., Varavei, A., Sepehrnoori, K., Podio, A., (2008). A Compositional Wellbore/Reservoir Simulator to Model Multiphase Flow and Temperature Distribution, International Petroleum Technology Conference, 3-5 December, Kuala Lumpur, Malaysia. https://doi.org/10.2523/ IPTC-12115-MS.

[57] Kreith, F., Bohn, M., (1997). Principles of Heat Transfer, 5th Edition, PWS Publishing Company.

[58] Ottenbacher, K.J., Smith, P.M., Illig, S.B., Linn, R.T., Fiedler, R.C., Granger, C.V., (2001). Comparison of logistic on and neural networks to predict rehospitalization in patients with stroke". Journal of clinical epidemiology. https://doi.org/10.1016/ s0895-4356(01)00395-x.

[59] Dowdy,S., Chilko D., (2004). Statistics for research:3rd edition". Hoboken, New Jersey: John Wiley & Sons, Inc. ISBN:0-471-26735-X

APPENDICE

List of publications

1- Gopdjim Noumo Prosper, Donatien Njomo, Zepang Nana Kevin, 2020. Numerical Simulation of the Minimum Insulation Thickness to Thermally Design a Subsea Pipeline Carrying an Oil and Gas flow. International Journal of Heat and Technology.

2- Gopdjim Noumo Prosper, Donatien Njomo, Zepang Nana Kevin (2019): Modeling and simulation of the temperature profile along offshore pipeline of an oil and gas flow: effect of insulation materials. International Journal of Innovative Science and Research Technology Volume 4, Issue 9, September - 2019

International Journal of Heat and Technology
Vol. 39, No. 3, June, 2021, pp. 763-774
Journal homepage: http://iieta.org/journals/ijht

Numerical Simulation of the Minimum Insulation Thickness to Thermally Design a Subsea Pipeline Carrying an Oil and Gas Flow

Prosper Gopdjim Noumo*, Donatien Njomo, Kevin Zepang Nana, Leonard Ribot Chuisseu Nguewo

Department of Physics, Faculty of Science, University of Yaounde 1, P.O.Box 812, Yaoundé, Cameroon

Corresponding Author Email: gopdjimnoumop@gmail.com

https://doi.org/10.18280/ijht.390310

Received: 16 September 2020
Accepted: 8 January 2021

Keywords:
thermal insulation, two-phase flow, heat transfer, numerical simulation, temperature profile, pressure profile

ABSTRACT

This paper considered an existing subsea pipeline transporting an oil and gas flow, and proposed to find the best thermal insulating material and the required thickness of insulation necessary to meet an output temperature of 40°C and a pressure of 2.4MPa so as to avoid flow assurance issues. MATLAB and PIPESIM software were employed to run the simulations of the temperature and pressure profiles along the considered pipeline. Data used for the simulations were obtained from open literature. Results obtained from our simulations in MATLAB are validated using PIPESIM software, measured values and prediction model from literature. The temperature model was then used to thermally design an insulation thickness for the 50 km long pipeline using three insulating materials which are: black aerogel, polyurethane and calcium silicate. Results from the analysis showed that the black Aerogel material with a critical thickness of 10.16 cm is most effective to satisfy the criterion design. The effect of the selected insulating material was also investigated on the phase envelop. Results shows that for proper insulation thickness the flowing fluid temperature can be maintained at a temperature above which no flow assurance issues can be observed.

1. INTRODUCTION

In deepwater oil production project, where wells are located far from platforms, offshore fluids generally consisting of oil gas and water are often transported over long distances in subsea pipelines [1]. During the transportation, the multiphase fluids is cooled on its way to the surface production due to heat transfer, through the pipelines walls, with the surrounding seawater [1]. If the production flow-line is not properly and sufficiently insulated against heat losses to the external surrounding, temperature of the flowing fluids inside the subsea pipeline will drop and this may lead to some flow assurance issues such as the precipitation of asphaltenes and/or paraffin wax and the formation of hydrates [2]. For example, it is shown by Ahmed [3] that at temperature around 288, 15°k, wax will start to form inside the pipeline and at temperature below 313, 15°k, combine with high-pressure gas hydrates will occur. As results of these issues, pipe effective flow area may reduce and if serious, blockage may occur [4]. In subsea area, the interaction between the cold surrounding water and the warm flowing fluids inside pipeline is a major cause of temperature drop, which is responsible of some flow assurance issues such as wax deposition, and risk of hydrates formation. Therefore, temperature drops must be prevented in oil and gas production in order to minimize flow assurance issues. This can be achieved by choosing a proper insulation material with an appropriate thickness for the pipeline.

Insulation of pipeline is becoming more and more increasingly important in any subsea project because of the increase in energy saving that it can provides. Optimum insulation thickness need then to be calculated for an appropriate selection of the insulating material with respect to a proper thickness. In recent years, many researches have been carried out on this topic in the open literature showing the interest of scientific for the pipeline thermal design. For examples: Nurfarah and William [5] carried out a study on the optimum thermal insulation design for subsea pipeline. One of theirs objectives was to establish a workflow procedure in selecting thermal insulation materials, thickness and number of layers required for protective coating. The pipeline length considered was comprised between 500 and 1500m and the design criterion was that the output temperature should be above 20°C. They used Visual Basic Application with Excel for the simulations purpose. Kiran [6], explored and compared the various types of insulation and find the optimum thickness of insulation required to maintain the temperature of the fluid inside the pipeline, above the hydrate/wax formation temperature of about 40°C to ensure smooth flow. Excel spreadsheet calculation was used to compare the effect of various insulation material with different thicknesses on the temperature profile of the fluid in deep-water environment. Ibrahim Masaud Ahmed [3], focuses he study on the thermal insulation pipelines used for subsea crude oil transportation. He used MATLAB and Ansys fluent CFD to validate the MATLAB model. Briggs et al. [7] carried out a study using PIPESIM software to investigate the effects of flowline sizes, flow rates, insulation material, type and configuration on flow assurance of waxy crude over 10.2 km between the wellhead and the first stage separator on the platform. Considering the implications of these factors for flow assurance. They used Polyurethane Foam, and pipe-in-pipe insulation type. Mobolaji et al. [8] investigated the best material that is suitable for the thermal insulation of subsea flowlines using the ANSYS software package, and then provided the best

composite arrangement of insulation materials for better heat optimization. They used different insulating materials such as Aerogel, Paraffin Wax, Mineral Wool and Grooved Mineral to fill the gap between the inner pipe and the outer pipe. Marfo et al. [9] used PIPESIM software to design a suitable pipeline for transporting condensate gas for the Jubilee and TEN Fields. The design comprises of two risers and two flowlines. Hydrate formation temperature was determined to be 72.5 °F at a pressure of 3 000 psig. The insulation thickness for flowlines 1 and 2 were determined to be 1.5 in. and 2 in. respectively. Marfo et al. [9] employed PIPESIM software to design a subsea pipeline for transportation of natural gas from Gazelle Field in Côte d'Ivoire to a processing platform located 30 km and to predict the conditions under which hydrate will form so as to be avoided. The found that an insulation thickness of 0.75 in.with specific pipe size of 10 in. could satisfy the arrival pressure condition of 800 psia. However, most of these studies thermally design insulation material for pipelines using computational method and commercial software. Moreover, some of them are based on single-phase flow. As far as two-phase gas and liquid flow is concerned, none of these studies calculated the optimum insulation thickness based on a coupled temperature-pressure model. Pressure and temperature are dependent variables that affect all the flow parameters.

Oluwaseun [10] carried out a study that focuses on choosing and sizing of an insulation material to meet an output temperature of an oil and gas wells. The criterion design output temperature was set at 20℃. the pipeline used was 1km long. The fluids properties was modeled using compositional model. Aspen Hysys software was used and Urethane Foam was used as the insulating material. Similarly to the work done by Zulkefli and Pao [5], this paper focuses on choosing and sizing of an insulation material to meet an output temperature of an oil and gas transporting pipelines in a subsea area from a wellhead to a surface processing plant. The particular points of this work that differ from [4] are:

- the pipeline is 50km long with undulation;
- the fluids properties are calculated using black oil model,
- the design output temperature used is 40℃
- three insulating materials: Calcium Silicate (CS), Black Aerogel (BA) and Polyurethane Foam (PUF) are used for the optimum insulation thickness
- MATLAB and PIPESIM software are used to perform numerical simulations

The aim of this study is to analyze the performance of different insulating materials along with the different insulation thickness. Then choice of the thermal insulation design should have the ability to maintain the flowline temperature above the critical point of hydrate formation temperature in order to prevent hydrate and wax crystals, which is usually 20℃. However, in this study the criterion temperature design was set to 40℃. More specifically, the study objectives are to:

- model the fluids properties with black oil model;
- model the temperature and pressure profiles of an oil and gas flow in an undulated subsea pipeline;
- build a computer program code in MATLAB for numerical simulations; model the temperature with PIPESIM software;
- use the temperature model for the thermal design of the subsea pipeline by performing numerical simulations analysis of different insulating materials with different thicknesses.

This research project is therefore devoted to the investigation of thermal insulation properties and fluid properties on the temperature profile in the pipeline system during steady state condition. The thermal insulation design should have a capability of maintaining the temperature above 40℃. This project is therefore restricted to: undulated subsea pipeline of 427m of altitude and 50km long; passive thermal insulation. This work contributes to a better understanding of the calculation of temperature and pressure distributions during gas and liquid flow in subsea pipeline using black oil model approach for fluids properties characterization, which lead to the optimal choice of the thermal insulation design.

This study is organized as follow: Section 2 presents the methodology and the propose algorithm for steady state flow analysis. Section 3 presents ours case study and field data. The results of our numerical analysis are presented and discussed. Section 4 conclude the work and presents recommendations and future work.

2. METHODOLOGY

2.1 Geometrical parameters of pipeline and insulation materials

The subsea pipeline geometry considered in this study is the same as that presented by Duan et al. [4] for the example 1 case. Figure 1 below represent a vertical section of the considered offshore pipeline. The figure was represented with MATLAB software based on data from the schematic in ref. [4].

Table 1. Geometrical parameters of pipeline and insulation [4]

Internal diameter of pipeline (m)	Outer diameter of pipeline (m)	Thickness of pipeline (m)	Length of pipeline (m)
0.3112	0.3239	0.0127	50,000

The geometrical parameters of the pipeline and insulation materials as well as the thermophysical properties of insulation materials are given in Table 1 and Table 2.

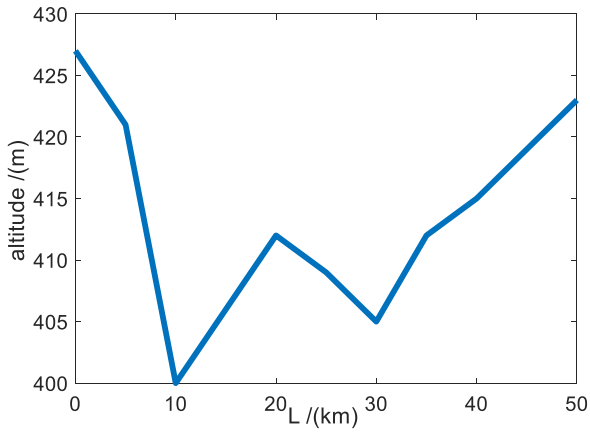

Figure 1. Vertical sectional profile of the pipeline [4]

Table 2. Thermophysical properties of the insulation materials [11, 12]

Insulation materials	Thermal conductivity (W/m K)	Specific heat (Kj/Kg K)	Density (Kg/m³)
Calcium Silicate	0.069	0.96	260
Polyurethane	0.04	1400	45
Black Aerogel	0.012	950	140

2.2 Fluids properties

The black oil model assumed that there are at most three distinct phase: Oil, gas and water. Water and oil are assumed to be immiscible and they do not exchange mass or change phase. Gas is assumed to be soluble in oil but not in water. In this work, the fluids properties were calculated using the black oil approached as follow. All black oil variables are given in S.I units unless precise.

2.2.1 Bubble point pressure P_b

The bubble point pressure can be determined by [13]:

$$\mathrm{P_b} = 1.255\left[\left(\frac{\mathrm{GOR}}{0.0059\gamma_g 10^{2.14/\gamma_o}10^{-0.00198\mathrm{T}}}\right)^{0.83} - 1.76\right] \quad (1)$$

with T is in °*k*, P_b in *Bar*.

2.2.2 Gas oil solution R_s

Standing in 1951 [14], proposed a correlation for the calculation of the gas-oil solution.

$$\mathrm{R_S} = 0.00590\gamma_g 10^{2.14/\gamma_o}10^{-0.00198\mathrm{T}}(0.797.10^{-5}\mathrm{P} + 1.4)^{1.205} \quad (2)$$

For pressures greater than bubble point pressure, R_s=GOR, with T in °*k* and P in *Pa, R_s in Sm³/Sm³.*

2.2.3 Oil formation volume factor B_o

B_o is defined as the ratio between the oil volume at flow conditions and the oil volume at standard conditions.

$$\mathrm{B_o} = \frac{\mathrm{V_o(P,T)}}{\mathrm{V_{o\_sc}}} = \frac{\mathrm{Q_o(P,T)}}{\mathrm{Q_{o\_sc}}} = \frac{\mathrm{V_{so}}}{\mathrm{V_{so\_sc}}} \quad (3)$$

Oil formation volume factors at or less than bubble point pressures can be estimated by using the correlation obtained by Standing [14].

$$\mathrm{B_o} = 0.9759 + 0.952.10^{-3}\left(\mathrm{R_S}\left(\frac{\gamma_g}{\gamma_{osc}}\right)^{0,5} + 0.401\mathrm{T} - 103\right)^{1.2} \quad (4)$$

For pressures greater than bubble point pressure, oil formation volume factor is calculated by [14]:

$$\mathrm{B_o} = \mathrm{B_{ob}}\exp[-\mathrm{C_o}(\mathrm{P} - 10^5\mathrm{P_b})] \quad (5)$$

The coefficient of oil isothermal compressibility is calculated by Vazquez and Beggs [15] using the correlation below:

$$\mathrm{C_o} = 10^{-9}\frac{2.81\mathrm{Rs} + 3.10\mathrm{T} + \frac{171}{\gamma_o} - 118\gamma_g - 1102}{\mathrm{P}} \quad (6)$$

With, T in °*k*, P in *Bar*, B_o in *m³/m³* and C_o in *Bar*$^{-1}$.

2.2.4 Oil viscosity μ_o

The oil viscosity is determined for three thermodynamic pressure levels

- For P=P_{atm}, the dead oil viscosity is calculated using the equation by Beal [16] as presented by [17]:

$$\mu_{od} = C_4\left(0.32 + \frac{1.8\times10^7}{API^{4.53}}\right)\left(\frac{360}{C_3 + 200}\right)^{10^{\left(0.43+\frac{8.33}{API}\right)}} \quad (7)$$

- For P_{atm}<P≤P_b, the live oil viscosity is calculated using Beggs and Robinson [17] formulation

$$\mu_o = 10.715C_4(C_1\mathrm{Rs} + 100)^{-0.515}\left(\frac{\mu_{od}}{C_4}\right)^{(5.44(C_1\mathrm{Rs}+150)^{-0.338})} \quad (8)$$

- For P>P_b, the relation from Vasquez and Beggs [18] is used

$$\mu_o = \mu_{ob}\left(\frac{\mathrm{P}}{\mathrm{P_b}}\right)^{\mathrm{m}} \quad (9)$$

where,

$$\mathrm{m} = 2.6(C_2\mathrm{P})^{1.187}\times e^{-11.513-8.9810^{-5}C_2\mathrm{P}} \quad (10)$$

μ_{ob} is the viscosity at the bubble-point pressure obtained using and setting R_s=GOR.

μ_o is given in *Pa.s.*

2.2.5 Oil specific gravity and oil density γ_o, ρ_o

In petroleum industry, the oil specific gravity and oil density are given by:

$$\gamma_o = \frac{141.5}{\mathrm{API} + 131.5} \quad (11)$$

$$\rho_{o\_sc} = \gamma_o\rho_{w\_sc} \quad (12)$$

$$\rho_o = \frac{\rho_{o\_sc} + \rho_{g\_sc}\mathrm{R_s}}{\mathrm{B_o}} \quad (13)$$

where,

ρ_{o_sc}, ρ_{w_sc} and ρ_{g_sc} are standard densities of oil, water and gas respectively. γ_o is the specific density of oil. ρ_o is the local density of oil at flow conditions.

2.2.6 Gas compressibility factor Z

Correlation presented by Andreolli et al. [11] approximating the abacus data in Standing and Katz [19] is given by:

$$\mathrm{Z} = 1 - \frac{3.52}{10^{0.9813\mathrm{T_{pr}}}} + \frac{0.274\mathrm{P_{pr}^2}}{10^{0.8157\mathrm{T_{pr}}}} \quad (14)$$

$$\mathrm{T_{pr}} = \frac{\mathrm{T}}{\mathrm{T_{pc}}} \quad (15)$$

$$\mathrm{P_{pr}} = \frac{\mathrm{P}}{\mathrm{P_{pc}}} \quad (16)$$

where, the pseudocritical properties were calculated using the Standing [15] correlation

$$T_{pc} = \frac{1}{C_5}\left(168 + 325\gamma_g - 12.5\gamma_g^2\right) \quad (17)$$

$$P_{pc} = \frac{1}{C_2}\left(677 + 15.0\gamma_g - 37.5\gamma_g^2\right) \quad (18)$$

2.2.7 Gas formation volume factor B_g

B_g is defined by the ratio of the free gas volume in flow condition to the volume at standard condition of the same mass of gas.

$$B_g = \frac{V_{g(P,T)}}{V_{g\_sc}} = \frac{\rho_{g\_sc}}{\rho_g} \quad (19)$$

$$B_g = \frac{P_{sc}}{T_{sc}}\frac{ZT}{P} \quad (20)$$

where, P_{sc} and T_{sc} are pressure and temperature at standard condition. T and P are temperature and pressure at flow conditions respectively.

2.2.8 Gas density ρ_g

$$\rho_g = 0.009225\frac{\gamma_g P}{ZT} \quad (21)$$

where, T is in °k, P in Pa.

2.2.9 Gas viscosity μ_g

For the gas viscosity calculation, we used the Lee et al. [18].

$$\mu_g = C_4 F_1 \exp\left(F_2\left(C_4\rho_g\right)^{F_3}\right) \quad (22)$$

$$F_1 = \frac{\left(9.379 + 16.07M_g\right)(C_5T)^{1.5}}{209.2 + 19260M_g + C_5T} \quad (23)$$

$$F_2 = 3.448 + \frac{986.4}{C_5T} + 10.09M_g \quad (24)$$

$$F_3 = 2.447 - 0.2224F_2 \quad (25)$$

where, T is in °k

2.2.10 Water formation volume factor B_W

B_W is defined as the ratio between the water volume at flow conditions and the water volume at standard conditions.

$$B_w = \frac{V_w(P,T)}{V_{w\_sc}} = \frac{Q_w(P,T)}{Q_{w\_sc}} \quad (26)$$

It can be calculated using the McCain correlation [20].

$$B_W = (1 + \Delta V_{wT})(1 + \Delta V_{wP}) \quad (27)$$

where, ΔV_{wT} and ΔV_{wP} are respectively the volume corrections for temperature and pressure, obtained by:

$$\Delta V_{wT} = -1.00010(10^{-2}) + 1.33391(10^{-4})C_3 + 5.50654(10^{-7})C_3{}^2 \quad (28)$$

$$\Delta V_{wP} = -1.95301(10^{-9})C_2C_3P - 1.72834(10^{-13})C_2{}^2C_3P^2 - 3.58922(10^{-7})C_2P - 2.25341(10^{-10})C_2{}^2P^2 \quad (29)$$

T is given in °k and P in Pa.

2.2.11 Water density

The water density at local flow condition is calculated as:

$$\rho_w = \frac{\rho_{w\_sc}}{B_w} \quad (30)$$

where, ρ_{wsc} and γ_{wsc} are respectively water density at standard conditions and specific gravity of water at standard condition.

2.2.12 Water viscosity

The water viscosity was estimated by using the correlation of Collins [21], neglecting salinity effect as presented by [11].

$$\mu_{w_{sc}} = 109.574C_4C_3^{-1.12166} \quad (31)$$

$$\mu_w = \mu_{w_{sc}}(0.999 + 4.029510^{-5}k_6 + 3.1062 \times 10^{-9}k_6^2) \quad (32)$$

$$k_6 = (C_2P + 14.7) \quad (33)$$

2.2.13 Volumetric flow rate

Volumetric flow rate of petroleum fluids (gas, oil and water) at flow conditions are defined as follow:

$$Q_g = \left(Q_{g\_sc} - RsQ_{o\_sc}\right)B_g = Q_{o\_sc}(GOR - Rs)B_g \quad (34)$$

$$Q_o = Q_{o\_sc}B_o \quad (35)$$

$$Q_w = Q_{w\_sc}B_w \quad (36)$$

$$Q_l = Q_{o\_sc}B_o + Q_{w\_sc}B_w = Q_{o\_sc}(B_o + WOR.B_w) \quad (37)$$

where, Q_{g_sc}, Q_{w_sc} and Q_{o_sc} are the flow rates of gas, water and oil at standard conditions. Q_g, Q_w, Q_o and Q_l are the flow rates of gas, water, oil and liquid at flow conditions. *GOR* and *WOR* are gas oil ratio and water oil ratio at surface.

2.3 Pressure gradient formulation

The pressure gradient is calculated using Dukler and Taitel correlation [22] in which, void fraction is determined based on drift-flux model using correlations from [23]. Eq. (1) below describes the pressure profile along a flow-line.

$$\left(\frac{dP}{dL}\right) = \frac{f_{tp}\rho_m V_m^2}{2D} + \rho_m g\sin(\theta) \quad (38)$$

where: P is the pressure given in P_a; L is the length of the pipeline in m; ρ_m is the mixture local density in $k_g.m^{-3}$; v_m is the mixture velocity in $m.s^{-1}$; D is the pipeline outer diameter in m; g is the gravitational acceleration given in $m.s^{-2}$ and θ is the inclinasion of the pipeline expressed in degrees. In Eq. (38), two necessary variables are to be determined: the friction factor of two-phase flow f_{tp} and the mixture density ρ_m.

$$\rho_m = \rho_L\left(\frac{\lambda^2}{1-\alpha}\right) + \rho_g\left(\frac{(1-\lambda)^2}{\alpha}\right) \quad (39)$$

$$\frac{1}{\sqrt{f_{tp}}} = -2\log\left[\frac{2\varepsilon/d}{3.7} - \frac{5.02}{Re}\log\left(\frac{2\varepsilon/d}{3.7} + \frac{13}{Re}\right)\right] \quad (40)$$

$$\lambda = \frac{Q_{o\_sc}B_o + Q_{w\_sc}B_w}{Q_{o\_sc}B_o + Q_{w\_sc}B_w + (Q_{g\_sc} - Q_{o\_sc}R_s)B_g} \quad (41)$$

$$\alpha = \frac{V_{sg}}{C_d V_m + V_d} \quad (42)$$

$$C_d = \frac{V_{sg}}{V_m}\left[1 + \left(\frac{V_{sl}}{V_{sg}}\right)^{\left(\frac{\rho_g}{\rho_L}\right)^{0.1}}\right] \quad (43)$$

$$V_d = 2.9\left[\frac{g.D.\sigma(1+\cos\theta)(\rho_L - \rho_g)}{\rho_L^2}\right]^{0.25}(1.22 + 1.22\sin\theta)^{\frac{P_{atm}}{P}} \quad (44)$$

From (Eq. (38)) to (Eq. (44)):

ρ_g, is the local density of the gas, $k_g.m^{-3}$; ρ_L is the local liquid density, $k_g.m^{-3}$; α is the void fraction of the gas phase given by drift flux correlation of Woldesemayat. For more details, see [23]. V_{sg} is the superficial velocity of the gas phase, $m.s^{-1}$; V_m is the mixture velocity, $m.s^{-1}$; C_d is the profile parameter and V_d is the drift velocity. σ is the surface tension calculated given in $N.m^{-1}$. P_{atm}, is the atmospheric pressure, in Pa. λ is the liquid input fraction. Q_{o_sc} and Q_{w_sc} are oil and water flowrate respectively at standard condition given in $m^3.s^{-1}$. Black oil parameters which are: B_w, $m^3.s^{-3}$; B_g, $m^3.m^{-3}$; B_o, $m^3.m^{-3}$; R_s, $Sm^3.Sm^{-3}$, ε, is the pipe roughness, d the pipe diameter and Re is the Reynolds number of the mixture given by (Eq. (45)) below:

$$Re = \frac{\rho_m V_m d}{\mu_m} \quad (45)$$

2.4 Temperature profile model using MATLAB

Difference material of thermal insulation will result to various temperature profile inside the subsea pipeline. Thus, we present here the temperature calculations model for an oil and gas flow inside subsea pipeline. The temperature are pressure dependent. From the general equation describing the temperature profile along pipeline considering that the kinetic energy is negligible as in ref. [24], we have:

$$\frac{\partial(T_m)}{\partial t} - \eta_m\frac{\partial P}{\partial t} = -v_m\frac{\partial(T_m)}{\partial L} - \frac{U_o\pi D(T_m - T_e)}{A_p\rho_m Cp_m} + v_m\eta_m\frac{\partial P}{\partial L} - v_m\frac{g\sin(\theta)}{C_{p_m}} \quad (46)$$

where, T_m is the average temperature of the fluid given in °k, A_p is the pipe cross-sectional area m^2, t is the time given in s, C_{p_m} is the mixture specific heat capacity in $J.k.k_g^{-1}$, η_m is the mixture Joule Thomson coefficient, $k.Pa^{-1}$, U_o is the overall heat transfer coefficient in $w.k.m^{-2}$, T_e is the environment temperature in °k.

In steady state conditions, (Eq. (47)) becomes:

$$\frac{dT_m}{dL} = -\frac{U_o\pi D(T_m - T_e)}{C_{p_m}w_m} + \eta_m\frac{dP}{dL} - \frac{g\sin(\theta)}{C_{p_m}} \quad (47)$$

where:

$$w_m = \rho_m V_m A_p \quad (48)$$

$$Cp_m = Cp_g\alpha\frac{\rho_g}{\rho_m} + Cp_L(1-\alpha)\frac{\rho_L}{\rho_m} \quad (49)$$

$$Cp_L = \left(\frac{Q_o}{Q_o + Q_w}\right)Cp_o + \left(\frac{Q_w}{Q_o + Q_w}\right)Cp_w \quad (50)$$

From (Eq. (47) to (Eq. (50)):

w_m is the mixture mass flow rate in $k_g.s$, Cp_m, is the average specific heat capacity calculated as in ref. [25], Cp_g and Cp_L are the specific heat capacity of the gas and liquid respectively. Cp_m, Cp_g and Cp_L are expressed in $J.k.k_g^{-1}$. Q_o and Q_w are respectively the local flowrates of the oil and water. η_m, is the average Joule-Thomson, coefficient calculated using (Eq. (51)) through (Eq. (54)) as shown below,

$$\eta_m = -\left(\frac{w_g Cp_g\eta_g + w_L Cp_L\eta_L}{w_m Cp_m}\right) \quad (51)$$

$$\eta_g = \left(\frac{1}{\rho_g C_{p_g}}\right)\left[\frac{T_m}{Z}\left(\frac{dZ}{dT}\right)_p\right] \quad (52)$$

$$\eta_L = \frac{1}{\rho_L\, Cp_L}(T_m\beta - 1) \quad (53)$$

$$\beta = \frac{WOR}{1+WOR}\frac{\partial B_w}{\partial T} + \frac{1}{1+WOR}\frac{\partial B_o}{\partial T} \quad (54)$$

Where is the thermal expansion coefficient and Z is the gas compressible factor.

The overall heat transfer coefficient U_o is calculated as

$$\frac{1}{U_o} = \left(\frac{r_{ins}}{r_i h_{in}} + r_{ins}\frac{\ln\left(\frac{r_o}{r_i}\right)}{k_{pipe}} + r_{ins}\frac{\ln\left(\frac{r_{ins}}{r_o}\right)}{k_{ins}} + \frac{r_{ins}}{h_o}\right) \quad (55)$$

k_{pipe} and k_{ins} represent the thermal conductivity of the metallic pipe and the insulation layer respectively, they are expressed in, $w.k^{-1}.m^{-1}$. r_{ins}, r_o and r_i are respectively the insulation material radius, the outer and the inner radius given in m. The surrounding heat transfer coefficient h_o expressed in $w.k^{-1}.m^{-2}$, is calculated using (Eq. (56)) below:

$$h_o = \frac{K_o Nu_o}{D} \quad (56)$$

where, $Nu_o = 0.027.R_{eo}^{0.8}P_{ro}^{0.3}$, represent the Nusselt number; $Re_o = \frac{\rho_o V_o D}{\mu_o}$, is the outer Reynolds number of the seawater; ρ_o is the density of the seawater, $k_g.m^{-3}$; V_o, is the seawater velocity, m/s; μ_o is the viscosity of the seawater, in Pa.s; $Pr_o = \frac{\mu_o Cp_o}{K_o}$, is the Prandtl number of the outer seawater; Cp_o is the specific heat capacity of the seawater, $J.k.k_g^{-1}$; K_o is the thermal conductivity of the seawater, $w.k^{-1}.m^{-1}$.

The internal heat transfer coefficient expressed in $w.k^{-1}.m^{-2}$, is calculated according to Pourafshary et al. [25] as follow:

$$h_{in} = \frac{K_{tp}Nu_{tp}}{D} \quad (57)$$

where, K_{tp} expressed in $w.k^{-1}.m^{-1}$, is the mixture thermal conductivity of the two-phase flow given as

$$K_{tp} = \alpha k_g + (1-\alpha)k_L \quad (58)$$

With k_g and k_L representing each the thermal conductivity of the gas and liquid respectively, expressed both in $w.k^{-1}.m^{-1}$.

Nu_{tp}, the Nusselt number of the two-phase flow determined as follow:

If flow is laminar ($Re_T \leq 2000$), for long pipe, we have:

$$Nu_{tp} = 1.86\left[Re_T Pr_m \left(\frac{D}{L}\right)\right]^{\frac{1}{3}} \quad (59)$$

If flow is turbulent flow ($Re_T \geq 6000$), for long pipe, we have:

$$Nu_{tp} = 0.023\, Re_T^{0.8} Pr_m^{0.33}\left(1+\left(\frac{D}{L}\right)^{0.7}\right) \quad (60)$$

For transition flow regime ($2000 \leq Re_T \leq 6000$)

$$Nu_{tp} = Nu_{laminar}\left[\frac{Re_T}{6000}\right]^a \quad (61)$$

with, parameter a given by:

$$a = \frac{\ln\left(\frac{Nu_{turbulent}}{Nu_{laminar}}\right)}{\ln\left(\frac{Re_{max}}{Re_{min}}\right)} \quad (62)$$

The total Reynolds number Re_T is calculated as follow:

$$Re_T = \frac{\rho_L V_{sL} D}{\mu_L} + \frac{\rho_g V_{sg} D}{\mu_g} \quad (63)$$

The Prandtl number of the mixture is given by:

$$Pr_m = \frac{\mu_m Cp_m}{K_{tp}} \quad (64)$$

2.5 Numerical simulations

The finite difference method was used to discretize the temperature model given by Eq. (47). All the equations in this study are solved simultaneously using MATLAB software. Numerically, we divide the pipeline into sections, and each section was divided into cells and consider average value of temperature and pressure in the cells. The numerical solution obtained using finite difference method is therefore given by:

$$\frac{T_m(i+1)-T_m(i)}{\Delta x} = \left(\frac{T_e - T_m}{A} + \eta_m \frac{dP}{dL} - \frac{g\sin(\theta)}{C_{p_m}}\right)_i \quad (65)$$

In which, the parameter A is:

$$A_i = \left(\frac{C_{p_m} w_m}{U_o \pi D}\right)_i \quad (66)$$

The temperature model presented above is first validated by using it to produce the same work done by [4]. The difference done here by this research is the methodology approach for the determination of the pressure gradient, the calculation of the Z-factor, the calculation of the liquid holdup and the determination of the of the joule Thomson coefficient of gas, liquid and thus, for the mixture. In Table 3 below, we present all the necessary inputs fluids data to run simulations.

Table 3. Operating parameters [4]

Oil flow rate	0.00955m³/s
Gas flow rate	9.05 Nm³
Density of natural gas	0.710 Kg/m³
Density of crude oil (20°C)	886.9 Kg/m³
Surrounding temperature	277.15 K
Inlet temperature	323.15 K
Outlet temperature	278.75 K
Inlet pressure	5 MPa
Outlet pressure	2.4 MPa
Over all heat transfer coefficient	2 (W/m² K)

2.6 Temperature model using PIPESIM

This study also uses the PIPESIM software to build and validate the temperature model presented above. The operating parameters are enter in the software. The fluid type is set as black oil. The simulations are

2.6.1 Pipeline model

The network schematic model was used to build the pipeline model in PIPESIM. Figure 2 below shows a sketch of the simulation modeling of the pipeline in PIPESIM.

2.6.2 Multiphase correlation

The multiphase model selected in PIPESIM was the revised correlation of Beggs and Brill [17] described by the following equation

$$\frac{dP}{dL} = \frac{\frac{f_{tp}\rho_n v_m^2}{2d} + \rho_m g\sin\theta}{1-E_k} \quad (67)$$

In which E_k is a dimensionless acceleration term that take into consideration the pressure gradient due to kinetic energy effects and is given by:

$$E_k = \frac{V_m V_{sg} \rho_m}{P} \quad (68)$$

The Beggs and Brill multiphase correlation deals with both the friction pressure loss and the hydrostatic pressure difference. First the appropriate flow regime for the particular combination of gas and liquid rates (Segregated, Intermittent or Distributed) is determined. The liquid holdup, and hence, the in-situ density of the gas-liquid mixture is then calculated according to the appropriate flow regime, to obtain the hydrostatic pressure difference. A two-phase friction factor is calculated based on the "input" gas-liquid ratio and the Moody friction factor table using Colebrook equation. From this, the friction pressure loss is calculated using "input" gas-liquid mixture properties. That is why this model was selected.

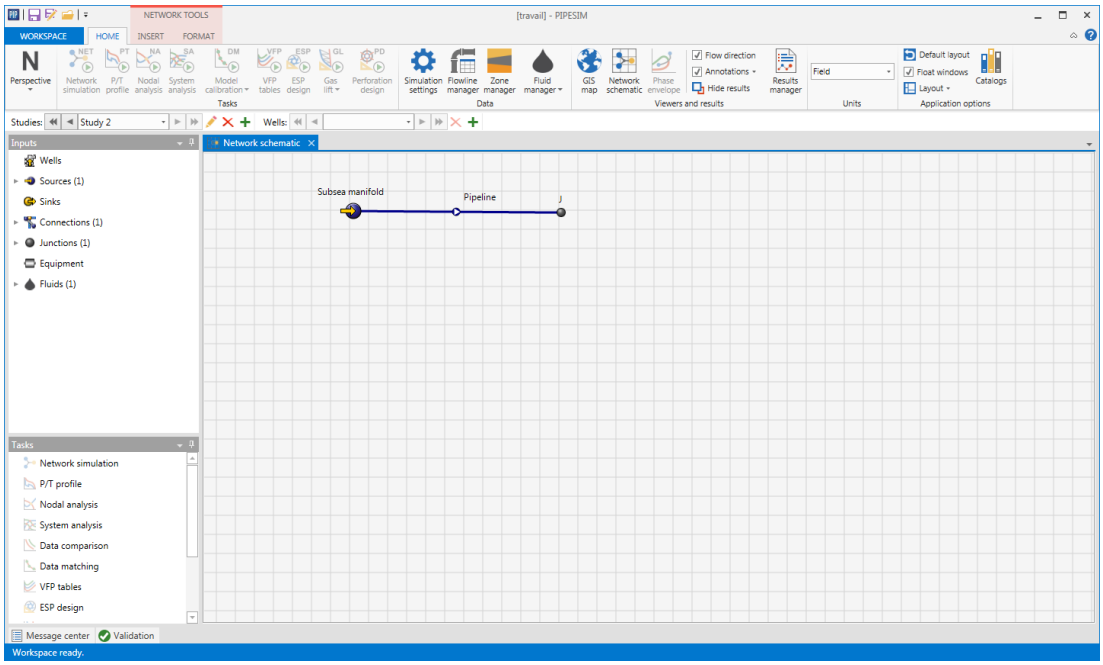

Figure 2. Sketch of the simulation modeling of subsea pipeline in PIPESIM

2.6.3 Energy equation

PIPESIM uses the first law of thermodynamics to perform a rigorous heat transfer balance on each pipe segment. The first law of thermodynamics is the mathematical formulation of the principle of conservation of energy applied to a process occurring in a closed system (a system of constant mass m). It equates the total energy change of the system to the sum of the heat added to the system and the work done by the system. For steady-state flow, it connects the change in properties between the streams flowing into and out of an arbitrary control volume (pipe segment) with the heat and work quantities across the boundaries of the control volume (pipe segment). For a multiphase fluid in steady-state flow, the energy equation is given by:

$$\Delta\left[\left(H+\frac{1}{2}V_m^2+gz\right)dm\right]=\sum\delta Q-\delta W \qquad (69)$$

where the specific enthalpy:

$$H=U+PV \qquad (70)$$

is a state property of the system since the internal energy U the pressure P and the volume V are state properties of the system. It is clear from the left-hand side of Eq. (69), the change in total energy is the sum of the change in enthalpy energy,

$$\Delta[Hdm]=\Delta[(U+PV)dm] \qquad (71)$$

the change in gravitational potential energy:

$$\Delta(E_p)=\Delta[(gz)dm] \qquad (72)$$

and the change in total kinetic energy (based on the mixture velocity)

$$\Delta(E_k)=\Delta\left[\left(\frac{1}{2}V_m^2\right)dm\right] \qquad (73)$$

which is assumed to be negligible.

On the right-hand side of Eq. (69), $\sum\delta Q$ includes all the heat transferred to the control volume (pipe segment) and δW represents the shaft work, that is work transmitted across the boundaries of the control volume (pipe segment) by a rotating or reciprocating shaft

2.6.4 Setup calculation

In PIPESIM, after the pipeline model is built and the fluid model is considered, the setup data for simulations can then be edited as it be seen in the Figure 3 below.

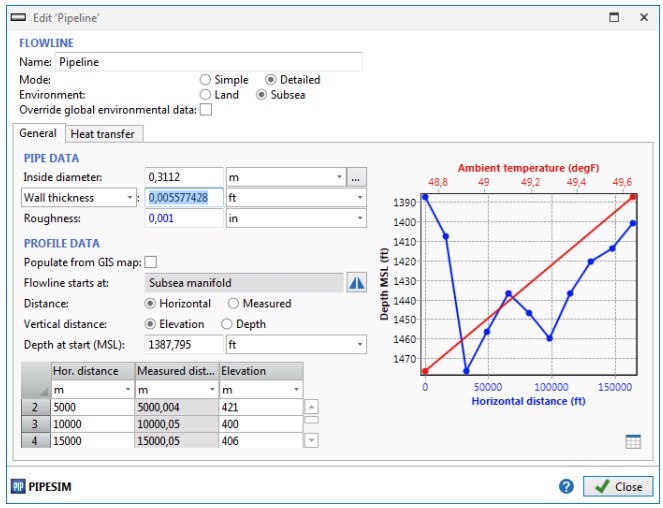

Figure 3. Sketch of data edit in PIPESIM

2.6.5 Run simulations

You can perform nodal analysis, reservoir simulation, and use other analytical tools (such as pressure/temperature (P/T) profiles, VFP tables, and network simulation) to calculate the distribution of flowrates, temperatures, and pressures throughout the system and plan new field developments. Figure 4 below presents a sketch of temperature simulation run using PIPESIM.

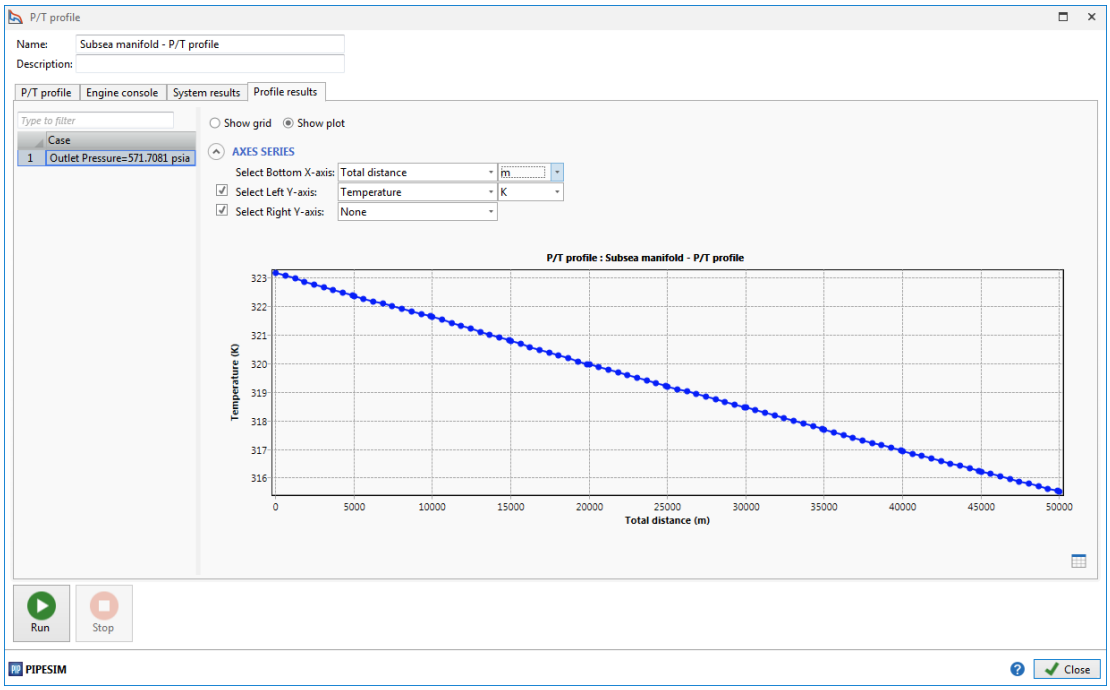

Figure 4. Sketch of temperature simulation with PIPESIM

3. RESULTS AND DISCUSSIONS

The given calculations are performed to select the insulation material and appropriate insulation layer thickness. The design criterion is to ensure that the temperature at any point on the flow line does not drop to below 40°C, as required by flow assurance. Insulating materials considered for this design are Calcium Silicate (CS), Black Aerogel (BA) and Polyurethane Foam (PUF). Firstly, MATLAB software was used to implement numerical simulations and PIPESIM software was used for numerical validation purpose of the temperature profile. Further simulations are run to thermally design the subsea pipeline. Finally, the effect of the selected insulation material on the heat flux and the phase envelop of the fluids was carried out

3.1 Pressure profile inside the subsea pipeline

As pressure and temperature are simultaneously dependent, we first present the result of the pressure profile along the considered subsea pipeline. In order to verify the pressure model describes above in Eq. (38), numerical simulation was performed with MATLAB software using data presented in Table 3 above. The validation of the predicted model is done using PIPESIM software and measure value data obtained from [4].

3.1.1 Validation with the PIPESIM model

In order to validate the model used for predicting the pressure profile, the output of the predicted model was compared to the output of the PIPESIM model. From Figure 5 above, we observed the Pressure drop is not linear because of the presence of more than phase. Predicted pressure decreases along the subsea pipeline from 5×10^6 Pa to 2.4327×10^6 Pa. The pressure obtained with the PIPESIM software have an end-point value of 3×10^6 Pa. The predicted used Dukler and Taitel model in which liquid holdup is calculated using drift-flux correlation while the PIPESIM model used the Beggs and Brill correlation. These different approaches could explain the difference observed when comparing the outputs of the models. However, the pressure drop from PIPESIM is closed to the one obtained by our predicted program with a relative error of about (3-2.4327)/3=19%. This shows that the predicted model presented in this study can be used for two-phase pressure drop calculation in an undulated subsea pipeline of about 50km. A greater pressure drop will cause a smaller displacement of the fluid, thus additional energy will be required to displace the fluid.

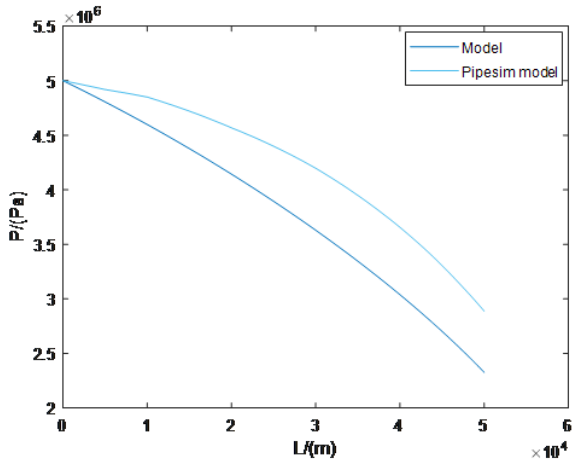

Figure 5. Pressure profile inside subsea pipeline obtained using proposed model with MATLAB software and validated with PIPESIM model

Table 4. Pressure comparison and validation [4]

Methods	Inlet pressure/ (MPa)	Endpoint pressure/ (MPa)	Pressure drop /(MPa)	REPD
Model	5	2.4327	2.5673	1.26%
Measured Value	5	2.4	2.6	

3.1.2 Validation with measured data

We compared in Table 4, the end-point value of the predicted model of pressure profile and the measured value from experiment in [4]. We then calculated the relative pressure difference (REPD). From Table 4, we noticed that the predicted pressure and the measured end-value are in good agreement with a relative error of 1.26% which shows that the proposed model capture well the two-phase flow pressure profile inside the subsea pipeline.

3.2 Temperature profile inside subsea pipeline

Temperature is one of the most important parameter in all thermal insulation design in subsea pipeline. Before investigating on the proper insulation material and the required insulation thickness, the temperature profile of the fluid flowing inside the pipeline must be well described. In order to make sure that the proposed temperature model is good for further simulations run, validation was carried out using PIPESIM model, measured value from experiment in [4] and literature calculation model from [4]. The predicted temperature from Eq. (65) was implement in MATLAB.

3.2.1 Validation with the PIPESIM model

Using the data presented in Table 3 above in conjunction with the above temperature model described by Eq. (65), the predicted temperature profile has been calculated using MATLAB software. The model was first validated numerically with the PIPESIM software as shown in Figure 6 below. It can be observed that the mixture of oil and gas enters the subsea pipeline with a temperature of 323.15°k and decreases along the subsea pipeline until it reaches the temperature of approximately 277.9934°k. This result was obtained for an overall heat transfer coefficient U = 2 W/(m² K) as presented by Duan et al. [4]. From the plot, it can be observed that the predicted model and the PIPESIM model show a good agreement. It can also be observed that the flowing temperature decreases rapidly to 313.15°K for a travelled distance of about 0.5 km, which represent the maximum distance the fluid moved before starting undergoing flow assurance issues such as paraffin wax formation and deposition. By considering the pipeline length of 50 km, the close match results shows that the model can predict the temperature distribution of an oil and gas flow through an undulated subsea pipeline.

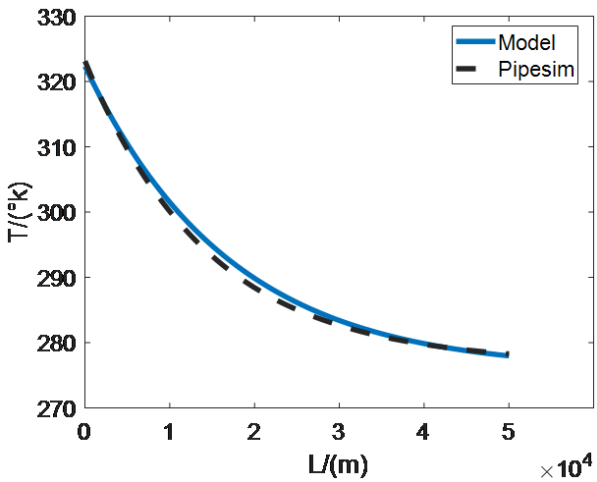

Figure 6. Temperature profile comparison between our model and PIPESIM model

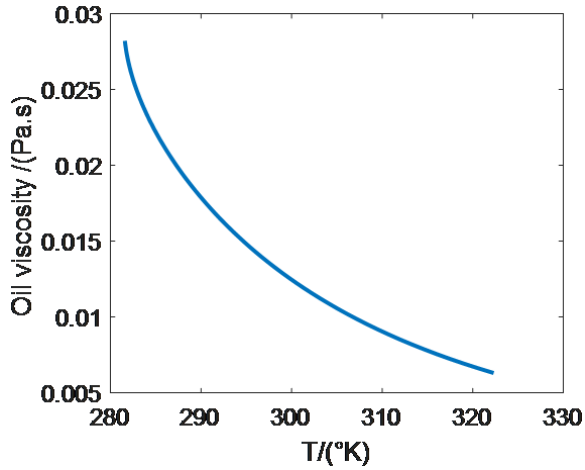

Figure 7. Oil viscosity variation with temperature

As the fluid temperature decreases along the pipeline due to the heat losses between the cold surrounding and the hot fluid, oil viscosity will increase as it is shown in Figure 7 above. Such situation may promote formation of solids such as wax in the pipeline resulting in pipeline obstruction thus to an increase in pressure drop of the fluid. Another problem, is the decrease of the oil production along the subsea production pipeline as can be seen in the Figure 8.

Figures 6, 7 and 8 show that the temperature is an important parameter for the analysis of fluid flow in subsea pipeline. A drop in temperature will cause a reduction in production due to a restriction of the flow area by solids deposition such as wax and hydrates resulting from a thermal unbalance between the surrounding cold water and the hot fluid flowing through the pipeline. This situation may required a more suitable insulation design for remediation.

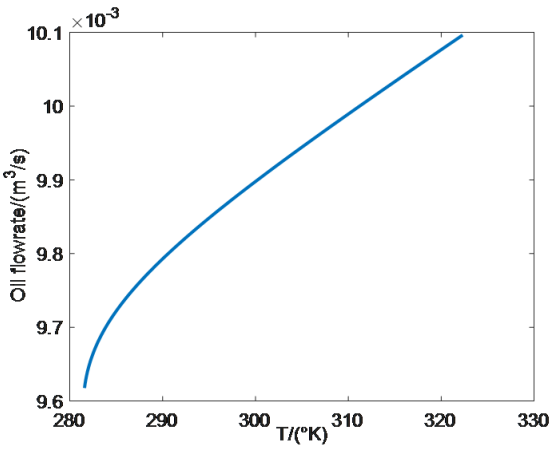

Figure 8. Oil flowrate variation with temperature

3.2.2 Validation with measured field data from literature model

The model was also validated using measured value from field data. The results was presented and compared in Table 5 below. From this table, it is show that the predicted temperature from our model is in good agreement with that of the measured value and the predicted model from [4]. The results show a relative error of 1.68% with the measured value, 1.04% with the PIPESIM model and 3.37% with the model presented by Duan et al. [4]. This result shows that the model can predict accurately the temperature profile inside the considered subsea pipeline for an overall heat transfer coefficient U = 2 W/(m² K).

Table 5. Validation of the temperature calculations with others models

Methods	Inlet temperature/(K)	Endpoint temperature/(K)	Temperature drop	RETD
Predicted model	323.15	277.99	45.1566	1.68%
MV	323.15	278.75	44.4	1.04%
PIPESIM prediction	323.15	278.28	44.86	
UPTP	323.15	277.25	45.9	3.37%

Form the results presented in Figure 6 and Table 5 above, it clear that the temperature model presented in this study can be further used for the thermal insulation design because of its good accuracy with other models. The main goal of the thermal design analysis was to select an appropriate insulation layer thickness and material. The design criterion is to ensure that the temperature at any point on the flow line does not drop to below 40°C, as required by flow assurance. Insulation materials considered for this design are Calcium Silicate, Polyurethane Foam and Black Aerogel.

3.3 Numerical simulations for the determination of the minimum insulation thickness of Calcium Silicate

Figure 9 below shows the effect of various Calcium Silicate thickness on the fluid temperature along the subsea pipeline.

The thickness is comprised between 2.54 to 66.04 cm. It can be seen that, for insulation thickness less than 66.04 cm, the fluid temperature would drop below the 313.15°K, leading to high risk of flow assurance issues inside the subsea pipeline. The minimum insulation thickness to be used in this case is 66.04 cm.

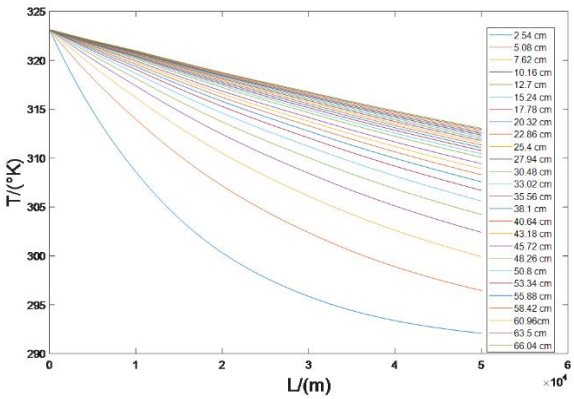

Figure 9. Temperature profiles of the flowing fluids inside subsea pipeline with different insulation thickness of Calcium Silicate

3.4 Numerical simulations for the determination of the minimum insulation thickness of Polyurethane Foam

Figure 10 below, shows the temperature profile for different Polyurethane Foam thickness taken between 2.54 cm and 25.4cm. It can be observed that the minimum insulation thickness that would achieved an output temperature of at least 313.15°K is 25.4cm.

3.5 Numerical simulations for the determination of the minimum insulation thickness of Black Aerogel

In Figure 11 below, we plotted the temperature profile for different insulation thickness of Black Aerogel. The thickness range from 1.27 cm and 10.16 cm. The minimum insulation thickness necessary to satisfy the design criterion is 10.16 cm as can be seen.

When comparing the temperature profiles plotted in figure 9 to Figure 11 for the various insulating materials with different thickness, we observed that either a 25.4 cm of Polyurethane or a 10.16cm of Black Aerogel material should be used as insulating material type for the subsea pipeline. However, only cost analyses can justify one of the options, which is beyond the scope of this work. In this study, because Black Aerogel has the smallest thermal conductivity and provide the smallest insulation thickness, it was chosen as the best insulating material with a thickness of 10.16cm for the design purpose.

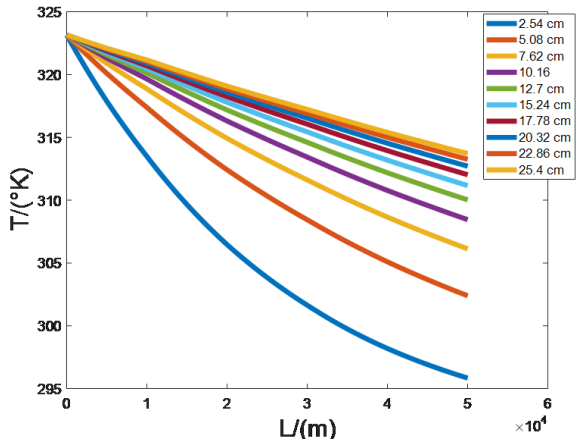

Figure 10. Temperature profiles of the flowing fluids inside subsea pipeline with different insulation thickness of Polyurethane Foam

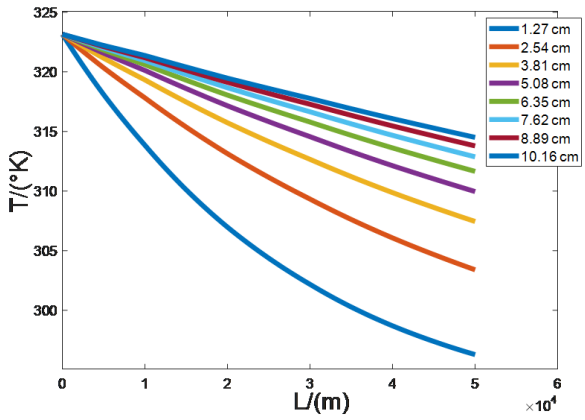

Figure 11. Temperature profiles of the flowing fluids inside subsea pipeline with different insulation thickness of Black Aerogel

The temperature profiles have also help us to investigate the risk of flow assurance issues by examined the phase envelop.

3.6 Effect of Black Aerogel on the phase diagram

Due to the low temperature and high pressure of deep water,

the pipe thermal insulation has important effects on the fluid temperature in pipeline. Effect of Black Aerogel on the formation area of some flow assurance issues under different insulating material thickness.

In Figure 12, F.A is for Flow Assurance. The effect of different insulating material thickness was investigated on the phase diagram. It can be seen that the flow assurance risk formation area decreases with the increase of the thickness of insulating material. Thus, this approach can also be used to optimize the thermal insulation design of subsea pipeline.

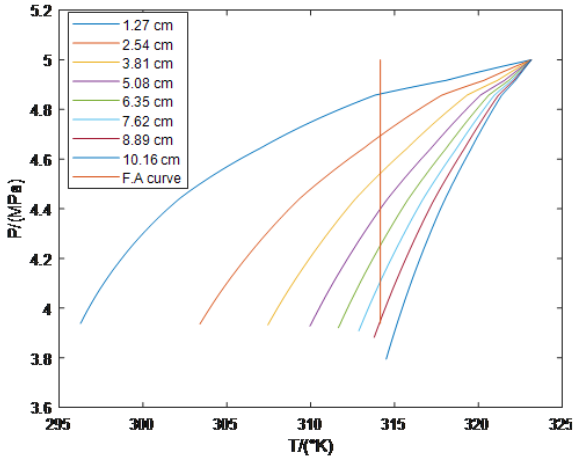

Figure 12. Pressure variation vs temperature

4. CONCLUSION

In this work, we proposed a model to thermally design a subsea pipeline for heat conservation purpose in subsea pipeline and therefore to avoid the formation of some flow assurance issues such as paraffin wax and hydrates. As temperature and pressure greatly influence the flow assurance issues caused by thermal unbalance, a temperature and pressure model were proposed and validated using field data and others models. The good agreement obtained shows that the predicted models are suitable for temperature and pressure prediction in subsea pipeline. Further simulations were run to find out the optimal insulation thickness among three different insulating materials with various thicknesses in order to achieve the subsea pipeline design. From the obtained results, it is concluded that a minimum of 10.16 cm Black Aerogel thermal insulation thickness is required to ensure that the discharge temperature at the discharge end of the subsea pipeline does not fall below 313.15 degree Kelvin. It was also observed that, the selected insulation material has direct impacts on the flow assurance issues formation area in the subsea pipeline. Because of this, flow assurance risk formation region can be shifted or avoided. The proposed model can therefore be used to thermally design a subsea pipeline during steady state operation. For future work, logistic regression can be used to predict hydrate formation probability in a subsea production and transportation pipeline for a given composition and operating conditions. Machine learning approach can also be used to risk assessment of hydrate and wax formation. Multi-variate Logistic Regression Model to Analyze hydrate formation risk can also be carried out. Thermal insulation design can be studied on transporting pipeline that crosses offshore and onshore pipeline. Transient analysis can also be considered to capture wax, hydrates deposition tendencies during shut down, and restart scenarios for subsea pipeline transporting liquid and gas flow. A comparative study using PIPESIM, Aspen Hysys and MATLAB can be done in order to choose the best software that properly offer a good estimation of optimal insulation thickness. Investigation should be carried out for optimal economic insulation thickness design in subsea pipeline.

ACKNOWLEDGMENT

Thanks to the director of Environmental Energy Technologies Laboratory (E.E.T.L) for his time, counseling, guidance and availability.

REFERENCES

[1] Phil, H. (2007). Oil and Gas Pipelines: Yesterday and Today. International Petroleum Technology Institute, ASME, New York.

[2] Guo, B.Y. (2007). Petroleum Production Engineering: A Computer-Assited Approach. 1st (Ed.), Elsevier Science & Technology Books.

[3] Ahmed, I.M. (2018). Modeling and development of insulation materials in subsea. Master thesis, University of Newfoundland.

[4] Duan, J.M., Wang, W., Zhang, Y., Zheng, L.J., Liu, H.S., Gong, J. (2013). Energy equation derivation of the oil-gas flow in pipelines. Oil & Gas Science and Technology – Rev. IFP Energies Nouvelles, 68(2): 341-353. https://doi.org/10.2516/ogst/2012020

[5] Zulkefli, N.H.B., Pao, W. (2016). Optimum thermal insulation design for subsea pipeline flow assurance. Report number: 17276Affiliation: Universiti Teknologi PETRONAS. https://doi.org/10.13140/RG.2.2.33853.05603

[6] Patil, K.D., Sadafule, S. (2014). Study on effect of insulation design on thermal-hydraulic analysis: an important aspect in subsea pipeline designing. Technical Report, Maharashtra Institute of Technology, 4(1). https://www.researchgate.net/publication/263426807.

[7] Briggs, T.A., Onyegiri, I.E., Ekwe, E.B. (2020). Investigation of the effects of flowline sizes, flow rates, insulation material, type and configuration on flow assurance of waxy crude. Innovative Systems Design and Engineering, 11(3). https://doi.org/10.7176/ISDE/11-3-02

[8] Abegunde, M., Adeyemi, A. (2020). Optimisation of thermal insulation of subsea flowlines for hydrates. Society of Petroleum Engineers. https://doi.org/10.2118/203721-MS

[9] Marfo, S.A., Opoku Appau, P., Kpami, L.A.A. (2018). Subsea pipeline design for natural gas transportation: A case study of côte d'ivoire's gazelle field. International Journal of Petroleum and Petrochemical Engineering (IJPPE), 4(3): 21-34. http://dx.doi.org/10.20431/2454-7980.0403003

[10] Alade, O. (2018). Sizing surface production flow line insulation thickness for a desired output temperature. Petroleum & Petrochemical Engineering Journal, 2(7). https://doi.org/10.23880/ppej-16000178

[11] Andreolli, I., Zortea, M., Baliño, J.L. (2017). Modeling offshore steady flow field data using drift-flux and black-

oil models. Journal of Petroleum Science and Engineering, 157: 14-26. https://doi.org/10.1016/j.petrol.2017.07.001
[12] Brill, J.P., Mukherjee, H. (1987). Multiphase flow in wells. J. Pet. Technol., 39(1): 15-21. https://doi.org/10.2118/16242-PA
[13] Standing, M.B. (1947). A Pressure-Volume-Temperature Correlation for Mixtures of California Oil and Gases. New York, New York: Standard Oil Co. of California.
[14] Standing, M.B. (1951). Volumetric and Phase Behavior of Oil Field Hydrocarbon Systems: PVT for Engineers. California Research Corp.
[15] Vazquez, M., Beggs, H.D. (1980). Correlations for fluid physical property prediction. Journal of Petroleum Technology, 32(6): 968-970. https://doi.org/10.2118/6719-pa
[16] Beal, C. (1946). The viscosity of air, water, natural gas, crude oil and its associated gases at oil field temperatures and pressures. Transactions of the AIME, 165(1): 94-115. https://doi.org/10.2118/946094-G
[17] Beggs, D.H., Robinson, J.R. (1975). Estimating the viscosity of crude oil systems. Journal of Petroleum Technology, 27(9): 1140-1141. https://doi.org/10.2118/5434-PA
[18] Lee, A.L., Gonzalez, M.H., Eakin, B.E. (1966). The viscosity of natural gases. Journal of Petroleum Technology, 18(8): 997-1000. https://doi.org/10.2118/1340-PA
[19] Standing, M.B., Katz, D.L. (1942). Density of natural gases. Transactions of the AIME, 146(1): 140-149. https://doi.org/10.2118/942140-G
[20] McCain, W.D. (1990). The Properties of Petroleum Fluids. PennWell Books, Tulsa.
[21] Collins, A.G. (1987). Petroleum Engineering Handbook. SPE, Dallas. Properties of Produced Waters.
[22] Taitel, Y., Dukler, A.E. (1976). A model for predicting flow regime transitions in horizontal and near horizontal gas-liquid flow. AIChE Journal, 22(1): 47-55. https://doi.org/10.1002/aic.690220105
[23] Woldesemayat, M., Ghajar, A.J. (2007). Comparison of void fraction correlations for different flow patterns in horizontal and upward inclined pipes. International Journal of Multiphase Flow, 33(4): 347-370. https://doi.org/10.1016/j.ijmultiphaseflow.2006.09.004
[24] Zerpa, L.E. (2013). A practical model to predict gas hydrate formation, dissociation and transportability in oil and gas flowlines. Phd Thesis, Faculty and the Board of Trustees of the Colorado School of Mines.
[25] Pourafshary, P., Varavei, A., Sepehrnoori, K., Podio, A. (2008). A compositional wellbore/reservoir simulator to model multiphase flow and temperature distribution. International Petroleum Technology Conference, December, Kuala Lumpur, Malaysia, pp. 3-5. https://doi.org/10.2523/IPTC-12115-MS

NOMENCLATURE

A	cross section area, m^2
B_o	oil formation volume factor, $m^3.m^{-3}$
B_w	water formation volume factor, $m^3.m^{-3}$
B_g	gas formation volume factor, $m^3.m^{-3}$
C_d	profile parameter
Cp	specific heat at constant pressure, $J.k_g{}^{-1}.k^{-1}$
D	inner diameter of pipe, m
f	friction factor
g	acceleration of gravity, $m.s^{-2}$
h_{in}	inner convective heat transfer coefficient, $w.k^{-1}.m^{-2}$
h_o	outer convection heat transfer coefficient, $w.k^{-1}.m^{-2}$
k	thermal conductivity of pipe, $w.k^{-1}.m^{-1}$
L	pipe length, m
P	pressure, Pa
q	heat flux rate
Q_w	local flow rate of water at flow conditions, $m^3.s^{-1}$
Q_o	local flow rate of oil at flow conditions, $m^3.s^{-1}$
Q_g	local flow rate of gas at flow conditions, $m^3.s^{-1}$
Q_{w_sc}	flow rate of water at standard conditions, $m^3.s^{-1}$
Q_{o_sc}	flow rate of water at standard conditions, $m^3.s^{-1}$
Q_{g_sc}	flow rate of water at standard conditions, $m^3.s^{-1}$
Re	Reynolds number
R_S	solution gas-oil ratio, $Sm^3.Sm^{-3}$
r	radius of pipe, m
T	temperature, k
U	overall heat transfer coefficient, $w.k.m^{-2}$
V_d	drift velocity, $m.s^{-1}$
V_{sw}	superficial velocity of water, $m.s^{-1}$
V_{so}	superficial velocity of oil, $m.s^{-1}$
V_{sg}	superficial velocity of gas, $m.s^{-1}$
V_g	velocity of the gas phase, $m.s^{-1}$
V_l	velocity of the liquid phase, $m.s^{-1}$
V_m	mixture velocity, $m.s^{-1}$
w	mass flow rate, $k_g.s^{-1}$
Z	gas compressibility factor

Greek symbols

ρ	density, $k_g.m^{-3}$
μ	viscosity, $k_g.m^{-1}.s^{-1}$
α	void fraction
η	joule Thomson coefficient, $k.Pa^{-1}$
θ	inclinasion angle of pipe, rad
σ	surface tension, $N.m^{-1}$

Subscripts

atm	atmospheric
o	oil, outer
g	gas
w	water
l	liquid
m	mixture
sc	standard conditions
tp	two phase
p	pipe
i	inner
ins	insulation
e	ambient

ISSN No:-2456-2165

Modeling and Simulation of the Temperature Profile along Offshore Pipeline of an Oil and Gas Flow: Effect of Insulation materials

Gopdjim Noumo Prosper
Dept. of Physics
University of Yaounde 1
Yaounde, Cameroon

Donatien Njomo.
Dept. of Physics
University of Yaounde 1
Yaounde, Cameroon

Zepang Nana Kevin
Dept. of Physics
University of Yaounde 1
Yaounde, Cameroon

Abstract:- In offshore area, flowing parameters such as temperature and pressure must be controlled in order to guarantee a safety and economical transportation of fluid along pipeline. This can be achieved by using numerical simulations. In this paper, a mathematical model for predicting temperature and pressure profile along offshore pipeline during oil and gas transportation is presented. The model obtained from general formulation of pressure and temperature equations during two-phase flow is discretized and solved iteratively using a Matlab code. The numerical simulations results, shows a good agreement with a relative error of 1.16% on a field data obtained from literature. Further, effect of three insulation layers consisting of calcium silicate, black aerogel and polyurethane foam along with different insulation material thickness ranges between 0.0254 m and 0.0635 m, as well as different oil flowrates, on the temperature profile are analyzed. Required insulation material, insulation thickness and minimum inlet temperature for maintaining a minimum flow temperature of 313.15°k at any point in the offshore pipeline are determined. Results shows that an inlet temperature of 343.15°k with a thickness of 0.0635 m of black aerogel satisfied the requirement. It is shown that, the proposed model has predicted the temperature distribution very well.

Keywords:- *Temperature Profile, Offshore Pipeline, Numerical Simulation, Insulation Material, Two Phase Flow.*

I. INTRODUCTION

During transportation of oil and gas inside offshore pipeline, the fluid inside pipeline losses heat because of the temperature difference between the cooler surrounding and the warmer fluids. Consequently, if the fluids temperature drop below the wax appearance temperature or the hydrate appearance temperature, wax and hydrates deposition will occur which may lead to a reduction of the effective flow area of pipe and if serious, blockage may occur [1]. Pipeline blockage significantly influence the economical operation and financial benefit of the oil and gas industry. With today's low oil price and high rig rate, the industry is struggling with cost reduction [2]. Therefore, it is very important to carefully manage the thermal design of offshore pipeline in order to control the heat loss and thus, to prevent additional loss resulting from maintenance operations related to the flow assurance issues. Temperature distribution is therefore of great importance in any design process of oil and gas transportation.

In the open literature, many authors have been interested in the topic of temperature modeling and simulation inside offshore pipelines and wellbores for single and multiphase flow as it is shown in [1, 2, 4-11] among others. From these studies, it comes out that:

- temperature and pressure are dependent;
- the temperature profile model obtained for multiphase flow is different from that of single-phase flow because of complexity of the dynamical behavior of the multiphase;
- fluids properties are determined using black oil or component model as presented in [5, 12, 15];
- pressure profile is modeled using homogeneous or separated phase model [11-145].
- single-phase temperature distribution can e determined using analytical or numerical solution.

Temperature profile investigation in offshore pipeline is mostly to find out the thermal management strategy appropriate to limit some of the flow assurance issues such as wax and hydrate formation and deposition. Insulation materials revealed to be one the various thermal strategy that can be used in order to maintain the flow temperature at any point in the pipeline above wax and hydrate formation region. As shown in [18], at temperature around 288, 15°k, wax will start to form inside the pipeline and at temperature below 313, 15°k, combine with high-pressure gas hydrates will occur. Therefore, it is also important to select the appropriate insulation material and required thickness that will be able to keep the flowing temperature to above 313.15°k. Recently, [3,16-18] among others, have investigated the effect of several insulation materials and several thickness on the temperature profile under steady and transient state condition in order to select and to determine the require thickness of insulation necessary to guarantee a continuous flowing of the fluid inside pipeline. However, most of these studies focuses on the case of single-phase flow and do not considered the pressure drop calculation.

In this study, are objectives are to model under steady state, the temperature profile during oil and gas flow in offshore pipeline and to determine by numerical simulation:

- the effect of oil flow rate change on the temperature profile,
- the effect of several insulation materials and several insulation thickness on the temperature profile
- the optimum operating condition that is, the appropriate insulation material and thickness necessary to meet the requirement temperature of 313.15°k at any point in the pipeline.

II. METHODOLOGY

A. Pipeline Geometry

The pipeline geometry considered in this study is the same as that presented in [1] for the example 1 case. Figure 1 below is a representation of the vertical section of the considered offshore pipeline.

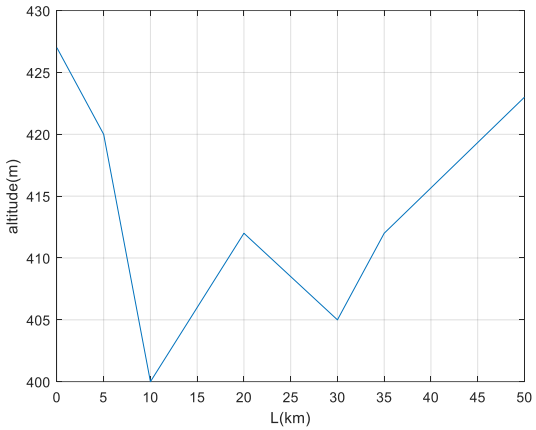

Fig. 1:- Vertical sectional profile of the pipeline [1].

Figure 2 below, show the cross sectional section of the pipeline covered with insulation.

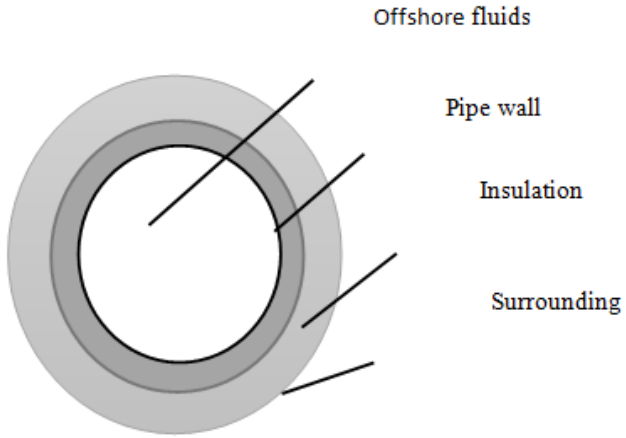

Fig. 2:- Pipeline with insulation material

The pipeline is consisting of a single metal carbon steel covered by coating insulation. The surrounding environment is seawater.

B. Fluids Properties

Fluids properties needs to be determined in order to perform the calculation of the pressure gradient along pipeline. These properties, which are local density, local viscosity, surface tension, local fluids flow rates, formation volume factors and the gas compressibility factor among others, depend on pressure and temperature and are determined using black oil model. In this work, we do not focused on fluids properties calculations but on the temperature calculation. The methodology of the determination of these fluids properties can be seen in the works done by [12], which provides in depth details equations needed for the calculations procedure using black oil model formulation.

C. Abbreviations and Acronyms

The pressure gradient dp/dL, where p is the pressure and L is the length along the pipeline is determined as:

$$\left(\frac{dP}{dL}\right) = \left(\frac{dP}{dL}\right)_f + \left(\frac{dP}{dL}\right)_h + \left(\frac{dP}{dL}\right)_{acc} \quad (1)$$

The first term on the right side of Equation (1), subscript "*f*", is the pressure gradient corresponding to the friction. The second term with subscripts "h", correspond to the gravity, and the last term with subscripts "acc", is relative to the pressure loss due to the acceleration. In this work, the pressure gradient is approximated by using Dukler and Taitel correlation [4] in which, void fraction is determined based on drift-flux model using correlations from [11,23].

$$\left(\frac{dP}{dL}\right) = \frac{f_{tp}\rho_m V_m^2}{2D} + \rho_m g \sin(\theta) \quad (2)$$

where: P is the pressure given in $\mathrm{P_a}$; L is the length of the pipeline in m; ρ_m is the mixture local density in $\mathrm{k_g/m^3}$; v_m is the mixture velocity in $\mathrm{m/s}$; D is the pipeline outer diameter in m; g is the gravitational acceleration given in $\mathrm{m/s^2}$ and θ is the inclinasion of the pipeline expressed in degrees. In equation (2), two necessary variables are to determine:

- f_{tp} is the two phase friction factor determined as in [4].
- ρ_m, which is calculated here using equation (3) below:

$$\rho_m = \rho_L\left(\frac{\lambda^2}{1-\alpha}\right) + \rho_g\left(\frac{(1-\lambda)^2}{\alpha}\right) \quad (3)$$

with, ρ_g, density of the gas, $\mathrm{k_g/m^3}$; ρ_L liquid density, $\mathrm{k_g/m^3}$; α is the void fraction of the gas phase given by drift flux correlation of Woldesemayat. For more details see [12, 26].

$$\alpha = \frac{V_{sg}}{C_d V_m + V_d} \quad (4)$$

where, V_{sg} is the superficial velocity of the gas phase, $\mathrm{m/s}$; V_m is the mixture velocity, $\mathrm{m/s}$; C_d is the profile parameter and V_d is the drift velocity. These two parameters are calculated as presented in [12] by:

$$C_d = \frac{V_{sg}}{V_m}\left[1+\left(\frac{V_{sl}}{V_{sg}}\right)^{\left(\frac{\rho_g}{\rho_L}\right)^{0.1}}\right] \quad (5)$$

$$V_d = 2.9\left[\frac{g.D.\sigma(1+\cos\theta)(\rho_L-\rho_g)}{\rho_L^2}\right]^{0.25}(1.22+1.22\sin\theta)^{\frac{P_{atm}}{P}} \quad (6)$$

In equation (6), σ, $\mathrm{N/m}$, is the surface tension calculated as presented in the work of [27]. P_{atm}, is the atmospheric pressure, in Pa.

From equation (2), λ is the liquid input fraction and is calculated as follow:

$$\lambda = \frac{Q_{o\ sc}B_o + Q_{w\ sc}B_w}{Q_{o\ sc}B_o + Q_{w\ sc}B_w + (Q_{g\ sc} - Q_{o\ sc}R_s)B_g} \quad (7)$$

where, $Q_{o\ sc}$ and $Q_{w\ sc}$ are oil and water flowrate respectively at standard condition given in $\mathrm{m^3/s}$. Black oil parameters which are: B_w, m³/m³; B_g, m³/m³; B_o, m³/m³; R_s, Sm³/Sm³ are calculated as presented in the work of Andreolli [12].

D. Temperature Model

From the general equation describing the temperature profile along pipeline considering that the kinetic energy is negligible [19] we have:

$$\frac{\partial(T_m)}{\partial t} - \eta_m\frac{\partial P}{\partial t} = -v_m\frac{\partial(T_m)}{\partial L} - \frac{U_o\pi D(T_m - T_e)}{A_p\rho_m Cp_m} + v_m\eta_m\frac{\partial P}{\partial L} - v_m\frac{g\sin(\theta)}{C_{p_m}} \quad (8)$$

where, T_m is the average temperature of the fluid given in $^{\circ}\mathrm{k}$, A_p is the pipe cross-sectional area $\mathrm{m^2}$, t is the time given in s, C_{p_m} is the mixture specific heat capacity in $\mathrm{J/k_g{}^{\circ}k}$, η_m is the mixture Joule Thomson coefficient, $^{\circ}\mathrm{k/Pa}$, U_o is the overall heat transfer coefficient in $\frac{\mathrm{W}}{\mathrm{m^2}}{}^{\circ}\mathrm{k}$, T_e is the environment temperature in $^{\circ}\mathrm{k}$.

In steady state conditions, equation (8) becomes:

$$\frac{dT_m}{dL} = -\frac{U_o\pi D(T_m - T_e)}{C_{p_m}w_m} + \eta_m\frac{dP}{dL} - \frac{g\sin(\theta)}{C_{p_m}} \quad (9)$$

where:

w_m is the mixture mass flow rate in $\mathrm{k_g/s}$, given by:

$$w_m = \rho_m V_m A_p \quad (10)$$

Cp_m , is the average specific heat capacity of the multiphase flow calculated using equations (11) and (12) below as in [28]:

$$Cp_m = Cp_g\alpha\frac{\rho_g}{\rho_m} + Cp_L(1-\alpha)\frac{\rho_L}{\rho_m} \quad (11)$$

$$Cp_L = \left(\frac{Q_o}{Q_o+Q_w}\right)Cp_o + \left(\frac{Q_w}{Q_o+Q_w}\right)Cp_w \quad (12)$$

Where, Cp_g and Cp_L are the specific heat capacity of the gas and liquid respectively. Cp_m, Cp_g and Cp_L are expressed in $\mathrm{J/(kg.{}^{\circ}k)}$. Q_o and Q_w are respectively the local flowrates of the oil and water given by $Q_o = Q_{o\ sc}B_o, \mathrm{m^3/s}$ and $Q_w = WOR.Q_{o\ sc}.B_w$, $\mathrm{m^3/s}$ are the oil and water local flowrate respectively.

η_m, is the average Joule-Thomson, coefficient calculated using equation (13) through equation (16) as shown below,

$$\eta_m = -\left(\frac{w_g Cp_g\eta_g + w_L Cp_L\eta_L}{w_m Cp_m}\right) \quad (13)$$

$$\eta_g = \left(\frac{1}{\rho_g C_{p_g}}\right)\left[\frac{T_m}{Z}\left(\frac{dZ}{dT}\right)_p\right] \quad (14)$$

$$\eta_L = \frac{1}{\rho_L C_{p_L}}(T_m\beta - 1) \quad (15)$$

$$\beta = \frac{WOR}{1+WOR}\frac{\partial B_w}{\partial T} + \frac{1}{1+WOR}\frac{\partial B_o}{\partial T} \quad (16)$$

where, η_g and η_l are respectively the Joule Thomson coefficients of the liquid and the gas given both in $^{\circ}\mathrm{k/Pa}$. β, is the thermal expansion of the liquid phase, $1/^{\circ}\mathrm{k}$. Z, is the gas compressibility factor determined by using new correlation presented in [29]. w_g and w_L are the mass flowrate of the gas and liquid phases respectively given in $\mathrm{kg/s}$.

From equation (9), the overall heat transfer coefficient U_o is given by equation (17) below:

$$\frac{1}{U_o} = \left(\frac{r_{ins}}{r_i h_{in}} + r_{ins}\frac{\ln\left(\frac{r_o}{r_i}\right)}{k_{pipe}} + r_{ins}\frac{\ln\left(\frac{r_{ins}}{r_o}\right)}{k_{ins}} + \frac{r_{ins}}{h_o}\right) \quad (17)$$

where, k_{pipe} and k_{ins} represent the thermal conductivity of the metallic pipe and the insulation layer respectively, they are expressed in , $\mathrm{w/(^{o}k.m)}$. r_{ins}, r_o and r_i are respectively the insulation material radius, the outer and the inner radius of the pipeline, all expressed in m.

The surrounding heat transfer coefficient h_o expressed in $\mathrm{w/(^{o}k.m^2)}$, is calculated using equation (18) below:

$$h_o = \frac{K_o Nu_o}{D} \tag{18}$$

where, $Nu_o = 0.027 \, . R_{eo}^{0.8} P_{ro}^{0.3}$, represent the Nusselt number; $Re_o = \frac{\rho_o V_o D}{\mu_o}$, is the outer Reynolds number of the seawater; ρ_o is the density of the seawater, $\mathrm{kg/m^3}$; V_o, is the seawater velocity, $\mathrm{m/s}$; μ_o is the viscosity of the seawater, in $\mathrm{Pa.s}$; $Pr_o = \frac{\mu_o Cp_o}{K_o}$, is the Prandtl number of the outer seawater; Cp_o is the specific heat capacity of the seawater, $\mathrm{J/(kg.^{o}k)}$; K_o is the thermal conductivity of the seawater, $\mathrm{w/(^{o}k.m)}$

The internal heat transfer coefficient expressed in $\mathrm{w/(^{o}k.m^2)}$, is calculated according to [24] as follow:

$$h_{in} = \frac{K_{tp} Nu_{tp}}{D} \tag{19}$$

where:

K_{tp} expressed in $\mathrm{w/(^{o}k.m)}$, is the mixture thermal conductivity of the two-phase flow given as

$$K_{tp} = \alpha k_g + (1-\alpha) k_L \tag{20}$$

With k_g and k_L representing each the thermal conductivity of the gas and liquid respectively, expressed both in $\mathrm{w/(^{o}k.m)}$.

Nu_{tp}, the Nusselt number of the two-phase flow determined as follow:

If flow is laminar ($Re_T \leq 2000$), for long pipe, we have:

$$Nu_{tp} = 1.86 \left[Re_T Pr_m \left(\frac{D}{L}\right) \right]^{\frac{1}{3}} \tag{21}$$

If flow is turbulent flow ($Re_T \geq 6000$), for long pipe we have:

$$Nu_{tp} = 0.023 \, \mathrm{Re_T^{0.8} Pr_m^{0.33}} \left(1 + \left(\frac{D}{L}\right)^{0.7}\right) \tag{22}$$

For transition flow regime ($2000 \leq Re_T \leq 6000$)

$$Nu_{tp} = Nu_{laminar} \left[\frac{Re_T}{6000}\right]^a \tag{23}$$

with, parameter a given by:

$$a = \frac{\ln\left(\frac{Nu_{turbulent}}{Nu_{laminar}}\right)}{ln\left(\frac{Re_{max}}{Re_{min}}\right)} \tag{24}$$

The total Reynolds number Re_T is calculated as follow:

$$Re_T = \frac{\rho_L V_{sL} D}{\mu_L} + \frac{\rho_g V_{sg} D}{\mu_g} \tag{25}$$

The Prandtl number of the mixture is given by:

$$Pr_m = \frac{\mu_m Cp_m}{K_{tp}} \tag{26}$$

The heat exchange between the hot fluids inside pipeline and the cooler environment is given by:

$$q = U_o (T_m - T_e) \tag{27}$$

where, q is the heat flux given in $\mathrm{w/m^2}$.

Numerical Solution

The finite difference method was used to discretize the temperature model given by equation (9). All the equations in this study are solved simultaneously using Matlab software. Pipesim software is used for comparison purpose. Numerically, we divide the pipeline into sections, and each section was divided into cells and consider average value of temperature and pressure in the cells. The numerical solution obtained using finite difference method is therefore given by:

$$\frac{T_m(i+1) - T_m(i)}{\Delta x} = \left(\frac{T_e - T_m}{A} + \eta_m \frac{dP}{dL} - \frac{g \sin(\theta)}{C_{p_m}}\right)_i \tag{28}$$

In which, the parameter A is:

$$A_i = \left(\frac{C_{p_m} w_m}{U_o \pi D}\right)_i \tag{29}$$

The temperature model presented above is first validated by using it to produce the same work done by [1]. The difference done here by this research is the methodology approach for the determination of the pressure gradient, the calculation of the Z-factor, the calculation of the liquid holdup and the determination of the of the joule Thomson coefficient of gas, liquid and thus, for the mixture. The operating parameters used is the same as those presented in table .1 of reference [1].

III. RESULTS AND DISCUSSIONS

In order to analyze the accuracy of the temperature model proposed in this study, the obtained results are to be compared with the results from, UPTP model and measured value (MV) as presented in [1] for the;

Case 1 example.

For that, the same operating parameters and the same pipeline geometry parameters as in [1] have been used in our Matlab computer program. By using this field data, we computed the pressure and temperature profile along the offshore pipeline. Fig. 3 and 4 represents the pressure and temperature profile of the oil and gas flow through offshore pipeline obtained using the proposed model.

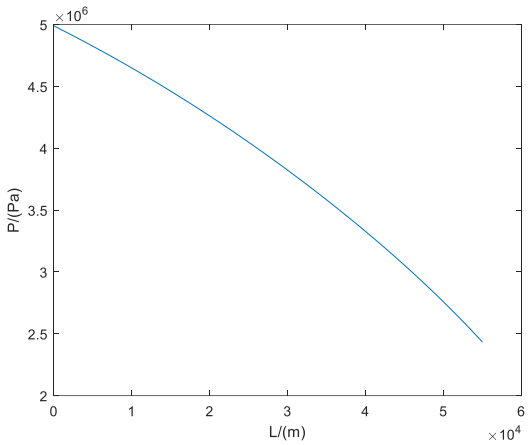

Fig. 3:- Pressure profile of oil and gas flow along offshore pipeline obtained using proposed model.

In fig.3, we observed that the pressure decreases along the offshore pipeline from 5×10^6Pato 2.4327×10^6Pa. Pressure drop is not linear because of the presence of more than phase.

Methods	Inlet pressure/ (MPa)	Endpoint pressure/ (MPa)	Pressure drop /(MPa)	REPD
Model	5	2.4327	2.5673	1.26%
MV	5	2.4	2.6	

Table 1:- Pressure comparison and validation [1].

Table.1 above shows the pressure drop comparison between results from our model and that obtained by measurement.

It comes out that the predicted pressure model matches with the measured value with a relative pressure drop (REPD) of 1.26%.

In fig.4, it is shown the comparison between the temperature profile of the oil and gas flow from our model and that from pipesim model. It can be seen, the temperature decreases along the pipeline for the both model from 323.15°k to an end point value of 278.2861°k for pipesim and 277.9934°k for our model. It is shown that our model prediction matches with the pipesim prediction with a relative error of 0.6%.

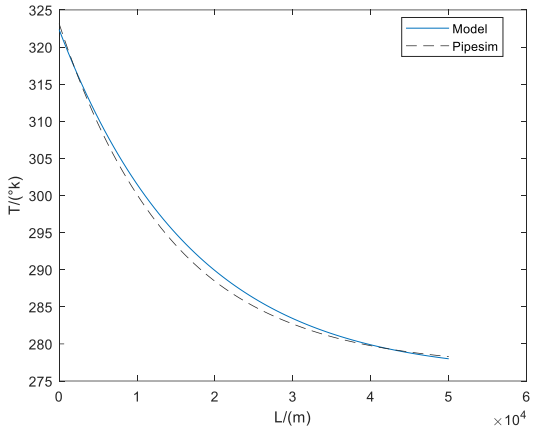

Fig. 4:- Temperature profile comparison between our model and pipesim model.

Table.2 below, presents comparison between the results of the temperature drop obtained from our model, pipesim model, UPTP model and measured value. In this table, the relative temperature drop (RETD) is calculated as follow:

$$RETD = \frac{Temperature\ drop\ predicted - Measured\ Value}{Temperature\ drop\ predicted} \times 100\%$$

It is shown in table.2 below that the result obtained from our model is in good agreement with results from others models and those of the measured value. These results indicates that the accuracy of the proposed model presented here is verified.

From fig.4 above, we also observed that the temperature decreases significantly after the first 1.5 km of flow. This is due to the rapid heat flux exchange between the warm fluid and the cooler environment as can be seen in fig.5 below.

Methods	Inlet temperature/ (°k)	Endpoint temperature/ (°k)	Temperature drop/(°k)	RETD
Model	323.15	277.9934	45.1566	1.68%
Pipesim	323.15	278.2861	44.8669	1.04%
UPTP	323.15	277.25	45.9	3.37%
MV	323.15	278.75	44.4	

Table 2:- Temperature drop validation (MV) as presented in [1]

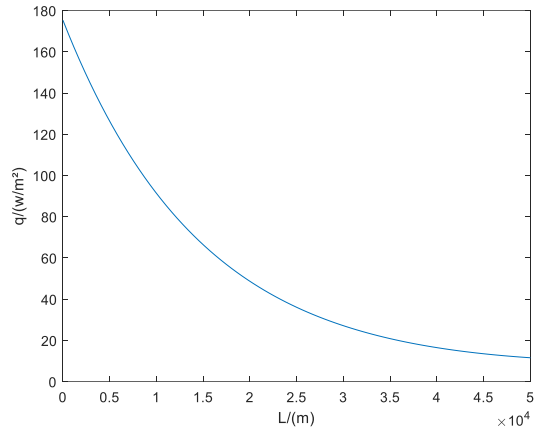

Fig. 5:- Heat flux exchange between the warm oil and gas flow and the seawater environment.

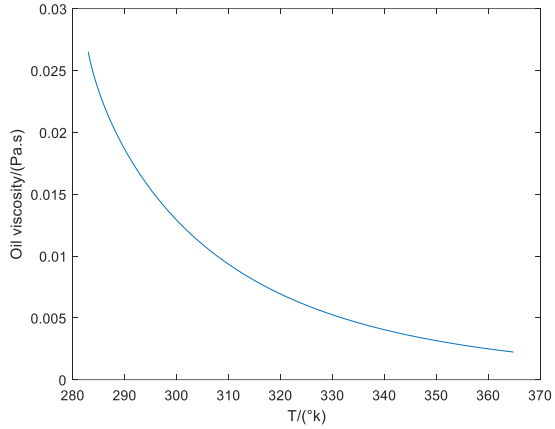

Fig. 6:- Variation of the oil viscosity with the temperature.

In fig.7 below, it is shown that the oil flowrate decreases as the temperature decreases.

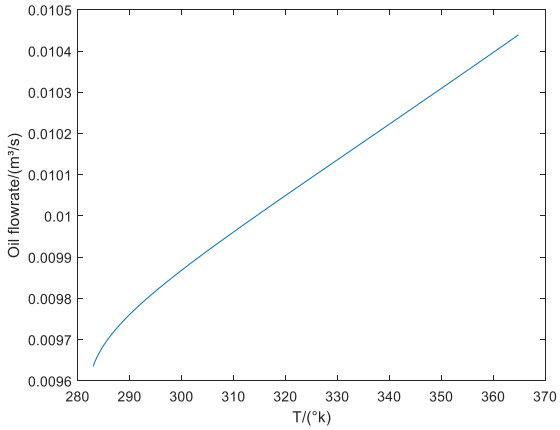

Fig. 7:- Variation of the oil flowrate with the temperature.

By considering the validation of the proposed model, sensibility runs are performed. We first analyzed the effect of three insulation materials, which are black aerogel, calcium silicate and polyurethane foam, with various thickness on the temperature profile. The following conditions were considered: the oil flowrate is maintained to 0.00955 m³/s, the inlet pressure is also fixed at 5MPa. The overall heat transfer coefficient is no longer set fix, but is determined using equation (17). Temperature profile is then calculated for each insulation and various thickness. Results are displayed in fig. 8, 9 and 10 below.

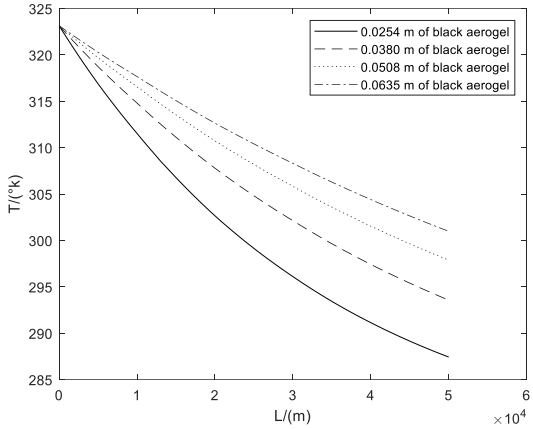

Fig. 8:- Effect of several thickness of black aerogel on the temperature profile of oil and gas flowing through offshore pipeline of 50 km.

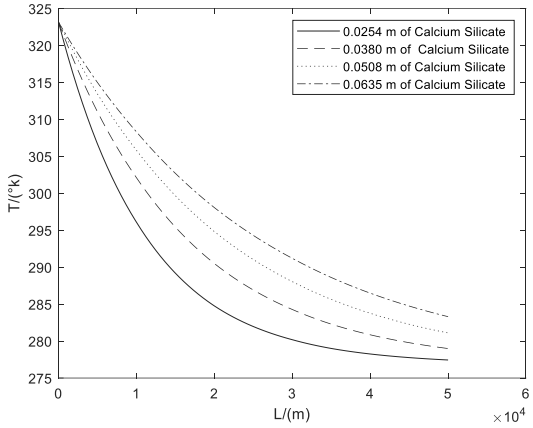

Fig. 9:- Effect of several thickness of calcium silicate on the temperature profile of oil and gas flowing through offshore pipeline of 50 km

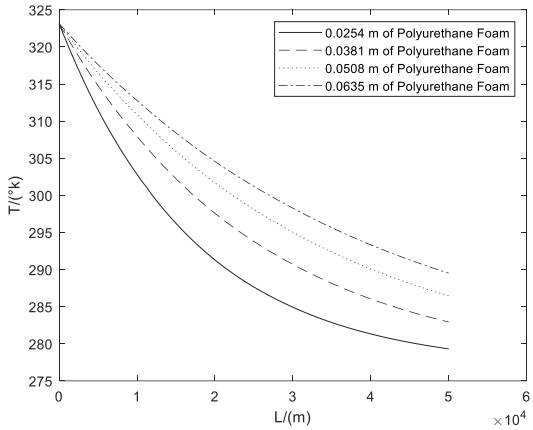

Fig. 10:- Effect of several thickness of polyurethane on the temperature profile of oil and gas flowing through offshore pipeline of 50 km.

It comes out from the figures above that, by increasing the insulation material thickness, the temperature drop decreases along the pipeline. It can also be observed that the

black aerogel material provides the best insulation than the others materials because of it very low thermal conductivity. However, none of the insulation material type and the selected thickness is able to withstand the flow assurance requirement.

Effect of the oil flowrate was also investigated. Results showed that as oil flowrate increases, the temperature drop decreases. This is because, increasing oil flowrate, increases the Reynolds number, which influence the overall heat transfer coefficient. Flow becomes rapid and the heat flux diminishes. For the considered range of the oil flowrate, the required minimum of the temperature is not achieve.

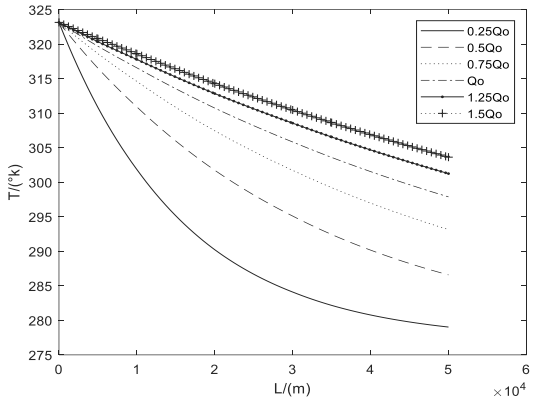

Fig. 11:- Variation of the oil flowrate with the temperature.

Further simulations have been carried out. The insulation material type used is the black aerogel because black aerogel provides better insulation than the others. The thickness selected are 0.0508 m and 0.0635 m, because the selected thickness have great impact on the temperature than the others as has been shown earlier. The oil flowrate is kept constant. The temperature profile for different inlet temperature and different insulation material thickness are calculated. Results are shown in fig.12 and 13 below. It is found that, from fig.12, the selected conditions is not suitable for maintaining the minimum temperature of 313.15°k while in fig.13, for an inlet temperature of 343.15°k with a thickness 0.0635 m, require minimum temperature in at any point in the pipeline is achieved.

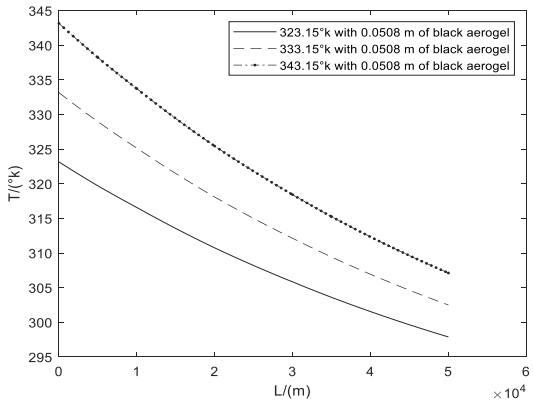

Fig. 12:- effect of different inlet temperature with 0.0508 m of black aerogel on the temperature profile of oil and gas flow in offshore pipeline

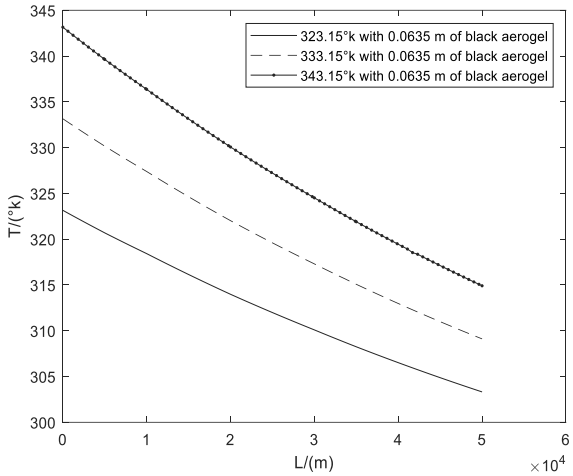

Fig. 13:- effect of different inlet temperature with 0.0635 m of black aerogel on the temperature profile of oil and gas flow in offshore pipeline.

The method presented in this study can be useful for the calculations of the temperature and pressure distribution along offshore pipeline as well as for thermal insulation management.

IV. CONCLUSION

In this paper, a mathematical model is proposed for predicting using numerical simulations, the temperature and pressure profile in long offshore pipeline of length 50 km during transportation of oil and gas. A drift flux model has been used to calculate the liquid holdup and the fluid properties where determined using black oil model. The overall heat transfer is modeled and incorporated in our computer program for sensitivity runs simulations. The results predicted by our model were compared against the results from measured value, UPTP model and pipesim model. Some of the significant points can be listed below:

- Good agreement is found between the predicted model results and field data, UPTP and pipesim models, which proves the accuracy of the model.
- When increasing the thickness of the insulation, the oil flowrate and the inlet temperature individually, the temperature drop decreases to a value below the require temperature at which no flow assurance issues such wax and hydrates formation can be observed.
- For an appropriate couple of inlet temperature and insulation thickness, obtained with a fix oil flowrate and a well-selected insulation material type, optimal operating condition that guarantee a continuous flow of the fluid inside offshore pipeline is achieved

ACKNOWLEDGMENT

Thanks to the director of Environmental Energy Technologies Laboratory (E.E.T.L) for his time, counseling, guidance and availability.

REFERENCES

[1]. J.M Duan, W. Wang, Y. Zhang, L.J. Zheng, H.S. Liu and J. Gong, Energy equation derivation of the oil-gas flow in pipelines, Oil & Gas Science and Technology – Rev. IFP Energies Nouvelles 68 (2013) 341-353.
[2]. Knut Vegard Løbergsli, Advanced temperature model for HPHT conditions, Master Thesis, Norwegian University of Science and Technology, Department of Petroleum Engineering and Applied Geophysics, 2015.
[3]. Kiran D. Patil, Study on effect of insulation design on thermal-hydraulic analysis: an important aspect in subsea pipeline designing. **Technical Report**, Maharashtra Institute of Technology, 2014, https://www.researchgate.net/publication/263426807.
[4]. Taitel, Y., & Dukler, A. E. (1976). A model for predicting flow regime transitions in horizontal and near horizontal gas-liquid flow, AIChE Journal, v.22, n. 1, 47-55. DOI:10.1002/aic.690220105.
[5]. Romero, O. J., Saad, H. C., Pereira, I. B., & Romero M. I., Influence of heat transfer on two-phase flow behavior in on-shore oil pipelines, Ingeniería e Investigación, 36(2016) 14-22.DOI: http://dx.doi.org/10.15446/ing.investig.v36n1.51570.
[6]. R.Sharifian, Temperature modeling for nodal analysis, Master of Science, Faculty of Civil Engineering & Geosciences, at Delft University of Technology, 2016.
[7]. Onuh Yunusa Charles, Temperature prediction model for flowing distribution in wellbores and pipelines, Master of Science in Petroleum Engineering, faculty of the African University of Science and Technology Abuja-Nigeria, 2011.
[8]. Shoham, O., Mechanistic modeling of gas-liquid two-phase flow in pipes, 2006, Chap. 6, 297-299.
[9]. B. Guo, S. Duan, and A. Ghalambor, A simple model for predicting heat loss and temperature profiles in insulated pipelines, Society of Petroleum, Engineers, Production and Operations, 21 (2006) 107–113.
[10]. Pourafshary, P., Varavei, A., Sepehrnoori, K., & Podio, A., *A* Compositional wellbore/reservoir simulator to model multiphase flow and temperature distribution, International Petroleum Technology Conference, 3-5 December, Kuala Lumpur, Malaysia, 2008, DOI: 10.2523/IPTC-12115-MS.
[11]. Alves, I.N., Alhanatl, F.J.S., Shoham, O., A unified model for predicting flowing temperature distribution in wellbores and Pipelines, SPE Prod. Eng. 20632 (1992) 363– 367.
[12]. Ting Dong Luis F. Ayala, Two-phase flow models for thermal behavior interpretation in horizontal wellbores, 6 (2016) 45–61, DOI 10.1007/s13202-015-0166-x. J Petrol Explor Prod Technol.
[13]. Andreolli, I., Zortea, M., Baliño, J.L., Modeling offshore steady flow field data using drift-flux and black-oil models, Journal of Petroleum Science and Engineering, 2017, doi:10.1016/j.petrol.2017.07.001.
[14]. Ishii, M., Zuber, N., Thermally induced ow instabilities in two-phase mixtures, 1970.
[15]. Hibiki, T., Ishii, M., Thermo-fluid dynamics of two-phase flow, 2006.
[16]. Brill J. P. and Mukherjee H, Multiphase flow in wells, Henry L. Doherty Memorial Fund of AIME, SPE, 1999.
[17]. S. Sadafule and K. D. Patil, Study on effect of insulation design on thermal hydraulic analysis an important aspect in subsea pipeline designing, Journal of Petroleum Engineering and Technology, 4 (2014) 2231-1785
[18]. Ibrahim Masaud Ahmed, Modeling and development of insulation materials in subsea, Master thesis, University of Newfoundland, 2018.
[19]. William Pao, Optimum thermal insulation design for subsea pipeline flow assurance, 2016 DOI: 10.13140/RG.2.2.33853.05603. https://www.researchgate.net/publication/311911773.
[20]. Luis E. Zerpa, A practical model to predict gas hydrate formation, dissociation and transportability in oil and gas flowlines Phd thesis, Faculty and the Board of Trustees of the Colorado School of Mines,.2013.
[21]. Beggs, H. D., & Brill J. P., A study of two phase flow in inclined pipes. Journal of Petroleum Technology, v. 25, n.5 (1973) 607-617. DOI: 10.2118/4007-PA.
[22]. Brill J. P. and Mukherjee H Multiphase flow in wells, Henry L. Doherty Memorial Fund of AIME, SPE, 1999
[23]. Beggs H. D, Optimization production using nodal analysis, OGCI, Inc., Petroskills, Tulsa, Oklahoma 74153 (2003) 80-90..
[24]. Zuber, N., Findlay, J. A., Average volumetric concentration in two-phase ow systems. Journal of heat transfer 87 (1965) 453-468.
[25]. Kreith, F. and Bohn, M. "Principles of Heat Transfer", 5th Edition, PWS Publishing Company, 1997.
[26]. Woldesemayat, M., Ghajar, A. J., Comparison of void fraction correlations for different flow patterns in horizontal and upward inclined pipes, International Journal of Multiphase Flow 33 (2007.) 347-370.
[27]. Vemund Flatebakken, Further development of a Network Solver with gas lift optimization. thesis, Novergian University of Science and Technology, Department of Geoscience and Petroleum, 2017.
[28]. Pourafshary, P., Varavei, A., Sepehrnoori, K., & Podio, A., A Compositional Wellbore/Reservoir Simulator to Model Multiphase Flow and Temperature Distribution, International Petroleum Technology Conference, 3-5 December, Kuala Lumpur, Malaysia. DOI: 10.2523/IPTC-12115-MS.
[29]. Lateef A.Kareem., Tajudeen M.Iwalewa., Muhammad Al-Marhoun ,New Explicit Correlation for the Compressibility Factor of Natural Gas: linearized z-factor isotherms, J Petrol Explor Prod Technol (2016), DOI: 10.1007/s13202-015-0209-3.